DISSERTATIONES PHYSICAE UNIVERSITATIS TARTUENSIS
27

ATOMIC LAYER DEPOSITION OF ARTIFICIALLY STRUCTURED DIELECTRIC MATERIALS

KAUPO KUKLI

TARTU 1999

DISSERTATIONES PHYSICAE UNIVERSITATIS TARTUENSIS

27

DISSERTATIONES PHYSICAE UNIVERSITATIS TARTUENSIS
27

ATOMIC LAYER DEPOSITION OF ARTIFICIALLY STRUCTURED DIELECTRIC MATERIALS

KAUPO KUKLI

TARTU UNIVERSITY
PRESS

This study was carried out at the Institute of Experimental Physics and Technology of Tartu University and at the Laboratory of Inorganic Chemistry of the University of Helsinki.

This Dissertation was admitted on December 16, 1998, in partial fulfilment of the requirements for the degree of Doctor of Philosophy in physics (applied physics), and allowed for defence by the Council of the Department of Physics, Tartu University.

Supervisor: Prof. Lembit Pung, Tartu University

Opponents: Prof. Martti M. Salomaa, Helsinki University of Technology
Prof. Enn Mellikov, Tallinn Technical University

Defence: February 10, 1999, at Tartu University, Tartu, Estonia.

The publication of this dissertation is granted by Tartu University

Tartu Ülikooli Kirjastuse trükikoda
Tiigi 78, Tartu 50410
Tellimus nr. 471

To Ruth

On mielekästä tehdä asioita,
joita tarvitaan.

Tuomo Suntola / Merja Haikkola

CONTENTS

LIST OF ORIGINAL PAPERS

I Kaupo Kukli, Jaan Aarik, Aleks Aidla, Oksana Kohan, Teet Uustare and Väino Sammelselg, Properties of Tantalum Oxide Thin Films Grown by Atomic Layer Deposition. *Thin Solid Films*, 260 (1995) 135–142.

II Jaan Aarik, Kaupo Kukli, Aleks Aidla and Lembit Pung, Mechanisms of Suboxide Growth and Etching in Atomic Layer Deposition of Tantalum Oxide from $TaCl_5$ and H_2O. *Applied Surface Science*, 103 (1996) 331–341.

III Kaupo Kukli, Mikko Ritala and Markku Leskelä, Atomic Layer Epitaxy Growth of Tantalum Oxide Thin Films from $Ta(OC_2H_5)_5$ and H_2O. *Journal of the Electrochemical Society*, 142 (1995) 1670–1675.

IV Kaupo Kukli, Jaan Aarik, Aleks Aidla, Hele Siimon, Mikko Ritala and Markku Leskelä, *In Situ* Study of Atomic Layer Deposition of Tantalum Oxide Thin Films from $Ta(OC_2H_5)_5$ and H_2O. *Applied Surface Science*, 112 (1997) 236–242.

V Kaupo Kukli, Mikko Ritala, Markku Leskelä and Reijo Lappalainen, Niobium Oxide Thin Films Grown by Atomic Layer Epitaxy. *Chemical Vapor Deposition*, 4 (1998) 29–34.

VI Kaupo Kukli, Mikko Ritala, Markku Leskelä and Janne Jokinen, Atomic Layer Epitaxy Growth of Aluminium Oxide Thin Films from a Novel $Al(CH_3)_2Cl$ Precursor and H_2O. *Journal of the Vacuum Science and Technology*, A15 (1997) 2214–2218.

VII Kaupo Kukli, Jarkko Ihanus, Mikko Ritala and Markku Leskelä, Properties of Ta_2O_5 Based Dielectric Oxide Multilayers Deposited by Atomic Layer Epitaxy. *Journal of the Electrochemical Society*, 144 (1997) 300–306.

VIII Kaupo Kukli, Jarkko Ihanus, Mikko Ritala and Markku Leskelä, Tailoring the Dielectric Properties of HfO_2-Ta_2O_5 Nanolaminates. *Applied Physics Letters*, 68 (1996) 3737–3739.

IX Kaupo Kukli, Mikko Ritala and Markku Leskelä, Properties of $(Nb_{1-x}Ta_x)_2O_5$ Solid Solutions and $(Nb_{1-x}Ta_x)_2O_5$-ZrO_2 Nanolaminates Grown by Atomic Layer Epitaxy. *Nanostructured Materials*, 8 (1997) 785–793.

1. PREFACE

The development of low-dimensional layered dielectric and semiconductor materials with precisely tuned composition and structure is an aim of the high-technology research [1]. Advanced dielectric coatings must demonstrate several reproducible features such as low defect density, temperature stability, excellent step coverage and high uniformity. The compound material and related defects affect the intrinsic physical properties while the conformality depends largely on the process technique. Depending on whether the film quality is first determined by conformality and/or electrical properties, the deposition technique is to be specified, generally preferring those enabling the growth at the lowest substrate temperature [2–4] to avoid undesired interfacial reactions, substrate damage and energetical cost.

Driven by the challenge for the realization of perfectly conformal growth at low temperatures, the Atomic Layer Epitaxy (ALE) [5] and Molecular Layering (ML) [6] techniques have been introduced where the substrate surface is alternately exposed to the chemical precursors of desired material carried into the reactor by inert gas and moving in the form of separate adsorption waves [7,8] along the surface. The adsorption can proceed, also at relatively low temperatures, until surface saturation. After refreshing the surface activity using proper chemicals, the adsorption of a new layer of precursor molecules becomes possible. Hence, one can develop a cyclic growth process by alternately adsorbing new molecular layers and recreating active adsorption sites. The growth rate of growing layer is determined by the amount of surface sites available for adsorption rather than by the temperature or precursor flux. The ideal ALE results in thin solid film with thickness determined by the number of adsorption cycles and the lattice constant of growing material, allowing easy modulation of device dimensions and providing sharp interfaces at atomic level between different functional layers.

It has been recognized for over 20 years that the device research is not meant to end up with simply a discovery but productive discovery [9]. At present, the ALE-technology is already a branch of strongly application-oriented research. Nevertheless, it is also a process of great academic interest, offering an opportunity to study rather fundamental phenomena related to the adsorption processes and formation mechanisms of thin solid films.

2. PURPOSE OF THE PRESENT STUDY

The claim of this study is the feasibility of atomic layer deposition for the highly reproducible fabrication of thin layered dielectrics. These structures demonstrate advanced size-dependent or composition-dependent physical properties in as-deposited state. Ta_2O_5 as a material of high permittivity and breakdown resistance has been selected as the basis oxide. The growth mechanism of Ta_2O_5 determines its composition and structure and was investigated in more detail by means of quartz crystal microbalances. The growth and properties of Ta_2O_5 [I–IV], Nb_2O_5 [V] and Al_2O_3 [VI] were studied in order to optimize their dielectric performance further evaluated by measuring their permittivity and leakage current density. The dielectric materials have been developed by tailoring the high dielectric constant and breakdown resistance of Ta_2O_5 to the higher resistivity or even higher permittivity of Nb_2O_5 [V,IX], Al_2O_3 [VI,VII], ZrO_2 [VII,IX] or HfO_2 [VIII]. The advanced performance of ZrO_2-Ta_2O_5, HfO_2-Ta_2O_5 and ZrO_2-$(Nb_{1-x}Ta_x)_2O_5$ nanolaminates was related to the nanocrystalline nature and phase changes in ZrO_2 [VII] and HfO_2 [VIII] layers and to the high permittivity of amorphous $(Nb_{1-x}Ta_x)_2O_5$ films [IX].

3. RESEARCH BACKGROUND

3.1. Chemical buildup of thin film structures

The surface activity towards chemisorption is determined by the nature, temperature resistance and surface density of certain functional groups, such as OH-groups, able to react with oncoming precursor molecules. For instance, the net reaction for silica supported modification of $(CH_3)_3SiCl$ cannot proceed without the aid of functional OH-groups created on silica surface after water adsorption [10]. The creation and recreation of OH-groups on the silicagel surface can be reproducibly controlled via successive heating and water re-adsorption cycles while the density of OH-groups is determined by the temperature rather than by the duration of annealing. This irreversible surface reaction and the following heat-treatment results in the mass of new SiO_2 layers added to the precipitate [10]. The extent and nature of surface reactions expressed, for instance, by the Cl to Ti ratio after $TiCl_4$ adsorption, changes with the density of active adsorption sites while the amount of Cl released decreases with the surface density of the OH-groups [11]. Along with the occupation of free sites, the surface becomes deactivated in relation to the adsorbing precursor. However, the surface is now terminated with other kind of radicals (chlorine) and may react with some alternative gaseous precursors (e.g. H_2O). The result is the creation of new atomic layer of solid compound and concurrent recreation of surface radicals — OH-groups. Such a molecular layering reaction [12] is highly reproducible also on monocrystalline (e.g. Si) substrate [13]. In general, multicomponent oxide films can be prepared in the molecular layering process, for instance, on Si surface via successive chemical reactions [14]:

1. $m(\text{-Si-OH}) + MCl_n \rightarrow (\text{-Si-O-})_mMCl_{n-m} + mHCl$
2. $(\text{-Si-O-})_mMCl_{n-m} + (n-m)H_2O \rightarrow (\text{-Si-O-})_mM(OH)_{n-m} + (n-m)HCl$
3. $(\text{-Si-O-})_mM(OH)_{n-m} + MCl_n \rightarrow (\text{-Si-O-})_mMO_{n-m}MCl_m + (n-m)HCl$
4. $(\text{-Si-O-})_mMO_{n-m}MCl_m + mH_2O \rightarrow (\text{-Si-O-})_mMO_{n-m}M(OH)_m + mHCl$
5. etc.,

if the chlorides of an arbitrary cation, M, and water are applied as reactants. Each subsequential stage of molecular layering results in the new overlayer of the same composition at the same energy state. As a consequence, the same structure should be formed at the each stage of the synthesis [6]. The exact reproduction of substrate or film structure can be expected if the density of similar active sites is the highest possible and is recovered after each layering step. Hence, the revolutionary aspect of the successive surface reactions is that providing the advantages of epitaxy even on amorphous substrates [5]. The

strongest possible bonds occur between adsorbent and adsorbate perpendicular to the surface. The film growth proceeds always stepwise, atomic plane by atomic plane and the ideal model of ALE [5,15,16] thus assumes the nucleation-free formation of compound film highly oriented in the growth direction. Heteroepitaxy can be, of course, realized whenever the lattice match between substrate and film allows it [17,18]. Alternative terms such as Atomic Layer Deposition (ALD), Digital Chemical Vapor Deposition, Sequential Binary Half-Reactions, Atomic Layer MOCVD, etc. can be met in literature [8,19–26] while the term Atomic Layer Chemical Vapor Deposition (AL-CVD) is recently accepted by Microchemistry Ltd. [27], the leader in the production of ALE-reactors. AL-CVD will be used in the further text as for a common denominator for all methods related to ML-ALE.

3.2. Capabilities of AL-CVD

Besides reproducibility and conformality, an additional advantage of the AL-CVD is the possibility to exploit highly reactive precursors with low reaction activation barriers allowing significant reduction in the deposition temperature, even down to the room temperature [17,21,28]. Possible problems concerning the relative slowness of stepwise growth could cease when considering the small thickness of functional layers in electronic devices, for instance, below 10 nm in memory cells [29]. Moreover, there will be decrease in the functional layer thickness in the future microelectronics down to the 4–5 times of the Si-O bond length [30].

By far the industrial manufacturing of sulfide-based phosphors and Al_2O_3-based insulators for thin film electroluminescent (TFEL) devices [5,31–33] has been the most outstanding application of AL-CVD. The fundamental aspects of the growth have been investigated for numerous microelectronic and optical materials [16,19,26,31,33–35], also considering metals [36,37], superconductors [25], transparent conductors [38], silicon [39] and ferroelectrics [23].

3.3. Features of real AL-CVD process

In AL-CVD, the adsorption process of a precursor should end up at the maximum surface coverage via occupation of all active sites excluded those inaccessible due to the steric hindrance. However, steric effects arising from the finite size of precursor molecules result in the screening of some active sites [26] usually resulting in a submonolayer deposition during one growth cycle.

The functional groups cannot be entirely consumed in surface reactions [40] at low temperatures. The precursor dose should be sufficiently high to approach the maximum coverage. For instance, the growth rate of TiO_2 films is higher the more complete is the dechlorination of $TiCl_4$ terminated surface during H_2O pulse. Long-term exposure to H_2O flux should replace the possible intermediates $TiCl_{4-n}(OH)_n$ entirely with Ti-OH [41]. Otherwise, Cl atoms in half-reacted $TiCl_{4-n}(OH)_n$ surface groups could block some active sites restricting the $TiCl_4$ adsorption in the next step.

Too long precursor pulses, in turn, may be accompanied by etching and consequent removal of the film material [42]. Also the atomic-level surface flatness may be destroyed by high fluxes, although the self-limiting adsorption mechanism itself is not necessarily violated. Excess precursor may adsorb on the sites of different energy when the precursor pulse lasts longer than the lifetime of surface radicals [43], resulting in the clustering and formation of unexpected structures. The existence of dissimilar surface sites should enhance the nucleation density while long exposures enable the completion of surface processes of different rates.

Sometimes, self-limiting surface reaction can be considered already in the conventional CVD process, manifesting itself as an asymptotic behaviour of the film growth rate when increasing with the precursor flow rate [44]. In AL-CVD process, the exposure times can be optimized to provide surface coverage close to the maximum. Eventually, the film growth rate may remain rather insensitive to the gas flow rate, precursor concentration, time parameters and substrate temperature. In principle, each of the parameters could have individual processing window where the self-limited and uniform adsorption is realized. More uniquely, the temperature range for constant growth rate is called ALE processing window [15]. At too low temperatures, the growth rate can be suppressed by the activation energy barriers or be increased due to the condensation effect. At too high temperatures, the growth rate may increase because of the thermal decomposition of the precursor or it can, in turn, decrease due to the thermal desorption or modification of surface groups.

The clear separation of reactant pulses by the purge periods is important when avoiding uncontrolled gas phase reactions [15,16]. In general, the periodic interruption of precursor beam accompanied by the increased time for surface-migration can increase the diameter of forming islands and enhance the two-dimensional growth on the expense of the surface density of islands [45]. In AL-CVD like processes, this results in the improved crystallinity, in addition to the better desorption and exhaust of byproducts, decreasing the residue content [46].

3.4. Real time monitoring of AL-CVD process

The surface coverage and structure can be investigated during the layer-by-layer growth process by optical monitoring [28,47] or reflection high energy electron diffractometry (RHEED) [48], respectively. The surface chemistry can be studied by means of Auger' electron spectroscopy (AES) or X-ray photo-electron spectroscopy (XPS) etc. [17]. Mass-spectroscopy can be applied in order to determine the molecular weight of volatile reaction byproducts and their fragmentation [49,50], while gravimetry [51] characterizes the nature of exchange reactions by sensing surface mass density changes.

The quartz crystal microbalances (QCM) is an alternative tool for direct monitoring of the mass of surface species, regularly applied to follow electrochemical reactions [52,53]. Anyhow, the QCM circuit has been originally developed [54] and is often applied for detecting film thickness in vacuum deposition process [55]. Also the parameters of thermal processes such as the sublimation enthalpies of fullerene layers [56] can be determined by QCM. Since the possibly first QCM studies on molecular layering of II–VI compounds [57], the QCM has also been applied to follow AL-CVD growth of Al_2O_3 [34,58], TiO_2 [59], Ta_2O_5 [42], SrS and SrO [50], CaS [60] and HfO_2 [61].

The working principle of the QCM is based on the mass-sensitivity of quartz piezocrystal mounted between metal electrodes forming an oscillator circuit. The alterations of QCM working frequency, Δf, are related to the additional mass adsorbed on the surface of crystal and electrodes, as follows [54]:

$$\Delta f / f = -\Delta d / d = -\Delta m / (\rho_q \times F \times d),$$

where f is the resonance frequency of unloaded crystal, d is the thickness of the quartz plate, Δd is the increase in film thickness, ρ_q is the density of quartz, F is the resonator (electrode) area and Δm is the mass load. Considering the decreased frequency, f_c, of coated quartz resonator in comparison to the unloaded one, one can modify the linear frequency-mass relationship for the direct measurement of oscillation period [62,63]:

$$m = \rho_q \times N \, (1/f_c - 1/f) = \rho_q \times N \times \Delta\tau ,$$

where $\Delta\tau$ is the change in vibration period and N is a constant. The temperature stability and mass sensitivity of QCM is potentially sufficient for detecting mass at (sub)monolayer level at the temperatures ranging from 1.4 K [64] up to the Curie point at 565 °C [63]. The initiation and termination points of adsorption processes are sharply defined (Fig. 1). Validity of linear relationship between mass load and frequency/period is maintained in sufficiently large limits, for instance, in case of 0.1 μm thick H_2O overlayer [52], but generally depending on the density of the growing material and atomic number of species weighed.

In gaseous environment and at low base pressures one can also neglect the vibration damping effect of viscosity of embracing fluid [65] as well as the hydrostatic pressure effect on frequency [65]. The nature of surface top layers formed during preceding cycles do not cause additional calculation errors sometimes affecting the results of optical monitoring [55].

In the AL-CVD process, one can record separately the QCM output signals stabilized after the first precursor pulse at some level, Δm_1, and that stabilized after the pulse of the second precursor, Δm_2 (Fig. 1). The mass added during completed growth cycle can be expressed as $\Delta m_0 = |\Delta m_1 - \Delta m_2|$. Measurement of absolute mass values is still complicated due to the calibration problems and sensitivity drift during successive mass loading cycles. Instead, the ratio $\Delta m_0/\Delta m_1$ can be calculated, representing the relative mass change in the particular cycle. Anyway, the changes in surface mass density can be correlated to the average molecular weight of chemical species adsorbed, reacted and released in the net reactions. For each heterogeneous reaction formally proposed, one can compare the molecular weight alterations calculated, $\Delta m_0/\Delta m_1$, to the experimental results. This should allow the selection of the most probable film growth mechanisms. Directly, QCM allows the monitoring of the relative rate of possible precursor decomposition or etching processes manifesting themselves via continuous increase and decrease in surface mass density, respectively.

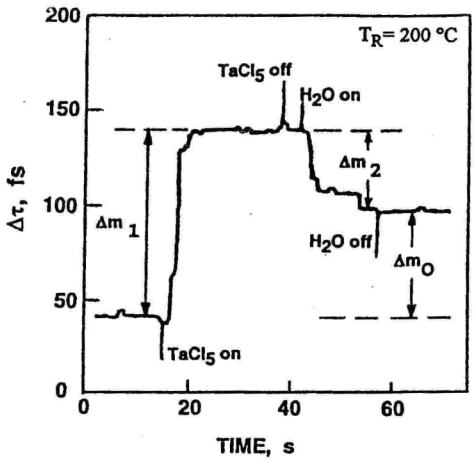

Figure 1. Alterations in QCM oscillation period upon mass load in AL-CVD process.

3.5. Structure of AL-CVD films

Generally, the structure of crystalline AL-CVD films corresponds to some known stable polymorph(s) of the particular compound. The bilateral growth mode favoured can result in the formation of densely packed crystalline structure even on amorphous substrates [66] but most often the films are weakly oriented or amorphous because of the kinetic limitations set by low temperatures. However, the heterogeneous nucleation proceeding on foreign surfaces is largely influenced by adsorption chemistry and occurs well below the homogeneous nucleation temperatures [67]. In AL-CVD, the irregular seeding of crystal growth takes place while the agglomeration probability and nucleation density depend on the growing material [68,69], substrate material [69], the chemical modification of adsorption sites [70] or difference in ionic radii of dopant and host matrix elements [71].

The proportional relationship between growth rate and number of growth cycles indicates the thickness-independent growth mechanism. The deviations can still be observed in the vicinity of film-substrate interface, referring to the phase changes [22,72–74] and/or to the different rates characterizing the reactivity of functional groups on surfaces of substrate and growing film [75]. At the early stages of molecular layering, it is possible to obtain different metastable forms varying in density while well-defined structural units of growing substance form after the minimization of the energy of layering products [6]. The crystallization "pathway" of stable solid from gas phase may contain one or several intermediate states with local free energy minima. So the TiO_2 and ZrO_2 can grow from metal chlorides and H_2O first forming the nanosize crystallites of high-pressure polymorph TiO_2-II [41,59] and high-temperature tetragonal ZrO_2 [70], respectively. The TiO_2-II forms easier the lower is the amount of OH-groups involved in the reactions while higher H_2O doses result in the preferred formation of rutile [41]. The rutile phase appears always but only after exceeding certain critical thickness depending on the precursor dose and purge time. In case of ZrO_2, it was noticed that the oxide agglomerate formed during the first successive molecular layering steps is not covered with the groups of the same activity as on the substrate surface [70]. Probably for this reason, the film formation proceeds initially with lower rate.

Some minimum surface group density is still required to obtain observable agglomerates [70]. In case of low density of adsorption sites, more space is left for surface migration and the agglomeration is favoured around these sites. The agglomeration is further enhanced by the chemistry of the growth mechanism. For instance, TiO_2 clusters might form on surface when the reaction product HCl, released in the reaction between $TiCl_4$ and OH-groups, itself reacts with OH-groups giving a secondary product H_2O which reacts, in turn, with $TiCl_4$ [40]. Whatever is the exact nucleation mechanism, such a growing nucleus has to be affected by the surface energy causing excess stress affecting the lattice

parameters. This favours the formation of lattice characteristic of the modification metastable in the bulk form.

High density of active sites, in turn, better repeats the structure of underlying surface and restricts the growth of nuclei initially formed. Consequently, the bilateral growth and instant formation of large supermolecular structures is enhanced while the growth of equilibrium phases with increased rate is favoured. Besides rutile TiO_2 [41], also the $ZrCl_x$ molecular layer and, consequently, the Zr atomic layer is completed easier the higher is the density of OH-groups, suppressing the formation of ZrO_2 agglomerates [70].

The formation of crystalline phases, regarded as metastable in the bulk form, is possible in AL-CVD films also without any obvious inclusion of stable polymorphs. For example, 100–400 nm thick La_2S_3 films with well-defined cubic structure can be grown on glass substrate at as low as 450–500°C [76], although the bulk cubic γ-La_2S_3 is stable at 1000°C and higher temperatures.

3.6. Binary metal oxides: reference studies

3.6.1. Ta_2O_5

Application fields

Ta_2O_5 is a material increasing integration densities in the dynamic random access memories (DRAM) on 265 Mbit — 1 Gbit levels [2,3,77]. The stability and resistance of Ta_2O_5 usually exceeds that of ferroelectrics, the long-term candidates for ultra-large-scale integrated (ULSI) dielectrics. Ta_2O_5-based technologies are compatible with the hemispherical-grain-silicon storage node [78] and 300-mm silicon wafer [79] fabrication technologies. Ta_2O_5 is also an outstanding optical material [80] because of its wide band-gap up to 4.5 eV and high transparency in the wavelength range of 0.6–2.0 μm.

Growth

Chemical vapor deposited (CVD) Ta_2O_5 thin films show better step coverage, lower leakage current and higher dielectric constant than those grown by physical vapor deposition (PVD) [81,82]. The pyrolysis and oxidation of tantalum ethoxide, $Ta(OC_2H_5)_5$, is a common low-temperature CVD route between 350 and 460°C [83–86]. The catalytic activity of Ta_2O_5 surface towards supplementary agent ethanol allows the creation of additional OH-groups enhancing the adsorption and growth rate, lowering the growth temperature below 300°C [87]. Even higher activity of $Ta(OC_2H_5)_5$ towards H_2O allows one to decrease the CVD temperature down to 100°C [88]. The growth rate limiting step is the competitive adsorption of H_2O and $Ta(OC_2H_5)_5$ molecules and surface reactions instead of gas-phase reactions or precursor transportation. Thus, the low-tempe-

rature CVD process is already surface-controlled, proceeding via reactions far from thermodynamic equilibrium. The results of thermodynamic calculations predict CH_4, CO, CO_2, H_2 and H_2O to be the main reaction products, while C_2H_5OH, CH_4 and C_2H_4 have been detected by mass-spectrometry [88].

Amorphous Ta_2O_5 films grow below 600–650°C, regardless of the deposition method used [84–86,89] and crystallize into hexagonal (δ), orthorhombic (β) or even into tetragonal (α) form either upon growth temperature increment [90] or during post-deposition annealing [84–86,89–92] above 600–650°C. The high-temperature form α-Ta_2O_5 [93] can be stabilized at low temperatures by doping with foreign metal oxides and shows enhanced ionic conduction, analogously to the stabilized zirconia.

Relatively large leakage currents observed in Ta_2O_5 can arise from the (hydro)carbon contamination in the range of 1–24 at %, coming from the carbon-containing precursors [86,91,94], in addition to the possible oxygen vacancies [29] or Ta interstitials [95]. The thermodynamics ruling the ethoxide decomposition may not favour the further reduction of carbon content [91]. The residue content and defect density can be reduced by annealing [82,96] or using alternative precursors [97]. Annealing temperatures above 450–500°C are already too high for IC processes after the first metallization level [82] and, therefore, the film quality has to be improved already in as-deposited state.

AL-CVD (ALE) has been applied for growing Ta_2O_5 thin films only from $TaCl_5$ and H_2O in the temperature range of 300–500°C [26,42,48,98–101]. $TaCl_5$ does not contain carbon, but increasing residual chlorine content is still observed in the films deposited below 500°C [99,100]. $TaCl_5$ also etches the underlying Ta_2O_5 film, increasing the thickness profile and decreasing the absolute growth rate [42].

Properties

The dielectric constant of highly oriented α-Ta_2O_5 is as high as 65 while that of low-temperature β-Ta_2O_5 phase does not exceed 24 [92]. The amorphous Ta_2O_5 also demonstrates local short-range order characteristic of β-Ta_2O_5 [102]. The low frequency dielectric constant of amorphous Ta_2O_5 films remains between 20–27 while polycrystalline films possess higher, although less stable, permittivity between 35 and 60 [83–86,89] upon the relative content of δ- and α-Ta_2O_5. Profound decrease in effective permittivity is often observed in annealed Ta_2O_5 films on silicon and is believed to arise due to the formation of interfacial leaky SiO_2 layer [97] or the lower oxidation state of tantalum in Ta-Si system possibly leading to the permittivity decrement [103]. The formation of SiO_2 can be restricted by depositing interfacial barrier electrodes [84,85]. Amorphous Ta_2O_5 is commonly accepted for DRAM and MOSFET processing [79,104] instead of crystalline material due to its higher stability and processing convenience. Moreover, low-temperature deposition below 425°C does not necessarily result

in the formation of SiO_2 interlayer [82,86] although the reaction between Ta_2O_5 and Si is favoured [105,106].

As-deposited Ta_2O_5 films are usually rather leaky [83,84,86] exhibiting, at the same time, large breakdown resistance. The high leakage may be explained by oxygen vacancies [107], high micropore density [108], high residue content [83,86], contaminating diffusion of substrate (Si) atoms into Ta_2O_5 layer [84,109] or the effect of high permittivity [92,110]. The thermal treatment carried out at high rate or below crystallization temperature can oxidize impurities or remove vacancies from the film bulk [78,81,83,87,107] but strong recrystallization of Ta_2O_5 upon long term annealing at high temperatures deteriorates the film resistivity [83,85].

3.6.2. Nb_2O_5

Application fields

Nb_2O_5 thin films have been studied, for instance, as a potential material for gas sensors [111] and 256 Mbit DRAM devices [2,112]. However, niobium is perhaps more recognized as a dopant, for instance, decreasing the work function of TiO_2 based solar cell materials [113] or restricting the degradation of $Pb(Ti,Zr)O_3$ ferroelectrics [114].

Growth

Below 500°C, $Nb(OC_2H_5)_5$ has been used as a Nb precursor [2,112] while $NbCl_5$ has been applied in the range of 850–1000°C [115]. Progress in CVD of Nb_2O_5 has still been hindered due to the expense, low stability and moisture sensitivity of niobium alkoxides and high residue (Cl) content arising from halide precursors [116].

Niobium and tantalum possess similar chemistries. Both Nb_2O_5 and Ta_2O_5 have complex structure built of MO_6 octahedra [95]. The low temperature orthorhombic γ-Nb_2O_5 (T-Nb_2O_5) and β-Ta_2O_5 forms are isostructural [117]. The Nb_2O_5 films crystallize when grown above 400–600°C or can be re-crystallized into T-Nb_2O_5 phase [118]. The recrystallization temperature is about 100–200°C lower than that of Ta_2O_5 [2,112,117,119], due to the lower binding energy and stability of Nb-O bonds compared to Ta-O bonds [117,119]. The stoichiometric deviations in Nb_2O_5 films as-deposited from $Nb(OC_2H_5)_5$ have been considerably stronger than usually observed in Ta_2O_5 [112]. Also the carbon content in Nb_2O_5 films grown at 470°C has been six times higher than that in Ta_2O_5 deposited in the same conditions [2].

Properties

The refractive index of Nb_2O_5 films is as high as 2.24–2.32 [2]. The dielectric constant of Nb_2O_5 films has been higher than that of Ta_2O_5, ranging from 14 to 143 [2,118,120], also depending on the deposition and annealing conditions.

The breakdown field can be 3–4 times lower than that in Ta_2O_5 [2]. Although the perfectly stoichiometric Nb_2O_5 is an insulator [121], already a minor excess of metal atoms in niobium oxide results in semiconducting behaviour [111,121].

3.6.3. Al_2O_3

Application fields

Al_2O_3 films have been studied for the application as ion diffusion barriers and protective dielectrics in thin film electroluminescent (TFEL) devices [31,32]. Al_2O_3 has been investigated for the application in capacitor devices [2].

CVD and AL-CVD growth of Al_2O_3

The growth of Al_2O_3 from various Al precursors, including chloride, alkoxides and metalorganics both in conventional CVD [122,123] and AL-CVD [20,34, 68,124–128] is influenced by rather weak tendency towards agglomeration and usually results in amorphous films showing smooth surfaces and roughness around several ångströms [68]. The content of residues (chlorine) increases towards lower deposition temperatures [34], still depending on the particular precursor chosen [128]. The physical properties may also depend on the nature of particular precursor. Despite the higher absolute residue concentration, the refractive index attained in the films grown from $Al(CH_3)_3$ and H_2O [126] have still been higher than that of the films grown from $AlCl_3$ and H_2O in the similar conditions [126,128]. MOCVD temperature for stoichiometric Al_2O_3 can be decreased down to 230°C, while the residual carbon content remains at around 2% and still consists mainly of the surface carbon [129]. The AL-CVD reactions between $Al(CH_3)_3$ and H_2O on silica can proceed at as low as 120°C [75]. Saturated surface reactions at temperatures above 450°C lead to the removal of resistant carbon-containing surface groups and continuation of contamination-free growth [75]. However, below 450°C, the carbon contamination probably cannot be eliminated entirely in $Al(CH_3)_3$-based process.

Properties

Amorphous Al_2O_3 is stable up to the annealing temperatures of 600–800°C. The dielectric constant in the films or bulk Al_2O_3 does not exceed 12 [2,120,124], while its band-gap can be as high as 7 eV [130]. In the AL-CVD films processed from $Al(CH_3)_3$ and H_2O, the band gap increases from 5 to 6 eV with the deposition temperature increasing from 150 to 310°C [125]. The breakdown field in $Al/Al_2O_3/Si$ capacitor structures fabricated by AL-CVD has been as high as 7–8.3 MV/cm [124,125,127] and is rather insensitive to the temperature changes, although the leakage current in as-deposited films monotonously increases with the growth temperature [127]. The leakage current can be decreased by about 2–3.5 orders after annealing, becoming independent of the sample history. Most probably, excess hydrogen is present in the CVD Al_2O_3

films as-deposited and can be removed in annealing process [122] accompanied by film shrinkage and densification.

3.6.4. ZrO_2

Application fields

ZrO_2 is a widely studied material for thermal barrier coatings, buffer layers for superconductors, oxygen sensors, catalytic supports and coatings, waveguides etc. ZrO_2 could be the most stable dielectric oxide in contact with silicon [106]. The MOCVD ZrO_2 films have exhibited quite low leakage currents [2,131] but also rather low refractive idex values as an indication of insufficient density [2]. More work is needed to improve the permittivity of polycrystalline ZrO_2 [131].

Growth

As a rule, the ZrO_2 films are polycrystalline regardless of the particular growth technique used. The main polymorphs of ZrO_2 are monoclinic, (m), tetragonal, (t), and cubic, (c), forms. The m-ZrO_2 is stable at room temperature, transforming into t-ZrO_2(II) at 1000–1200°C. Further transformation from t-ZrO_2 to c-ZrO_2 proceeds at 2300°C. The t-ZrO_2 phase is denser than m-ZrO_2 by approximately 4% due to its smaller unit cell dimensions [132,133]. The lattice parameters of t-ZrO_2 are very close to those of c-ZrO_2. Two additional high-pressure phases — the t-ZrO_2(IV) [134], and orthorhombic ZrO_2(V) [134,135] have been described as well.

A characteristic feature of zirconia is the possibility to stabilize large t- or c-ZrO_2 crystallites by using certain trivalent dopants (e.g. Y) for Zr^{4+} in the solubility limits [136], although the stabilization mechanism itself is not well understood [134,135]. The oxygen deficiency can be an important factor stabilizing t-(c-)ZrO_2 [137]. For comparison, alloying metal ions of valency higher than 4+ with ZrO_2 creates excess oxygens ending up at the ordered arrangement of ternary oxide such as $Ta_2Zr_8O_{21}$ [138], instead of t-ZrO_2.

The heterogeneous nucleation characteristic of the (ZrO_2) film growth [139] seems to be the easy way to initiate the formation of t-ZrO_2 in the vicinity of film-substrate interface rather independently of the growth method, temperature and substrate. Upon further growth, possible phase change into m-ZrO_2 is recognized as a nucleation controlled [139] and stress-assisted [140] displacive (martensitic) transformation process, induced by the lattice vibrations and the probability of finding oxygen atoms beyond some critical displacement value [141]. In this case, the average m-ZrO_2 particle size is expected to be comparable to or larger than that of t-ZrO_2. The martensitic transformation is not proceeding until full completion but to a certain extent depending on the temperature or the presence of extrinsic constraints [142] and, therefore, the t-ZrO_2 may not disappear completely.

The formation probability of t-ZrO_2 can be related to the process rate in the processes substantially differing in their nature. For instance, the long-term heating of disordered precursor in sol-gel process at relatively low temperatures may result in the high density of nuclei hindering the growth of stable crystals and enhancing the formation of nanosize t-ZrO_2 [143]. At higher heating rates, the crystal growth is faster compared to nucleation and, therefore, the stable polymorph m-ZrO_2 forms. Analogously to the ALE ZrO_2 process, more hydroxyls can be created in sol-gel process, in particular, by the rapid addition of excess H_2O to the $ZrCl_4$, followed by fast crystallization and preferred formation of m-ZrO_2 while slow precipitation and lower amount of OH-groups gives predominantly t-ZrO_2 [144]. Low processing rates, long heating periods and variable density of active radicals could be the universal factors favouring the (initial) formation of t-ZrO_2.

Little is reported on the formation of pure t-ZrO_2 in the thicker films. Undoped t(c)-ZrO_2 films can be grown, for instance, by MOCVD in the range of 390–700°C [145–147] preferably in a diffusion-controlled growth mode [146]. The undoped bulk t-ZrO_2 is usually stable until the size of crystallites exceeds 30 nm, approximately [143,148,149]. There is no strict correlation between the actual phase content and crystallite size as the further development of t-ZrO_2 is affected by chemical factors and the source of raw materials [144]. The size of m-ZrO_2 crystallites transformed from amorphous phase can be smaller than that of t-ZrO_2, because the smaller size and, consequently, larger number of embryonic parent nuclei is needed to transform a domain of critical size to t-ZrO_2 [150].

Properties

Stabilized t-ZrO_2 is a well-known ionic conductor [136] while the electronic conduction should dominate in undoped (m-)ZrO_2. Optical band-gap value of ZrO_2 is in the range between 5.0–5.85 eV [151]. ZrO_2 deposited at 450°C on Si possess relative permittivity of 19–22 [2,131], even together with a native SiO_2 layer. The permittivity of stabilized t-ZrO_2 is found to be higher than that of m-ZrO_2, ranging between 28 and 40 [132,152]. The breakdown field can reach 3 MV/cm [131]. Annealing can increase the breakdown resistance [131] and film density [2] but reduces the permittivity [131]. The defective nature of MOCVD ZrO_2 has still restricted its accommodation with DRAM technology [2].

AL-CVD of ZrO_2

The experiments on the ZrO_2 CVD via low temperature hydrolysis of $ZrCl_4$ in the temperature range 300–500°C are rare [153] and, apparently, not carried out below 300°C. The $ZrCl_4$ is a precursor prone to gas-phase reactions [145] and therefore particularly well-suited for the use in the AL-CVD process. Ritala *et al.* [19,154] have grown 100–210 nm thick ZrO_2 films by AL-CVD (ALE) from $ZrCl_4$ and H_2O on glass substrates at 500°C. In these films, the chlorine and

hydrogen content remained below 0.5 and 0.4 at %, respectively. The films were moderately crystallized but highly transparent with high refractive index of 2.2 at 580 nm. Strong agglomeration [73,154] and formation of t-ZrO_2 nanocrystallites [70,73] has been observed at the earliest stages of the growth on two-dimensional soda lime glass surface as well as on porous silica and alumina substrates. The agglomeration can be restricted by providing higher amount of OH-groups participating in surface reactions [155]. The calculated growth rate of ZrO_2, best fitted considering the hypotetical adsorption of only $ZrCl_2^{+2}$ species [26], is still 20% higher than the experimental result from the convenient process [154]. This has been tentatively explained by the random packing of adsorbed species [26], but can also indirectly refer to the deviations from the optimum coverage with OH-groups.

3.6.5. HfO_2

Application fields

HfO_2 thin films are used where good adhesion and stability, low intrinsic stress, negligible absortion and light scattering and controlled refractive index is needed. HfO_2 or HfO_2-based composites have been investigated for the use in optical multilayers [156], in TFEL systems [157,158] as well as for DRAM applications [2,100]. HfO_2 is still much less studied material than ZrO_2.

Growth and structure

HfO_2 and ZrO_2 are isomorphic oxides [159] with similar chemistries. However, the phase transition temperatures of HfO_2 are higher than those of ZrO_2. Undoped HfO_2 transforms from m-HfO_2 into t-HfO_2 phase at 1510–2000°C and from t-HfO_2 to c-HfO_2 at 2700°C [160]. The HfO_2 films deposited between 250 and 300°C can be rather disordered, crystallizing upon the post-deposition heat-treatment [2]. The high-temperature phases can be stabilized at room temperature by doping with rare-earth oxides [160]. Undoped metastable phases of HfO_2, however, cannot be obtained as easily as in case of ZrO_2. For example, Hf-containing acetate gels crystallized directly into the stable m-HfO_2 around 500–540°C, while the heating of Zr-containing gels first results in the formation of pure t-ZrO_2 and already at 450°C [161]. The critical crystallite size of HfO_2 for t→m transformation is between 4 and 10 nm which is a markedly lower range than that for ZrO_2 (15–30 nm) [162].

Properties

The optical band gap value of HfO_2 is about 5.3 eV [151]. The permittivity of evaporated HfO_2 films has been 18 (at 1 kHz) and the breakdown field was as high as 3.6 MV/cm [158]. Doping with 21–34 wt. % Nd_2O_3 has increased the permittivity and breakdown field in HfO_2 films up to 27 and 7.0 MV/cm [158], respectively. However, earlier reports on MOCVD HfO_2 films deposited at

250–300°C have described rather porous substance hardly acceptable as a capacitor material [2].

AL-CVD of HfO_2

HfO_2 films have been grown by AL-CVD from $HfCl_4$ and H_2O in the temperature range of 180–600°C [26, 61,100,163]. The growth rate decreases monotonously with the increase in the temperature [61,100] as the density and role of OH-groups assumptionally diminishes. The overall surface reaction at above 400°C should proceed, partially, via adsorption of $HfCl_4$ on the less active oxygen bridges, releasing less chlorine [61]. The proportional relationship between film thickness and the number of growth cycles was violated in case of the thinnest films studied (15 and 45 nm), growing with slightly lower rate [163]. Similarly to ZrO_2, the average growth rate of HfO_2, best fitted considering the hypotetical adsorption of only $HfCl_2^{+2}$ species [26], is still higher than the experimental result from the convenient process of thicker films [26, 163].

The 15–400 nm thick HfO_2 films grown at above 300°C [61,100,163] were essentially crystallized showing the most intense m-HfO_2 (200) and (020) reflections together with low intensity (–111) and (111) peaks. In the thinnest films, the intensity of the weak reflections of (111) t-HfO_2 was comparable to m-HfO_2 peaks [163]. In the HfO_2 films grown onto Si-substrates, the apparent reflections of the phase, metastable in the bulk form, were most easily attributed to the orthorhombic polymorph [61].

The chlorine content in the films grown at 225°C was 2.5 at. % [61], further diminishing below 1 at. % [61], even down to 0.2 at. % [100] at 500°C. The hydrogen content was less than 0.4 at. % [163] in the films grown at 500°C. The permittivity of the HfO_2 films grown at 500°C was 13–14 [100]. The refractive index was as high as 2.0 already in the films grown at 225°C, measured at 580 nm [61]. The leakage current through the Al/HfO_2/ITO capacitor structure was few $\mu A/cm^2$ at 1 MV/cm. The destructive breakdown took place at an unpredictable electric field value between 1.5–5 MV/cm [100].

3.7. Composite dielectrics: reference studies

Application fields

Composite dielectric films are investigated in order to find alternative electronic materials with substantially improved relative dielectric constant, leakage current density and charge storage capability. For instance, amorphous oxide films, such as Zr-Ti-Sr-O system deposited below 300°C [164] could be considered as alternatives challenging both Ta_2O_5 and ferroelectrics in developing memory devices. High power storage capacitors can also be prepared from the

$RuTaO_x$ or $MoTaO_x$ oxide systems [165]. However, advanced electrical properties are most often demonstrated by highly ordered powders typically processed at temperatures unsuitable for microelectronic applications. Amorphicity, texture and conformality requirements make the thin film technology essentially different from the powder technology putting challenges for finding appropriate low-temperature deposition technique for high permittivity composite films.

Powder composites

The behaviour of permittivity has been studied in Ta_2O_5 powders mixed, for instance, by TiO_2 [166], Al_2O_3 [167], Nb_2O_5 [168] or ZrO_2 [169]. The measurements have been carried out after firing the samples at temperatures 1300°C and higher. In the $(TiO_2)_x$-$(Ta_2O_5)_{1-x}$ samples, the permittivity reached 143 at x=0.08 while the permittivity of bulk Ta_2O_5 did not exceed 35 [166]. Moreover, in $(Nb_{1-x}Ta_x)_2O_5$ the permittivity reached the maximum value, 180, at x=0.15 [168]. For the rest of dopants, the increase in the dielectric constant has been rather moderate.

The relation between permittivity increment and structural changes is not clarified. Titanium demonstrates poor solubility in Ta_2O_5 matrix [170]. Only tantalum suboxide TaO_2 and rutile TiO_2 could form a continuous series of solid solutions [171]. Recent Raman and XRD investigations on $(TiO_2)_x$-$(Ta_2O_5)_{1-x}$ ceramics [172] allow one to rely on the periodical arrangement of TaO_n^{5-2n} or $Ta_6O_{12}^{+6}$ clusters and TiO_6 octahedra as a superstructure in case of TiO_2 contents below 13%. For the best match state (at x=0.08), the displacement of Ta ions and the net dipole polarization is enhanced due to the effect of Ti ions. In the $(Nb_{1-x}Ta_x)_2O_5$ samples of high temperature α-Nb_2O_5 structure, at the same time, the enhancement of permittivity was proposed to be a consequence of distortions of weakly ferroelectric Nb_2O_5 lattice with the Ta_2O_5 polyhedral structural units [168]. Due to the identical ionic radii and valences, Nb_2O_5 and Ta_2O_5 could form a continuous series of homogeneous solid solutions [173], viz. particular crystalline phase having variable composition. However, due to the mismatch between stable crystallographic forms, the actual solubility of Nb_2O_5 in Ta_2O_5 should be quite limited [174,175]. The permittivity increment in $(Nb_{1-x}Ta_x)_2O_5$ powders was observed below the Ta solubility limit x=0.25 [168] while the range strongly exceeding the limit has, apparently, not been studied.

Composite dielectric films

Fujikawa *et al.* [176,177] have noticed the enhanced permittivity in case of Nb_2O_5 addition to the Ta_2O_5 matrix while Al_2O_3 and SiO_2 were the additives effectively increasing breakdown field, supposedly due to the defect compensation in sputtered films [176]. Low leakage $(1-x)Ta_2O_5$-xAl_2O_3 (x=0.1) films have also been fabricated via metalorganic solution deposition and annealed on Si substrates at 750°C [178] where also the increase in the dielectric constant up to 42.8 has been achieved.

Probably the first Ta-Ti-O dielectric films were obtained by Umezawa *et al.* [179] at 200°C. The permittivity in these 20-150 nm thick sputtered films increased from 30 to 70 with the Ti content increased from 10 to 90%. The leakage current value was an intermediate between those characterizing pure Ta-O and Ti-O films. The films were amorphous in accord with XRD results but showed some ordering when studied by RHEED analysis. Recent investigations by Gan *et al.* [180] showed that in the amorphous $(TiO_2)_x$-$(Ta_2O_5)_{1-x}$ films the permittivity was the highest when x = 0.08, but not exceeding 30. After annealing and recrystallization at 800°C, the permittivity increased up to 55. Also the refractive index of Ta-Ti-O films increases above the value characteristic of Ta_2O_5 [181].

3.8. Dielectric multilayers: reference studies

Alternately assembled layers of two or more distinct compounds with adjustable one-dimensional periodicity can be termed as multilayers, whereas the term "nanolaminate" should specify the multilayers with the repeat distance in the superlattice dimensions between 2 and 20 nm. When growing nanostructures, one has to provide precise control over composition and dimensions of functional layers applying methods, such as Molecular Beam Epitaxy [182], allowing alternate dosing of film components. To keep sharp interfaces, the materials used in functional multilayers must also demonstrate high chemical inertness restricting spontaneous interface reactions and structure modifications. Structures with improved characteristics can be obtained by combining the best properties of single constituent layers. For example, in the TFEL Ta_2O_5-Al_2O_3 dielectrics, the low deposition rate and low permittivity of Al_2O_3 has been compensated by high growth rate and high permittivity of Ta_2O_5, while the good adhesion and high temperature stability of Al_2O_3, in turn, compensated the insufficient adhesion and lower temperature stability of Ta_2O_5 [183]. Another beneficial effect is coming from the lowered breakdown probability likely due to the breakdown channels broken at the interface between different materials [184].

The permittivity of binary oxides [108] or solution films [1,185] often decreases with the layer thickness. However, very thin superlattices of two distinct materials can possess effective permittivity comparable to that of the thick homogeneous mixture of the same materials [1,185]. The effect is explained by the influence of phase changes initiated by the increased lateral stress at the multilayer interfaces.

ZrO_2-based laminates have so far been of interest as hard protective coatings [186,187]. Partial stabilization of nondoped nanosize t-ZrO_2 between various ceramic layers — elastic constraints — is possible in sputtering process

[187,188]. To the best of my knowledge, possible application of (t-)ZrO_2 as a component of nanolaminates grown for electronic purposes has not been published, neither has ZrO_2 been used in Ta_2O_5-based multilayers.

Multilayers deposited by AL-CVD.
AL-CVD (ALE) is capable for precise adjustment of interlayer thickness, for instance, in Fabry-Perot filters consisting of Al_2O_3 and ZnS layers [189], or X-ray mirrors consisting of 1.6 nm thick Al_2O_3 and TiO_2 layers [190]. In dielectric films, the intermediate layers of alternative compound deposited into the host matrix inhibit rapid crystal growth and suppress concurrent interface roughening, reducing optical losses [191].

Regarding capacitor materials, the nanolaminates of thin HfO_2 or Al_2O_3 and Ta_2O_5 have been deposited [100,101,192,193] to combine the high permittivity and self-healing breakdown mechanism of Ta_2O_5 with lower leakage current of HfO_2 or Al_2O_3. These amorphous films consisted of 3 nm thick 4–34 double layers of Ta_2O_5 and another oxide. The thickness-independent permittivity of HfO_2-Ta_2O_5 laminates was 20–26 in the films deposited in the range of 300–400°C and did not show loss up to 1 Ghz of measurement frequency. The films did not show destructive breakdown below 4–5 MV/cm. The leakage currents were about 150nA/cm^2 at 1 MV/cm [192]. Moderate annealing temperatures did not affect the dielectric characteristics. The AL-CVD of these nanolaminates is already a CMOS compatible technology [193].

3.9. Nanocrystalline materials

General properties
Nanomaterials can be regarded as a special class of materials consisting of extremely small crystallites whose diameter range between 2 and 50 nm, having an appreciable fraction (20–50%) of their atoms residing in defect environments at the grain boundary or surface region [194]. Intrinsic strains but no dislocations are naturally present in such materials [194]. Controlled crystallite size is one of the fundamental issues in the field of nanostructured materials [195,196]. Appropriate scaling of the device dimensions relates the size effects to the dielectrical behaviour of the particular device.

Spatial confinement of charge carriers occurs in the crystallite when the Bohr radius of the first exciton becomes comparable or larger than the diminishing cluster radius, R [197]. Electronic eigenstates and phonons are localized within the nanocrystal owing to the sudden change in the potential arising from the Fermi level difference between grain bulk and disordered environment. According to Heisenberg uncertainty relation, the range of momentum is broadened due to the spatial confinement of electron position.

Hence, the energy will be determined dimensionally rather than by its chemical origin [195]. Electrons, when localized, loose their freedom which leads to further discretization of energy states. Well-defined states appear underneath the top of the valence and above the bottom of the conductance bands [197,198], decreasing the electron affinity [199]. The separation of these states — the effective band gap, E_g, — increases with the decrease in crystallite size [197,199] as follows:

$$E_g(R) = E_g(R_\infty) + (h\pi)^2(2R)^{-2}\,(1/m_e^{eff} + 1/m_h^{eff}) - 1.8e^2/(\varepsilon R),$$

where $E_g(R)$ denotes the first excitonic state of a cluster with radius R. The second term corresponds to the confinement energies for the electron and hole with effective masses m_e^{eff} and m_h^{eff}, respectively, shifting $E_g(R)$ to higher energy. The last term is the Coulomb interaction energy which, in turn, shifts $E_g(R)$ toward the lower values significantly below the cluster diameter of 15 Å, together with the decrease in permittivity [200].

In addition, the ionization energy of (shallow) impurities given by the Rydberg constant corrected for the carrier effective mass and permittivity:

$$E_I = 0.5(4\pi\varepsilon)^{-2}e^4m^{eff}h^{-2},$$

cannot usually be applied to impurities in a quantum wells but quantum well potential is to be considered in addition to the Coulomb potential [201]. Therefore, also the impurity activation energy could be higher when compared to the large polycrystalline samples.

Quantum confinement increases the band gap, for instance, in nanosize TiO_2 particles [202] or in a number of semiconductors, inducing blue-shift in their absorption spectra [197,199]. The increase in experimental permittivity value has also been observed in some nanocrystalline materials [203–205]. The changes in permittivity, though, arise most likely from the polarizability and space charge changes due to the larger contribution of grain boundaries. At the same time, the enlarged bandgap and ionization energy together with grain boundary barriers could contribute to the lower electronic conductivity expected in nanocrystalline materials.

Relationship between size and structure

At low growth temperatures, the diffusion and bilateral growth is kinetically limited and nonequilibrium structures can be nucleated [206,207]. An additional stress caused by excess surface energy acts along the boundary of forming crystallite [149,208]. The excess energy arises due to the unsaturated coordination value of the surface atoms owing to their broken bonds. In the nuclei or nanocrystallite of the particular compound, the Gibbs free energy, ΔG_{nano}, is higher owing to the contribution of the positive surface energy:

$$\Delta G_{nano} = \Delta G^{o} + 4\pi r^{2}\gamma_{surf},$$

where $\Delta G^{o} < 0$ is the free energy of the monocrystal and $\gamma_{surf} > 0$ is the specific free energy of of the surface. The polymorph which crystallizes first instead of the lowest free energy structure, is likely that offering greater freedom for cation placement as well as higher probability of oxygen vacancies. Further growth can proceed via partial or complete transformation into more stable phase. It is not exactly known whether nanocrystals change phase by a simultaneous coherent deformation of all unit cells, or the deformation occurs locally and propagates afterwards across the nanocrystal [199,209,210].

In CVD, the shift in the reaction equilibrium towards the sublimation or formation of gaseous products is stronger the smaller is the crystallite size and absolute value of Gibbs free energy of the product [198]. Thus, larger crystallites tend to grow on the expense of smaller ones. Therefore, preparation of fine-grained samples should be easier the lower is the growth temperature.

Case study: nanophase ZrO_2

The formation of fine-grained t-ZrO_2 is determined by the layer thickness rather than by the substrate material and growth conditions. The main factor stabilizing t(c)-ZrO_2 crystallite has to be its lower surface energy compared to the m-ZrO_2 of the same size [211]. In addition, the (PVD) growth of c-ZrO_2 on sapphire [212] could be supported also by the relatively small lattice misfit but the c-ZrO_2 was stable until the film thickness exceeded 40 nm. Also the fourfold increase in the sputtering (film growth) rate resulted in the preferred growth of m-ZrO_2 instead of c-ZrO_2 already at the initial stage of growth [212]. Besides size factors, the formation of nanocrystalline m-ZrO_2 is thus controlled by the reduced migration time and mobility of species adsorbed, putting kinetic limitations to the achievement of the lowest energy configuration [212], which in ultrathin films is t-ZrO_2. Thus, the t-ZrO_2 is actually the stable phase in ultrathin layers instead of m-ZrO_2.

In the sputtered (t-)ZrO_2-Al_2O_3 nanolaminates [188], the additional m-ZrO_2 appeared and its contribution started to increase when the ZrO_2 layers grew thicker than 5 nm. The general relation of Gibbs free energy for a hemispherical cap crystallite forming on a substrate could be accommodated [188]:

$$\Delta G = (2\pi/3)r^{3}\Delta g + 2\pi r^{2}\Delta\gamma_{fv},$$

where g is the volume free energy associated with a particular polymorph and γ_{fv} is the surface energy of the film-vapor interface. In multilayers, the supplementary solid-solid interface stress factor [213] should be considered as well. Equalizing the free energy change upon transformation to zero in equilibrium [149,188], one gets an expression for the critical radius, r_c, initiating the transformation [188]:

$$r_c = 3.79[1-(T/1448\ K)^{-1}]\ nm.$$

According to this relation, the critical grain diameter for t→m transformation increases, rather moderately, from 5.8 to 6.5 nm with growth temperature from 230 to 350°C. Although the absolute diameter eventually varies upon growth method or substrate, one can rely on the reproducible fabrication and size adjustment of nanocrystallites in a considerably wide temperature range, especially in the superlattices with certain repeat distance.

When using $ZrCl_4/H_2O$ precursor system in the present study, the relative density of active OH-groups, created after water exposure, should be decreased below the maximum coverage by the elevated substrate temperatures rather than determined by the underlying oxide surface sites. Epitaxial growth is inhibited already due to the surface heterogeneity and the thermodynamics allow easy formation of t-ZrO_2 nanocrystallites.

Once stabilized, the t-ZrO_2 crystallites might show advanced dielectric properties. Due to the smaller unit cell volume, V, and higher polarizability, α, of t-ZrO_2 [132], the increase in permittivity should be observed already in accord with the Clausius-Mosotti equation:

$$\varepsilon\text{-}1/(\varepsilon+2) = \alpha/(3V\varepsilon_0).$$

The fine-grained ZrO_2 has been of interest as a component of superhard coatings [148,186,187] rather than the electronic material. Nonetheless, it is known that the dopant-stabilized nanocrystalline ZrO_2 is a material with particularly high diffusivity and ionic conductivity [214]. In the non-doped nanocrystalline materials as in the present study, the electronic conduction is probably the dominant mechanism, being largely determined by the band structure and potential barriers at grain boundaries or interfaces.

3.10. Electrical characterization of thin films

Permittivity

The performance of a given material can be evaluated by measuring the basic dielectric properties of capacitor structures with small aspect ratio [215] consisting of the film of particular material between the underlying (e.g. sputtered indium-tin-oxide, ITO) electrode and top counterelectrode (e.g. evaporated Al). The effective permittivity, ε, can then be calculated from the capacitance, C, measured at certain frequency (e.g. 10 kHz) in accord with the simple electrostatics of parallel-plate capacitor, assuming uniform charge density and neglecting possible edge effects:

$$C = \varepsilon\varepsilon_0 S/d\ ,$$

where S is the effective electrode area, d is the thickness of insulator layer, ε is the dielectric permittivity of the material and ε_0 is the dielectric constant of free space.

In simple dielectric materials, e.g. Si_3N_4 and SiO_2, the bandgap is inversely proportional to the square root of the dielectric permittivity [216]. Also in (transition) metal oxides the energy of polarization is lower the higher is the permittivity while the electronic polarization reduces the electron ionization/ exitation energy and decreases the band-gap [217].

In the frequency range of 1 kHz – 10 Mhz, the relation between polarizability and the real part of the dielectric constant, ε, for binary and composite oxides follows the Clausius-Mosotti equation [218]. For composite materials consisting of randomly distributed regions of pure constituent phases, the permittivity can be calculated in accord with the effective medium approximation [219] and remains between the permittivity values of pure constituents [220]. For a number of ternary compounds or solid solutions such as $Zr_{0.92}Y_{0.08}O_{1.96}$, the polarizability can be calculated using the oxide additivity rule [152,218]. In these composites the permittivity value may exceed that of its constituents [152]. However, the additivity rule cannot be applied in $(Nb_{1-x}Ta_x)_2O_5$ solid solutions [168]. Moreover, thin films can consist of different phases (e.g. m-ZrO_2 and t-ZrO_2), remain amorphous or show distorted structure in relation to the bulk crystalline samples. In practice, it remains unclear which phase exactly is that describing the local order in the film bulk.

Pre-breakdown leakage currents in thin films

Charge transport in dielectrics is limited due to their large band gaps [104,221]. The charge carriers can be trapped either at stable (impurity) defects or at neutral interatomic sites [222]. Large currents are correlated with some critical detrapping fields, degrading the capacitor material and inducing dielectric breakdown [222]. Ohm's law is still observed at relatively low electric fields where injection of excess carriers and/or excitation of trapped charges is negligible. The conduction current, I, and external electric field, E, are then related as follows:

$$I \sim E \cdot \exp(-\Delta E_{ae}/kT),$$

where ΔE_{ae} is a thermal activation energy of electrons. Along with the increase in external field strength, the leakage currents exit ohmic region and increase rapidly with voltage. The rapid increase in the current density is often treated as an indication of (di)electric breakdown [223,224]. In the large band gap materials such as Ta_2O_5, Al_2O_3 or SiO, the existence of donor/acceptor centers is necessary to get detectable currents [224] while the trapping builds up some critical space sharge concentration and the field-enhanced detrapping initiates

the breakdown [222, 225]. The existence of impurity levels is actually the intrinsic property of real insulators [224,225] also determining the leakage characteristics in Ta_2O_5 [29]. However, the lowest leakage currents have generally been obtained in non-crystalline Ta_2O_5 [104] influenced by both lower dielectric permittivity and higher density of deep traps. The nonohmic conduction, sometimes denoted as simple exponential law [226], is already dependent on the permittivity as follows [221]:

$$I = \text{const} \cdot \exp[E\varepsilon\varepsilon_0/(eN_tkTd)]$$

where e is the electronic charge, N_t is the trap density and d is the insulator layer thickness. In practice, high dielectric constant when achieved at the expense of resistance still allows the use of reduced field strength for charge storage and so the high degrading currents are not that critical [104,221].

At even higher fields of several MV/cm or in the films thicker than 10–50 nm, the $I \sim E \times \exp(E^{1/2})$ dependence is generally dominant, instead of bulk tunnelling or Schottky injection mechanisms expressed by the $I \sim E^2 \times \exp(E^{1/2})$ and $I \sim \exp(E^{1/2})$ dependences, respectively [122,226,227]. In thicker films and high fields, one can account for the Frenkel-Poole conduction due to the field-enhanced thermal excitation of trapped electrons into the conduction band. The leakage current and electric field applied are related as follows [221,224,228]:

$$I = e\mu N_c(N_d/N_t)^{1/2}E \cdot \exp\left[(e^{3/2}\varepsilon^{-1/2}E^{1/2} - e(\Phi_d + \Phi_t))/2kT\right],$$

where μ is the carrier mobility, N_c is the carrier density, N_d is the donor density, N_t is the density of traps, Φ_d and Φ_t are the potential barriers for the excitation of donors and traps, respectively. The equation holds regardless of the absolute and relative amounts of defect levels. After the excitation/ionization of an atom in the bulk film, the electron moves freely in the medium consisting of neutral polarized atoms. The polarization screens the field of the positive ion created after removal of excited electron. Thus the excitation energy is decreased ε times from the value without screening effect.

In the (Ta_2O_5) films thicker than 50–100 nm, the pre-breakdown current is rather insensitive to the oxide thickness, voltage applied and the electrode material [229]. The determination of carrier and trap densities as well as the detailed study of the conduction mechanism remains beyond the scope of the present study. The attention has been paid on the composition-dependent shifts in the onset of high-field pre-breakdown region of the current vs voltage curves. The increment in the critical pre-breakdown field depends on the chemical quality and related physical breakdown resistance of insulator material. In special cases, e.g. in TFEL devices, the breakdown resistance at high fields of several MV/cm is particularly important because electroluminescence is a high field process and the brightness and aging of pixels is dependent on the charge

density — amount of trapping centers — especially in the vicinity of insulator/ phosphor interface [230].

Charge storage capability

The charge storage factor, Q, can be used as a figure of merit for the evaluation of different dielectric materials providing combined information about the capacitance density and the maximum working voltage [108,164,176]:

$$Q = U_{cr}\, C/S = \varepsilon_0\, \varepsilon\, E_{cr}\,,$$

where C is the capacitance measured, S is the electrode area, U_{cr} and E_{cr} are defined as the arbitrary critical voltage and electric field, inducing some conventional pre-breakdown leakage current density, e.g. 1 $\mu A/cm^2$ in this study. The Q-value can be used in the experimental series consisting of similar capacitors, when evaluating comparatively the changes in the nature of dielectric material.

4. EXPERIMENTAL TECHNIQUES

The Ta_2O_5 thin films were partially grown at the University of Tartu using the hot-wall flow-type ALE reactor equipped with quartz crystal microbalances (QCM) for the real time studies [I,II,IV]. Otherwise the metal oxides and their composites were deposited using a commercial F-120 reactor (by Microchemistry Ltd.) at the University of Helsinki [III,V–IX] applying constant precursor flow rates and water dosing. The films were not heat-treated after deposition.

The thickness and optical characteristics of the films have been analysed using optical transmission spectroscopy [I–IX] and optical absorption spectroscopy [I]. Computer-aided thermodynamical calculations have been carried out by using *HSC Chemistry for Windows* software at the University of Helsinki [II].

The electrical properties of the films grown have been measured using HP4275A LCR meter and HP4140B d.c.-source at Planar International Ltd. [VI–IX] or HP4192A impedance analyzer and HP4142B d.c. source at the Technical Research Centre of Finland [III]. The permittivity was measured at 10 kHz. The measurements were carried out at room temperature.

The structure and morphology of the films have been examined by the scanning electron microscope (SEM) and reflection high-energy electron diffraction (RHEED) at the University of Tartu [I,II], and SEM or X-ray diffraction (XRD) analysis carried out at the University of Helsinki [I,VII–IX].

Film composition has been analysed using energy-dispersive X-ray spectrometry (EDX) [IX], time-of-flight elastic recoil detection analysis (TOF-ERDA) [VI], (Rutherford) backscattering analysis (RBS) [III,V] and nuclear reaction analysis (NRA) [III] at the University of Helsinki; X-ray photoelectron spectroscopy (XPS) [III] at Helsinki University of Technology; electron-probe microanalysis (EPMA) and Auger' electron spectroscopy (AES) at the University of Tartu [I].

5. EXPERIMENTAL RESULTS

5.1. Ta_2O_5 growth from $TaCl_5$ and H_2O

Growth mechanism

The self-controlled $TaCl_5$ adsorption, expressed by the stabilization of the QCM output level [Fig. 2 in II], was achieved in the approximate temperature range 200–275°C [I,II]. Although the self-limiting adsorption mechanism can be realized, there is no true AL-CVD temperature window but the growth rate decreases monotonously with increasing temperature [Fig. 3 in II], rather similarly to other metal oxides grown from chloride precursors [34,61]. This is most probably related to the gradually decreasing density of the most active functional groups — hydroxyls. The intermediate formation and contribution of OH-groups is based on the reaction of $TaCl_5$ in the first step of AL-CVD cycle [II]:

$$n(\text{-OH})(s) + TaCl_5\,(g) \rightarrow (\text{-O-})_nTaCl_{5-n}\,(s) + nHCl(g).$$

In the second molecular layering step of AL-CVD cycle, the exposure of chlorinated oxide surface to H_2O results in the recreation of surface OH-groups:

$$(\text{-Cl})(s) + H_2O(g) \rightarrow (\text{-OH})(s) + HCl(g),$$

or bridging oxygen, created instantly or after dehydroxylation:

$$2(\text{-Cl})(s) + H_2O(g) \rightarrow (>O)(s) + 2HCl(g).$$

The conversion of OH-groups to the less reactive oxygen bridges requires certain activation energy [231] and takes place preferably at higher temperatures. In AL-CVD, this results in the decrease in the film growth rate. In addition, the byproduct, HCl, is likely to form supplementary adsorption wave [8,232] moving in front of $TaCl_5$ pulse. The secondary reaction between HCl and OH-groups [40,73,232,233] could result in the partial blocking of the most active surface sites by chlorine, limiting the adsorption of metal chloride [232] and possibly decreasing the observed growth rate towards the trailing edge of substrate [42].

The etching process expressed as a continuous mass decrease detected by the QCM at above 275°C [42,II] is probably a consequence of the release of oxychlorides:

$$3TaCl_5(g) + Ta_2O_5(s) \rightarrow 5TaOCl_3(g).$$

At temperatures above the etching threshold, uniform Ta_2O_5 films can be grown only after balancing the etching and blocking effects by appropriate choice of exposure and purge times.

Although no equilibrium is attained in the flow-type reactor, the free energy of the net reaction can be calculated [39] to evaluate the most facile reaction pathways. The calculated equilibrium amount of gaseous $TaOCl_3$ increases with growth temperature and exceeds the amount of alternative, solid $TaOCl_3$ at 275°C [II], which coincides with the onset of etching experimentally detected by means of QCM. The alternative etching product, TaO_2Cl, is not stable at these temperatures and should decompose if formed. The oxychlorides of tantalum might be formed first as intermediates bound to the surface. QCM studies allowed one to decide on the decrease of Cl/O ratio in intermediate surface species, created after $TaCl_5$ pulse, along with the increase in growth temperature [II]. Rather abrupt decrement in the Cl/O ratio was observed between 250 and 300°C, referring to the desorption of volatile chlorine-containing species exhausted in the etching process from the vicinity of the surface.

Composition and structure

Featureless growth of transparent Ta_2O_5 took place in the temperature range of 80–300°C [I]. The oxygen deficiency was detected by EPMA in the films regardless of the growth temperature. The residual chlorine content, 1% at 160°C, vanished down to the virtually undetectable amounts at 400 and 500°C [I]. The crystallization is obviously initiated at 300°C where the first oval crystallites giving tetragonal TaO_2 and hexagonal δ-Ta_2O_5 reflections appeared [I], as detected by RHEED and XRD, respectively. The TaO_2 predominantly exists on the surface formed at 400°C [I], not at 500°C. The crystallization intensity somewhat increases with the H_2O flow. The films possessed δ-Ta_2O_5 stucture with pronounced (100) orientation [I].

The stability of Ta_2O_5 against reducing agents is known [171]. It is likely that the AL-CVD-grown suboxide is rather a product of surface reactions with low-coordinated intermediates. Layered oxides with polar (preferably oxygen- or metal-terminated) surfaces can be reduced rather easily due to the non-completed coordination sphere of terminal metal atoms [234]. One can suggest, that layer-by-layer growth conditions fulfilled by AL-CVD growth mode might cause an "intrinsic" tendency for the easy modification of coordination numbers in the surface reactions. Thus, the reduction of the Ta oxidation state proposed might actually be the stabilization of low-coordinated inclusions or even Ta interstitials. The stabilization of lower oxides occurs during the water exposure after the partial destruction of Ta coordination sphere by the etching influence of $TaCl_5$. The TaO_2 is always regarded as a supplementary phase in addition to Ta_2O_5. It is, however, to be kept in mind that the TaO_2 structure was detected only at the surface. It is possible that the stoichiometric deviations in the film bulk may be partially due to the oxychloride residues.

Properties

The refractive index increased from 1.97 to 2.20 with the increase in growth temperature from 80 to 300°C. The optical absorption in the amorphous films was much lower than in the polycrystalline films [I]. The optical band-gap, E_g, in the amorphous films was close to 4.2 eV [I]. For polycrystalline films grown at 400 and 500°C, two regions of steep increase in absorption vs. wavelength curves were observed for both temperatures, giving two distinct values of E_g: 3.9 and 4.5 eV [I]. These values correspond to those reported for Ta suboxides and Ta_2O_5, respectively [235] while the lower absorption edge is to be attributed to the intrinsic properties of the TaO_2 phase.

The permittivity of the films grown at 250–325°C was 25–27 [236]. The leakage current density was about 1×10^{-6} and 5×10^{-5} A/cm^2 measured at 0.35 MV/cm in the films grown at 300 and 325°C, respectively [236].

The suboxide growth increases the optical and structural instability. It could also be considered as a potentially detrimental factor in Si-based capacitor structures causing lower effective permittivity.

5.2. Ta_2O_5 grown from $Ta(OC_2H_5)_5$ and H_2O

Growth mechanism

The self-controlled $Ta(OC_2H_5)_5$ adsorption was achieved in the temperature range 150–275°C [III]. The two-step molecular layering reactions proceeding via intermediate formation of surface hydroxyls and their exchange reactions with $Ta(OC_2H_5)_5$ can be written [IV]:

$$n(\text{-OH}) + Ta(OC_2H_5)_5 \rightarrow (\text{-O-})_nTa(OC_2H_5)_{5-n} + nC_2H_5OH,$$

$$(\text{-O-})_nTa(OC_2H_5)_{5-n} + (5\text{-}n)H_2O \rightarrow (\text{-O-})_nTa(OH)_{5-n} + (5\text{-}n)C_2H_5OH,$$

The desorption of $Ta(OC_2H_5)_5$ was not observed [III,IV]. The partial dehydroxylation of the surface is a thermally enhanced process which is likely responsible for the reduction of growth rate above 230°C. At the same time, thermal decomposition of $Ta(OC_2H_5)_5$ above 275°C [IV] acted as a process counteracting with dehydroxylation. In case of relatively long $Ta(OC_2H_5)_5$ pulse and purge times, the decomposition mechanism overwhelms the mass load and the growth rate increased monotonously with growth temperature [IV]. In case of the long purge times applied before the shortest possible $Ta(OC_2H_5)_5$ pulse, the dehydroxylation was more pronounced manifesting itself as a local minimum of the growth rate vs. temperature curve, at about 275°C [III].

In case of short $Ta(OC_2H_5)_5$ pulses, the surface mass exchange ratio $\Delta m_0/\Delta m_1$ decreased with increasing substrate temperature [IV]. In case of $Ta(OC_2H_5)_5$

pulse lengths 6.0 s and longer, the mass exchange ratio increased with increasing substrate temperature. The accessible OH-groups become exhausted before the maximum coverage is achieved in $Ta(OC_2H_5)_5$ adsorption process. This could reduce the sticking probability of $Ta(OC_2H_5)_5$ molecules lowering the related growth rate [IV].

The sticking coefficient values 0.004 and 0.035 were calculated at 250°C for $Ta(OC_2H_5)_5$ [IV] and $TaCl_5$ [237], respectively, indicating the lower rate for ethoxide adsorption. The low sticking coefficient is still advantageous, considering the resulting higher degree of conformality in three-dimensional, trenched substrate systems [238].

Properties

The films were amorphous exhibiting very flat and smooth surface [III]. The thickness decreased slightly and linearly with the distance from the leading edge of the substrate. The composition of films grown at 250 and 325°C was $Ta_{2\pm0.2}O_{5\pm0.2}$ and $Ta_{2\pm0.1}O_{5\pm0.1}$, respectively [III]. The carbon contamination was considerable only at the surface layer [III]. The average hydrogen content was 4 at. % and 0.6 at. % in the films grown at 250 and 325°C, respectively, still being the highest at the surface.

The permittivity was 23 and 25 in the films grown at 250 and 325°C, respectively. The respective leakage current densities were 3×10^{-4} and 7×10^{-5} mA/cm^2 at 0.35 MV/cm. As demonstrated by the nearly linear part of the log I/E vs $E^{1/2}$ curves (Fig. 2), the Poole-Frenkel conduction mechanism can be considered in the dielectric films studied.

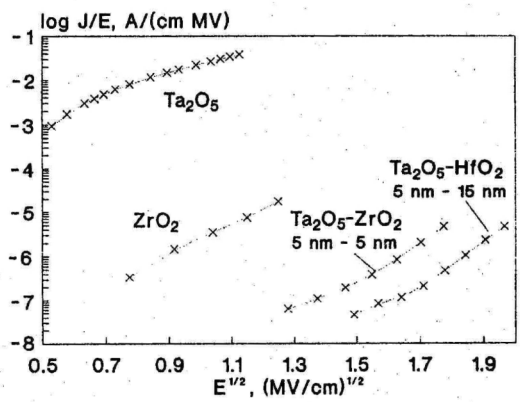

Figure 2. Log I/E vs $E^{1/2}$ curves of selected binary oxides and nanolaminates.

It is also noteworthy that the amorphous films grown from $Ta(OC_2H_5)_5$ did not exhibit structural and morphological dependence on the substrate material, while the films grown from $TaCl_5$ crystallized on ITO surface and showed enhanced thickness profile and haziness on soda lime glass, compared to the

films grown onto Corning 7059 glass substrate. Although the dielectric properties were quite similar, the structural stability and assumptionally higher stoichiometric homogeneity make the $Ta(OC_2H_5)_5$ more promising precursor also for AL-CVD.

5.3. Nb_2O_5 films

Nb_2O_5 thin films have been successfully grown from $Nb(OC_2H_5)_5$ and H_2O in the temperature range of 230–350°C [V]. The behaviour of the growth rate of Nb_2O_5 films vs temperature was analogous to that of Ta_2O_5 grown from $Ta(OC_2H_5)_5$, exhibiting a local minimum at about 265–280°C. Below 275°C, approximately, the film thickness tended to decrease linearly along the gas flow direction, analogously to Ta_2O_5. At 250°C, the growth rate of Nb_2O_5 films was about 25% lower than that of Ta_2O_5. Between 215 and 275°C, very flat films with weak thickness deviations about 1–2% could be achieved. Differently from Ta_2O_5, the Nb_2O_5 films deposited at 270°C and higher possessed inverted thickness profile. The films deposited at 275°C and higher were clearly thicker at the trailing edge of the substrate.

The films were amorphous, transparent, exhibited flat and smooth surface and possessed high refractive index close to 2.40 when deposited above 230°C. No heavy contaminants were detected in the film bulk. The Nb to O contents in the films deposited at 325°C corresponded to that in Nb_2O_5 in the accuracy limits of the backscattering analysis. Nb_2O_5 films crystallized when grown directly on the polycrystalline ITO surface showing XRD reflection peak of monoclinic (040) orientation. These films were too leaky for reliable capacitance measurements.

5.4. Al_2O_3 films

Amorphous Al_2O_3 films grown from $AlCl_3$, $Al(CH_3)_3$ or $Al(CH_3)_2Cl$ and H_2O exhibited pre-breakdown leakage current density values 6×10^{-7}, 2.5×10^{-7}, and 7.5×10^{-8} A/cm^2, respectively, at 2 MV/cm [VI, VII]. The permittivity and refractive index were not influenced by the precursor chosen but were dependent on the substrate temperature. The charge storage factor of Al_2O_3 films was 16 nC/mm^2, already twice of that in Ta_2O_5.

Carbon content in the films grown using $Al(CH_3)_2Cl$ was below 2 at. % already in the films grown at 95°C. The chlorine content in these films was 6.5 at. %. The films grown at low temperatures contained large amount of residual hydrogen, reaching 12 at. % already at 200°C. The hydrogen, chlorine

and carbon contents decreased rapidly with the increase in growth temperature down to 2, 0.5 and 0.1 at. % at 300°C, and further below 0.1 at. % at 400°C.

The refractive index increased from 1.64 to 1.68 with the temperature increasing from 200 to 500°C while the permittivity increased, respectively, from 7.5 to 8.7 [VI]. At the same time, the onset field of pre-breakdown conduction regime increased with the decrease in the deposition temperature until 200°C. Probably, the permittivity effect to the Poole-Frenkel potential barrier governs the conduction which otherwise should be higher in the more contaminated films. Considerably larger band-gap ascribed to Al_2O_3 and the lowest permittivity measured still makes this material the least leaky one among binary metal oxide dielectrics.

5.5. Al_2O_3-Ta_2O_5 nanolaminates

Al_2O_3-Ta_2O_5 nanolaminates were grown using the liquid precursors $Ta(OC_2H_5)_5$ and $Al(CH_3)_3$ [VII] and were arranged as 8 successively deposited Al_2O_3 and Ta_2O_5 double layers. The nominal repeat distance was 20 nm, while the thickness of one binary oxide layer was varied between 5 and 15 nm.

The Al_2O_3-Ta_2O_5 nanolaminates did not exhibit resistance improved in comparison to the Al_2O_3 films. The permittivity and refractive index decreased with the increase in the Al_2O_3 contribution but remained higher than that of Al_2O_3. Therefore, considering their low conductivity, the charge storage factor of Al_2O_3-Ta_2O_5 nanolaminates was increased in relation to their constituent oxides reaching 30 nC/mm^2 [VII] and showed, in this respect, already improved dielectric performance.

5.6. HfO_2 films

The 160 nm thick HfO_2 films grown in accord with the recipe established [163] were polycrystalline consisting mainly of m-HfO_2 [VIII] with trace t-HfO_2 (Fig. 3, 4). The (200), (020) and (002) reflections of the m-HfO_2 were the most intense ones (Fig. 3). A 10 nm thick amorphous Ta_2O_5 buffer layer, deposited between glass substrate and the HfO_2 film, obviously had a detrimental effect on the crystal growth [VIII]. At the same time, the m-HfO_2 crystallite growth was enhanced remarkably by polycrystalline ITO underlayer (Fig. 3). The crystallization affected by ITO could be suppressed by depositing thin Ta_2O_5 layer between ITO and HfO_2 (Fig. 3). The film structure was obviously profiled throughout the film depth, as confirmed by grazing-incidence X-ray diffraction (GID) measurements (Fig. 5). Obviously, the growth starts with the formation

of t-HfO_2 nanocrystallites and continues with preferential m-HfO_2 growth. At low incidence angles, the (111) t-HfO_2 peak disappears while the m-HfO_2 reflections remain.

The permittivity of polycrystalline HfO_2 films deposited between ITO and Al electrodes was typically 16. The leakage currents in polycrystalline HfO_2 films were several orders of magnitude lower than in Ta_2O_5. On the other hand, the breakdown resistance in the HfO_2 films was inferior to that of Ta_2O_5. The charge storage factor of HfO_2 capacitors was 8 nC/mm^2, similarly to Ta_2O_5 [VIII].

5.7. HfO_2-Ta_2O_5 nanolaminates

HfO_2-Ta_2O_5 nanolaminates were grown at 325°C [VIII]. The nominal thickness of HfO_2 interlayers was varied between 2.5 and 20 nm. The (–111) and (111) reflections of m-HfO_2 and concurrent t-HfO_2 (111) peak of comparable intensity appeared immediately when the HfO_2 interlayer thickness exceeded 5 nm. The (200) and (020) reflections of m-HfO_2 did not appear in the nanolaminates (Fig. 4). The relative crystallite size increased with nominal HfO_2 layer thickness [VIII] stabilizing at around 15 nm (Fig. 6a). Most likely, the total amount of HfO_2 nanocrystallites and, therefore, the amount of grain boundaries somewhat increases with HfO_2 layer thickness.

The permittivity value decreased monotonously with the increase in the HfO_2 layer thickness from that of pure Ta_2O_5 (25) to that of the pure HfO_2 (16) [VIII]. The breakdown resistance was much higher than in Ta_2O_5 films (Fig. 2). The breakdown resistance increased monotonously with the increase in the HfO_2 thickness from 2.5 nm up to 13–15 nm [VIII]. Further increase in the thickness was no more beneficial because of the increased breakdown probability.

5.8. ZrO_2 films

ZrO_2 films were obtained by using the well-established AL-CVD (ALE) process [154] at 230 [IX], 275 [IX] and 325°C [VII, IX]. All the films were polycrystalline containing predominantly m-ZrO_2 (Fig. 4) with trace inclusions of t-ZrO_2. In fact, there is an overlap between the m-ZrO_2 (020) and (200) and t-ZrO_2 (002) and (020) peaks, making the phase determination somewhat ambiguous. However, there is only minor discrepancy in the unit cell dimensions between HfO_2 and ZrO_2 [133,159] while the d-values corresponding to the (200), (020) and (002) reflections of m-HfO_2 (Fig. 4) [VII] have been clearly distinguished from those of t-HfO_2. Based on the analogy with HfO_2, only the XRD peak appearing at 30.3° is to be assigned as t-ZrO_2, while other peaks of

even higher intensity are regarded as the reflections of m-ZrO_2. Similarly to HfO_2, the growth of ZrO_2 starts with the formation of t-ZrO_2 crystallites (Fig. 5) detectable only closer to the film-substrate interface, i.e. at higher incidence angles in the GID measurements. Analogously to the HfO_2, the amorphous Ta_2O_5 underlayer obviously decreased the intensity of the m-ZrO_2 XRD peaks [VII].

The permittivity of ZrO_2 films approached 20. The leakage currents in ZrO_2 films were several orders of magnitude lower than in Ta_2O_5 (Fig. 2) and even lower than in HfO_2. The breakdown in the ZrO_2 films occurred at fields comparable to those in HfO_2. The charge storage factor of ZrO_2 capacitors was 19 nC/mm^2 which is a markedly higher value than those of Ta_2O_5 and HfO_2.

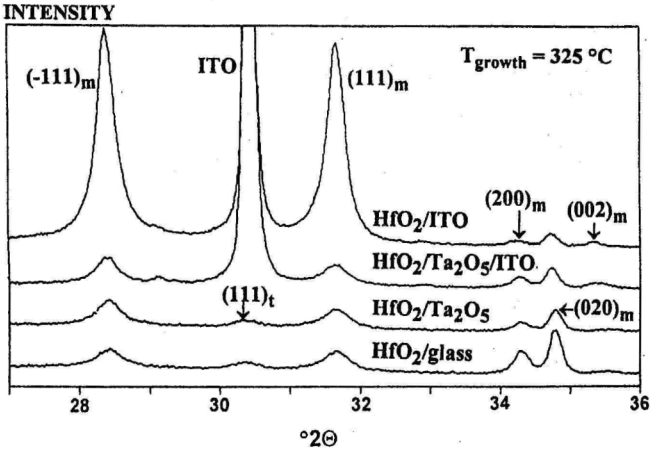

Figure 3. X-ray diffractograms of ca. 160 nm thick HfO_2 films deposited on substrates of different materials.

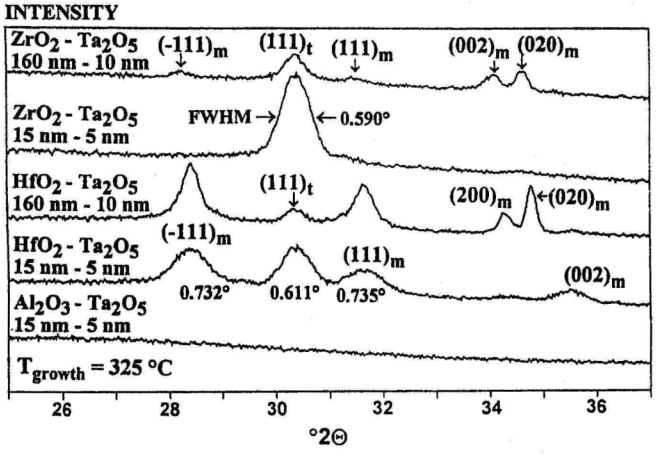

Figure 4. Typical X-ray diffractograms of ca. 160 nm thick Al_2O_3, HfO_2 and ZrO_2 films deposited on Ta_2O_5 underlayer and of Ta_2O_5-based nanolaminates.

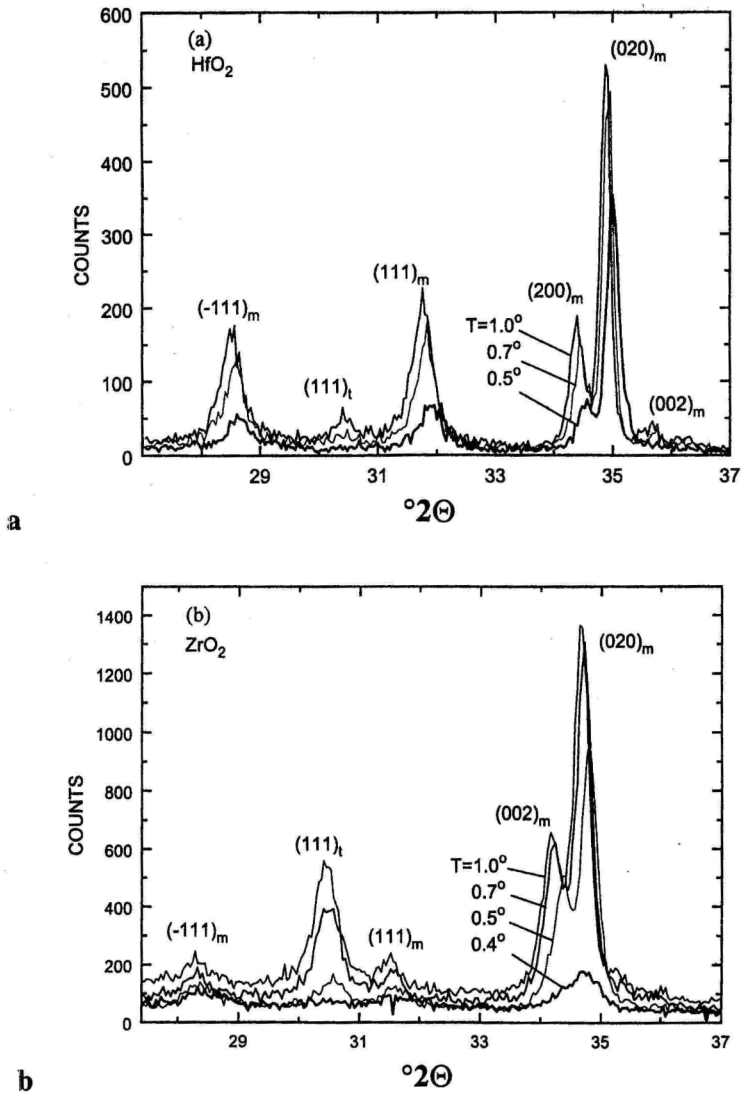

Figure 5. GID patterns of 160 nm thick HfO_2, (a), and ca. 120 nm thick ZrO_2, (b), films grown at 325°C. The information depth was lower than 100 nm for incidence angle, T, values of 0.4 and 0.5°. (The measurements have been performed by M. Schuisky at The Ångström Laboratory, Uppsala University)

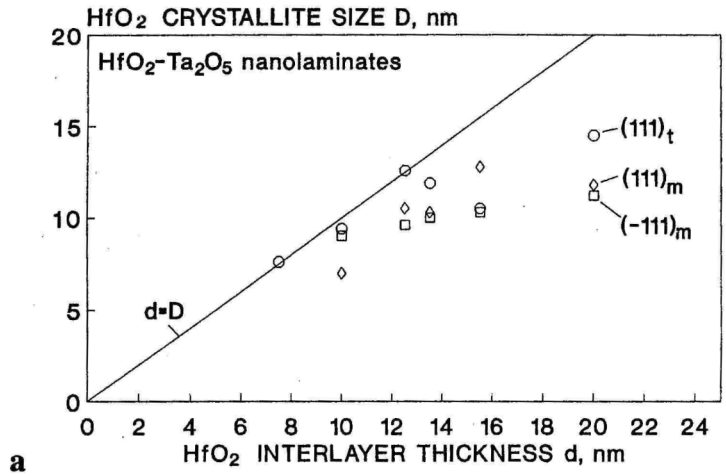

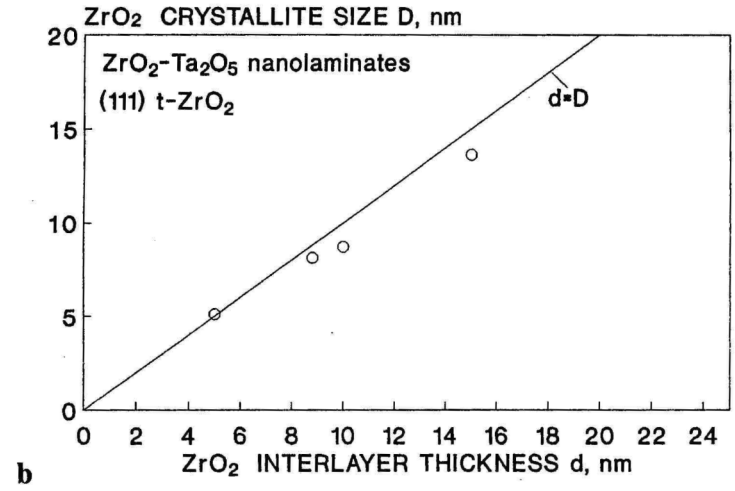

Figure 6. Dependence of the estimated relative size of HfO_2 (a) and ZrO_2 (b) nanocrystals on the nominal thickness of respective oxide interlayers in Ta_2O_5-based nanolaminates.

5.9. ZrO_2-Ta_2O_5 nanolaminates

ZrO_2-Ta_2O_5 nanolaminates were grown at 325°C [VII] with nominal thickness of ZrO_2 layers varied between 2.5 and 20 nm. The periodical structure of the nanolaminate is well-defined (Fig. 7). According to the TEM results, the ZrO_2 layers are crystallized, while only weak ordering was observed in the Ta_2O_5

layers undetectable by XRD. The gradual increase in the ZrO_2 layer thickness above 5 nm was accompanied by the appearance of the only XRD peak of considerable intensity at 30.3°, attributable to the (111) t-ZrO_2. The crystallite size in Ta_2O_5-ZrO_2 nanolaminates was well comparable to the nominal ZrO_2 layer thickness (Fig. 6).

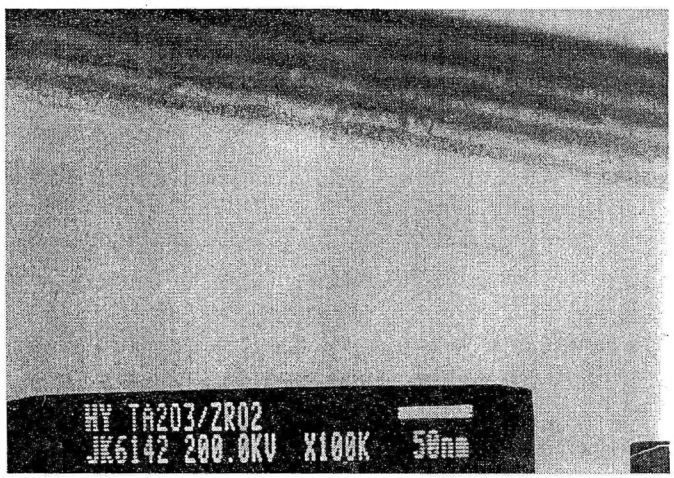

Figure 7. The structure of ZrO_2-Ta_2O_5 nanolaminate visualized by transmission electron microscope. (The image has been taken in the Centre for Electron Microscopy, Tampere University of Technology)

The relative ZrO_2 layer thickness did not seem to affect the high-field current density [VII]. The breakdown resistance was higher in these Ta_2O_5-ZrO_2 nanolaminates where the Ta_2O_5/ZrO_2 repeat distance was decreased down to 10 nm (Fig. 2) instead of the 20 nm initially chosen. Further reduction in the multilayer period down to 5 nm inhibited the crystal growth and increased the leakage current. At the same time, the permittivity was dependent on the relative content of ZrO_2, increasing slightly with ZrO_2 layer thickness above that of pure ZrO_2 (20) and even that of pure Ta_2O_5 (25) reaching 29 [Fig. 6 in VII]. The permittivity increment was detectable only in the nanolaminates with ZrO_2 layers thick enough for appreciable crystallization. The best charge storage factor obtained in the present study was 64 nC/mm^2 [Fig. 7 in VII].

5.10. Composite oxides

$Ta_xTi_yO_z$ films

Some $Ta_xTi_yO_z$ films were grown applying well-established AL-CVD recipes for Ta_2O_5 [III] and TiO_2 [19] at 325°C by successive supply of certain number

of either metal oxide deposition cycles [236]. No traces of crystallization were detected by the conventional XRD analysis. The TiO_2:Ta_2O_5 ratio was modified by the numbers of successive TiO_2 and Ta_2O_5 deposition cycles set at 1:9, 2:9, 3:12 and 21:300 while the total film thickness was kept around 150 nm. In case of less than 3–4 cycles, a submonolayer growth was expected, thus hardly resulting in true multilayer growth. Anyway, due to the low solubility of Ti in Ta_2O_5 [170], some segregation is likely also in the most homogeneous films grown.

The binary TiO_2 films were too leaky for reliable measurements. At the same time, the leakage currents in $Ta_xTi_yO_z$ films were already lower than those in their binary constituents, differing from the results by Umezawa *et al.* [179]. The sample leakage current densities, measured at 1 MV/cm, were 2×10^{-3} A/cm^2 in Ta_2O_5 films and 1×10^{-5}, 1×10^{-6}, 2×10^{-7}, and 6×10^{-8} A/cm^2 in TiO_2:Ta_2O_5 films with cycling ratios of 1:9, 2:9, 3:12 and 21:300, respectively. The pre-breakdown conduction current could be suppressed by the influence of potential barriers at the interfaces forming between distinct oxide layers.

The permittivity value was not higher than 32 in the films grown with the pulsing ratio of 1:9. In the rest of the samples, the permittivity remained at 28. The highest permittivity value, 37, was still obtained in TiO_2-Ta_2O_5 nanolaminate grown in a separate experiment by alternately supplying 167 TiO_2 and 512 Ta_2O_5 growth cycles creating a stack of 8 bilayers. The nanolaminate, however, was almost as leaky as the pure TiO_2 film.

$(Nb_{1-x}Ta_x)_2O_5$ films

Amorphous $(Nb_{1-x}Ta_x)_2O_5$ films [IX] were prepared by applying respective recipes [III,V] for both binary oxides analogously to the $Ta_xTi_yO_z$ films, at 230, 270 and 325°C. The segregation in $(Nb_{1-x}Ta_x)_2O_5$ films is neither enforced by valence difference nor by the inequality in ionic radii. Some segregation can still be expected due to the layer-by-layer growth provided by AL-CVD technique. The composition of the $(Nb_{1-x}Ta_x)_2O_5$ films could be easily tuned by adjusting the number of deposition cycles. The Ta/(Ta+Nb) ratio corresponded to that calculated using numerical values of the growth rates of respective binary oxides and the number of deposition cycles for both constituent oxides. The value of x measured was varied between 0.22 and 0.60, between the solid solubility limits recognized for Nb in Ta_2O_5 and Ta in Nb_2O_5 bulk crystalline samples [175].

Clear correlation between leakage current value and pulsing sequence has not been observed. The high-field leakage current density was somewhat lower than in Ta_2O_5 [IX] but still higher than in $Ta_xTi_yO_z$ films [239]. The permittivity was correlated with the refractive index and growth temperature, increasing also with the relative content of Nb_2O_5 and also with the number of deposition cycles for both binary oxides. The observed increase in dielectric constant from 25 to

the maximum value, 98, achieved in the thin $(Nb_{1-x}Ta_x)_2O_5$ films at such low temperatures is a remarkable result.

Ordering in amorphous solids is nondetectable with conventional XRD analysis but is generally expected as in the form of dispersed short-range ordered regions. In Ta_2O_5 the short-range order could correspond, for instance, to the low-temperature modification β-Ta_2O_5 [102]. There is only two structurally distinct forms of low-temperature Ta_2O_5 consisting of chains built from octahedral or pentagonal bipyramidal groups sharing two opposite vertices [240] which can be joined by still larger number of Nb_2O_5 polymorphs, containing octahedral NbO_6 groups sharing vertices and edges in various combinations [240]. The exchange energy of the niobium and tantalum atoms located at their polyhedral sites should not be too high considering the moderate difference in metal-oxygen bond energies. Therefore, charged defects and distortions might arise already due to the coordinational misfit owing to Nb atoms sitting at the pentagonal sites and Ta atoms replacing Nb at one of its polytype unit. This creates the additional space sharge, analogously to the mechanism discussed for manganese aluminates [241], which in the $(Nb_{1-x}Ta_x)_2O_5$ films polarizes under the external field applied enhancing the permittivity value. It is also known that metastable composite oxides have extended solubility limit compared to the ordered structures with defined equilibrium solubility [242]. So it appears also to be easier to imagine why the permittivity increment was observed in case of Ta contents similar to that of Nb [IX] whereas in the crystalline bulk samples [168] the permittivity does not increase for Ta concentrations above the solubility limits around 20–25%.

5.11. ZrO_2-$(Nb_{1-x}Ta_x)_2O_5$ nanolaminates

Some ZrO_2-$(Nb_{1-x}Ta_x)_2O_5$ nanolaminates were grown at 230, 275 and 325°C [IX]. In these films, Ta_2O_5 layers were replaced by higher permittivity $(Nb_{1-x}Ta_x)_2O_5$ in order to further enhance the effective dielectric constant. The nominal ZrO_2 single layer thickness in these nanolaminates has been set 5 nm at 230°C and 10 nm, approximately, at 270 and 325°C.

As expected, the distinct reflection of (111) t-ZrO_2 appeared in the XRD pattern taken from the nanolaminate deposited at as low as 270°C (Fig. 8). Although crystalline ZrO_2 films grew already at 230°C [IX] and the crystallization was detected in the 5 nm thick ZrO_2 layers in the nanolaminates [VII], the crystal growth was not detected in the nanolaminates deposited at 230°C [IX]. However, so far the influence of the further increase in ZrO_2 thickness is not investigated.

The leakage current was comparable to that in the other nanolaminates described above. The permittivity has increased, indeed, above those in Ta_2O_5,

ZrO_2, $(Nb_{1-x}Ta_x)_2O_5$ and ZrO_2-Ta_2O_5 films [239] up to 33. Further increase in permittivity is possible while the composition and relative layer thickness have not yet been optimized. The charge storage factor already reached 83 nC/mm^2 [IX].

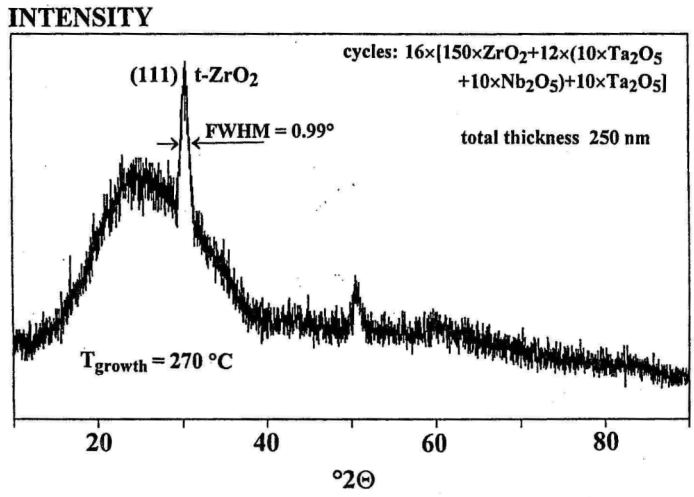

Figure 8. Typical X-ray diffractogram of the ZrO_2-$(Nb_{1-x}Ta_x)_2O_5$ nanolaminates.

6. DIELECTRIC PERFORMANCE OF NANOLAMINATES

Permittivity

Apparently due to the smaller critical crystallite size of HfO_2 for t→m transformation compared to ZrO_2, both m-HfO_2 and t-HfO_2 appear in the HfO_2-Ta_2O_5 nanolaminates while only t-ZrO_2 is observable in the ZrO_2-Ta_2O_5. In the latter films, the higher permittivity of t-ZrO_2, compared to that of m-ZrO_2, eventually gives rise to the effective permittivity of the whole structure above the respective value of Ta_2O_5. Similar behaviour cannot be examined in the HfO_2-Ta_2O_5 nanolaminates probably because of the interfering contribution of m-HfO_2. The effective permittivity could be predictable rather with the aid of some effective medium approximation, if the true values of the permittivity of the particular phases stabilized between the constraint layers were known.

Pre-breakdown leakage currents

In the nanocrystalline HfO_2-Ta_2O_5 and ZrO_2-Ta_2O_5 films, the breakdown resistance was remarkably higher in comparison to the constituent oxide films. The increase in the breakdown resistance might be considered as a barrier effect arising when high permittivity insulator layers are incorporated into the host dielectrics [243]. The formation of space charge trapped at the interface between two different dielectric layers is followed by the formation of permittivity/conductivity gradients. This is a sufficient condition for the bending of the breakdown channel, breaking the pathway of electronic avalanche and consequent increase of breakdown voltage. Moreover, the barrier effect is not accompanied by the decrease in capacitance otherwise characteristic of the series connection of dielectric layers [243]. However, although the highest permittivity difference exists between Al_2O_3 and Ta_2O_5, the Al_2O_3-Ta_2O_5 nanolaminates were not more resistive than the Al_2O_3 films. Thus, one can suggest that the potential barriers at the interfaces between different oxide interlayers is not the only mechanism reducing leakage currents although being probably the contributing one.

The increase in the resistance could, at least in some extent, be considered as a consequence of confinement effects in nanocrystalline materials such as the increase in band-gap and ionization energy. In addition, the inreasing amount of grain boundaries and interfaces should be accompanied by the creation of charge depletion regions and potential barriers, affecting the resistivity.

The capacitor of (nano)crystalline dielectric material could be modelled as a system of perfectly conducting grains and perfectly insulating grain boundaries while the total breakdown field in polycrystalline dielectrics is inversely proportional to the linear dimensions of grains [244]. In the HfO_2-Ta_2O_5 nanolaminates, the excess resistance may arise due to the carrier depletion within the space charge layer at the grain boundary core dispersed between the

grains, hindering the electronic transport from grain to grain [245]. The inrease in the number of grains along the field direction can thus be followed by the gradual decrease of leakage current. Local reduction of extrinsic electric field when divided by the (increasing) number of boundaries decreases the breakdown probability. Thus, the growing relative thickness of HfO_2 layers likely increases the amount of nanocrystallite boundaries perpendicular to the extrinsic electric field applied (Fig. 6) [Fig. 3 in VIII], fluently depressing the high-field conductivity [Fig. 2 in VIII].

At the same time, the t-ZrO_2 nanocrystallites seemed to be, approximately, of the same size as the nominal thickness of ZrO_2 layers (Fig.6). Therefore, the increase in the amount of grain boundaries with the layer thickness cannot be as pronounced as in the HfO_2 layers. Indeed, the leakage current in the ZrO_2-Ta_2O_5 nanolaminates seems to be mostly affected by the number of ZrO_2-Ta_2O_5 bilayers rather than by the relative ZrO_2 layer thickness [Fig. 5 in VII]. The leakage currents in the ZrO_2-containing nanolaminates also remained higher than in HfO_2-Ta_2O_5 (Fig. 2) [239]. Nonetheless, due to the permittivity difference, the charge storage factors are comparable.

In the nanolaminate structures, one could choose the most stable material to be deposited first in contact with the substrate, e.g. Si wafer. The varying material of the bottom and top layers does not affect the overall dielectric performance of the multilayer capacitor. In the present study, neither the permittivity nor leakage current was affected substantially when changing the material — Ta_2O_5, HfO_2 or ZrO_2 — for the bottom and top layers.

The periodicity of the nanolaminated structures determines their dielectric behaviour. Similar advanced dielectric features are expected to characterise also thinner structural units consisting, in principle, of one or few bilayers. For instance, in order to obtain functional layer containing only t-ZrO_2, one 5–10 nm thick ZrO_2 film has to be deposited, desirably using amorphous constraint layers. High relative dielectric constant and low leakage is expected to be shown by such kind of structured dielectrics, although the actual studies on these materials could require more sensitive technique with the emphasis on the surface analysis.

7. CONCLUSION

Artificially structured dielectric materials — thin films, mixtures of metal oxides and nanolaminates of Ta_2O_5, HfO_2, ZrO_2, Nb_2O_5 and Al_2O_3 — can be successfully grown in atomic layer chemical vapour deposition (AL-CVD) process. Advanced dielectric properties can be obtained in the films grown at temperatures as low as 200–230°C.

The dielectric performance of the binary metal oxides is determined by their chemical nature and structure. In certain extent, the residue content, film density and dielectric permittivity can be improved by increasing the deposition temperature or using better precursors. Further improvement in the film quality can be achieved by aiming at the formation of high-permittivity solid solutions by mixing different oxides like Ta_2O_5 and Nb_2O_5. The leakage currents can also be decreased by making use of the nanocrystalline nature of ultrathin ZrO_2 or HfO_2 layers between amorphous Ta_2O_5 or $(Nb_{1-x}Ta_x)_2O_5$ constraints in the multilayer structures. The charge storage capability of such advanced dielectric structures may be increased by ten times compared to the binary materials.

It is obvious that, besides inherent thickness control, AL-CVD technique allows the precise tuning of the film composition. Moreover, the control over size-dependent dielectric properties is achieved. These advantages can be used for creating high-quality structured materials applicable in (large area) microelectronics such as integrated circuit (IC) processing or TFEL devices.

8. FURTHER PERSPECTIVES

The further development of low temperature processing of materials characterized by the enhanced permittivity and increased breakdown resistance is definitely of importance. For this reason, the formation of moderately crystallized Ta_2O_5 from $TaCl_5$ and H_2O at around 300°C is under more detailed investigation. The effect of the $TaCl_5$ exposure time on the crystallization is clarified. The ongoing studies are aimed at the influence of the fluently varying amount of Nb substituted for Ta in weakly crystallized or amorphous Ta_2O_5 films as well as in the Nb_2O_5-Ta_2O_5 nanolaminates. The limits and positive effect of the Nb doping on the permittivity and leakage current changes are examined. Possible effect of the different Ta precursors on the film conformality and electrical properties is investigated as well.

In situ mass-spectrometry studies on the behaviour of different Ta and Nb precursor chemicals in AL-CVD reactions are going on. The effect of deposition temperature and pulse time parameters on the reaction mechanisms is to be clarified for the binary oxide as well as for composite oxide formation, including ternary ferroelectric compounds.

The low temperature deposition of ZrO_2 thin films should be studied in more detail on different substrate materials *in situ* and *ex situ*. The effect of the growth temperature on the crystallization and morphology should be investigated. Thickness series of the ultrathin ZrO_2 films could be provided while the structure profile and phase changes upon the film thickness should be detemined. The processing windows should be established for the t-ZrO_2 stabilization and optimized morphology. Also the properties and application of more volatile Hf and Zr-precursors should be studied to avoid the possible technical problems connected with uncontrolled particle transport and deposition [192] — factors possibly interfering the scale-up of the deposition process for industrial purposes.

The optical characterization of growing oxide (nano)crystallites as well as nanolaminates should be carried out. For instance, the X-ray absorption [246] and Raman spectroscopy [247] techniques could be descriptive when studying the crystal structure, electronic system and phase distributions in the oxide thin films.

Parallel studies on the (di)electric properties of the films under investigation should be organized while the measurements of the leakage currents should be carried out also below the high-field region. Studies on the accommodation of ultrathin films with the technology of integrated circuits should be continued.

TEHISSTRUKTUURIGA DIELEKTRILISTE MATERJALIDE AATOMKIHTSADESTAMINE

Kokkuvõte

Käesolevas töös demonstreeritakse keemilise aatomkiht-aurufaassadestuse meetodi sobivust ja eeliseid tehisstruktuuriga dielektriliste metalloksiidide Ta_2O_5, TiO_2, HfO_2, ZrO_2, Al_2O_3 ja Nb_2O_5 õhukeste tahkiskilede, segakoostisega kihtide ja nende nanolaminaatide kasvatamisel. Kiled moodustati H_2O ja metallide kloriidide või alkoksiidide molekulaarsete kihtide vahelistes järjestikustes pinnareaktsioonides. Hea kvaliteediga kiled saadi vägagi madalatel kasvutemperatuuridel, näiteks 200–230°C juures. See on väga oluline faktor, arvestades elektroonikatehnoloogias esitatavaid nõudeid võimalikult madalatele protsessitemperatuuridele.

Kirjeldatud meetodil kasvatatud binaarsete oksiidide reas Al_2O_3, HfO_2, ZrO_2, Ta_2O_5 suureneb dielektriline läbitavus väärtusest 8 väärtuseni 25. Kõrges elektriväljas jälgitav läbilöögieelne lekkevool suureneb koos materjali dielektrilise läbitavusega. Dielektrilist läbitavust võib teatud piirides samuti suurendada, tõstes kasvutemperatuuri, millega seoses langeb jääklisandite kontsentratsioon ja suureneb kile tihedus. Samas võib siiski suureneda lekkevool, mis käesolevas töös on tõestatud Al_2O_3 näitel.

Mahtuvuslike omaduste üldiseks parendamiseks tuleb antud materjalide omadused kombineerida. Madalsageduslikku dielektrilist konstanti võib märkimisväärselt suurendada (selles töös kuni 98) näiteks $(Nb_{1-x}Ta_x)_2O_5$ segaoksiidkiledes. Võib kasvatada ja uurida korrusstruktuure — nanolaminaate — milles binaarsest oksiidist või seguühendist koosneva vahekihi nominaalne paksus on suurusjärgus 2,5–20 nm. Nii väheneb näiteks HfO_2-Ta_2O_5-nanolaminaatides lekkevool monotoonselt koos monokliinse ja tetragonaalse HfO_2 faasi kristalliitide arvu suurenemisele HfO_2 kihtide paksenemisel. ZrO_2-Ta_2O_5-nanolaminaatides suureneb dielektriline läbitavus väärtuseni 29 vastavalt ainsana tuvastatud tetragonaalse ZrO_2 faasi kristalliitide kasvamisele ZrO_2 vahekihtides. Dielektrilist läbitavust võib veelgi suurendada, kasvatades Ta_2O_5 asemel $(Nb_{1-x}Ta_x)_2O_5$ kihte. Üldiselt ületab kombineeritud oksiidide kvaliteet nende komponentide kvaliteedi.

On näidatud, et aatomkihtsadestamine on hea reprodutseeritavusega protsess, mis lubab täpselt reguleerida dielektrikkihi paksust, keemilist koostist ja dimensioonidega määratud struktuurseid erinevusi. Struktuur omakorda mõjutab oluliselt füüsikalisi karakteristikuid. Töös saadud tulemusi võib kasutada kõrgekvaliteediliste dielektrikstruktuuride loomisel mikroelektroonikas, näiteks kiipide tehnoloogias või lamedates maatriksekraanides.

ACKNOWLEDGEMENTS

I am greatly indebted to my supervisors Mr. Jaan Aarik and Prof. Lembit Pung for their advises and support during my PhD studies.

The thesis work was completed after the tightest co-operative research carried out at the University of Helsinki, Laboratory of Inorganic Chemistry. My gratitude belongs to Dr. Mikko Ritala and Prof. Markku Leskelä for their expertise and encouraging supervision. For me, the interconnections between physics, chemistry and technology are crystallized.

I am very thankful to my co-authors or co-workers Dr. Aleks Aidla, Mr. Jarkko Ihanus, Mr. Andres Jaek, Dr. Janne Jokinen, Ms. Alma-Asta Kiisler, Ms. Oksana Kohan, Dr. Reijo Lappalainen, Dr. Hele Siimon, Dr. Väino Sammelselg and Dr. Teet Uustare. Hele is thanked also for the technical help in preparing the thesis manuscript. I appreciate the pleasant working atmosphere created by the staff with the Laboratory of Inorganic Chemistry, University of Helsinki and Institute of Experimental Physics and Technology, University of Tartu. Many interesting discussions have been carried out together with Dr. Malle Krunks from Tallinn Technical University, Dr. Kaido Tammeveski from the University of Tartu, Mr. Per Mårtensson and Mr. Mikael Schuisky from Uppsala University.

The facilities enabling electrical characterization of dielectric structures have been provided by Dr. Hannu Kattelus at the Technical Research Centre of Finland and Dr. Erkki Soininen, Dr. Juha Viljanen and Dr. Runar Törnquist at Planar International Ltd. I also appreciate the fruitful collaboration and discussions with all staff at the Color Research Laboratory, Planar International Ltd.

I am thankful to Prof. Lauri Niinistö for the opportunity to broaden my knowledge of the ALE research in the field of electroluminescent devices and rare earth elements at the Laboratory of Inorganic and Analytical Chemistry, Helsinki University of Technology.

My deepest gratitude belongs to my family for their continuous support and encouragement.

REFERENCES

[1] T. Kawai, M. Kanai and H. Tabata, Harmonic integration of functional metal oxide artificial lattices, *Mater. Sci. Eng.*, B41 (1996) 123.

[2] H. Treichel, A. Mitwalsky, G. Tempel, G. Zorn, D. A. Bohling, K. R. Coyle, B. S. Felker, M. George, W. Kern, A. P. Lane and N. P. Sandler, Deposition, annealing and characterization of high-dielectric-constant metal oxide films, *Adv. Mater. Opt. Electr.*, 5 (1995) 163.

[3] H. Treichel, G. Ruhl, R. Würl, P. Ansmann, Ch. Müller and M. Dietlmeier, Dielectric materials and insulators for microelectronics, *Electrochem. Soc. Proc.*, 97–25 (1997) 1125.

[4] D. R. Cote, S. V. Ngyen, W. J. Cote, S. L. Pennington, A. K. Stamper and D. V. Podlesnik, Low-temperature chemical vapor deposition process and dielectrics for microelectronic circuit manufacturing at IBM, *IBM J. Res. Develop.*, 39 (1995) 437.

[5] T. Suntola and J. Antson, Menetelmä ja laite yhdisteohutkalvojen kasvattamiseksi. Finnish Patent 52359 (1974), Method for producing compound thin films. U. S. Patent 4,058,430 (1977).

[6] V. B. Aleskovskii, Chemistry and technology of solids, *J. Appl. Chem. USSR*, 47 (1975) 2207.

[7] I. M. Klotz, The adsorption wave, *Chem. Rev.*, 39 (1946) 241.

[8] H. Siimon and J. Aarik, Modelling of precursor flow and deposition in atomic layer deposition reactor, *J. Phys. IV*, 5 (1995) 245.

[9] C. Hilsum, A constructive philosophy on display research, *IEEE Transact. Electron Devices*, ED-24 (1977) 791.

[10] H. W. Kohlschütter, P. Best and G. Wirzing, Umsetzung von Tri-methylsilicium-monochlorid mit Silicagel, *Z. anorg. allg. Chem.*, 285 (1956) 236.

[11] S. I. Kol'tsov and V. B. Aleskovskii, Vlijanie stepeni degidratatsii silikagelya na mekhanism gidroliza adsorbirovannogo chetyrekhkhloristogo titana. *Zh. Fiz. Khim.*, 42 (1968) 1210.

[12] S. I. Kol'tsov, G. I. Kuznetsova and V. B. Aleskovskii, Study of the stoichiometry of the products formed in the reaction of trichlorosilane with the functional groups of polysilicic acid, *J. Appl. Chem. USSR*, 40 (1967) 2644.

[13] G. V. Sveshnikova, S. I. Kol'tsov and V. B. Aleskovskii, Formation of a silica layer of predetermined thickness on silicon by the molecular-layering method, *J. Appl. Chem. USSR*, 43 (1970) 1155.

[14] S. I. Kol'tsov, A. N. Volkova and V. B. Aleskovskii, Preparation and investigation of the chemical composition of the products formed by successive chemisorption of titanium and phosphorus chlorides on the surface of silica gel, *J. Appl. Chem. USSR*, 42 (1969) 980.

[15] T. Suntola, Atomic layer epitaxy, in: Handbook of Crystal Growth 3, Thin Films and Epitaxy, Part B: Growth Mechanisms and Dynamics, Ed. D. T. J. Hurle, Elsevier 1994, Ch. 14.

[16] T. Suntola, Atomic layer epitaxy, *Mater. Sci. Rep.*, 4 (1989) 261.

[17] Y. Luo, D. Slater, M. Han, J. Moryl and R. M. Osgood, Jr., Low-temperature, chemically driven atomic-layer epitaxy: *In situ* monitored growth of CdS/ZnSe (100), *Appl. Phys. Lett.*, 71 (1997) 3799.

[18] R. A. Bisengaliev, B. V. Novikov, V. B. Aleskovskii, V. E. Drozd, D. A. Ageev, V. I. Gubaidullin and A. P. Savchenko, Molecular layering of 2D films and superlattices based on II-VI compounds, *Phys. Solid State* (*Fiz. Tverd. Tela*), 40 (1998) 754.

[19] M. Ritala, Atomic layer epitaxy growth of titanium, zirconium and hafnium dioxide thin films, *Ann. Acad. Sci. Fenn.*, Ser. A, 257 (1994).

[20] S. M. George, A. W. Ott and J. W. Klaus, Surface chemistry for atomic layer growth, *J. Phys. Chem.*, 100 (1996) 13121.

[21] J. W. Klaus, O. Sneh and S. M. George, Growth of SiO_2 at room temperature with the use of catalyzed sequential half-reactions, *Nature*, 278 (1997) 1934.

[22] V. Sammelselg, A. Rosental, A. Tarre, L. Niinistö, K. Heiskanen, K. Ilmonen, L.-S. Johansson and T. Uustare, TiO_2 thin films by atomic layer deposition: a case of uneven growth at low temperature, *Appl. Surf. Sci.*, 134 (1998) 78.

[23] T. Hirai, K. Teramoto, T. Goto and Y. Tarui, Preparation of perovskite oriented $PbZr_xTi_{1-x}O_3$ films with suppressed vapor phase reactions by a digital chemical vapor deposition method, *Jpn. J. Appl. Phys.*, 34 (1995) 539.

[24] B. Sang, A. Yamada and M. Konagai, Textured ZnO thin films for solar cells grown by a two-step process with the atomic layer deposition technique, *Jpn. J. Appl. Phys.*, 37 (1998) L206.

[25] S. Yamamoto, A. Kawaguchi and S. Oda, Preparation of thin films of $YBa_2Cu_3O_x$ with a smooth surface by atomic layer MOCVD, *Mater. Sci. Eng.*, B41 (1996) 87.

[26] M. Ylilammi, Monolayer thickness in atomic layer deposition, *Thin Solid Films*, 279 (1996) 124.

[27] URL: http://www.microchem.fi

[28] H. Kumagai and K. Toyoda, In situ ellipsometric diagnostics for controlled growth of metal oxides with surface chemical reactions, *Appl. Surf. Sci.*, 82/83 (1994) 481.

[29] W. S. Lau, L. Zhang, A. Lee, C. H. See, T. Han, N. P. Sandler and T. C. Chang, Detection of defect states responsible for leakage current in ultrathin tantalum pentoxide (Ta_2O_5) films by zero-bias thermally stimulated current spectroscopy, *Appl. Phys. Lett.*, 71 (1997) 500.

[30] S. Asai, Y. Wada and E. Takeda, Downscaling ULSIs by using nanoscale engineering, *Microelectronic Eng.*, 32 (1996) 31.

[31] L. Niinistö, M. Ritala and M. Leskelä, Synthesis of oxide thin films and overlayers by atomic layer epitaxy for advanced applications, *Mater. Sci. Eng.*, B41 (1996) 23.

[32] M. Tiitta and L. Niinistö, Volatile metal β-diketonates: ALE and CVD precursors for electroluminescent device thin films, *Chem. Vap. Deposition*, 3 (1997) 167.

[33] L. Niinistö, Atomic layer epitaxy, *Curr. Opinion Solid State Mater. Sci.*, 3 (1998) 147.

[34] See articles by Aarik *et al.* and Siimon *et al.*, in: *Acta Comment. Univ. Tartuensis*, Vol. 908 (1990) and Vol. 964 (1993).

[35] M. Leskelä and M. Ritala, Atomic layer epitaxy in deposition of various oxide and nitride thin films, *J. Phys. IV*, 5 (1995) C5-937.

[36] P. Mårtensson and J.-O. Carlsson, Atomic layer epitaxy of copper on tantalum, *Chem. Vap. Deposition*, 3 (1997) 45.

[37] M. Juppo, M. Vehkamäki, M. Ritala and M. Leskelä, Deposition of molybdenum thin films by an alternate supply of $MoCl_5$ and Zn, *J. Vac. Sci. Technol.*, A 10 (1998) 2845.

[38] M. Ritala, T. Asikainen and M. Leskelä, Enhanced growth rate in atomic layer epitaxy of indium oxide and indium-tin oxide thin films, *Electrochem. Solid-State Lett.*, 1 (1998) 156.

[39] S. M. Gates, Comparison of chemical schemes for Si atomic layer epitaxy, *J. Phys. Chem.*, 96 (1992) 10439.

[40] S. Haukka, E.-L. Lakomaa and A. Root, An IR and NMR study of the chemisorption of $TiCl_4$ on silica, *J. Phys. Chem.*, 97 (1993) 5085.

[41] J. Aarik, A. Aidla, V. Sammelselg, H. Siimon and T. Uustare, Control of thin film structure by reactant pressure in atomic layer deposition of TiO_2, *J. Cryst. Growth*, 169 (1996) 496.

[42] J. Aarik, A. Aidla, K. Kukli and T. Uustare, Deposition and etching of tantalum oxide films in atomic layer epitaxy process, *J. Cryst. Growth*, 144 (1994) 116.

[43] M. Ishii, S. Iwai, T. Ueki and Y. Aoyagi, Surface reaction mechanism and morphology control in AlP atomic layer epitaxy, *Thin Solid Films*, 318 (1998) 6.

[44] W. N. Gill and S. Ganguli, Gas phase and surface reactions in subatmospheric chemical vapor deposition of tetraethylorthosilicate-ozone, *J. Vac. Sci. Technol.*, B15 (1997) 948.

[45] P. Jensen and B. Niemeyer, The effect of a modulated flux on the growth of thin films, *Surf. Sci.*, 384 (1997) 2823.

[46] H. J. Cho and H. J. Kim, Improvement of dielectric properties of (Ba,Sr)TiO_3 thin films deposited by pulse injection chemical vapor deposition, *Appl. Phys. Lett.*, 72 (1998) 786.

[47] A. Rosental, P. Adamson, A. Gerst and A. Niilisk, Monitoring of atomic layer deposition by incremental dielectric reflection, *Appl. Surf. Sci.*, 107 (1996) 178.

[48] Z. Zhu, M. Hagino, K. Uesugi, S. Kamiyama, M. Fujimoto and T. Yao, Surface processes in ALE and MBE growth of ZnSe: Correlation of RHEED intensity variation with surface coverage, *Jpn. J. Appl. Phys.*, 28 (1989) 1659.

[49] J. Hyvärinen, M. Sonninen and R. Törnquist, Mass spectrometry study of ZnS atomic layer epitaxy process, *J. Cryst. Growth*, 86 (1988) 695.

[50] J. Aarik, A. Aidla, A. Jaek, M. Leskelä and L. Niinistö, *In Situ* study of a strontium β-diketonate precursor for thin film growth by atomic layer epitaxy, J. *Mater. Chem.*, 4 (1994) 1239.

[51] A. Koukitu, N. Takahashi, and H. Seki, In situ monitoring of the GaAs growth process in halogen transport atomic layer epitaxy, *J. Cryst. Growth*, 33 (1994) L613.

[52] M. Rodahl and B. Kasemo, On the measurement of thin liquid overlayers with the quartz-crystal microbalance, *Sensors and Actuators*, A 54 (1996) 448.

[53] R. Ortega-Borges and D. Lincot, Mechanism of chemical bath deposition of cadmium sulfide thin films in the ammonia-thiourea system. *In Situ* kinetic study and modelization, *J. Electrochem. Soc.*, 140 (1993) 3464.

[54] G. Sauerbrey, Verwendung von Schwingquartzen zur Wägung dünner Schichten und zur Mikrowägung, *Z. Phys.*, 155 (1959) 206.

[55] C. J. vd Laan and H. J. Frankena, Monitoring of optical thin films using a quartz crystal monitor, *Vacuum*, 27 (1977) 391.

[56] L. Norin, Interaction of C_{60} with transition metals for thin film applications, Dissertation, *Acta Univ. Upsaliensis*, Uppsala, 1998., p. 24.

[57] A. I. Romanychev, V. E. Drozd and V. B. Aleskovskii, Growth of zinc and cadmium sulfide films with the aid of ellipsometry and a quartz resonance balance, *J. Appl. Chem. USSR*, 62 (1989) 11.

[58] J.-F. Fan and K. Toyoda, Self-limiting behaviour of the growth of Al_2O_3 using sequential vapor pulses of TMA and H_2O_2, *Appl. Surf. Sci.*, 60/61 (1992) 765.

[59] J. Aarik, A. Aidla, V. Sammelselg and T. Uustare, Effect of growth conditions on formation of TiO_2-II thin films in atomic layer deposition process, *J. Cryst. Growth*, 181 (1997) 259.

[60] J. Aarik, A. Aidla, A. Jaek, M. Leskelä and L. Niinistö, Precursor properties of calcium β-diketonate in vapor phase atomic layer epitaxy, *Appl. Surf. Sci.*, 75 (1994) 33.

[61] J. Aarik, A. Aidla, A.-A. Kiisler, T. Uustare and V. Sammelselg, Influence of substrate temperature on atomic layer growth and properties of HfO_2 thin films, *Thin Solid Films*, in press.

[62] K. H. Behrndt, Long-term operation of crystal oscillators in thin film deposition, *J. Vac. Sci. Technol.*, 8 (1971) 622.

[63] V. M. Mecea, J. O. Carlsson and R. V. Bucur, Extensions of the quartz-crystal-microbalance study, *Sensors and Actuators* A 53 (1996) 371.

[64] A. D. Migone, J. Krim, J. G. Dash and J. Suzanne, Incomplete wetting of ^4He films on Ag and Au(111) surfaces, *Phys. Rev.*, B 31 (1985) 7643.

[65] V. Tsionsky, L. Daikhin, M. Urbakh and E. Gileadi, Behaviour of quartz crystal microbalances in nonadsorbed gases at high pressures, *Langmuir*, 11 (1995) 674.

[66] M. Ritala, M. Leskelä, E. Rauhala and J. Jokinen, Atomic layer epitaxy growth of TiN thin films from TiI_4 and NH_3, *J. Electrochem. Soc.*, 145 (1998) 2914.

[67] N. Marasli and J. D. Hunt, The use of measured values of surface energies to test heterogeneous nucleation theory, *J. Cryst. Growth*, 191 (1998) 558.

[68] M. Ritala, H. Saloniemi, M. Leskelä, T. Prohaska, G. Friedbacher and M. Grasserbauer, Studies on the morphology of Al_2O_3 thin films grown by atomic layer epitaxy, *Thin Solid Films*, 286 (1996) 54.

[69] J. Ihanus, M. Ritala, M. Leskelä, T. Prohaska, R. Resch, G. Friedbacher and M. Grasserbauer, AFM studies on ZnS thin films grown by atomic layer epitaxy, *Appl. Surf. Sci.*, 120 (1997) 43.

[70] A. Kytökivi, E.-L. Lakomaa and A. Root, Controlled formation of ZrO_2 in the reaction of $ZrCl_4$ vapor with porous silica and γ-alumina surfaces, *Langmuir*, 12 (1996) 4395.

[71] Y. Charreire, R. Cortes, E. Nykänen, L. Niinistö, P. Soininen and M. Leskelä, Speciation of activators in electroluminescent thin films: an EXAFS study of cerium and terbium doped strontium sulfide, *Fresenius J. Anal. Chem.*, 362 (1998) 41.

[72] N. V. Dolgushev, A. A. Malkov, A. A. Malygin, S. A. Suvorov, A. V. Shchukarev, A. V. Beljaev and V. A. Bykov, Synthesis and characterization of nanosized titanium oxide films on the (0001)-Al_2O_3 surface, *Thin Solid Films*, 293 (1997) 91.

[73] A. Kytökivi, E.-L. Lakomaa, A. Root, H. Österholm, J.-P. Jacobs and H. H. Brongersma, Sequential saturating reactions of $ZrCl_4$ and H_2O vapors on the modification of silica and γ-alumina with ZrO_2, *Langmuir*, 13 (1997) 2717.

[74] M. Ritala, M. Leskelä, L. Niinistö, T. Prohaska, G. Friedbacher and M. Grasserbauer, Development of crystallinity and morphology in hafnium dioxide thin films grown by atomic layer epitaxy, *Thin Solid Films*, 250 (1994) 72.

[75] E.-L. Lakomaa, A. Root and T. Suntola, Surface reactions in Al_2O_3 growth from trimethylaluminium and water by atomic layer epitaxy. *Appl. Surf. Sci.*, 107 (1996) 107.

[76] K. Kukli, H. Heikkinen, E. Nykänen and L. Niinistö, Deposition of lanthanum sulfide thin films by atomic layer epitaxy, *J. Alloys Comp.*, 275–277 (1998) 10.

[77] H. Treichel, A. Mitwalsky, G. Tempel, G. Zorn, W. Kern, N. Sandler and A. P. Lane, Deposition, annealing, and characterization of tantalum pentoxide films, *Mater. Res. Soc. Symp. Proc.*, 282 (1993) 557.

[78] G.-T. Jeong, K.-C. Lee, D.-W. Ha, K.-H. Lee, K.-H. Kim, I.-G. Kim, D.-H. Kim and K. Kim, A high performance 16 Mb DRAM using giga-bit technologies, *IEEE Transact. Electron Devices*, 44 (1997) 2064.

[79] J.-L. Autran, R. Devine, C. Chaneliere and B. Balland, Fabrication and characterization of Si-MOSFET's with PECVD amorphous Ta_2O_5 gate insulator, *IEEE Electron Device Lett.*, 18 (1997) 447.

[80] J. D. T. Kruschwitz and W. T. Pawlewitcz, Optical and durability properties of infrared transmitting thin films, *Appl. Opt.*, 36 (1997) 2157.

[81] G. B. Alers, R. M. Fleming, Y. H. Wong, B. Dennis, A. Pinczuk, G. Redinbo, R. Urdahl, E. Ong and Z. Hazan, Nitrogen plasma annealing for low temperature Ta_2O_5 films, *Appl. Phys. Lett.*, 72 (1998) 1308.

[82] G. B. Alers, D. J. Werder, Y. Chabal, H. C. Lu, E. P. Gusev, E. Garfunkel, T. Gustafsson and R. S. Urdahl, Intermixing at the tantalum oxide/silicon interface in gate dielectric structures, *Appl. Phys. Lett.*, 73 (1998) 1517.

[83] T. Aoyama, S. Saida, Y. Okayama, M. Fujisaki, K. Imai and T. Arikado, Leakage current mechanism of amorphous and polycrystalline Ta_2O_5 films grown by chemical vapor deposition, *J. Electrochem. Soc.*, 143 (1996) 977.

[84] T. Aoyama, S. Yamazaki and K. Imai, Ultrathin Ta_2O_5 capacitor with Ru bottom electrode, *J. Electrochem. Soc.*, 145 (1998) 2961.

[85] K. Kishiro, N. Inoue, S.-C. Chen and M. Yoshimaru, Structure and electrical properties of thin Ta_2O_5 deposited on metal electrodes, *Jpn. J. Appl. Phys.*, 37 (1998) 1336.

[86] C. Chaneliere, S. Four, J. L. Autran, R. A. B. Devine and N. P. Sandler, Properties of amorphous and crystalline Ta_2O_5 thin films deposited on Si from a $Ta(OC_2H_5)_5$ precursor, *J. Appl. Phys.*, 83 (1998) 4823.

[87] H. Shinriki, M. Sugiura, Y. Liu, K. Shimomura and T. Nakajima, Ethanol-addition-enhanced, chemical vapor deposited tantalum oxide films from $Ta(OC_2H_5)_5$ and oxygen precursors, *J. Electrochem. Soc.*, 145 (1998) 3247.

[88] X. Li, M. L. Hitchman and S. H. Shamlian, Low temperature CVD of tantalum oxide films, *Electrochem. Soc. Proc.*, 97–25 (1997) 1246.

[89] J. V. Grahn, P.-E. Hellberg and E. Olsson, Effect of growth temperature on the properties of evaporated tantalum pentoxide thin films on silicon deposited using oxygen radicals, *J. Appl. Phys.*, 84 (1998) 1632.

[90] K. Chen, M. Nielsen, G. R. Yang, E. J. Rymaszewski and T.-M. Lu, Study of amorphous thin films by DC magnetron reactive sputtering, *J. Electronic Mater.*, 26 (1997) 397.

[91] D. Laviale, J. C. Oberlin and R. A. B. Devine, Low pressure microwave electron cyclotron resonance plasma deposition of amorphous Ta_2O_5 films, *Appl. Phys. Lett.*, 65 (1994) 2021.

[92] S. Shibata, Dielectric constants of Ta_2O_5 thin films deposited by r.f. sputtering. *Thin Solid Films*, 277 (1996) 1.

[93] G. M. Choi, H. L. Tuller and J. S. Haggerty, Alpha-Ta_2O_5. An intrinsic fast oxygen ion conductor, *J. Electrochem. Soc.*, 136 (1989) 835.

[94] K.-A. Son, A. Y. Mao, Y.-M. Sun, B. Y. Kim, F. Liu, A. Kamath, J. M. White, D. L. Kwong, D. A. Roberts and R. N. Vrtis, Chemical vapor deposition of ultrathin Ta_2O_5 films using $Ta[N(CH_3)_2]_5$, *Appl. Phys. Lett.*, 72 (1998) 1187.

[95] F. A. Cotton and G. Wilkinson, Advanced inorganic chemistry, John Wiley & Sons, New York, 1980, p. 831.

[96] W. S. Lau, P. W. Qian, N. P. Sandler, K. A. McKinley and P. K. Chu, Evidence that N_2O is a stronger oxidizing agent than O_2 for the post-deposition annealing of Ta_2O_5 on Si capacitors, *Jpn. J. Appl. Phys.*, 36 (1997) 661.

[97] R. A. B. Devine, C. Chaneliere, J. L. Autran, B. Balland, P. Paillet and J. L. Leray, Use of carbon-free Ta_2O_5 thin films as a gate insulator, *Microelectronic Eng.*, 36 (1997) 61.

[98] M. Pessa, R. Mäkelä and T. Suntola, Characterization of surface exchange reactions used to grow compound films, *Appl. Phys. Lett.*, 38 (1981) 131.

[99] J. Aarik, A. Aidla and K. Kukli, In situ characterisation of ALE growth by reagent pulse delay times in a flow-type reactor, *Appl.Surf. Sci.*, 75 (1994) 180.

[100] H. Kattelus, M. Ylilammi, J. Salmi, T. Ranta-aho, E. Nykänen and I. Suni, Electrical properties of tantalum based composite oxide films, *Mater. Res. Soc. Symp. Proc.*, 284 (1993) 511.

[101] H. Kattelus, M. Ylilammi, J. Saarilahti, J. Antson and S. Lindfors, Layered tantalum-aluminium oxide films deposited by atomic layer epitaxy, *Thin Solid Films*, 225 (1993) 296.

[102] V. V. Bryksin, M. N. Dyakonov and S. D. Khanin, Pryschkovy perenos v nekristallicheskom okisle tantala , *Fiz. Tverd. Tela*, 22 (1980) 1403.

[103] H. Morisaki, S. Masaki and S. Watanabe, New oxidation state of tantalum oxide formed by reactive ion-beam sputtering of Ta and Si, *J. Vac. Sci. Technol.*, A 5 (1987) 1767.

[104] P. Balk, Dielectrics in microelectronics — problems and perspectives, *J. Non-Cryst. Solids*, 187 (1995) 1; Dielectrics for field-effect technology, *Adv. Mater.*, 7 (1995) 703.

[105] K. J. Hubbard and D. G. Schlom, Thermodynamic stability of binary oxides in contact with silicon, *J. Mater. Res.*, 11 (1996) 2757.

[106] Outokumpu HSC Chemistry for Windows, Program package, Version 3.02, Outokumpu Research OY, Pori, Finland, 1997.

[107] G. Eftekhari, Electrical characteristics of Ta_2O_5 films on Si prepared by dc magnetron reactive sputtering and annealed rapidly in N_2O, *J. Vac. Sci. Technol.*, B 16 (1998) 2115.

[108] S. Roberts, J. Ryan and L. Nesbit, Selective studies of crystalline Ta_2O_5 films, *J. Electrochem. Soc.*, 133 (1986) 1405.
[109] S. Ezhilvalavan and T.-Y. Tseng, Conduction mechanisms in amorphous and crystalline Ta_2O_5 thin films, *J. Appl. Phys.*, 83 (1998) 4797.
[110] X. M. Wu, S. R. Soss, E. J. Rymaszewski and T.-M. Lu, Dielectric constant dependence of Poole-Frenkel potential in tantalum oxide thin films, *Mater. Chem. Phys.*, 38 (1994) 297.
[111] L. Chambon, C. Maleysson, A. Pauly, J. P. Germain, V. Demarne and A. Grisel, Investigation, for NH_3 gas sensing applications, of the Nb_2O_5 semiconducting oxide in the presence of interferent species such as oxygen and humidity, *Sensors and Actuators*, B 45 (1997) 107.
[112] A. P. Lane, A. Chen and B. S. Page, Advanced dielectrics deposited by LPCVD, *Mater. Res. Symp. Soc. Proc.*, 250 (1992) 331.
[113] A. Bernasik, M. Radecka, M. Rekas and M. Sloma, Electrical properties of Cr- and Nb-doped TiO_2 thin films, *Appl. Surf. Sci.*, 65/66 (1993) 240.
[114] K. Miura and M. Tanaka, Effect of Nb doping on fatique in lead zirconate titanate, *Jpn. J. Appl. Phys.*, 36 (1997) 226.
[115] H. R. Brunner, F. P. Emmenegger, M. L. A. Robinson and H. Rötschi, Growth and properties of thin film capacitors, *J. Electrochem. Soc.*, 115 (1968) 1287.
[116] Y. Narendar and G. L. Messing, Synthesis, decomposition and crystallization characteristics of peroxo-citrato-niobium: an aqueous niobium precursor, *Chem. Mater.*, 9 (1997) 580.
[117] F. Fairbrother, The chemistry of niobium and tantalum. Elsevier Publishing Company, Amsterdam, 1967, p.30.
[118] N. Hara, E. Takahashi, J. H. Yoon and K. Sugimoto, Ellipsometric analysis of growth process and corrosion resistance of Nb_2O_5 films formed by MOCVD, *J. Electrochem. Soc.*, 141 (1994) 1669.
[119] T. Ikeya and M. Senna, Change in the structure during amorphization and metallization of Ta_2O_5 under mechanical stressing. A comparative study with Nb_2O_5, *J. Non-cryst. Solids*, 113 (1989) 51.
[120] A. K. Vijh, Solid state properties of some valve metal oxides, *J. Electrochem. Soc.*, 116 (1969) 353.
[121] E. H. Greener, D. H. Whitmore and M. E. Fine, Electrical conductivity of near-stoichiometric α-Nb_2O_5, *J. Chem. Phys.*, 34 (1961) 1017.
[122] D. A. Mehta, R. S. Butler and F. J. Feigel., Effect of post-deposition annealing treatments on charge trapping in CVD Al_2O_3 films on Si, *J. Electrochem. Soc.*, 120 (1973) 1707.
[123] W. Koh, S.J. Ku and Y. Kim, Chemical vapor deposition of Al_2O_3 films using highly volatile single sources, *Thin Solid Films*, 304 (1997) 222.
[124] V. E. Drozd, A. P. Baraban and I. O. Nikiforova, Electrical properties of Si-Al_2O_3 structures grown by ML-ALE, *Appl. Surf. Sci.*, 82/83 (1994) 583.
[125] A. P. Baraban, V. V. Bulavinov, V. E. Drozd, I. O. Nikiforova and M. V. Sergijenko, Electrophysical characteristics of AL-Al_2O_3 structures synthesized by the molecular stratifying technique, *Zh. Tekhn. Fiz. (Sov. J. Techn. Phys.)*, 65 (1995) 203.

[126] Y. Kim, S. M. Lee, C. S. Park, S. I. Lee and M. Y. Lee, Substrate dependence on the optical properties of Al_2O_3 films grown by atomic layer deposition, *Appl. Phys. Lett.*, 71 (1997) 3604.

[127] P. Ericsson, S. Bengtsson and J. Skarp, Properties of Al_2O_3-films deposited on silicon by atomic layer epitaxy, *Microel. Eng.* 36 (1997) 91.

[128] S. J. Yun, K.-H. Lee, J. Skarp, H.-R. Kim and K.-S. Nam, Dependence of atomic layer-deposited Al_2O_3 films characteristics on growth temperature and AL precursors of $Al(CH_3)_3$ and $AlCl_3$, *J. Vac. Sci. Technol.*, A 15 (1997) 2993.

[129] J. S. Kim, H. A. Marzouk, P. J. Reucroft, J. D. Robertson and C. E. Hamrin, Fabrication of aluminium oxide thin films by a low-pressure metalorganic chemical vapor deposition technique, *Appl. Phys. Lett.*, 62 (1993) 681.

[130] A. K. Vijh, A thermochemical approach to the bandgap of semiconducting and insulating materials, *J. Mater. Sci.*, 5 (1970) 379.

[131] J. Shappir, A. Anis and I. Pinsky, Investigation of MOS capacitors with thin ZrO_2 layers and various gate materials for advanced DRAM applications, *IEEE Transact. Electron Devices*, ED-33 (1986) 442.

[132] D. P. Thompson, A. M. Dickins and J. S. Thorp, The dielectric properties of zirconia, *J. Mater. Sci.*, 27 (1992) 2267.

[133] J. Nawrocki, M. P. Rigney, A. McCormick and P. W. Carr, Chemistry of zirconia and its use in chromatography, *J. Chromatography*, A 657 (1993) 229.

[134] S. B. Qadri, C. M. Gilmore, C. Quinn, E. F. Skelton and C. R. Gossett, Structural stability of ZrO_2-Al_2O_3 thin films deposited by magnetron sputtering, *J. Vac. Sci. Technol.*, A 7 (1989) 1220.

[135] M. Pulver and G. Wahl, MOCVD of zirconia films using β-diketonates, *Electrochem. Soc. Proc.*, 97–25 (1997) 960.

[136] M. S. Khan, M. S. Islam and D. R. Bates, Cation doping and oxygen diffusion in zirconia: a combined atomistic simulation and molecular dynamics study, *J. Mater. Chem.*, 8 (1998) 2299.

[137] X. Lu, K. Liang, S. Gu, Y. Zheng and H. Fang, Effect of oxygen vacancies on transformation of zirconia at low temperatures, *J. Mater. Sci.*, 32 (1997) 6653.

[138] M. Lerch and J. Lerch, Nitrogen incorporation into Ta_2O_5-containing zirconia ceramics, *J. Mater. Sci. Lett.*, 16 (1997) 1454.

[139] I.-W. Chen and Y.-H.Chiao, Martensitic nucleation in ZrO_2, *Acta Metall.*, 31 (1983) 1627.

[140] A. H. Heuer and M. Rühle, On the nucleation of the martensitic transformation in zirconia (ZrO_2), *Acta Metall.*, 33 (1985) 2101.

[141] B.-Y. Kim and H. Hamaguchi, Role of oxygen phonons in the martensitic phase transformation of yttria stabilized tetragonal zirconia polycrystals, *J. Mater. Sci. Lett.*, 26 (1997) 645.

[142] A. L. Roytburd, T. S. Kim, Q. Su, J. Slutsker and M. Wuttig, Martensitic transformation in constrained films, *Acta Mater.*, 46 (1998) 5095.

[143] A. Mehner, H. Klümper-Westkamp, F. Hoffmann and P. Mayr, Crystallization and residual stress formation of sol-gel-derived zirconia films, *Thin Solid Films*, 308–309 (1997) 363.

[144] R. Srinivasan, B. Davis, O. B. Cavin and C. R. Hubbard, Crystallization and phase transformation process in zirconia: An in situ high-temperature X-ray diffraction study, *J. Am. Ceram. Soc.*, 75 (1992) 1217.

[145] S. B. Desu, T. Shi and C. K. Kwok, Structure, composition and properties of MOCVD ZrO_2 thin films, *Mat. Res. Soc. Symp. Proc.*, 168 (1990) 349.
[146] N. Bourhila, F. Felten, J. P. Senateur, F. Schuster, R. Madar and A. Abrutis, Deposition and characterization of ZrO_2 and yttria-stabilized ZrO_2 films using injection-LPCVD, *Electrochem. Soc. Proc.*, 97–25 (1997) 417.
[147] Z. Xue, B. A. Vaartstra, K. G. Caulton, M. H. Chisholm and D. L. Jones, Chemical vapor deposition of cubic-zirconia thin films from zirconium alkoxide complexes, *Eur. J. Solid State Inorg. Chem.*, 29 (1992) 213.
[148] R. C. Garvie, R. H. Hannink and R. T. Pascoe, Ceramic steel ?, *Nature*, 258 (1975) 703.
[149] R. C. Garvie, Stabilization of the tetragonal structure in zirconia microcrystals, *J. Phys. Chem.*, 82 (1978) 218.
[150] W. Stichert and F. Schüth, Influence of crystallite size on the properties of zirconia, *Chem. Mater.*, 10 (1998) 2020.
[151] N. I. Medvedeva, V. P. Zhukov, M. Ya. Khodos and V. A. Gubanov, The electronic structure and cohesive energy of HfO_2, ZrO_2, TiO_2 and SnO_2 crystals, *Phys. Stat. Sol.*, (b) 160 (1990) 517.
[152] M. A. Subramanian and R. D. Shannon, Dielectric constant of Y-stabilized zirconia, the polarizability of zirconia and the oxide additivity rule, *Mater. Res. Bull.*, 24 (1989) 1477.
[153] J. Gavillet, T. Belmonte, D. Hertz and H. Michel, Low temperature zirconia thin films synthesis by a chemical vapour deposition process involving $ZrCl_4$ and O_2-H_2-Ar microwave post-discharges. Comparison with a conventional CVD hydrolysis process, *Thin Solid Films*, 301 (1997) 35.
[154] M. Ritala and M. Leskelä, Zirconium oxide thin films deposited by ALE using zirconium tetrachloride as precursor, *Appl. Surf. Sci.*, 75 (1994) 333.
[155] M. Lindblad, S. Haukka, A. Kytökivi, E.-L. Lakomaa, A. Rautiainen and T. Suntola, Processing of catalysts by atomic layer epitaxy: modification of supports, *Appl. Surf. Sci.*, 121/122 (1997) 286.
[156] M. Fadel, O. A. Azim, O. A. Omer and R. R. Basily, A study of some optical properties of hafnium dioxide (HfO_2) thin films and their applications, *Appl. Phys.* A, 66 (1998) 335.
[157] J. W. Li, Y. K. Su and M. Yokoyama, Current density- voltage characteristics of AC thin-film electroluminescent devices with different dielectric-phosphor interfaces, *Jpn. J. Appl. Phys.*, 32 (1993) 5591.
[158] Yu. G. Sukharev, I. L. Akulyushin, V. V. Zherevchuk, A. A. Savel'ev, A. V. Andriyanov, V. S. Mironov and O. V. Polyarush, Electrical and optical properties of HfO_2-Nd_2O_3 dielectric films, *Inorg. Mater.*, 33 (1997) 1254.
[159] I.-A. El-Shanshoury, V. A. Rudenko and I. A. Ibrahim, Polymorphic behaviour of thin evaporated films of zirconium and hafnium oxides, *J. Am. Ceram. Soc.*, 53 (1970) 264.
[160] M. Yashima, H. Takahashi, K. Ohtake, T. Hirose, M. Kakihana, H. Arashi, Y. Ikuma, Y. Suzuki and M. Yoshimura, Formation of metastable forms by quenching of the HfO_2-$RO_{1.5}$ melts (R=Gd, Y and Yb), *J. Phys. Chem. Solids*, 57 (1996) 289.

[161] M. Yashima, T. Kato, M. Kakihana, M. A. Gulgun, Y. Matsuo and M. Yoshimura, Crystallization of hafnia and zirconia during the pyrolysis of acetate gels, *J. Mater. Res.*, 12 (1997) 2575.

[162] J. Wang, H. P. Li and R. Stevens, Hafnia and hafnia toughened ceramics, *J. Mater. Sci.*, 27 (1992) 5397.

[163] M. Ritala, M. Leskelä, L. Niinistö, T. Prohaska, G. Friedbacher and M. Grasserbauer, Development of crystallinity and morphology in hafnium dioxide thin films grown by atomic layer epitaxy, *Thin Solid Films*, 250 (1994) 72.

[164] R. B. van Dover, L. F. Schneemeyer and R. M. Fleming, Discovery of a useful thin-film dielectric using a composition-spread approach, *Nature*, 392 (1998) 162.

[165] C. Z. Deng, R. A. J. Pynenburg and K. C. Tsai, Improved porous mixture of molybdenum nitride and tantalum oxide as a charge storage material, *J. Electrochem. Soc.*, 145 (1998) L61.

[166] R. J. Cava, W. F. Peck Jr. and J. J. Krajewski, Enhancement of the dielectric constant of Ta_2O_5 through substitution with TiO_2, *Nature*, 377 (1995) 215.

[167] R. J. Cava, W. F. Peck Jr., J. J. Krajewski, G. L. Roberts, B. P. Barber, H. M. O. Bryan and P. L. Gammel, Improvement of the dielectric properties of Ta_2O_5 through substitution with Al_2O_3, *Appl. Phys. Lett.*, 70 (1997) 1396.

[168] R. J. Cava, W. F. Peck Jr., J. J. Krajewski and G. L. Roberts, Dielectric properties of the $(Nb_{1-x}Ta_x)_2O_5$ solid solution, *Mater. Res. Bull.*, 31 (1996) 295.

[169] R. J. Cava, J. J. Krajewski, W. F. Peck Jr. and G. L. Roberts, Dielectric properties of Ta_2O_5-ZrO_2 polycrystalline ceramics, *J. Appl. Phys.*, 80 (1998) 1613.

[170] H.-J. Lee, R. Sinclair, M.-B. Lee and H.-D. Lee, Interfacial reaction in the poly-Si/Ta_2O_5/TiN capacitor system, *J. Appl. Phys.*, 83 (1998) 139.

[171] N. Schönberg, An X-ray investigation of the tantalum-oxygen system, *Acta Chem. Scand.*, 8 (1954) 240.

[172] J. F. Meng, B. K. Rai, R. S. Katiyar and A. S. Bhalla, Raman investigation on $(Ta_2O_5)_{1-x}(TiO_2)_x$ system at different temperatures and pressures. *J. Phys. Chem. Solids*, 58 (1997) 1503.

[173] H. Schäfer, A. Dürkop and M. Jori, Über die Affinitätsverhältnisse bei der Phase-Umwandlung im System Nb_2O_5-Ta_2O_5, *Z. anorg. allg. Chem.*, 275 (1954) 19.

[174] F. Holtzberg and A. Reisman, Sub-solidus equilibria in the system Nb_2O_5-Ta_2O_5, *J. Phys. Chem.*, 64 (1960) 1192.

[175] G. P. Mohanty, L. J. Fiegel and J. H. Healy, On the system niobium pentoxide — tantalum pentoxide, *J. Phys. Chem.*, 68 (1964) 208.

[176] H. Fujikawa and Y. Taga, Effects of additive elements on electrical properties of tantalum oxide films, *J. Appl. Phys.*, 75 (1994) 2538.

[177] H. Fujikawa, K. Noda, S. Tokito and Y. Taga, Electrical properties of Ta-Sn-O films on indium tin oxide electrodes, *Appl. Phys. Lett.*, 70 (1997) 270.

[178] P. C. Joshi, S. Stowell and S. B. Desu, Structural and electrical properties of crystalline (1-x)$Ta_2O_{5-x}Al_2O_3$ thin films fabricated by metalorganic solution deposition technique, *Appl. Phys. Lett.*, 71 (1997) 1341.

[179] T. Umezawa, S. Yajima and K. Matsumoto, The electrical properties of resistive and dielectric thin films prepared by reactive sputtering from a tantalum titanium composite target, *Thin Solid Films*, 52 (1978) 69.

[180] J.-Y. Gan, Y. C. Chang and T. B. Wu, Dielectric property of $(TiO_2)_x$-$(Ta_2O_5)_{1-x}$ thin films, *Appl. Phys. Lett.*, 72 (1998) 332.
[181] J. Rivory, Characterization of inhomogenous dielectric films by spectroscopic ellipsometry, *Thin Solid Films*, 313 (1998) 333.
[182] O. Kilpelä, J. Sinkkonen and S. Novikov, MBE growth of material systems for semiconductor nanostructures, *Reports in Electron Physics*, Helsinki Univ. Technol., 15 (1997).
[183] S. K. Tiku and S. H. Rustomji, Dielectrics for bright EL displays, *IEEE Transact. Electron Devices*, 36 (1989) 1947.
[184] J. Ohwaki, H. Kozawaguchi and B. Tsujiyama, Stacked insulator structure thin-film electroluminescent display devices, *J. Electrochem. Soc.*, 137 (1990) 340.
[185] B. D. Qu, M. Evstigneev, D. J. Johnson and R. H. Prince, Dielectric properties of $BaTiO_3/SrTiO_3$ multilayered thin films prepared by pulsed laser deposition, *Appl. Phys. Lett.*, 72 (1998) 1394.
[186] J. S. Moya, Layered ceramics, *Adv. Mater.*, 7 (1995) 185.
[187] C. R. Aita, Multilayer nanolaminates containing polycrystalline zirconia, U. S. Patent 5,472,795 (1995).
[188] C. R. Aita, M. D. Wiggins, R. Whig, C. M. Scanlan and M. Gajdardziska-Josifovska, Thermodynamics of tetragonal zirconia formation in a nanolaminate film, *J. Appl. Phys.*, 79 (1996) 1176.
[189] D. Riihelä, M. Ritala, R. Matero and M. Leskelä, Introducing atomic layer epitaxy for the deposition of optical thin films, *Thin Solid Films*, 289 (1996) 250.
[190] H. Kumagai, K. Toyoda, K. Kobayashi, M. Obara and Y. Iimura, Titanium oxide aluminium oxide multilayer reflectors for water-window wavelengths, *Appl. Phys. Lett.*, 70 (1997) 2338.
[191] M. Ritala, M. Leskelä, L. Niinistö, T. Prohaska, G. Friedbacher and M. Grasserbauer, Surface roughness reduction in atomic layer epitaxy growth of titanium dioxide thin films, *Thin Solid Films*, 249 (1994) 155.
[192] T. Kanniainen, J. Skarp and H. Kattelus, Growth of dielectric HfO_2/Ta_2O_5 thin film nanolaminate capacitors by atomic layer epitaxy, *Electrochem. Soc. Proc.*, 97–31 (1998) 36.
[193] H. Kattelus, H. Ronkainen, T. Kanniainen and J. Skarp, Thin-film capacitors with tantalum-hafnium oxide nanolaminate insulator, The 28th European Solid State Device Res. Conf., ESSDERC'98, Bordeaux, 8–10. Sept. 1998, Proceedings, p. 444.
[194] R. W. Siegel, What do we really know about the atomic-scale structures of nanophase materials ?, *J. Phys. Chem. Solids*, 55 (1994) 1097.
[195] J. Dutta, Electrical properties of nanocomposites, *Analusis Mag.*, 24 (1996) M16.
[196] J. Dutta and H. Hoffmann, Nanomaterials: Bridging the gap between solid-state physics and materials science, *Analusis Mag.*, 24 (1996) M8.
[197] A. Hagfeldt and M.Grätzel, Light-induced redox reactions in nanocrystalline systems, *Chem. Rev.*, 95 (1995) 49.
[198] S. Veprek, Electronic and mechanical properties of nanocrystalline composites when approaching molecular size, *Thin Solid Films*, 297 (1997)145.
[199] L. E. Brus, Electron-electron and electron-hole interactions in small semiconductor crystallites: The size dependence of the lowest excited electronic state, *J. Chem. Phys.*, 80 (1984) 4403; Chemical approaches to semiconductor nano-

crystals, *J. Phys. Chem. Solids*, 59 (1998) 459; Metastable dense semiconductor phases, *Science*, 276 (1997) 373.
[200] W. T. Tsang, E. F., Schubert and J. E. Cunningham, Doping in semiconductors with variable activation energy, *Appl. Phys. Lett.*, 60 (1992) 115.
[201] R. Tsu, D. Babic and L. Ioriatti, Jr., Simple model for the dielectric constant of nanoscale silicon particle, *J. Appl. Phys.*, 82 (1997) 1327.
[202] A. Goossens, Bandgap enlargement in anodic oxide films on titanium, *Surf. Sci.*, 371 (1997) 390.
[203] M. Abdulkhadar and B. Thomas, Study of dielectric properties of nanophase silver iodide, *Bull. Mater. Sci.*, 19 (1996) 631.
[204] B. Thomas and M. Abdulkhadar, Dielectric properties of nano-particles of zinc sulfide, *Pramana*, 45 (1995) 431.
[205] L. D. Zhang, H. F. Zhang, G. Z. Wang, C. M. Mo and Y. Zhang, Dielectric behaviour of nano-TiO_2 bulks, *Phys. Stat. Sol.*, (a) 157 (1996) 483.
[206] J. M. McHale, A. Auroux, A. J. Perrotta and A. Navrotsky, Surface energies and thermodynamic phase stability in nanocrystalline aluminas, *Science*, 277 (1997) 788.
[207] F. F. Lange, Chemical solution routes to single-crystal thin films, *Science*, 273 (1996) 903.
[208] R. C. Cammarata, Surface and interface stress effects on interfacial and nanostructured materials, *Mater. Sci. Eng.*, A 237 (1997) 180.
[209] T. Eisenhammer and A. Trampert, Formation of quasicrystalline AlCuFe by physical vapor deposition: phase selection via nanocluster nucleation, *Phys. Rev. Lett.*, 78 (1997) 262.
[210] C.-C. Chen, A. B. Herhold, C. S. Johnson and A. P. Alivisatos, Size dependence of structural metastability in semiconductor nanocrystals, *Science*, 276 (1997) 398.
[211] H. F. Holmes, E. L. Fuller Jr. and R. B. Gammage, Heats of immersion in the zirconium oxide — water system, *J. Phys. Chem.*, 76 (1972) 1497.
[212] S. C. Moulzolf, Y. Yu, D. J. Frankel and R. J. Lad, Properties of ZrO_2 films on sapphire prepared by electron cyclotron resonance oxygen-plasma-assited deposition, *J. Vac. Sci. Technol.*, A 15 (1997) 1211.
[213] S. A. Dregia, R. Banerjee and H. L. Fraser, Polymorphic phase stability in thin multilayers, *Scripta Mater.*, 39 (1998) 217.
[214] I. Kosacki, B. Gorman and H. U. Anderson, The microstructure and electrical conductivity correlation in nanocrystalline oxide thin films, The 1997 Joint Int. Meeting ES and ISE, Paris, 31.08.–05.09.1997, Book of Abstracts, Vol. 97–2, p. 2565.
[215] H. Nishiyama and M. Nakamura, Capacitance of disk capacitors, *IEEE Transact. Comp. Hybrids Manufact. Technol.*, 16 (1993) 360.
[216] S. A. Campbell, D. C. Gilmer, X. Wang, M. Hsieh, H.-S. Kim, W. L. Gladfelter and J. Yan, MOSFET transistors fabricated with high-permittivity TiO_2 dielectrics, *IEEE Transact. Electron Devices*, 44 (1997) 104.
[217] A. Muñoz-Paez, Transition metal oxides: geometric and electronic structures, *J. Chem. Education*, 71 (1994) 381.
[218] R. D. Shannon, Dielectric polarizabilities of ions in oxides and fluorides, *J. Appl. Phys.*, 73 (1993) 348.

[219] Y. Ishibashi and M. Iwata, Physical properties of composites, *Jpn. J. Appl. Phys.*, 35 (1996) 5157.
[220] B. Sareni, L. Krähenbühl, A. Beroual and C. Brousseau, Effective dielectric constant of random composite materials, *J. Appl. Phys.*, 81 (1997) 2375.
[221] H. Demiryont, L. R. Thompson and G. J. Collins, Optical and electrical characterization of laser-chemical-vapor-deposited aluminium oxynitride films, *J. Appl. Phys.*, 59 (1986) 3238.
[222] C. Coudray and G. Blaise, Charge trapping induced electromechanical energy, *J. Appl. Phys.*, 80 (1996) 5248.
[223] J. C. Jackson, T. Robinson, O. Oralkan, D. J. Dumin and G. A. Brown, Differentiation between electric breakdowns and dielectric breakdown in thin silicon oxides, *J. Electrochem. Soc.*, 145 (1998) 1033.
[224] J. G. Simmons, Conduction in thin dielectric films, *J. Phys. D: Appl. Phys.*, 4 (1971) 613.
[225] C. Rambaut, K. H. Oh, H. Jaffrezic, J. Koharoff and S. Fayeulle, Molecular dynamic simulation of electron trapping in sapphire, *J. Appl. Phys.*, 81 (1997) 3263.
[226] R. H. Walden, A method for the determination of high-field conduction laws in insulating films in the presence of charge trapping, *J. Appl. Phys.*, 43 (1972) 1178.
[227] J. M. Mohaidat and R. N. Ahmad-Bitar, Current voltage characteristics of metal-insulator-semiconductor structures via quantum mechanical tunneling, *Appl. Phys. Lett.*, 72 (1998) 2256.
[228] J. Frenkel, On pre-preakdown phenomena in insulators and electronic semiconductors, *Phys. Rev.*, 54 (1938) 647.
[229] V. A. Laleko, I. I. Dragan and N. Yu. Ershova, Investigation of the kinetics of electrical breakdown of tantalum oxide layers, *Phys. Stat. Sol.*, (a) 141 (1994) K11.
[230] A. N. Krasnov, R. C. Bajcar and P. G. Hofstra, Optimization of alternating-current thin-film electroluminescent displays, *J. Vac. Sci. Technol.*, A 16 (1998) 906.
[231] B. Lee, J. N. Kondo, F. Wakabayashi and K. Domen, Infrared spectroscopic study of high-temperature behaviour of the Brønsted acidic hydroxyl groups on zeolites, *Bull. Chem. Soc. Jpn.*, 71 (1998) 2149.
[232] H. Siimon and J. Aarik, Thickness profiles of thin films caused by secondary reactions in flow-type atomic layer deposition reactors, *J. Phys. D., Appl. Phys.*, 30 (1997) 1725.
[233] H. Siimon, J. Aarik and T. Uustare, Effects of HCl readsorption on film growth in atomic layer CVD of TiO_2, *Electrochem. Soc. Proc.*, 97–25 (1997) 131.
[234] M. A. Barteau, Site requirements of reactions on oxide surfaces, *J. Vac. Sci. Technol.*, A 11 (1993) 2162; V. E. Henrich and P. A. Cox, Fundamentals of gas-surface interactions on metal oxides, *Appl. Surf. Sci.*, 72 (1993) 277.
[235] H. Demiryont, J. R. Sites and K. Geib, Effects of oxygen content on the properties of tantalum oxide films deposited by ion-beam sputtering, *Appl. Opt.*, 24 (1985) 90.
[236] K. Kukli, M. Ritala and M. Leskelä, unpublished results.
[237] H. Siimon and J. Aarik, Reactivities of $TaCl_5$ and H_2O as precursors for atomic layer deposition, *J. Phys.* IV, 5 (1995) C5-277.

[238] J.-H. Yun, S.-W. Rhee, Experimental and theoretical study of step coverage in metal-organic chemical vapor deposition of tantalum oxide thin films, *Thin Solid Films*, 292 (1997) 324.
[239] K. Kukli, M. Ritala and M. Leskelä, Dielectric oxide nanolaminates deposited by atomic layer epitaxy, *Electrochem. Soc. Proc.*, 97–25 (1997) 1137.
[240] A. F. Wells, Structural inorganic chemistry, Fourth edition, Clarendon Press, Oxford, 1975, p. 453–454.
[241] R. Ray, Model for interface reaction control in superplastic deformation of non-stoichiometric ceramics, *Mater. Sci. Eng.*, A 166 (1993) 89.
[242] C. G. Levi, Metastability and microstructure evolution in the synthesis of inorganics from precursors, *Acta Mater.*, 46 (1998) 787.
[243] O. S. Gefle, S. M. Lebedev and V. Ya. Uschakov, The mechanism of the barrier effect in solid dielectrics, *J. Phys. D: Appl. Phys.*, 30 (1997) 3267.
[244] T. Nagaya and Y. Ishibashi, Dielectric breakdown in polycrystalline system, *Jpn. J. Appl. Phys.*, 36 (1997) 6136.
[245] J. Jamnik and J. Maier, Charge transport and chemical diffusion involving boundaries, *Solid State Ionics*, 94 (1997) 189.
[246] R. Ruus, A. Kikas, A. Saar, A. Ausmees, E. Nõmmiste, J. Aarik, A. Aidla, T. Uustare and I. Martinson, Ti 2p and O 1s X-ray absorption of TiO_2 polymorphs, *Solid State Comm.*, 104 (1997) 199.
[247] J. Männik, J. Aarik, I. Sildos, A. Kasikov and A. Aidla, Spectroscopic study of thin titanium dioxide films grown by atomic layer deposition, *Proc. Estonian Acad. Sci. Phys. Math.*, 47 (1998) 56.

PUBLICATIONS

I

Reprinted from *Thin Solid Films*, Vol. 260 (1995),
K. Kukli, J. Aarik, A. Aidla, O. Kohan, T. Uustare and V. Sammelselg,
Properties of tantalum oxide thin films grown by atomic layer deposition,
pp. 135–142, Copyright 1998, with permission from Elsevier Science

ELSEVIER

Thin Solid Films 260 (1995) 135–142

thin solid films

Properties of tantalum oxide thin films grown by atomic layer deposition

Kaupo Kukli[a,*], Jaan Aarik[a], Aleks Aidla[a], Oksana Kohan[a], Teet Uustare[a], Väino Sammelselg[b]

[a]*University of Tartu, Institute of Experimental Physics and Technology, EE2400 Tartu, Estonia*
[b]*Institute of Physics of Estonian Academy of Sciences, EE2400 Tartu, Estonia*

Received 27 July 1994; accepted 28 September 1994

Abstract

Thin tantalum oxide films were deposited using atomic layer deposition from $TaCl_5$ and H_2O at temperatures in the range 80–500 C. The films deposited at temperatures below 300 C were predominantly amorphous, whereas those grown at higher temperatures were polycrystalline containing the phases TaO_2 and Ta_2O_5. The oxygen to tantalum mass concentration ratio corresponded to that of TaO_2 at all growth temperatures. The optical band gap was close to 4.2 eV for amorphous films and ranged from 3.9 to 4.5 eV for polycrystalline films. The refractive index measured at $\lambda = 550$ nm increased from 1.97 to 2.20 with an increase in growth temperature from 80 to 300 C. The films deposited at 80 C showed low absorption with absorption coefficients of less than 100 cm^{-1} in the visible region.

Keywords: Deposition process; Optical coatings; Oxides; Structural properties

1. Introduction

Tantalum oxide has been studied extensively due to its good potential for industrial applications, in particular in electronic and optoelectronic technology. Tantalum oxide films have been employed as optical coatings and waveguides [1–6]. Because of its high dielectric constant, tantalum oxide is a promising candidate for capacitor insulators in high-density dynamic memories (DRAM) [7,8] and in devices of ultra-large-scale integration (ULSI) [9]. Tantalum oxide is also used as a gate dielectric in thin film transistors (TFTs) [10], as an active layer in solid state chemical sensors [11] and as a dielectric material in electroluminescent devices [12]. In addition, crystalline Ta_2O_5 films have shown piezoelectric and surface acoustic wave (SAW) characteristics [13]. The high chemical stability of Ta_2O_5 films allows the application of this material as a corrosion-resistant oxide coating [14].

A number of deposition methods and several source materials can be used for the deposition of tantalum oxide films. Physical deposition methods, such as reactive evaporation (RE), reactive sputtering (SP), reactive ion plating (IP) [1,6,9] and pulsed-laser-assisted evaporation [5], are accepted for tantalum oxide film growth. Tantalum oxide thin films of extreme geometries have been deposited chemically through surface reactions using chemical vapour deposition (CVD) [3,7,9,13–15]. The application of plasma-enhanced CVD (PECVD) [8,16] and photo-CVD processes using $Ta(OC_2H_5)_5$ [17], $Ta(OCH_3)_5$ [18], $Ta(DPM)_4Cl$ [13] or $TaCl_5$ [9,19] as source materials has been discussed recently. In addition to the methods listed above, atomic layer deposition (ALD) has also been used for growing tantalum oxide films [21–23]. It should be noted that, in the latter references, the growth process was described as atomic layer epitaxy (ALE) where the word "epitaxy" was used to emphasize the sequential deposition of film constituents.

Differences in the material stoichiometry have been observed when different techniques are used to grow

* Corresponding author.

SSDI 0040-6090(94)06388-5

tantalum oxide films [6,16]. These differences, correlated with the deposition conditions, have a strong influence on the optical parameters [6]. Stoichiometric Ta_2O_5 deposited by ion-beam sputtering [2] and pulsed-laser-assisted evaporation [5] is a non-absorbing, non-dispersive material for optical coatings, whereas suboxide films with progressively decreasing oxygen ratios show an increase in refractive index and absorption coefficient [2]. A low absorption coefficient (less than 1000 cm^{-1}) below the fundamental absorption edge ($h\nu < 4.2$ eV) has been found for Ta_2O_5 films deposited by magnetron reactive sputtering [1].

According to some investigations [3,9], tantalum oxide films grown by CVD from $Ta(OC_2H_5)_5$ contain less oxygen than samples deposited by physical methods. Two different reactions resulting in the composition of Ta_2O_5 and TaO_2 have been considered in the CVD process [3]. Again, the suboxide (TaO_2) is proposed to be responsible for the increase in the absorption coefficient.

As a rule, tantalum oxide films as-deposited at temperatures below 700 °C exhibit an amorphous structure [1,5,14–17,19–21]. However, some deposition techniques allow the deposition of ordered tantalum oxide films. Oriented Ta_2O_5 films have been grown by conventional low-pressure CVD on quartz and Si(100) substrates at 625 °C and higher temperatures using $Ta(OC_2H_5)_5$ and $Ta(DPM)_4Cl$ as precursors [13]. Crystalline films have also been deposited by laser-CVD [18] from $Ta(OCH_3)_5$ on quartz substrates. The presence of a crystalline phase has also been detected in predominantly amorphous Ta_2O_5 films grown by PECVD [8] from $Ta(OC_2H_5)_5$.

There are relatively few data concerning the ALD of tantalum oxide films. $TaCl_5$ and H_2O have been used as precursors with growth at reactor temperatures of 500 °C [20] and 300 °C [21,22]. The structure of tantalum oxide films grown on glass substrates is amorphous. The films deposited at 500 °C have been reported to be stoichiometric Ta_2O_5 with smooth, uniform surfaces [19].

The main advantage of ALD is the possibility to control the film thickness very precisely and to grow films of uniform thickness on large areas and profiled substrates. This is due to the specific feature of ALD whereby the exposures of the substrate surface to different precursors are separated in real time. The adsorption of every precursor is self-limited and is independent of the exposure time and the precursor pressure if sufficient precursor doses are used [24].

However, recent studies have demonstrated that the conditions for self-limited growth of tantalum oxide are not completely achieved at substrate temperatures above 300 °C [25]. On the other hand, it is desirable that low deposition temperatures be used in some applications. Therefore the investigation of the properties of tantalum oxide grown by ALD over a wide temperature range, including temperatures below 300 °C, is of great interest. Furthermore, to our knowledge, no data concerning the effect of the substrate structure on the properties of tantalum oxide films grown by ALD from $TaCl_5$ and H_2O have been published. Thus we have studied the characteristics of tantalum oxide films grown by ALD on different substrates. In this study, we investigate the properties of tantalum oxide films grown on soda lime glass, fused silica and monocrystalline silicon at temperatures in the range 80–500 °C.

2. Experimental details

The experiments were carried out in a horizontal flow-type ALD reactor. The equipment parameters used in our experiments have been described previously [23].

The films were grown on glass, fused silica and silicon substrates. The maximum size of the glass substrates was 30 mm × 60 mm, whereas the typical sizes of the silica and silicon substrates were 30 mm × 40 mm and 10 mm × 10 mm respectively. The glass substrates were placed at 60 mm and the silica and silicon substrates at 80 mm distances from the gas inlets. Films were grown at reactor temperatures of 80, 160, 300, 400 and 500 °C. N_2 was used as carrier gas at a pressure of 250 Pa at the reactor outlet.

A single ALD cycle consisted of a sequence of pulses of volatilized precursors separated by purge times. The substrate surface was exposed to $TaCl_5$ and H_2O beams for 1–2 s, while purge times of 0.3 and 1.7–2.7 s were used after $TaCl_5$ and H_2O pulses respectively. The number of cycles used for a particular sample growth was varied from 1000 to 6000. Suitable conditions for film growth were established using real time measurements carried out with a quartz microbalance before the beginning of the growth process. The mass sensor of the microbalance was placed in the reaction zone at a distance of 135 mm from the gas inlet. Other details of the apparatus for these measurements have been published previously [26,27]. The reactant doses and purge times were adjusted to sufficiently high values to achieve a growth rate which was independent of a further increase in the $TaCl_5$ source temperature, H_2O flow rate and purge times. The typical value of the H_2O molecular flow was 733 Pa cm^3 s^{-1}. At the growth temperatures of 300 and 500 °C, the H_2O doses were varied between 440 and 1340 Pa cm^3 s^{-1} in order to investigate the influence of changes in H_2O vapour pressure on the film structure.

The thermal stability of the films was studied by annealing for 6 h at 700 °C in air and pure N_2.

Optical transmittance spectra were taken from films grown on silica substrates using a Specord 40 M optical

spectrometer. Refractive indices, absorption coefficients and film thicknesses were calculated using a method based on the analysis of the transmittance spectrum of a weakly absorbing film and non-absorbing substrate system [28]. The absorption coefficient for the spectral region of low transparency was recorded directly by a Hitachi 340 spectrometer. The absorption spectra were used for optical band gap estimation. The IR absorption spectra of films formed on silicon substrates at 80, 160 and 300 °C were measured using a Specord 75 IR (Carl Zeiss, Jena) spectrometer in the wavenumber range 400–4000 cm^{-1}.

The composition of films deposited on silicon substrates was examined via electron probe X-ray microanalysis (EPMA) using a JSM-35 (Jeol Ltd.) equipment supplied with an energy dispersive X-ray spectrometer 860 Series 2 (Link Systems). As the films were very thin, the measurements were carried out using a low-energy (4–6 kV) primary electron beam. The signal of Si Kα radiation generated in the Si substrate was used to determine the upper limit of the probe energy. Tantalum foil was used as a standard for the determination of the tantalum mass concentration, ZnO and Al_2O_3 for oxygen concentration analysis and KCl for chloride concentration analysis.

Refraction high energy electron diffraction (RHEED) and X-ray diffractometry (XRD) using Cu Kα radiation were applied to investigate the film structure and crystallinity. XRD analysis was carried out using a Philips MPD 1880 powder X-ray diffractometer at the Department of Chemistry, University of Helsinki.

3. Results

3.1. Growth rate

The growth rate of the films shows a strong dependence on the reactor temperature T_R (Fig. 1). It reaches 0.16 nm per cycle at 80 °C and decreases to 0.043 nm per cycle at 500 °C. This decrease is probably due to changes in the growth mechanism. According to the mechanism proposed earlier for Al_2O_3 film growth [29], the hydroxyl groups which appear on the film surface at lower temperatures may be responsible for the stimulation of exchange reactions during the adsorption of aluminium chloride. We assume that analogous processes take place in the case of tantalum chloride. A certain amount of chlorine with a relatively high ionic radius is released during the adsorption process and therefore tantalum (with remaining chloride) can deposit more densely on the sites available on the surface. However, the contribution of OH groups in film formation seems to be limited to the participation in surface reactions because the amount of residual O–H bonds in the TaO_x films grown at 80, 160 and 300 °C is below

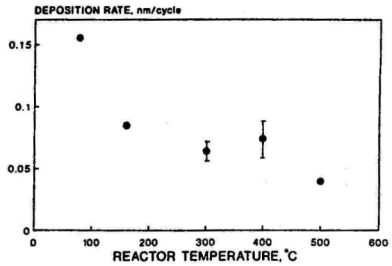

Fig. 1. Temperature dependence of the growth rate for films deposited on silica substrates.

the detection limit of IR spectroscopy. In contrast, for the amorphous Al_2O_3 film grown in separate experiments from $AlCl_3$ and H_2O by ALD at 70 °C, the absorption peak corresponding to O–H bonds was easily detected in the IR spectra.

3.2. Composition and structure

Fig. 2 shows the results of the compositional analysis of the films carried out by EPMA. The relatively high content of chlorine residues at a growth temperature of 80 °C (6.08%) decreases rapidly to 0.99% at 160 °C and is undetectable at 400 and 500 °C. The data presented in Fig. 2 also allow the calculation of the oxygen to tantalum mass concentration ratios $C(O)/C(Ta)$. The variation in $C(O)/C(Ta)$ is less than 5% over the entire temperature range investigated, while the mean value of $C(O)/C(Ta)$ is equal to 0.170. The latter value is similar to the oxygen to tantalum mass ratio for TaO_2 (0.1768). For Ta_2O_5, $C(O)/C(Ta) = 0.2209$. Thus the oxygen deficiency in our tantalum oxide films is evident.

The structures of the films grown on silicon and glass substrates were studied by RHEED and XRD respectively. RHEED analysis shows that all of the

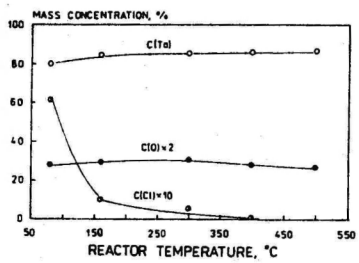

Fig. 2. Composition of tantalum oxide films as a function of the growth temperature.

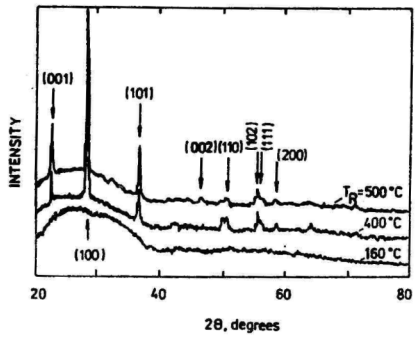

Fig. 3. X-Ray diffraction patterns of tantalum oxide films grown on glass substrates. Arrows indicate the reflections corresponding to the distances between the lattice planes for δ-Ta_2O_5.

films grown at 80 and 160 °C are amorphous and those grown at 400 and 500 °C are polycrystalline. The reflections corresponding to both hexagonal δ-Ta_2O_5 and tetragonal TaO_2 were observed in the RHEED patterns of the films deposited at 400 and 500 °C. The tetragonal structure dominated at 400 °C, whereas the hexagonal structure prevailed at 500 C. XRD studies confirmed that the films deposited at 80 and 160 C were amorphous. For the films grown at 400 and 500 C, peaks characteristic of hexagonal δ-Ta_2O_5 (Fig. 3) were recorded. It should be noted that no crystallization was observed after annealing of the amorphous films at 700 °C.

The intense background caused by scattering from material in an amorphous state was observed in RHEED patterns for films grown at 400 C. This indicates a low crystallinity of these films. In the RHEED patterns for films grown at 500 C, the background was somewhat weaker. However, the reflections corresponding to smaller interplanar distances were still not resolved from the background. Therefore crystallization was incomplete even at growth temperatures as high as 500 °C. As the ratio of $C(O)/C(Ta)$ determined by EPMA was even smaller than that for pure TaO_2, the existence of a low-ordered phase with a high oxygen deficiency is evident. We could not determine the ratio of δ-Ta_2O_5 to TaO_2 reliably because of the presence of the amorphous background.

Amorphous and polycrystalline films were grown at 300 C. RHEED studies demonstrated that changes in the H_2O dose due to the variation of the H_2O flow rate caused detectable changes in the film structure. The films grown at the highest H_2O flow rate (1340 Pa cm^3 s^{-1}) were amorphous, whereas those grown at 1106 Pa cm^3 s^{-1} and lower H_2O flow rates were polycrystalline. The polycrystalline films had a tetragonal structure with

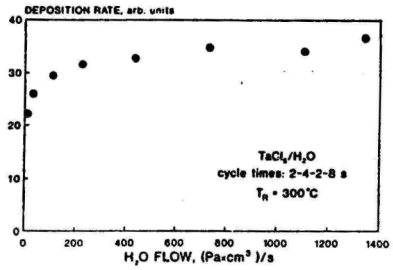

Fig. 4. Deposition rate measured by a mass sensor as a function of the H_2O molecular flow. Purge times significantly higher than those applied during film growth were used in order to enhance the accuracy of the measurements.

lattice parameters of $a = 4.49 \pm 0.02$ Å and $c = 2.915 \pm 0.005$ Å which are slightly lower than the values published earlier for TaO_2 by Schonberg [30] ($a = 4.709$ Å and $c = 3.065$ Å). Lower values of the lattice parameters should indicate oxygen deficiency. However, reflections corresponding to the lower oxides were not observed. The possible variations in the film composition were unfortunately below the detection limit of EPMA. The real time deposit mass measurements demonstrate that an increase in the H_2O flow rate from 440 to 1340 Pa cm^3 s^{-1} causes an increase in the growth rate by approximately 10% (Fig. 4). No changes in the film structure were observed when the $TaCl_5$ dose was varied. However, the $TaCl_5$ dose was varied by a factor of only three, because the etching of the growing film by $TaCl_5$ occurred at high doses [25] and low doses were not sufficient to provide self-limited growth.

It is evident that the effect of precursor doses on the film composition and structure needs more detailed study. However, at the moment, we can note that a reactor temperature of 300 C seems to be the "critical" temperature at which the crystallization of TaO_2 starts in the ALD process.

3.3. Optical properties

Fig. 5 shows the transmittance spectrum of a tantalum oxide film deposited at 80 C. It can be seen that the film is of good optical quality. The absorption coefficient α, calculated from this transmittance spectrum, is below 100 cm^{-1} in the visible spectral range. However, such low values of α were not obtained for films grown at higher reactor temperatures. Fig. 6 demonstrates that α increases monotonically for two orders of magnitude when the growth temperature is increased to 500 C. Comparing the data presented in Fig. 6 with the surface morphology of the films (Fig. 7), we can conclude that the high values of α corresponding

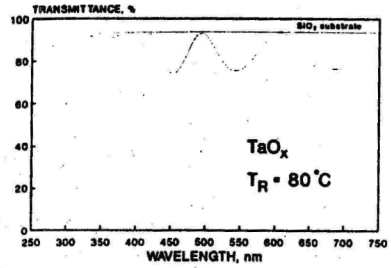

Fig. 5. Transmittance spectrum of tantalum oxide film grown at 80 °C. The film thickness calculated from this spectrum is 433 nm.

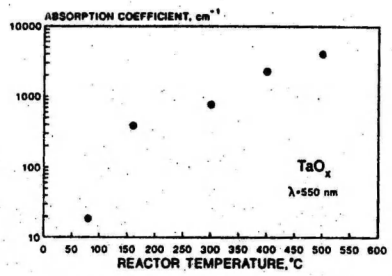

Fig. 6. Dependence of the absorption coefficient on the reactor temperature used for film growth.

to high growth temperatures are mainly caused by the light scattering on the rough surfaces of the films (Figs. 7(c)–7(e)). On the other hand, the surface roughness is strongly enhanced by the formation of crystallites. Indeed, we demonstrated in Section 3.2 that the films grown at 300 °C using lower H_2O doses are polycrystalline. The surface roughness of these films is higher (Figs. 7(d) and 7(e)) than that of films grown at higher H_2O doses when crystallization is not observed.

The high optical losses of the films grown at 400 and 500 °C did not enable us to calculate the refractive index n reliably. However, the dispersion curves of the refractive index were obtained for films grown at lower temperatures (Fig. 8). The values of n at $\lambda = 550$ nm are equal to 1.97 ± 0.05, 2.11 ± 0.06 and 2.2 ± 0.06 for films grown at 80, 160 and 300 °C respectively. The last value is, within experimental error, the same as that obtained by Kattelus et al. [22] ($n = 2.23$) for tantalum oxide grown by ALD (ALE) at 300 °C.

Proceeding from the dependence of the absorption coefficient on the photon energy, we estimated the optical band gap E_g using the extrapolation of the approximately linear parts of the $(h\nu\alpha)^{1/2}$ vs. $h\nu$ curves ($h\nu$ is the photon energy) to $\alpha = 0$ [2] (broken lines in Fig. 9). Fig. 9 shows that, for the films grown at 80–300 °C, the absorption coefficient above a threshold follows well the $(h\nu - E_g)^2$ energy dependence characteristic of indirectly allowed transitions. For polycrystalline films grown at 400 and 500 °C, two regions of steep increase of the absorption coefficient with an increase in the photon energy are observed. Therefore two different values of E_g can be found for these films (Figs. 9 and 10). The possible reasons for this behaviour of the $(h\nu\alpha)^{1/2}$ vs. $h\nu$ curves are discussed below.

4. Discussion

The results presented in Section 3.2 clearly indicate that suboxides are preferentially formed during the low-temperature ALD growth of tantalum oxide when $TaCl_5$ and H_2O are used as precursors. This is not surprising because oxygen deficiency has also been observed in ion-beam-sputtered [6] and CVD-grown [3] tantalum oxide films, as well as in those deposited by laser-assisted CVD [16]. However, the suboxides presented in these films were amorphous [3,6,16]. Also, the tantalum oxide films grown to date by ALD (ALE) by Pessa et al. [20] and Kattelus et al. [21,22] have been amorphous. In contrast, the films studied in this work tended to be crystalline when grown at temperatures as low as 300 °C. Moreover, as shown above, crystalline films can be grown on amorphous substrates.

Proceeding from the last circumstance, secondary crystallization can be considered as a possible reason for the growth of polycrystalline films. An amorphous layer is formed first and crystallization takes place inside the as-grown layer.

In the case of Ta_2O_5, this type of crystallization has been observed at 625 °C and higher temperatures [13–16]. However, annealing of our amorphous films at 700 °C during a time period equal to the duration of the longest ALD process did not cause detectable crystallization. Consequently, the formation of the crystalline structure is caused by other effects. Most probably, surface migration of chemisorbed intermediates and/or selective chemisorption of the precursors are responsible for crystallization. In order to understand the mechanisms of surface migration and to determine the species responsible for crystallization, the growth kinetics should be studied in more detail. At present, it seems that volatile oxochlorides, formed as a result of surface reactions between tantalum oxide and gaseous $TaCl_5$ [31], may be the migrating intermediates which strongly affect the atomic layer growth of tantalum oxide.

It should be noted that significant agglomeration occurs at temperatures as low as 160 °C, even when a

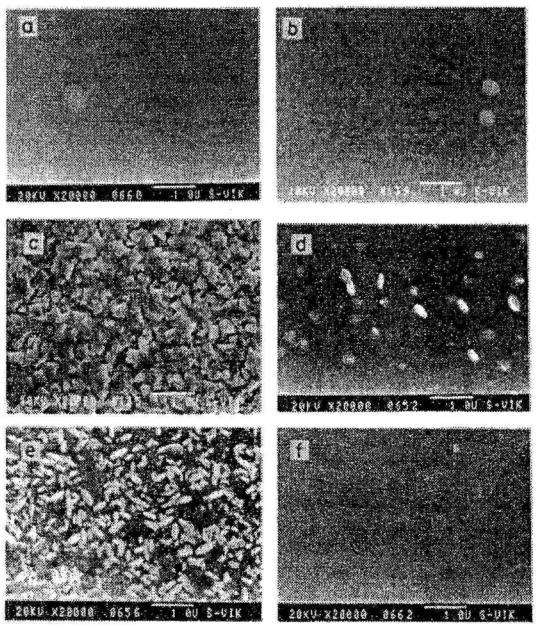

Fig. 7. Surface morphology of tantalum oxide films grown at 80 °C (a), 160 °C (b), 400 °C (c), and 300 °C (d–f). H_2O molecular flows are 733 (a–d), 1106 (e) and 1440 Pa cm^3 s^{-1} (f).

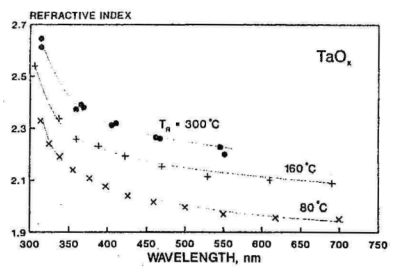

Fig. 8. Dispersion curves for tantalum oxide films grown on silica substrates. Refractive indices are calculated from the transmittance spectra.

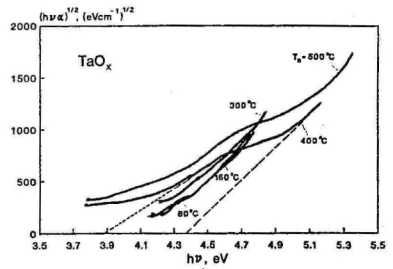

Fig. 9. $(h\nu\alpha)^{1/2}$ vs. $h\nu$ plots for tantalum oxide films grown at different reactor temperatures.

detectable structure is not formed. This agglomeration seems to precede the crystallization and is the reason for the strong relationship between the absorption coefficient and the growth temperature in the range 80–300 °C where the most significant changes in absorption take place. There are two explanations for the suppressed agglomeration at low temperatures. Firstly, the surface mobility of the adsorbed particles is lower. Secondly, the surface reactions may be incomplete. For this reason, the chlorine residues remain in the film (Fig. 2) and can restrict the formation of agglomerates.

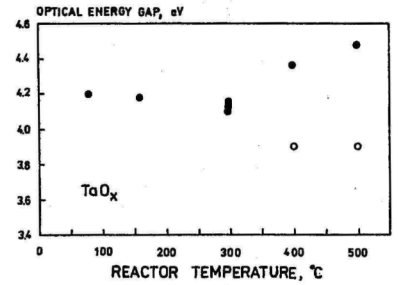

Fig. 10. Optical energy gap for tantalum oxide films grown at different reactor temperatures. At lower growth temperatures, up to 300 °C, only single values for the optical energy gap were detected. At higher growth temperatures, lower and higher energy gap values for the same sample film were detected and are marked with open and filled circles respectively.

The significant difference between the ionic radius of oxygen and chlorine may prevent ordering inside a single agglomerate. This ordering seems to be the main reason for the stability of the agglomerates.

The role of chlorine residues was demonstrated in recent experiments where TiO_2 was grown from $TiCl_4$ and H_2O. Using different doses of H_2O we could control the concentration of chlorine as well as the absorption coefficient. We established that α increases with a decrease in the chlorine content [32].

Comparing the data on the structure and composition of our tantalum oxide films, it can be seen that the crystalline structure occurs at temperatures at which the concentration of residual chlorine decreases to near zero. Thus the expectation that the maintenance of a certain stoichiometry is a precondition for crystallization seems to be confirmed. However, the effect of H_2O dose on the film structure at 300 °C demonstrates that the surface reactions taking place at these temperatures and H_2O doses are not complete in spite of the fact that chlorine is removed at low H_2O doses. In this context, it could be supposed that, initially, the suboxides (in particular TaO_2) are formed in the reaction between surface-bound oxochlorides and impinging H_2O molecules. Simultaneously, the chlorine is completely removed from the adsorbate. Furthermore, the oxidation of these suboxides takes place in the H_2O flow. Presumably, the latter process is slower and thus higher H_2O pressures and substrate temperatures are needed to realize it.

An unexpected result of this study is that the appearance of lower oxides in the films does not cause an increase in optical losses as observed previously [2]. Moreover, we obtained the lowest value of a for the film of highest non-stoichiometry, while the absorption coefficient of this film was even lower than that for stoichiometric ion-beam-sputtered films [2]. At the same time, we observed an increase in optical losses and the appearance of a long-wave tail in the absorption spectrum when agglomeration and crystallization occurred. Thus we can suppose that the presence of lower oxides in the films grown by ion-beam sputtering [2] renders agglomeration more favourable and this agglomeration (but not the non-stoichiometry itself) is responsible for the changes observed in the absorption coefficient and absorption spectrum.

The long-wave tail which appears in the absorption spectrum of polycrystalline tantalum oxide (Fig. 9) is very similar to that observed for polycrystalline silicon [33]. It has been shown that the absorption coefficient of polycrystalline silicon is significantly higher than that of amorphous silicon [33], while this effect is most clearly observable near the absorption edge.

The dependence of the optical band gap on the structure of the tantalum oxide films is also similar to that observed for silicon [30]. The transition from the amorphous phase to the crystalline phase causes a decrease in the band gap in both cases. Similarly, two different values of E_g can be found by approximation of different regions of the $(h\nu\alpha)^{1/2}$ vs. $h\nu$ plots for both tantalum oxide and silicon. Thus we must consider that the changes in the absorption spectrum, particularly in the long-wave tail, can be strongly influenced by the film structure and light scattering on the surface and/or bulk inhomogeneities. However, for our films grown at 300 °C and lower temperatures, the values of the optical band gap seem to be reliable because in this case the tail of the absorption edge is short.

The situation is more complicated for films grown at 400 and 500 °C. These films contain crystalline TaO_2 as well as Ta_2O_5. Therefore it seems reasonable to assume that the higher transition energy for these films (Fig. 10) is caused by the contribution of hexagonal Ta_2O_5 crystallites, while the lower value of the transition energy can be associated with the presence of lower oxides, in particular TaO_2. Unfortunately, when considering analogous changes in the absorption spectrum of silicon caused by variations in structure [33], no straightforward conclusions about the effect of film composition on the experimental values of E_g could be made. However, the values of the optical band gap assigned to our films are close to those obtained by other workers and range from 4.0 eV for films with a significant suboxide content [2] to 4.5 eV for stoichiometric Ta_2O_5 [2,34].

5. Conclusions

The present study shows that the properties of tantalum oxide films grown by ALD from $TaCl_5$ and

H_2O depend significantly on the growth conditions. The films deposited below 300 °C were predominantly amorphous, whereas those grown at 400 and 500 °C exhibited a polycrystalline structure. The structure of the films deposited at 300 °C was dependent on the deposition conditions, such as the H_2O flow in the ALD reactor. Both TaO_2 and Ta_2O_5 crystalline phases were detected in the polycrystalline films. The oxygen to tantalum mass concentration ratio was close to the ratio of TaO_2 at all deposition temperatures. The value of the optical band gap for amorphous films was close to 4.2 eV, whereas E_g values ranging from 3.9 to 4.5 eV could be assigned to the films grown at 400 and 500 °C. The refractive index measured at $\lambda = 550$ nm increased from 1.97 to 2.20 with an increase in the growth temperature from 80 to 300 °C. The films deposited at 80 °C exhibited low absorption with an absorption coefficient of less than 100 cm^{-1} in the visible region.

The low absorption index, together with a relatively high refractive index in the visible region, makes the tantalum oxide films grown at temperatures below 300 °C suitable for solar cell antireflection coatings, especially when low deposition temperatures are required to avoid the destructive effect of high temperature on the device structure. With regard to this application, ALD, which provides excellent in situ thickness control, seems to be a promising method for tantalum oxide thin film growth.

Acknowledgements

The authors are grateful to J. Asari, A.-A. Kiisler, H. Kelle and A. Jaek for technical assistance. Gratitude is also expressed to M. Leskelä and M. Ritala for use of the XRD equipment at the University of Helsinki. The scanning electron microscopy and EPMA studies were carried out using the equipment JSM-35 donated by Studsvik AB (Sweden) to the University of Tartu. This work was supported by the Estonian Science Foundation (Grants 213 and 750).

References

[1] F. Rubio, J. Denis, J.M. Albella and J.M. Martinez-Duart, *Thin Solid Films, 90* (1982) 405.
[2] H. Demiryont, J.R. Sites and K. Geib, *Appl. Opt., 24* (1985) 490.
[3] S.B. Desu, *Mater. Chem. Phys., 31* (1992) 341.
[4] A.J. Waldorf, J.A. Dobrowolski, B.T. Sullivan and L.M. Plante, *Appl. Opt., 32* (1993) 5583.
[5] H.O. Sankur and W. Gunning, *Appl. Opt., 28* (1989) 2806.
[6] K. Gürtler, K. Bange, W. Wagner, F. Rauch and H. Hantsche, *Thin Solid Films, 175* (1989) 185.
[7] G.Q. Lo, D.L. Kwong and S. Lee, *Appl. Phys. Lett., 62* (1993) 97.
[8] P.A. Murawala, M. Sawai, T. Tatsuta, O. Tsuji, Shizuo Fujita and Shigeo Fujita, *Jpn. J. Appl. Phys., 32* (1993) 368.
[9] K. Shimizu, M. Katayama, H. Funaki, E. Arai, M. Nakata, Y. Ohji and R. Imura, *J. Appl. Phys., 74* (1993) 375.
[10] M. Matsui, H. Nagayoshi, G. Muto, S. Tanimoto, K. Kuroiwa and J. Tarui, *Jpn. J. Appl. Phys., 29* (1990) 62.
[11] U. Teravaninthorn, Y. Miyahara and T. Moriizumi, *Jpn. J. Appl. Phys., 26* (1987) 2116.
[12] C.T. Hsu, Y.K. Su and M. Yokoyama, *SPIE Display Technol., 1815* (1992) 288.
[13] K. Tominaga, R. Muhammet, I. Kobayashi and M. Okada, *Jpn. J. Appl. Phys., 31* (1992) L585.
[14] C.H. An and K. Sugimoto, *J. Electrochem. Soc., 139* (1992) 1956.
[15] A.P. Lane, *Mater. Res. Soc. Symp. Proc., 250* (1992) 331.
[16] S.-O. Kim, J.S. Bun and H.J. Kim, *Thin Solid Films, 206* (1991) 102.
[17] Y. Nishimura, K. Tokunaga and M. Tsuji, *Thin Solid Films, 226* (1993) 144.
[18] A. Watanabe, M. Mukaida, Y. Imai, K. Osato, T. Kameyama and K. Fukuda, *J. Mater. Sci., 28* (1993) 5363.
[19] S. Tanimoto, M. Matsui, K. Kamisako, K. Kuroiwa and Y. Tarui, *J. Electrochem. Soc., 139* (1992) 320.
[20] M. Pessa, R. Mäkelä and T. Suntola, *Appl. Phys. Lett., 38* (1981) 131.
[21] H. Kattelus, M. Ylilammi, J. Saarilahti, J. Antson and S. Lindfors, *Thin Solid Films, 225* (1993) 296.
[22] H. Kattelus, M. Ylilammi, J. Salmi, T. Ranta-aho, E. Nykänen and I. Suni, *Mater. Res. Soc. Symp. Proc., 284* (1993) 511.
[23] J. Aarik, A. Aidla and K. Kukli, *Appl. Surf. Sci., 75* (1994) 180.
[24] T. Suntola, *Mater. Sci. Rep., 7* (1989) 266.
[25] J. Aarik, A. Aidla, K. Kukli and T. Uustare, *J. Cryst. Growth, 144* (1994) 116.
[26] J. Aarik, A. Aidla, A. Jaek, M. Leskelä and L. Niinistö, *J. Mater. Chem., 4* (1994) 1239.
[27] J. Aarik, A. Aidla, A. Jaek, M. Leskelä and L. Niinistö, *Appl. Surf. Sci., 75* (1994) 33.
[28] A.S. Valeev, *Opt. Spectrosc. USSR, 15* (1963) 269.
[29] J. Aarik, A. Aidla, A. Jaek, A.-A. Kiisler and A.-A. Tammik, *Acta Polytech. Scand., 195* (1990) 201.
[30] N. Schonberg, *Acta Chem. Scand., 8* (1954) 240.
[31] H. von Schäfer and E. Sibbing, *Z. Anorg. Allg. Chem., 305* (1960) 341.
[32] J. Aarik, A. Aidla, T. Uustare and V. Sammelselg, *J. Cryst. Growth*, in press.
[33] Y. He, C. Jin, G. Cheng, L. Wang, X. Liu and G.Y. Hu, *J. Appl. Phys., 75* (1994) 797.
[34] E.E. Khawaja and S.G. Tomlin, *Thin Solid Films, 30* (1975) 361.

II

Reprinted from *Applied Surface Science*, Vol. 103 (1996),
J. Aarik, K. Kukli, A. Aidla and L. Pung,
Mechanisms of suboxide growth and etching in atomic layer deposition of tantalum oxide from $TaCl_5$ and H_2O, pp. 331–341,

ELSEVIER

Applied Surface Science 103 (1996) 331–341

applied surface science

Mechanisms of suboxide growth and etching in atomic layer deposition of tantalum oxide from $TaCl_5$ and H_2O

Jaan Aarik, Kaupo Kukli *, Aleks Aidla, Lembit Pung

University of Tartu, Institute of Experimental Physics and Technology, EE-2400 Tartu, Estonia

Received 17 January 1996; accepted 22 June 1996

Abstract

In the present study, the possible surface processes during the atomic layer deposition (atomic layer epitaxy) of tantalum oxide thin films from $TaCl_5$ and H_2O were studied. Surface mass exchange was detected by means of quartz crystalline mass sensor (QCM) during the growth process. Using the results of QCM measurements and those of electron-probe composition analysis, Cl/Ta and O/Ta atomic ratios as well as stable surface concentration of Ta and Cl atoms in the intermediate surface layer were calculated versus growth temperature. The mechanisms of suboxide growth and etching in the continuous precursor flow was evaluated on the basis of the measurement results and thermodynamical probability for different reactions.

1. Introduction

Tantalum oxide thin films have been intensively studied because of their wide applicability in technology. Dielectric layers in capacitor technology [1] and electroluminescent devices [2] as well as antireflection coatings for solar cells [3,4] and optical waveguides [5] have been the main applications of the Ta_2O_5 films.

Physical deposition [2,6,7] as well as chemical vapor deposition (CVD) [1,8–10] methods have been used for Ta_2O_5 film growth. Different tantalum precursors such as $Ta(thd)_5$ [10], $Ta(OCH_3)_5$, $Ta(OC_2H_5)_5$, $Ta[N(CH_3)_2]_5$ and $TaCl_5$ [9] have been applied in the CVD deposition of Ta_2O_5. Among other precursors $TaCl_5$ has been preferred in order to avoid the carbon contamination in growing films [11].

Atomic layer deposition (ALD, frequently referred to as atomic layer epitaxy – ALE) as well as related digital chemical vapor deposition method [8] has been also used for tantalum oxide film growth using $TaCl_5$ [8,12–16] or $Ta(OC_2H_5)_5$ [17] as tantalum sources, and H_2O [12–17] or O_2 [8] as oxygen sources. The characteristic feature of the ALD process is that the active components are introduced into the reaction zone subsequently. The desired solid film is formed via saturative, self-controlled surface reactions allowing the homogeneous distribution of the active species throughout the surface area. For this reason, ALD allows the deposition of thin films with high precision thickness control, high uniformity and low defect density [18]. In the case of the

* Corresponding author. University of Helsinki, Department of Chemistry, Laboratory of Inorganic Chemistry, P.O. Box 55, University of Helsinki, FIN-00014 Helsinki, Finland. Fax: +358-0-19140198; e-mail: Kaupo.Kukli@Helsinki.fi.

PII S0169-4332(96)00554-5

self-limited precursor adsorption the ALD growth rate should saturate along with increasing precursor doses. However, the tantalum oxide ALD process, especially at high temperatures, is different from this idealized model.

Effects of the reactor temperature and $TaCl_5$-precursor dose on the ALD growth and properties of tantalum oxide films have been studied earlier [15,16]. In the case of optimum precursor doses the growth rate was equal to 0.06 nm per cycle at 300°C growth temperature. However, etching instead of growth of as-deposited layers took place at temperatures of 280°C and higher when too high $TaCl_5$ doses were used. The etching rate was enhanced by the increase in the reactor temperature.

Hypothesis about the excess of weakly bound species, particularly tantalum oxychlorides, which desorb resulting in the etching process at the film surface, has been outlined on the basis of these results [15]. Unfortunately, no detailed description of the etching mechanism has been presented because of the lack of experimental data. There is neither data published concerning the growth kinetics below 240°C where the growth rate significantly depends on the substrate temperature [16]. At the same time, this temperature range is of interest because the films with high optical quality can be grown at these temperatures [16]. At last, it has been shown that ALD can be used for growing crystalline TaO_2 with rutile structure [16]. To our knowledge, this is the only technique which has yielded this kind of films. However, the reasons for the growth of TaO_2 instead of thermodynamically more favorable Ta_2O_5 are still not understood.

Therefore the aim of this study is to lighten these problems proceeding from the kinetics of $TaCl_5$ and H_2O adsorption in the ALD process. On-line microweighing by quartz-crystal microbalance (QCM) is applied as a relatively simple method to investigate the deposition kinetics experimentally during the film growth. Because of its high sensitivity [19] this method enables one to measure the adsorption of less than one monolayer and is already used for the investigation of the adsorption interactions during the ALD growth of ZnS and CdS [20], TaO_x [14,15] and Al_2O_3 [21] as well as for characterization of precursor properties of strontium [22] and calcium β-diketonates [23].

In order to deduce the growth mechanism from QCM measurements, one should proceed from thermodynamically probable surface reactions. Therefore some reactions which can take place during ALD growth of tantalum oxide from $TaCl_5$ and H_2O are analyzed in Section 2. The agreement of one or another reaction with our real-time QCM measurement data is discussed in Section 4 while the technique for QCM studies is described in Section 3.

2. Adsorption reactions

In the ALE process, the precursor pulses are separated in real time. Therefore the solid film is formed via surface reactions only. Unfortunately, the theoretical analysis of surface reaction probabilities is usually rather complicated because thermodynamic data for intermediate surface species are generally not known. In addition, the solid surfaces may be much different from the respective bulk materials. Nevertheless, it has been found, for instance, that the quasimolecules produced in the reaction between Cl_2 and alumina surface can be described as aluminium oxychloride (AlOCl) while the equilibrium constant for the surface reaction compares to that for bulk reaction in this case when the final Cl surface coverage after surface reaction is close to unity [24]. Of course the thermodynamical calculations cannot describe the kinetics of surface reactions because, due to the continuous purging of the ALD reactor, the thermodynamic balance can be driven towards the products unfavored for equilibrium state [25]. However, these calculations enable one to exclude less-favored reactions. Thermodynamical calculations have been successfully applied, for instance, in order to study solid phase [26] and vapor-phase [25,27] equilibria in the CVD and ALE-processed oxides, respectively. Moreover, one can suggest that the continuous etching process itself is most likely very close to bulk reactions even in ALD which also supports the reliability of calculations.

In order to study which reactions are responsible for the tantalum oxide growth and etching in ALD process, we analyze the reactions corresponding to the chemisorption of $TaCl_5$ and H_2O on the surfaces treated by H_2O and $TaCl_5$, respectively. In addition, reaction mechanisms leading to suboxide growth will be discussed below.

2.1. Adsorption of $TaCl_5$ on Ta_2O_5

Oxide surfaces exposed to water vapor are usually hydroxyl terminated at modest temperatures. At low pressures and high temperatures, however, surface hydroxyls decompose leaving bridging oxygens on the solid surface. Therefore the reactions of $TaCl_5$ with hydroxylated as well as dehydroxylated surfaces should be considered.

The surface hydroxyls generally act as adsorption/reaction sites for metal chloride. A model earlier proposed for Al_2O_3 [21] and for TiO_2 [28] growth from respective metal chlorides and H_2O assumes that hydroxyl groups are responsible for the stimulation of exchange reactions during the adsorption of chlorides. By the simple analogy with these papers we suggest that this mechanism could be taken into account for Ta_2O_5 growth as well:

$$n(-OH)(s) + TaCl_5(g) \rightarrow (-O-)_nTaCl_{5-n}(s) + nHCl(g), \quad (1)$$

where $n = 1, 2, 3, 4$.

Formally, the equation is also valid in case of completely dehydroxylated surface when $n = 0$. However, most probably chloride does not adsorb molecularly in this case but reacts with oxide [28]. Thus we can describe this surface reaction more exactly as:

$$n(=O)(s) + TaCl_5(g) \rightarrow (-O-)_nTaCl_{5-n}(s) + n(-Cl)(s). \quad (2)$$

The interaction of $TaCl_5$ with Ta_2O_5 has been earlier described in the form of following chemical reactions [29]:

$$3TaCl_5(g) + Ta_2O_5(s) \rightarrow 5TaOCl_3(s, g) \quad (3)$$

$$TaCl_5(g) + 2Ta_2O_5(s) \rightarrow 5TaO_2Cl(s) \quad (4)$$

In order to correlate the film composition and the reaction products with the changes in growth conditions, we have calculated the equilibrium composition of the solid and gas phases and possible etching products for different process conditions. The reactor temperature and pressure were chosen to be consistent with the experimental conditions in the reactor chamber during $TaCl_5$ pulse. We have used a commercial computer program, HSC Chemistry for Windows [30] which implements the calculations based on predetermined thermochemical data on the chemical species to be considered in the system. Calculations have been made using the $TaCl_5(g)$ as a feed reactant and Ta_2O_5 as the reactant assumptionally represented in the as-deposited solid film. The program calculates the equilibrium amounts of chemical species, assumed to be stable, minimizing the total Gibbs free energy of the system of species. It has to be noted that thermochemical data for TaO_2Cl and solid $TaOCl_3$ at temperatures above 600 K are not available [29,30] referring to the instability of these compounds at high temperatures. Insert data for these compounds are thus extrapolated for the calculations. No thermochemical data are available also for describing the surface species formed according to Eqs. (1) and (2). Therefore only the calculations for bulk-like reactions could be carried out.

The results of the calculations are depicted in Fig. 1. The calculations show that $TaOCl_2$ is formed first when Ta_2O_5 is exposed to $TaCl_5$. In addition, a remarkable amount of $TaOCl_3$ is formed at higher $TaCl_5$ doses. At lower temperatures $TaOCl_3$ appears in the solid phase preferably while the formation of gaseous $TaOCl_3$ is favored at temperatures above 250°C, approximately. Correspondingly one can suppose that the chlorine abundance after $TaCl_5$ pulse should be higher at lower growth temperatures. Moreover, probable desorption of $TaOCl_3$ can explain the etching of tantalum oxide in $TaCl_5$ flow at high temperatures.

Of course the real ALD process is probably more complicated. First, reactions described by Eqs. (1) and (2) can go simultaneously. Further, the possibility for re-adsorption of HCl, released in the reaction (1), should be considered. During re-adsorption HCl can react with OH-groups:

$$(-OH)(s) + HCl(g) \rightarrow (-Cl)(s) + H_2O(g). \quad (5)$$

as well as with bridging oxygen on partially dehydroxylated surface:

$$(=O)(s) + HCl(g) \rightarrow (-OH)(s) + (-Cl)(s). \quad (6)$$

Moreover, it should be considered that the reactions described by Eq. (1), (2), (5) and (6) can occur in the deposition process simultaneously.

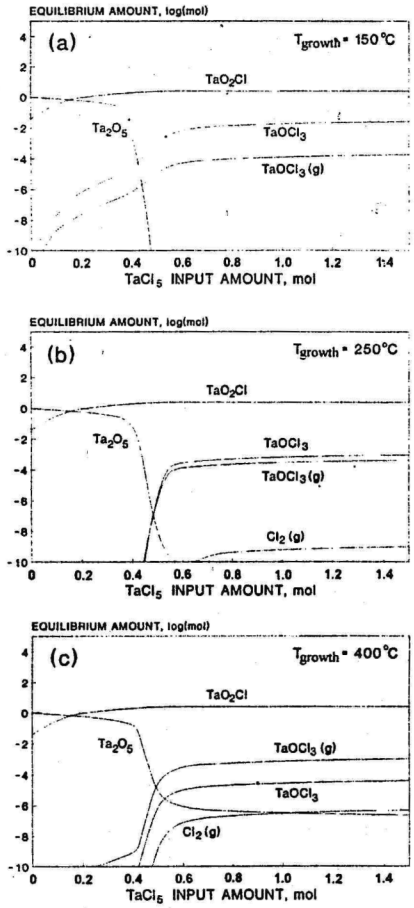

Fig. 1. Calculated amounts of reaction products as functions of $TaCl_5$ dose when 1 mol Ta_2O_5 is exposed to $TaCl_5$ at (a) 150°C, (b) 250°C and (c) 400°C.

However, all the reactions discussed above form intermediate surface species which can be described as oxychlorides. Therefore we believe that the general conclusions concerning the temperature dependence of chlorine abundance and desorption of $TaOCl_3$ at high temperatures should be still usable in order to explain our experimental results presented below.

2.2. Adsorption of H_2O

Exposure of the chlorinated oxide surface to H_2O can result in the replacement of the surface chlorines either by hydroxyl groups:

$$(-Cl)(s) + H_2O(g) \rightarrow (-OH)(s) + HCl(g). \quad (7)$$

or by bridging oxygens:

$$2(-Cl)(s) + H_2O(g) \rightarrow (=O)(s) + 2HCl(g). \quad (8)$$

The reactions cause appearance of hydroxylated and dehydroxylated surfaces, respectively. Of course, the reactions can occur simultaneously as well, forming partially hydroxylated surface layer. It should be noted, however, that HCl unlikely re-adsorbs in this reaction step because the surface is already chlorinated.

It is of importance to point out that subsequent ALD cycles are identical in that case, only, when the number of OH-groups reacting with $TaCl_5$ and HCl in the first reaction step is equal to the number of those appearing on the surface in the second reaction step. This requirement sets some additional limitations to the possible combinations of reactions which can be considered when plausible growth mechanisms are discussed.

2.3. Growth of TaO_2

Growth of TaO_2 films is not an exceptional case because suboxides have been observed in ion-sputtered films [6,7]. There are also some evidences that the films grown from $TaCl_5$ and O_2 in photo-assisted CVD-process can contain suboxides [31]. Nevertheless, no mechanism leading to the formation of suboxides in the ALD process has been suggested. Neither are thermodynamic data available for solid tetravalent tantalum compounds.

It has been shown that $TaCl_5$ tends to decompose and form subchlorides at temperatures above 150°C [9]. This decomposition can be a reason for the reduction of tantalum oxidation state during chloride adsorption. Another possibility is that $TaCl_5$, react-

ing with nonstoichiometric oxide, forms tetravalent oxychloride. For instance, it is known that a reaction between $TaCl_5$, Ta and Ta_2O_5 produces $TaOCl_2$ [32], a tetravalent oxychloride of tantalum. Further it depends probably on the dose of H_2O whether OH-groups and/or oxygen atoms replace the chlorines, only, or occupy the unsaturated bond, too, during the second reaction step.

Despite possible decomposition of $TaCl_5$ this precursor has been used for the ALD growth of tantalum oxide at temperatures up to 500°C [12,16]. Moreover, it has been shown that crystalline phases of tantalum oxide can be obtained by ALD technique from $TaCl_5$ and H_2O at temperatures above 300°C, only. Thus it is of particular interest to study the corresponding surface reactions at these temperatures.

Probably the chlorines released during decomposition of $TaCl_5$ also adsorb on the oxide [33]. Therefore Eq. (2) can be used for the description of the adsorption process of $TaCl_5$ on dehydroxylated TaO_2 as well.

The reaction with hydroxyl groups can be written as:

$$n(-OH)(s) + TaCl_5(g) \rightarrow (-O-)_nTaCl_{4-n}(s) + nHCl(g) + \tfrac{1}{2}Cl_2(g), \quad (9)$$

where $n = 1, 2, 3$.

It is possible that the oxidation state of tantalum is reduced from 5 to 4 during the second growth step when H_2O reacts with the chlorinated oxide surface. In this case some amount of adsorbed chlorine should be used for the formation of volatile chlorine oxides and removed from the surface in this way. Although this mechanism seems to be thermodynamically unfavored, that has been discussed in order to explain etching of tantalum suboxides in the Cl_2 flow [33]. In the case when a completely filled chlorine layer is present on the outermost surface of adsorbate, this hypothesis may be reasonable because the H_2O molecules reaching chlorinated surface, first interact with chlorine rather than with tantalum. Therefore, in the very early stage of this reaction step the formation of chlorine oxide could be probable. This explanation is consistent with the observation that the reaction between H_2O and chlorinated tantalum oxide has at least two stages described by different time constants [34].

3. Experimental

The experiments were carried out in a horizontal flow-type ALD reactor [16,22,23] at the pressure of 250 Pa using N_2 as the carrier gas. Tantalum oxide was deposited directly onto the sensor crystal of QCM. The mass sensor position corresponded to that of the trailing edge of substrates [16]. To reduce the possible disturbing effect of the structure and surface species of layers deposited earlier, we coated the QCM surface with tantalum oxide buffer layer at each reactor temperature before the mass measurements were started. Single ALD cycles were applied for the investigation of growth mechanisms in the temperature range from 50 to 400°C. Each cycle was a sequence of $TaCl_5$ pulse, purge time and H_2O pulse. Sufficiently long purge times which enabled the mass-sensor temperature to reach its initial level were used after every ALD cycle. The purge time between $TaCl_5$ and H_2O pulses was inevitable to avoid intermixing of reactants and, consequently, the gas phase reactions following this intermixing. The $TaCl_5$ pulse time was varied from 0.3 to 20 s while the H_2O pulse time was 5–15 s. The $TaCl_5$ source was kept at 65°C and the H_2O flow equalled 440 Pa cm^3 s^{-1}.

In order to determine the intermediate surface species formed as a result of $TaCl_5$ adsorption, we measured the mass increase corresponding to this reaction step and that corresponding to the complete ALD cycle. Using these mass changes and the film composition, the Cl/Ta ratio was found for the surface intermediate species. Changes in the adsorbate masses were measured for several ALD cycles separately at each reactor temperature and averaged afterwards in order to get experimental points. The experimental temperature range was limited due to the increased sensitivity to the temperature deviations markedly influencing the QCM signal at high temperatures. At temperatures 100–300°C the method enabled us to detect the changes corresponding to 0.02–0.05 monolayers of tantalum oxide while at temperatures below 100°C the sensitivity reached 0.01 monolayers. The film composition was deter-

mined by ex situ electron-probe microanalysis (EPMA). The details of these measurements have been published earlier [16].

4. Results and discussion

QCM signals recorded at 160, 240 and 370°C are shown in Fig. 2. The self-limited behavior of adsorption at 240°C is obvious. However, deviations from the saturation of QCM signal during $TaCl_5$ pulse are observable at other temperatures. The etching process starts at higher temperatures while a slow but continuous increase of mass sensor signal occurs at temperatures below 200°C (Fig. 2). The latter effect can be caused by the decomposition of $TaCl_5$ as well as by gas phase reactions [22] between $TaCl_5$ and H_2O residues possibly existing in the carrier gas. In order to minimize the role of etching and gas phase and/or decomposition reactions, the data shown in Fig. 3 were recorded at short $TaCl_5$ pulse times.

The absence of changes in the QCM signal during purge times was typical for all temperatures. This indicates that the surface intermediates formed during precursor pulses do not desorb or release gaseous decomposition products spontaneously under these conditions. An abrupt increase of the QCM signal after switching on the $TaCl_5$ pulse, Δm_1, and decrease of that during H_2O pulse, Δm_2, were also typical for all temperatures used in this work. The former is due to the adsorption of $TaCl_5$ and possibly to re-adsorption of HCl and/or Cl_2. The latter is due to the exchange of adsorbed chlorine atoms by hydroxyl groups and/or oxygen.

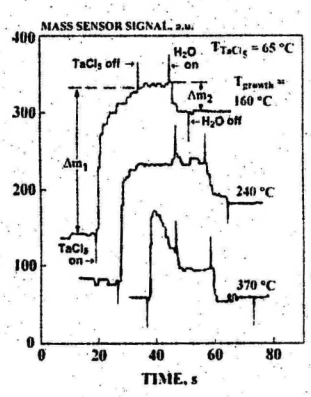

Fig. 2. Time dependence of mass sensor signal during ALD cycle at 200 (a) and 400°C (b).

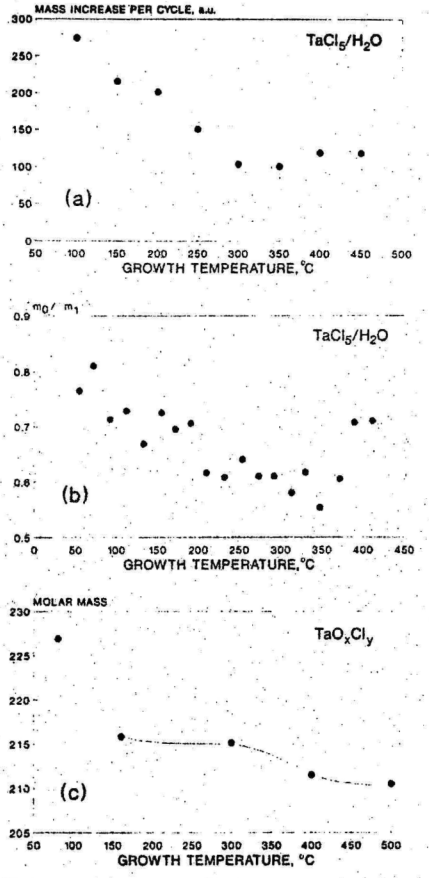

Fig. 3. Deposition rate measured by QCM (a), experimental mass exchange ratio $\Delta m_0/\Delta m_1$ measured by QCM (b) and molar mass of TaO_xCl_y in the solid phase (c) as functions of growth temperature. Solid line is drawn for convenience.

Δm_1 as well as the overall change in QCM signal, $\Delta m_0 = \Delta m_1 - \Delta m_2$, obtained as a result of completed ALD cycle, depend on the growth temperature. The dependences of Δm_0 and $\Delta m_0/\Delta m_1$ on the reactor temperature are depicted in Fig. 3(a) and (b), respectively. The curves correspond to 3 s long $TaCl_5$ pulse times and 10 s long H_2O pulse times. Thus the precursor doses used compare to those applied in our previous study [16]. In addition, it should be noted that the dependence of $\Delta m_0/\Delta m_1$ ratio on the $TaCl_5$ pulse time did not exceed the deviation of experimental points in Fig. 3(b) when the $TaCl_5$ pulse time was varied from 0.3 to 3 s at temperatures up to 400°C.

Fig. 3(c) shows the effect of growth temperature on the molar mass of the compound TaO_xCl_y, formed in the ALD process. The values of x and y are presented in Fig. 4. The data shown in Fig. 3(c) and 4 are obtained from the results of EPMA. In the calculations, we also took into account that no OH-groups were detected in the films [16]. One can see in Fig. 4 that besides the Cl/O ratio the oxidation state of tantalum depends on the growth temperature. However, the dependence of M_f on growth temperature as well as that of tantalum oxidation state is rather weak.

As mentioned above the composition of surface intermediates formed during $TaCl_5$ pulse can be estimated using composition and molar mass of the film material and the changes in QCM signal caused by precursor pulses. However, we have to assume that no desorption of Ta-containing species takes place during H_2O pulse. In addition, we assume for the sake of simplicity that chlorine atoms escape the surface because of exchange reactions according to Eqs. (7) and (8).

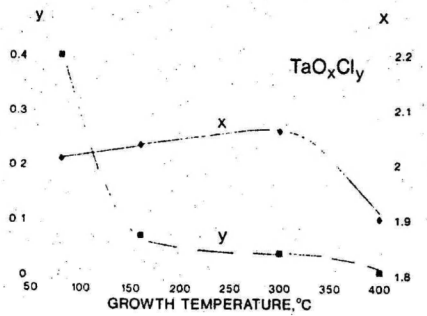

Fig. 4. Composition of films versus growth temperature. Lines are guides to eye.

In this case n_{Cl} chlorine atoms adsorbed together with a tantalum atom are replaced by hydroxyl groups and/or oxygen atoms while each hydroxyl group and oxygen atom replaces one and two chlorine atoms, respectively. Corresponding mass balance can be written as:

$$M_f(\Delta m_1/\Delta m_0) - M_f = M_{Cl}(n_{Cl} - y) - (M_O n_O)/2 - M_{OH} n_{OH}. \quad (10)$$

where M_{Cl}, M_O and M_{OH} are the molar masses of chlorine, oxygen and hydroxyl groups, respectively. n_0 and n_{OH} are the numbers of chlorine atoms coordinated to one tantalum atom and exchanged by oxygen or hydroxyl groups, respectively. The left side of Eq. (10) represents the mass change occurring during H_2O pulse per tantalum atom adsorbed during previous $TaCl_5$ pulse. The first term on the right side is the mass of chlorine atoms released during H_2O pulse per tantalum atom adsorbed. The second and third terms are the masses of oxygen and hydroxyl groups, respectively, replacing the chlorine atoms released. Our assumptions made above require that $n_O + n_{OH} = n_{Cl} - y$.

As none of the values n_O and n_{OH} nor the relationship between them is known, we can calculate the dependence of n_{Cl} on temperature for some extreme cases, only. The data used in the calculations are shown in Table 1. They are obtained from interpolations of experimental results depicted in Figs. 3 and 4. The results of calculations are presented in Table 2.

As one can see in Table 2, the probable values of the Cl/Ta ratio range from 3.1 and 4.5 at 100°C. The former value is obtained provided that no hydroxyl groups participate in surface reactions. This assumption, however, is unlikely fulfilled at such low temperatures. Therefore Cl/Ta ratios higher than 3.1 are more probable. The last result, in turn, shows that whether the average number of hydroxyl groups reacting with a $TaCl_5$ molecule is rather low ($n < 1.9$ in Eq. (1)) or HCl released in this reaction re-adsorbs (Eqs. (5) and (6)).

Table 1
Mass changes in ALD cycle and composition of deposited films versus growth temperature

Temperature (°C)	Δm_0 (au)	Δm_1 (au)	$\Delta m_0/\Delta m_1$	x	y	M_F (amu)
100	276	373	0.740	2.02	0.27	227
150	218	306	0.706	2.03	0.08	217
200	201	300	0.669	2.05	0.05	218
250	150	244	0.614	2.06	0.04	215
300	102	171	0.596	2.06	0.03	215
350	99	168	0.590	2.01	0.02	214
400	117	171	0.682	1.91	0.01	212

At temperatures 200–300°C, the Cl/Ta ratios in the adsorbate layer exceed even that of $TaCl_5$ when the calculations are carried out assuming that only OH-groups react with $TaCl_5$. This result cannot be explained by a simple exchange reaction where $TaCl_5$ reacts with OH-groups and HCl is released. Thus one must conclude that whether the reactions go via oxygen bridges or the readsorption of gaseous reaction products takes place. Proceeding from the data of Sakharov et al. [35] one can suppose, however, that the abundance of hydroxyl groups on tantalum oxide should be rather low at these temperatures. Correspondingly the reactions via oxygen bridges characterized by Cl/Ta ratios close to 5 are more probable than those via OH-groups. On the other hand one cannot exclude the possibility that Cl_2 or HCl released because of $TaCl_5$ decomposition or surface reactions at reactor inlet, can re-adsorb and really result in Cl/Ta ratios higher than 5. So high Cl/Ta ratios indicate that the reduction of the oxidation state of tantalum leading to the growth of TaO_2 is not caused by the deficiency of chlorine in the intermediate surface layer formed at $T \leq 350$°C during $TaCl_5$ pulse. Consequently the reaction going according to Eq. (9) is not probable and the main reason for suboxide growth at these temperatures is low reactivity of H_2O towards surface tantalum. The last conclusion is in agreement with reactant pulse delay time measurements [34] which indicate that the reactivity of H_2O towards the chlorinated surface is significantly lower than that of $TaCl_5$ towards the surface treated by H_2O.

At temperatures close to 400°C, the Cl/Ta ratio decreases in the intermediate adsorbate layer. OH-groups unlikely take part in surface reactions at these temperatures because hydrated tantalum oxide significantly dehydroxylates at 230–330°C [35]. Therefore, most probably some free chlorine is released while about 3.5 chlorine atoms adsorbs together with each tantalum atom at 400°C. This Cl/Ta ratio is very close to the oxidation state of tantalum in the films grown at those temperatures (Fig. 4). Hence, at temperatures about 400°C, the oxidation state of Ta characteristic to suboxides can be obtained during

Table 2
Surface concentration of tantalum atoms deposited in a single ALD cycle and Cl/Ta ratio in intermediate surface layer after $TaCl_5$ pulse, calculated for different reaction mechanisms

Temperature (°C)	N_{Ta} (nm^{-2})	Cl/Ta ratio			
		A Cl replaced by OH	B 2Cl replaced by O	C $(n_{Cl}-y)$Cl replaced by xOH	D $(n_{Cl}-y)$Cl replaced by xO
100	3.8	4.52	3.13	3.45	3.39
150	3.2	4.97	3.37	3.60	3.54
200	2.9	5.83	3.94	4.04	3.99
250	2.2	7.34	4.95	4.83	4.77
300	1.5	7.90	5.33	5.12	5.06
350	1.5	8.06	5.43	5.17	5.11
400	1.8	5.35	3.59	3.70	3.65

adsorption of $TaCl_5$ already. This result is in agreement with the results of thermodynamic calculations shown in Fig. 1. Indeed, one can see that Cl_2 is released in the reaction between Ta_2O_5 and $TaCl_5$ at 400°C. Therefore decomposition of chloride or oxychlorides as well as reduction of oxidation state of Ta should really take place in this reaction step.

In the calculations discussed above we assumed that during H_2O pulse no chlorine is removed from substrate surface without exchange of that with oxygen or OH-groups. Nevertheless, we also estimated the Cl/Ta ratio provided that $n_{Cl} - y$ chlorine atoms are replaced by x oxygen atoms or OH groups while the rest of chlorine is released with no exchange. Here, x oxygen atoms per tantalum atom adsorbed is the minimum amount which ensures the formation of the film with the composition TaO_xCl_y. The dependences obtained in this way are very close to that calculated for the mechanism which assumes complete exchange of chlorine by oxygen (Table 2). Therefore the conclusions concerning the surface concentration of Ta and Cl adsorbed are also valid in the case when some chlorine is released due to the formation of volatile chlorine oxide as discussed in Section 2.3.

Our data combined with those published earlier [15,16] allow us to estimate the surface concentration of Ta adsorbed during an ALD cycle, N_{Ta}, as well as that of chlorine adsorbed during $TaCl_5$ pulse, N_{Cl}. We take into account that the growth rate of TaO_2 films is 0.06 nm per cycle at 300°C [15]. High refractive index of the films [16] and the circumstance that crystallized films grow at this temperature [16] indicate the high density of the material. Therefore proceeding from the estimations made previously [17] we take the packing density of our film material equal to 0.9 of that for bulk TaO_2. The X-ray density of TaO_2 has been shown to range from 9.884 [36] to 10.41 g/cm^3 [37]. We use the value 9.95 g/cm^3 [36]. From these data we find that 1.5 tantalum atoms is adsorbed per 1 nm^2 at 300°C during an ALD cycle. Using this value and data presented in Fig. 3(a) and (c) we can find N_{Ta} as a function of growth temperature (Table 2).

The data presented in Table 2 enable us to estimate the surface concentration of chlorine adsorbed during $TaCl_5$ pulse. The values of N_{Cl} corresponding to the reaction mechanisms presented in Table 2,

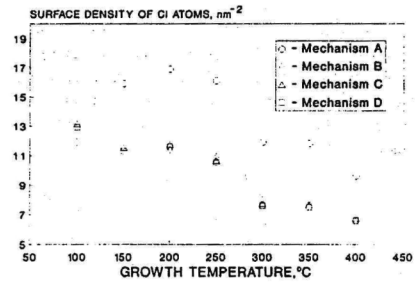

Fig. 5. Surface concentration of Cl atoms in intermediate surface layer after $TaCl_5$ pulse as a function of growth temperature. The Cl surface concentration is calculated for reaction mechanisms described in Table 2.

are depicted in Fig. 5. Unfortunately the real N_{Cl} values can be different from those shown in this figure because the contribution of OH-groups, possible re-adsorption of reaction products and reduction of tantalum oxidation state is not exactly known. However, the curves determine the most probable range of N_{Cl}. The highest possible values of N_{Cl} correspond to the reaction mechanism where surface chlorine is equivalently replaced by OH-groups. The other three mechanisms give significantly lower N_{Cl} values while they are rather close to each other at all temperatures studied. As the role of surface dehydroxylation and chloride decomposition should increase together with growth temperature, the real values of N_{Cl} should be close to those predicted by mechanisms B, C and D at higher temperatures. At low temperatures where the surface is hydroxylated after the H_2O pulse, the chlorine release without exchange with OH-groups is less probable. Thus the lower the growth temperature, the closer the real N_{Cl} values to those predicted by mechanism A.

It is noteworthy that at 100°C, possible N_{Cl} values exceed the surface concentration of Cl^--ions in the close packed plane monolayer by a factor ranging from 1.3 to 1.9. Although this can be partly due to the increase of effective surface area caused by film roughness, one should not neglect the possibility that chlorine forms more than one atomic monolayer on the film surface. In the latter case chlorine atoms should be coordinated to tantalum atoms incorporated into oxide film already as well as to those

adsorbed during $TaCl_5$ pulse. It is interesting to note that despite high surface concentration of chlorine there is no concentration saturation with decreasing substrate temperature. The latter result indicates the absence of steric hindrance at least on a chlorine monolayer level.

It should be noted that this kind of temperature dependence of chlorine abundance can be qualitatively predicted by thermodynamical calculations if one assumes that the available amount of surface oxygen, e.g. the topmost monolayer, limits the reaction between $TaCl_5$ and oxide. Indeed, the calculations presented in Section 2 show that oxychloride with higher Cl/O ratio more readily appears in the solid phase at lower temperatures rather than at higher ones.

Another interesting feature is that N_{Cl} reaches the values comparable to that of close-packed Cl^- monolayer at temperatures 300–400°C. These temperatures are very close to the lowest values of those at which etching of tantalum oxide film by $TaCl_5$ was observed [15]. Thus one can conclude that the oxychloride with higher desorption energy (and lower Cl/O ratio) does not block the adsorption sites of $TaCl_5$. As a consequence, $TaCl_5$ further reacts with oxide and forms oxychlorides with lower desorption energy and higher Cl content. These oxychlorides desorb at higher temperatures causing the etching of film. Along with the temperature decrease, however, they stay on the solid surface causing the increase of chlorine abundance discussed above.

5. Conclusions

We have shown that the composition and surface coverage in the intermediate surface layer formed during $TaCl_5$ pulse significantly depends on substrate temperature. Intermediate surface species with high Cl/Ta ratio close to 5 are formed at 200–350°C. At 400°C, the ratio is significantly lower than 5. The reduction of Cl/Ta ratio with increasing growth temperatures indicates that the oxidation state of tantalum should be reduced at about 400°C during $TaCl_5$ adsorption.

There is no direct evidence about steric hindrance of the adsorbate formation during $TaCl_5$ pulse. Chlorine surface coverage created by $TaCl_5$ pulse monotonously decreases with increasing growth temperature. At temperatures where etching can be observed, the stable surface coverage of chlorine is lower than in the close-packed Cl^- surface monolayer. These experimental observations can be explained on the basis of existing thermodynamic data. Thermodynamic calculations show that oxychlorides with higher Cl/O ratio which are preferably produced at higher $TaCl_5$ doses tend to volatilize with increasing growth temperature. In particular, $TaOCl_3$ occurs in the gas phase at temperatures above 250°C.

Therefore we can conclude that the reason for tantalum oxide etching in the continuous $TaCl_5$ flow is the desorption of oxychlorides with high chlorine content. The effect is most significant at temperatures where the stable abundance for surface oxychlorides is too low to avoid reaction between $TaCl_5$ and oxide. The temperature dependence of stable surface abundance for oxychlorides also explains the effect of reactor temperature on the growth rate at $T < 240$°C where no etching has been observed.

The mechanism of suboxide growth depends on temperature. There is no clear evidence that the oxidation state of tantalum may be reduced at temperatures below 350°C during $TaCl_5$ adsorption. Most probably, this reduction takes place during the H_2O pulse. At temperatures above 350°C the oxidation state of tantalum can be reduced during $TaCl_5$ pulse, already. This conclusion is also consistent with thermodynamic calculations which predict the appearance of free chloride in the reaction between $TaCl_5$ and Ta_2O_5 at $T > 250$°C.

Acknowledgements

The authors are thankful to A.-A. Kiisler for the assistance in the study and to M. Ritala for useful discussions. The authors are also indebted to M. Leskelä and Magnus Ehrnrooth Foundation for the possibility to carry out computer-aided thermodynamical calculations using HSC Chemistry for Windows at the University of Helsinki.

References

[1] E.P. Burte and N. Rauch, J. Non-Cryst. Solids 187 (1995) 425.

[2] H. Yang, F. Tanoue, S. Hibino, S. Sakakibara, K. Yokoi and T. Hotta, Jpn. J. Appl. Phys. 34 (1995) L757.
[3] A. Scheipers, C. Kötter, J. Eshold, H. Hinkers and M. Knoll, in: Proc. 12th Eur. Photovoltaic Solar Energy Conf., Amsterdam, 1994, p. 731.
[4] S.-C. Chiao, J.-L. Zhou and H.A. Macleod, Appl. Opt. 32 (1993) 5557.
[5] T. Doumuki, H. Tamada and M. Saitoh, Appl. Phys. Lett. 65 (1994) 2519.
[6] H. Demiryont, J.R. Sites and K. Geib, Appl. Opt. 24 (1985) 490.
[7] X.M. Wu, P.K. Wu, T.-M. Lu and E.J. Rumaszewski, Appl. Phys. Lett. 62 (1993) 3264.
[8] S. Tanimoto, N. Shibata, K. Kuroiwa and Y. Tarui, J. Electrochem. Soc. 141 (1994) 1339.
[9] H. Koyama, S. Tanimoto, K. Kuroiwa and Y. Tarui, Jpn. J. Appl. Phys. 33 (1994) 6291.
[10] K. Tominaga, R. Muhammet, I. Kobayashi and M. Okada, Jpn. J. Appl. Phys. 31 (1992) L585.
[11] P.A. Murawala, M. Sawai, T. Tatsuta, O. Tsuji, S. Fujita and S. Fujita, Jpn. J. Appl. Phys. 32 (1993) 368.
[12] M. Pessa, R. Mäkelä and T. Suntola, Appl. Phys. Lett. 38 (1981) 131.
[13] H. Kattelus, M. Ylilammi, J. Salmi, T. Ranta-aho, E. Nykänen and I. Suni, Mater. Res. Soc. Symp. Proc. 284 (1993) 511.
[14] J. Aarik, A. Aidla and K. Kukli, Appl. Surf. Sci. 75 (1994) 180.
[15] J. Aarik, A. Aidla, K. Kukli and T. Uustare, J. Cryst. Growth 144 (1994) 116.
[16] K. Kukli, J. Aarik, A. Aidla, O. Kohan, T. Uustare and V. Sammelselg, Thin Solid Films 260 (1995) 135.
[17] K. Kukli, M. Ritala and M. Leskelä, J. Electrochem. Soc. 142 (1995) 1670.
[18] T. Suntola, in: Handbook of Crystal Growth 3, Thin Films and Epitaxy, Part B, Growth Mechanics and Dynamics, Atomic Layer Epitaxy, Ed. D.T.J. Hurle (Elsevier, Amsterdam, 1994) ch. 14.
[19] V. Mecea, Sens. Actuators A 40 (1994) 1.
[20] A.I. Romanychev, J. Appl. Chem. USSR 65 (1993) 2218.
[21] J. Aarik, A. Aidla, A. Jaek, A.-A. Kiisler and A.-A. Tammik, Acta Polytech. Scand. Chem. Technol. Ser. 195 (1990) 201.
[22] J. Aarik, A. Aidla, A. Jaek, M. Leskelä and L. Niinistö, J. Mat. Chem. 4 (1994) 1239.
[23] J. Aarik, A. Aidla, A. Jaek, M. Leskelä and L. Niinistö, Appl. Surf. Sci. 75 (1994) 33.
[24] F. Réti, V.K. Josepovits and I.V. Perczel, Appl. Surf. Sci. 65/66 (1993) 271.
[25] K.-E. Elers, M. Ritala, M. Leskelä and E. Rauhala, Appl. Surf. Sci. 82/83 (1994) 468.
[26] J.H. Han, H.-K. Ryu, C.-H. Chung, B.-G. Yu and S.H. Moon, J. Electrochem. Soc. 142 (1995) 3980.
[27] T. Asikainen, M. Ritala and M. Leskelä, J. Electrochem. Soc. 141 (1994) 3210.
[28] M. Ritala, M. Leskelä, E. Nykänen, P. Soininen and L. Niinistö, Thin Solid Films 225 (1993) 288.
[29] O. Knacke, O. Kubaschewski and K. Hesselmann, Eds., Thermochemical Properties of Inorganic Substances II (Springer, Berlin, 1991) pp. 1956–1958.
[30] Outokumpu HSC Chemistry for Windows, program package, Version 1.10, Outokumpu Research OY, Pori, Finland (1993).
[31] S. Tanimoto, M. Matsui, K. Kamisako, K. Kuroiwa and Y. Tarui, J. Electrochem. Soc. 139 (1992) 320.
[32] D.V. Drobot and E.A. Pisarev, Russ. J. Inorg. Chem. 29 (1984) 1561.
[33] L.-A. Delouise, Surf. Sci. 324 (1995) 233.
[34] H. Siimon and J. Aarik, J. Phys. IV, 5 (1995) C5-277.
[35] V.V. Sakharov, N.B. Korovkina, B.G. Korshunov and Yu.B. Muravlev, Rus. J. Inorg. Chem. 28 (1983) 1093.
[36] Y. Syono, M. Kikuchi, T. Goto and K. Fukuoka, J. Solid State Chem. 50 (1983) 133.
[37] N. Schönberg, Acta Chem. Scand. 8 (1954) 240.

III

Reprinted from *Journal of the Electrochemical Society*, Vol. 142 (1995),
K. Kukli, M. Ritala and M. Leskelä,
Atomic layer epitaxy growth of tantalum oxide thin
films from $Ta(OC_2H_5)_5$ and H_2O, pp. 1670–1675,

Reprinted from JOURNAL OF THE ELECTROCHEMICAL SOCIETY
Vol. 142, No. 5, May 1995
Printed in U.S.A.

Atomic Layer Epitaxy Growth of Tantalum Oxide Thin Films from $Ta(OC_2H_5)_5$ and H_2O

Kaupo Kukli,* Mikko Ritala, and Markku Leskelä

Department of Chemistry, University of Helsinki, FIN-00014, Helsinki, Finland

ABSTRACT

The deposition of thin Ta_2O_5 films by atomic layer epitaxy (ALE) was investigated in the temperature range of 150 to 450°C using $Ta(OC_2H_5)_5$ and water as precursors. Because of the thermal self-decomposition of $Ta(OC_2H_5)_5$ the self-limiting ALE growth was achieved only below 350°C. All the films grown were amorphous as examined by x-ray diffraction analysis. The films grown at 250 and 325°C were stoichiometric within the accuracy of Rutherford backscattering spectrometry and contained 4 and 0.6 atom percent (a/o) hydrogen as determined by nuclear reaction analysis, respectively. Except for the outermost surface, the content of carbon residues was below 3 a/o as analyzed by x-ray photoelectron spectroscopy. The films exhibited smooth surfaces as observed by scanning electron microscopy and relatively uniform thicknesses with 7% deviation in the gas flow direction. The refractive index of the films increased with deposition temperature stabilizing at 2.23 at temperatures higher than 300°C. The permittivities for the films grown at 250 and 325°C were 21 and 25, respectively, and leakage current densities at 1 MV/cm electric field were 4.0 and 2.3 mA/cm^2, respectively.

Introduction

Ta_2O_5 is characterized by high chemical and thermal stability, high dielectric (ϵ = 22...35) and optical (n = 2.25) constants, and ionic conductivity. Therefore Ta_2O_5 thin films have been used in a number of applications such as dielectric materials for storage capacitors[1-14] and thin film transistors,[15] antireflection coatings for solar cells,[16,17] optical waveguides,[18] and filters,[19-21] chemical sensors,[22] as well as corrosion resistant materials.[23]

Both chemical and physical methods have been applied for Ta_2O_5 thin film deposition. In general, the films deposited using chemical vapor deposition (CVD) have possessed higher density, homogeneity, and purity[19,23] than films obtained by means of alternative techniques. CVD has also a distinct advantage in terms of a conformal step coverage[3,6,7,11] necessary for the creation of three-dimensional memory structures. Several tantalum precursors such as $Ta(OC_2H_5)_5$,[1,3-6,9-12,19,24] $Ta(OCH_3)_5$,[7,23] $Ta(thd)_4Cl$,[24] and $TaCl_5$[13,15,25] have been employed for the CVD growth of Ta_2O_5 films. In the case of the tantalum alkoxide precursors relatively high levels of carbon residues have been left in the films causing higher leakage currents and lower breakdown voltages when compared with films grown using the chloride precursor.[12,13] However, according to Ref. 5 stoichiometric Ta_2O_5 films with carbon contents below the sensitivity limit of Auger electron spectroscopy (AES) could have been grown from $Ta(OC_2H_5)_5$ by conventional CVD. Nevertheless, postannealing[4-6] as well as photoassisted CVD[1,7,15,25] and plasma-enhanced CVD (PECVD)[11,12] have been applied effectively to improve the dielectric properties of the films derived from the alkoxides.

Atomic layer epitaxy (ALE) is an advantageous chemical deposition method which allows the controlled growth of solid films with high thickness uniformity and low defect density.[26] The ALE growth is based on sequential exposures of the substrate surface to different precursors. Between the precursor pulses the reactor is purged with an inert gas. In the ideal case, the desired solid film forms via subsequent saturative surface reactions in a layer-by-layer mode. A characteristic feature of the ALE growth is the self-limited adsorption of a given precursor onto the substrate surface. Therefore, the film thickness depends only on the number of deposition cycles used.

Recently, metal alkoxides have been applied as precursors in ALE growth of aluminium and titanium oxide thin films.[27-30] Since in ALE the alternate dosing of the reactants eliminates inherently all gas-phase reactions, occasionally troublesome in CVD, water could be used as the other precursor in these studies without any difficulties. Owing to the facile hydrolysis reaction the alkoxide groups became effectively removed from the films; no carbon could be detected with AES and x-ray photoelectron spectroscopy

* Permanent address: Institute of Experimental Physics and Technology, University of Tartu, EE2400 Tartu, Estonia.

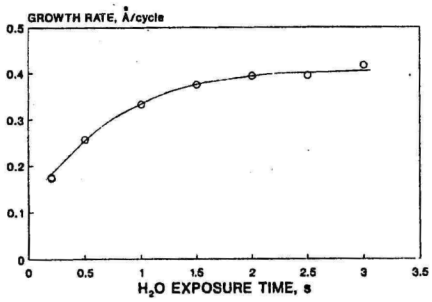

Fig. 1. Dependence of growth rate on H_2O exposure time.

(XPS). In the present work we have studied the possibility of growing Ta_2O_5 films by ALE using $Ta(OC_2H_5)_5$ and H_2O as precursors.

Experimental

Tantalum oxide films were grown onto 5 × 5 cm soda lime glass using a hot-wall flow-type F-120 ALE reactor (Microchemistry Ltd., Espoo, Finland).[31] Nitrogen was used as a carrier and purging gas. The total pressure in the reactor was about 10 mbar. $Ta(OC_2H_5)_5$ was evaporated from an open boat held at 105°C inside the reactor. The pulsing of the $Ta(OC_2H_5)_5$ vapor was accomplished by means of inert gas valving.[31] Water vapor was generated in an external reservoir at 20°C and led into the reactor through needle and solenoid valves.

Transmittance spectra of the films were measured within a wavelength range of 380 to 1100 nm using a Hitachi U-2000 spectrophotometer. A fitting method developed and described by Ylilammi and Ranta-aho[32] was exploited for evaluating film thicknesses and refractive indexes from these spectra. Comparative thickness measurements and verification of the film stoichiometry were obtained by RBS of 2.0 MeV $^4He^+$ ions from the 2.5 MV Van de Graaff accelerator of the Accelerator Laboratory at the University of Helsinki.[33] Carbon residues were analyzed by means of XPS and argon ion sputtering using a PHI Small Spot ESCA 5400 electron spectrometer and a PHI 04-300 ion gun. XPS spectra were excited by nonmonochromatized MgK_α radiation and measured using 89 eV analyzer energy and 0.5 eV channel width. The films were also profiled for hydrogen by the nuclear reaction analyses (NRA) technique using a $^{15}N^{2+}$ beam from the 5 MV tandem accelerator EGP-10-II of the Accelerator Laboratory to excite the 6.385 MeV resonance of the $^1H(^{15}N,\alpha\gamma)^{12}C$ reaction.[34] Structural analysis was carried out with a Philips MPD 1880 powder x-ray diffractometer using CuK_α radiation. Surface morphology and cross sections of the films were examined by means of a Zeiss DSM 962 scanning electron microscope at the Department of Electron Microscopy at the University of Helsinki.

In order to measure the basic electrical characteristics, tantalum oxide films with thicknesses of 150 nm were deposited onto sputtered indium-tin oxide (ITO) electrodes at 250 and 325°C. An array of aluminium electrodes was evaporated onto the tantalum oxide layer as-deposited enabling the measurement of the dielectric properties over an approximate surface area of 6 cm^2. The effective area of a single electrode was 0.2 mm^2. Capacitances and loss factors were measured at a frequency of 100 kHz using an HP 4192A impedance analyzer, and the current-voltage characteristics with an HP 4142B modular dc source at a ramp rate of 1 to 3 V/s. Probe contacts were established on two adjacent aluminium electrodes (inset in Fig. 8), doubling the effective thickness of the tantalum oxide film.

Results and Discussion

Film growth.—Figure 1 shows the dependence of the film growth rate on H_2O exposure time. The stabilization of the growth rate at 0.4 Å/cycle with pulse times longer than 2.0 s is evident. The effect of the $Ta(OC_2H_5)_5$ pulse length was also studied but no differences in thicknesses or thickness profiles were found between films grown using 0.2 and 0.4 s pulses. It is noteworthy that the films grown using even longer $Ta(OC_2H_5)_5$ exposure times (1.0 s) became slightly profiled. Therefore, $Ta(OC_2H_5)_5$ and water pulse lengths of 0.2 and 2.0 s, respectively, were chosen to be employed in subsequent experiments.

Figure 2 demonstrates the dependence of the growth rate on the deposition temperature. The constant growth rate of approximately 0.4 Å/cycle is achieved in the temperature range of 225 to 325°C. The decrease of the growth rate below 225°C is apparently due to kinetic factors. Within a temperature region of 325 to 400°C the growth rate decreases slightly with increasing temperature. This decrease can be attributed to either re-evaporation of the chemisorbed species, dehydroxylation of the film surface, or reduction of the $Ta(OC_2H_5)_5$ flux due to its decomposition in the source line. Above 400°C the growth rate exhibits a strong increase. As verified by the special experiments where only $Ta(OC_2H_5)_5$ was dosed onto the substrate surface, this increase is due to the self-decomposition of $Ta(OC_2H_5)_5$ resulting in a CVD-like growth (Fig. 2). At 300°C the decomposition rate was no more than 9% of that achieved with the hydrolysis reaction. These changes in the deposition rate are in a good accordance with the relationship between substrate temperature and CVD deposition rate of Ta_2O_5 found by Tominaga *et al.*[24] When only $Ta(OC_2H_5)_5$ was used, the deposition of Ta_2O_5 film began at about 300°C and the deposition rate increased monotonically with substrate temperature up to 600°C.[24]

One of the characteristic features of ALE is simple and accurate thickness control. The proportional relationship between the film thickness and the number of ALE cycles was verified also in the present work (Fig. 3). The films grown at 250°C using optimum cycle times exhibited only 7% deviation in thickness, as maximum, in the gas flow direction (Fig. 4) and less than 5%, perpendicular to the gas flow.

Film composition.—Since the main goal of the present work was to develop an ALE process for Ta_2O_5 films, in the following chapters we concentrate mainly on those films which were deposited under the self-limiting growth conditions, *i.e.*, at temperatures below 350°C. The RBS spectrum for the film deposited at 250°C is depicted in Fig. 5. As determined in RBS measurements, the compositions of the films grown at 250 and 325°C were $Ta_{2\pm0.2}O_{5\pm0.2}$ and $Ta_{2\pm0.1}O_{5\pm0.1}$, respectively. In other words, these films con-

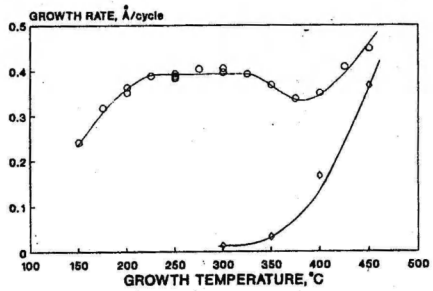

Fig. 2. The growth rate as a function of substrate temperature (○) conventional ALE growth; (◇) film growth caused by thermal decomposition of tantalum ethoxide when only $Ta(OC_2H_5)_5$ was dosed on the substrate. The curves are drawn for convenience.

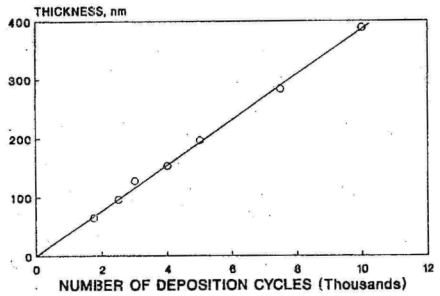

Fig. 3. Dependence of Ta_2O_5 film thickness on the number of ALE cycles.

sisted of stoichiometric Ta_2O_5 within the accuracy of the analysis.

NRA measurements showed the average hydrogen contents to be close to 0.6 and 4 a/o in the films grown at 325 and 250°C, respectively. The hydrogen content was higher at the surface region and diminished abruptly in the bulk region. The results of NRA measurements published earlier[20,21,35] showed that the H content of the ion plated (IP) tantalum oxide films deposited onto glass substrates did not exceed 2 a/o in the bulk region while the H content in reactively evaporated films was one order of magnitude higher. It has been pointed out[20,35] that the higher H content of evaporated films is probably due to their higher porosity and, as a consequence, higher moisture uptake after the process as compared with the IP films. The average hydrogen content in our films deposited at 325°C seems to be closer to that for Ta_2O_5 obtained by ion plating. Thus we suggest that the density of our films deposited at 325°C should be quite close to that of IP films while the film deposited at 250°C should be more porous or possess higher amount of residual hydrogen originating already from the film formation process.

In XPS analysis a considerable amount of carbon, ascribed to a postdeposition contamination, was observed on the outermost surfaces of the films grown at 250 and 325°C. The symmetric shape of the C1s peak, *i.e.*, the absence of inelastically scattered C1s photoelectrons, suggested that no significant amounts of carbon were located below the outermost layer. Indeed, when the film was depth profiled, the carbon exhibited a sharp decrease already after a gentle sputtering. However, even after a prolonged sputtering about 2 to 3 a/o carbon was detected. Whether this observation, in contradiction with the symmetric C1s peak detected at the outermost surface, is due to a true carbon contamination of the bulk of the film or due to a sputtering artefact, *e.g.*, knock-in of the residual carbon from the surface, remains unclear. In this context it is also worth emphasizing that the low hydrogen contents measured in the film bulk imply that no large amounts of carbon could have been incorporated in the form of ethoxide residues, $-OC_2H_5$.

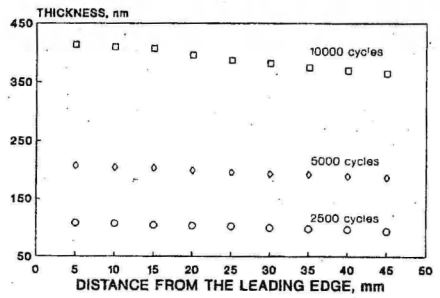

Fig. 4. Thickness profiles, measured along the gas flow direction, of Ta_2O_5 films grown at 250°C using different numbers of ALE cycles.

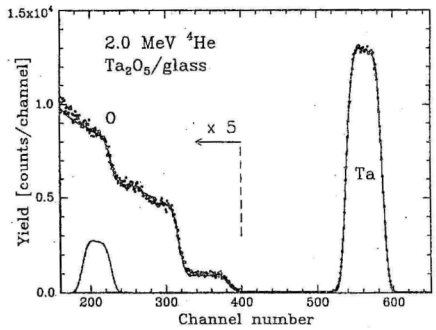

Fig. 5. RBS spectrum of Ta_2O_5 film grown at 250°C onto soda lime glass substrate (●) experimental data; (—) fitted spectrum.

Film properties.—All the films grown in the present experiments were amorphous as examined by XRD. This is consistent, in general, with several data published about the structure of tantalum oxide films as-deposited onto various substrate materials using different deposition methods and source materials.[1,3,5,7,12,17,23]

Figure 6 shows the cross-sectional SEM image of the film deposited at 250°C. No cracks or pinholes were observed. As compared with many other films grown by ALE onto

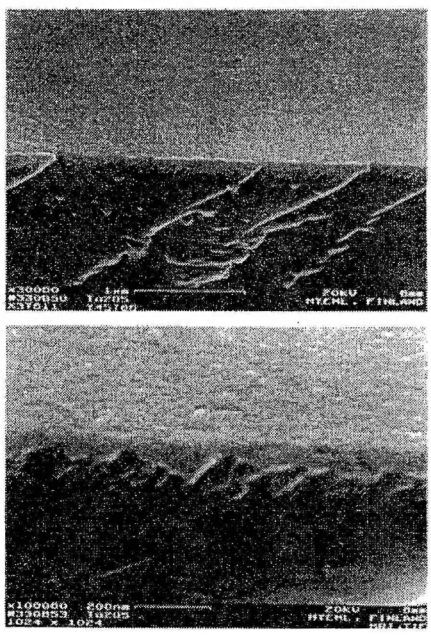

Fig. 6. Cross-sectional SEM images of Ta_2O_5 films deposited at 250°C taken with different magnifications.

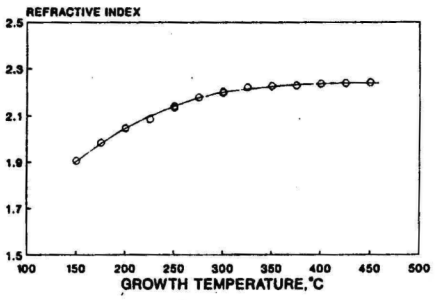

Fig. 7 Refractive index vs. deposition temperature.

glass substrates,[36-39] the Ta_2O_5 films prepared in the present work exhibit extremely smooth surfaces which is most likely due to their amorphous structure.

The refractive index was dominantly determined by the growth temperature and almost independent of other deposition conditions.The refractive index measured at a wavelength λ = 580 nm increased with the deposition temperature, evidently stabilizing at 2.23 when temperatures higher than 300°C were used (Fig.7). The films grown at 250°C with thicknesses between 96 and 388 nm exhibited the same refractive index at the mean value of 2.14 with 0.5% experimental error. As has been reported earlier,[11,20] the refractive index is strongly dependent on the stoichiometry of the Ta_2O_5 film as well as on the film density and structure. Therefore, in the present study, the latter properties are probably independent of the film thickness at a given temperature.

The refractive index of tantalum oxide films obtained using physical deposition methods are reported to be in the range of 1.90 to 2.21 for sputtered,[16,17] 2.05 for reactively evaporated,[21] and 2.20 to 2.25 for IP films.[21] It is well-known that IP films can possess good stoichiometry and a density of 95% of the bulk density of the corresponding crystalline material.[20,35] The high refractive index of the IP films has been directly attributed to their high density which was also verified by their lower H uptake as compared with the evaporated films.[20] In the case of CVD-grown films prepared from $TaCl_5$ by photo-CVD [7,13,25] as well as from $Ta(OC_2H_5)_5$ by laser-assisted CVD [1] the refractive index depends on the substrate temperature very similarly to the present work, reaching values of about 2.2 and 2.3, respectively, at 300°C or higher temperatures. The refractive index of the Ta_2O_5 bulk material has been reported to be as high as 2.42 at λ = 632.8 nm. [40] However, the value of n = 2.2 achieved in the thin Ta_2O_5 film growth is reported to be already close to that of bulk material.[13] The value of n = 2.22 has been also evaluated for the films grown by low-pressure CVD in a substrate temperature range of 375 to 500°C. [25] Kattelus *et al.*[41] measured a value of n = 2.23 for tantalum oxide films grown by ALE at 300°C from $TaCl_5$ and H_2O. Thus, there is no difference between the refractive indexes of Ta_2O_5 films grown by ALE from different tantalum precursors.

In comparison with the data referred to above, the values of n measured for the films grown at 325°C were among the highest ones. These tantalum oxide films grown in the present experiment possessed refractive indexes close to those of the bulk material. The high refractive index of these films refers directly to their high density. Indeed, when the density of the Ta_2O_5 bulk material (8.2 g/cm^3 [42]) was employed in converting the atomic densities measured by RBS to geometrical thicknesses, we obtained a good agreement between thicknesses calculated from optical and RBS measurements for the film deposited at 325°C. By contrast, the thickness for the film grown at 250°C calculated on the basis of RBS data was only 89% of the thickness value obtained from optical spectra. This suggests that the real density of the film grown at 250°C is approximately 11% lower than the density of the bulk material.

Our samples exhibited an approximate deviation of 5% in capacitance over the 6 cm^2 measurement area consistently with the thickness profile. The averaged values of permittivity, ϵ, obtained from capacitance measurements were 21 and 25 for samples grown at 250 and 325°C, respectively. In comparison, Zaima *et al.*[4] and Rauch *et al.*[3] evaluated values of ϵ = 25 and 24.5, respectively, for as-deposited LPCVD films (thickness about 100 nm) prepared at 340 to 500°C using tantalum ethoxide precursor as well. Tanimoto *et al.*[25] measured ϵ = 23 and 25 for films grown by photo-CVD. Kattelus *et al.*[41] reported ϵ = 24 for ALE-grown Ta_2O_5 films using $TaCl_5$ as a tantalum precursor.

Our samples grown at 250 and 325°C possessed dielectric losses of 0.01 and 0.02, respectively, without any prior surface treatment before electrode deposition. Kattelus *et al.*[41] have already reported the loss factor in ALE-grown tantalum oxide films derived from $TaCl_5$ to be in order of 10^{-2}.

Samples measured in the present study exhibited uniform current-voltage (I-V) dependences over the 6 cm^2 measurement area. Typical I-V curves for the films grown at different temperatures are depicted in Fig. 8. The values of leakage current densities at the 1 MV/cm electric field strength are 4.0 and 2.3 mA/cm^2 for the films deposited at 250 and 325°C, respectively (Fig. 8). It is noteworthy that these values are about one-order of magnitude smaller than those reported by Kattelus *et al.*[41] for the as-deposited ALE-grown films grown from $TaCl_5$ at 300°C. The latter films contained 1 to 2 a/o chlorine impurities.

In the case of postannealing procedures, which were not employed in the present study, the leakage current reduction has been attributed directly to the recovery of the stoichiometry in the CVD films, and also to the reduction of carbon residues. However, leakage currents of as-grown as well as annealed films have been reported to be considerably affected by changes in deposition conditions, such as deposition temperature[25] which influences the film properties, *e.g.*, refractive index. In general, increases in n and ϵ mean an increase in film density and, as a result, a reduction in the leakage current.[25] It is worth noting that the leakage current of the film grown at 325°C ($n \approx 2.23$) is somewhat smaller than that of the film grown at 250°C ($n \approx$ 2.14). This can possibly be explained by higher amount of hydrogen uptake in the films grown at 250°C caused by their lower density when compared to the film deposited at 325°C. Earlier the effect of water on the electrical properties of Ta_2O_5 films has already been observed[14] when the presence of H_2O in the oxidizing ambient has shown a detrimental effect on the leakage of the resulting Ta_2O_5 films obtained by thermal oxidation. When the oxidation took place only via H_2O, the observed leakage current was extremely high.[14]

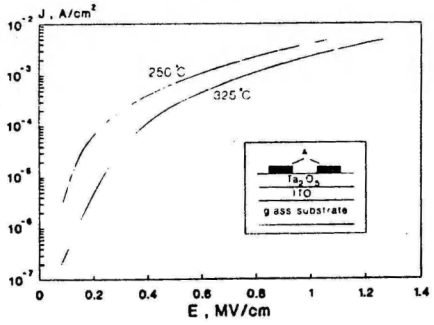

Fig. 8. Dependence of the leakage current density of Ta_2O_5 films on electric field strength as measured using the electrode configuration shown in the inset.

Comparison of our results with most of the data published recently is complicated because of the differences in substrate and electrode materials. Leakage currents exhibited by our samples are in the order of $10^{-2}...10^{-3}$ A/cm^2 at 1 to 1.2 MV/cm field strength applied. These values are comparable with those of Ta_2O_5 films as-deposited by CVD mainly onto silicon substrates.[12,13,15,25] However, in case of lower electric fields, below 1 MV/cm field strength, the leakage currents in our films are several orders of magnitude higher, approximately, than those in the films deposited on silicon substrates. This can be due to the native interfacial SiO_2 layer in metal-oxide-semiconductor structures responsible for lowering the electric fields and, therefore, the leakage currents,[11,13,43] what is not the case in the present study. However, the leakage current densities in our as-deposited films were even smaller than those measured by Rauch and Burte,[3] who deposited stoichiometric Ta_2O_5 from $Ta(OC_2H_5)_5$ onto silicon and used aluminium gate electrodes.

It is noted by Young[43] that dielectric properties of sputtered Ta_2O_5 films with aluminium electrodes appear to deteriorate with time yielding higher currents, probably due to the interaction between the aluminium electrode and the tantalum oxide creating a film with larger oxygen deficiency. Stanley and Maissel have, in their early work,[44] compared current-voltage curves for several sputtered tantalum oxide diodes with various metal counterelectrodes and found that the voltage required for a given current density was somewhat smaller in case of Al electrodes than that in case of Cu or Au counterelectrodes, for instance. Recently, TiN and Mo have been reported to be optimum materials for low- and high-temperature processes, respectively, for Ta_2O_5 capacitors.[10] The detailed study of conduction mechanisms in as-deposited as well as annealed films is beyond the scope of the present work. However, the creation of convenient capacitor structures using silicon substrates and alternative electrode materials will be the basis for future investigations.

Conclusions

Tantalum oxide thin films were deposited by atomic layer epitaxy in temperature range of 150 to 450°C using $Ta(OC_2H_5)_5$ and H_2O as precursors. The temperature independent growth rate of 0.4 Å/cycle was determined for the films grown in the temperature range of 225 to 325°C using the optimum precursor pulse lengths. The self-decomposition of tantalum ethoxide became considerable above 325°C, approximately, causing film growth via the CVD-mode and, consequently, an increase in the film growth rate.

All the films grown were amorphous as examined by XRD. The SEM image of the film grown at 250°C showed extremely smooth and uniform film surface which is probably due to its amorphous nature.

The films grown at 325 and 250°C were stoichiometric Ta_2O_5 within the accuracy of the RBS analysis. NRA measurements showed the hydrogen contents to be close to 0.6 and 4 a/o in the films grown at 325 and 250°C, respectively. According to XPS measurements our films contained less than 3 a/o carbon.

The refractive index measured at the wavelength λ = 580 nm increased with the deposition temperature, stabilizing at 2.23 when temperatures higher than 300°C were used. The values of permittivity, ϵ, obtained from capacitance measurements were 21 and 25 for samples grown at 250 and 325°C, respectively. Leakage current densities at the 1 MV/cm electric field strength were 4.0 and 2.3 mA/cm^2 for films deposited at 250 and 325°C, respectively.

Acknowledgments

The authors are indebted to Dr. Leena-Sisko Johansson for carrying out the XPS analysis. Dr. Eero Rauhala and Pekka Haussalo are acknowledged for the RBS and NRA measurements. Dr. Hannu Kattelus is appreciated for the access to the electrical measurements. This work was supported in part by the Academy of Finland and the Technology Development Centre (TEKES), Helsinki, Finland. K.Kukli expresses gratitude to the government of Finland for the research Grant VIRO-75v.

Manuscript submitted Oct. 18, 1994; revised manuscript received Jan 23, 1995.

The University of Helsinki assisted in meeting the publication costs of this article.

REFERENCES

1. Y. Nishimura, K. Tokunaga, and M. Tsuji, *Thin Solid Films*, **226**, 144 (1993).
2. K. Sundaram, W. K. Choi, and C. H. Ling, *ibid.*, **230**, 145 (1993).
3. N. Rauch and E. P. Burte, *Microel. J.*, **24**, 421 (1993).
4. S. Zaima, T. Furuta, Y. Yasuda, and M. Iida, *This Journal*, **137**, 1297 (1990).
5. W. R. Hitchens, W. C. Krusell, and D. M. Dobkin, *ibid.*, **140**, 2615 (1993).
6. K. Shimizu, M. Katayama, H. Funaki, E. Arai, M. Nakata, Y. Ohji, and R. Imura, *J. Appl. Phys.*, **74**, 375 (1993).
7. K. Yamagishi and Y. Tarui, *Jpn. J. Appl. Phys.*, **25**, L306 (1986).
8. S. Tanimoto, M. Matsui, M. Aoyagi, K. Kamisako, K. Kuroiwa, and Y. Tarui, *ibid.*, **30**, L330 (1991).
9. H. Shinriki, T. Kisu, S.-I. Kimura, Y. Nishioka, Y. Kawamoto, and K. Mukai, *IEEE Trans. Electron. Devices*, **ED-37**, 62 (1990).
10. H. Matsuhashi and S. Nishikawa, *Jpn. J. Appl. Phys.*, **33**, 1293 (1994).
11. S.-O. Kim, J. S. Byun, and H. J. Kim, *Thin Solid Films*, **206**, 102 (1991).
12. P. A. Murawala, M. Sawai, T. Tatsuta, O. Tsuji, S. Fujita, and S. Fujita, *Jpn. J. Appl. Phys.*, **32**, 368 (1993).
13. M. Matsui, S. Oka, K. Yamagishi, K. Kuroiwa, and Y. Tarui, *ibid.*, **27**, 506 (1988).
14. G. S. Oehrlein, *J. Appl. Phys.*, **59**, 1587 (1986).
15. M. Matsui, H. Nagayoshi, G. Muto, S. Tanimoto, K. Kuroiwa, and Y. Tarui, *Jpn. J. Appl. Phys.*, **29**, 62 (1990).
16. F. Rubio, J. Denis, J. M. Albella, and J. M. Martinez-Duart, *Thin Solid Films*, **90**, 405 (1982).
17. H. Demiryont, J. R. Sites, and K. Geib, *Appl. Opt.*, **24**, 490 (1985).
18. W. M. Paulson, F. S. Hickernell, and R. L. Davis, *J. Vac. Sci. Technol.*, **16**, 307 (1979).
19. S. B. Desu, *Mat. Chem. Phys.*, **31**, 341 (1992).
20. C. R. Ottermann, K. Bange, W. Wagner, F. Rauch, and H. Hantche, *Thin Solid Films*, **175**, 185 (1989).
21. K. Gürtler, K. Bange, W. Wagner, M. Laube, and F. Rauch, *Surf. Interface Anal.*, **19**, 435 (1992).
22. U. Teravaninthorn, Y. Miyahara and T. Moriizumi, *Jpn. J. Appl. Phys.*, **26**, 2116 (1987).
23. C. H. An and K. Sugimoto, *This Journal*, **139**, 1956 (1992).
24. K. Tominaga, R. Muhammet, I. Kobayashi, and M. Okada, *Jpn. J. Appl. Phys.*, **31**, L585 (1992).
25. S. Tanimoto, M. Matsui, K. Kamisako, K. Kuroiwa, and Y. Tarui, *This Journal*, **139**, 320 (1992).
26. T. Suntola, *Mat. Sci. Rep.*, **7**, 266 (1989).
27. L. Hiltunen, H. Kattelus, M. Leskelä, M. Mäkelä, L. Niinistö, E. Nykänen, P. Soininen, and M. Tiitta, *Mat. Chem. Phys.*, **28**, 379 (1991).
28. M. Ritala, M. Leskelä, and E. Rauhala, *Chem. Mater.*, **6**, 556 (1994).
29. M. Ritala, M. Leskelä, L. Niinistö, and P. Haussalo, *ibid.*, **5**, 1174 (1993).
30. H. Döring, K. Hashimoto, and A. Fujishima, *Ber. Bunsenges. Phys. Chem.*, **96**, 620 (1992).
31. T. Suntola, *Thin Solid Films*, **216**, 84 (1992).
32. M. Ylilammi and T. Ranta-aho, *ibid.*, **232**, 56 (1993).
33. E. Rauhala, J. Keinonen, K. Rakennus, and M. Pessa, *Appl. Phys. Lett.*, **51**, 973 (1987).
34. H. J. Whitlow, J. Keinonen, M. Hautala, and A. Hautojärvi, *Nucl. Instrum. Methods Phys. Res., Sect. B*, **5**, 505 (1984).
35. W. Wagner, F. Rauch, and K. Bange, *Fresenius Z. Anal. Chem.*, **333**, 478 (1989).
36. M. Ritala, M. Leskelä, L. Niinistö, T. Prohaska, G. Friedbacher, and M. Grasserbauer, *Thin Solid Films*, **249**, 155 (1994).
37. M. Ritala, M. Leskelä, L. Niinistö, T. Prohaska, G. Friedbacher, and M. Grasserbauer, *ibid.*, **250**, 72 (1994).

38. T. Asikainen, M. Ritala, and M. Leskelä, *This Journal*, **141**, 3210 (1994).
39. K.-E. Elers, M. Ritala, M. Leskelä, and E. Rauhala, *Appl. Surf. Sci.*, **82&83**, 468 (1994).
40. P. W. Black and J. Wales, *Infrared Phys.*, **8**, 209 (1968).
41. H. Kattelus, M. Ylilammi, J. Salmi, T. Ranta-aho, E. Nykänen, and I. Suni, *Mat. Res. Soc. Symp. Proc.*, **284**, 511 (1993).
42. *Handbook of Chemistry and Physics*, 52nd ed., R. C. Weart, Editor, The Chemical Rubber Co., Cleveland, OH (1971-1972).
43. P. L. Young, *J. Appl. Phys.*, **47**, 235 (1976).
44. C. L. Stanley and L. I. Maissel, *ibid.*, **35**, 1530 (1964).

IV

Reprinted from *Applied Surface Science*, Vol. 112 (1997),
K. Kukli, J. Aarik, A. Aidla, H. Siimon, M. Ritala and M. Leskelä,
In Situ study of atomic layer deposition of tantalum oxide
thin films from $Ta(OC_2H_5)_5$ and H_2O, pp. 236–242,

ELSEVIER

Applied Surface Science 112 (1997) 236–242

applied surface science

In situ study of atomic layer epitaxy growth of tantalum oxide thin films from $Ta(OC_2H_5)_5$ and H_2O

Kaupo Kukli [a,*], Jaan Aarik [a], Aleks Aidla [a], Hele Siimon [a], Mikko Ritala [b], Markku Leskelä [b]

[a] *University of Tartu, Institute of Experimental Physics and Technology, EE2400 Tartu, Estonia*
[b] *University of Helsinki, Department of Chemistry, P.O. Box 55, FIN-00014 Helsinki, Finland*

Abstract

Ta_2O_5 thin films have been deposited in atomic layer epitaxy process from $Ta(OC_2H_5)_5$ and H_2O. A quartz crystalline mass-sensor was exploited to detect the adsorption processes at the gas–solid interface during the film growth. It is suggested that $Ta(OC_2H_5)_5$ reacts with surface hydroxyls producing intermediate surface species $(-O)_nTa(OC_2H_5)_{5-n}$ where n varies with the reactor temperature. During the subsequent water pulse these species react further converting the surface back to the hydroxyl-terminated one. The uncontrolled deposition due to the temperature-induced decomposition of tantalum ethoxide with the activation energy of 100 ± 6 kJ/mol contributes to the film growth above 275°C. The value of the diffusion coefficient $D = 0.0075$ m^2/s for gas-phase $Ta(OC_2H_5)_5$ has been calculated at 250°C. Estimated sticking coefficient of $Ta(OC_2H_5)_5$ is about one order of magnitude higher than that of H_2O and nearly one order of magnitude lower than that of $TaCl_5$.

PACS: 68.45.Da; 77.84.Bw; 81.15.Gh; 82.40.−g

Keywords: Atomic layer epitaxy; Tantalum oxide; Tantalum ethoxide; Quartz crystal microbalance

1. Introduction

Ta_2O_5 is known as a high-quality dielectric material for capacitor technology [1–5], electroluminescent and field emission displays [6–8], optical [9] and corrosion resistant coatings [10]. Ta_2O_5 films have been deposited by chemical vapor deposition (CVD) using several precursor materials such as $Ta(OC_2H_5)_5$ [5,11–14], $Ta(OCH_3)_5$, $TaCl_5$ and $Ta[N(CH_3)_2]_5$ [11]. Among these precursors $Ta(OC_2H_5)_5$ is often the most preferred one because of its 100% volatility and superior thermal stability [11].

Besides conventional CVD techniques, atomic layer epitaxy (ALE) [15] as a digital chemical vapor deposition method has been applied to deposit Ta_2O_5 thin films. A common tantalum precursor in ALE growth has been $TaCl_5$ [15–18]. The adsorption of $TaCl_5$ and H_2O has been investigated in situ using highly sensitive oscillating quartz crystalline mass-sensor (QCM) [16,17] enabling detection of mass

* Corresponding author. Tel.: +372-7-433276; fax: +372-7-465570; e-mail: kaupo.kukli@helsinki.fi.

PII S0169-4332(96)00989-0

changes equal to less than one monolayer. $Ta(OC_2H_5)_5$ and H_2O have also been exploited for the ALE deposition of amorphous and stoichiometric Ta_2O_5 thin films [19] as well as high-quality Ta_2O_5–HfO_2 [20] and Ta_2O_5–ZrO_2 [21] dielectric nanolaminates.

The aim of this study was to investigate the sequential adsorption of the $Ta(OC_2H_5)_5/H_2O$ precursor system in real time by QCM in order to obtain quick information about the effects of temperature and precursor exposure times on film growth as well as film formation mechanisms and adsorption properties of the precursors.

2. Experimental

A low pressure flow-type hot-wall ALE reactor was used in our experiments. Details of the reactor design and mass monitoring have been published elsewhere [22]. Nitrogen (purity 99.9997%), additionally purified by the liquid nitrogen adsorption trap, was exploited as carrier gas. The pressure inside the reactor was held at 250 Pa, approximately. The tantalum ethoxide (Aldrich, claimed purity 99.98%) was evaporated from an open boat inside the reactor at temperatures ranging from 88 to 103°C. The reactor temperature in the deposition chamber was varied between 70 and 375°C.

The precursors were led directly onto QCM placed at the precursor inlet. The AT-cut quartz crystals of 30 MHz oscillation frequency were used in these measurements. Before starting the measurements, a tantalum oxide buffer layer was deposited by ALE onto silver electrodes of the QCM. In order to investigate the growth kinetics in more details, supplementary substrates of tantalum foil were placed face-to-face between reactant gas inlet and the QCM forming an array of precursor propagation channels [17,23]. The length of the channels was 50 mm. These channels were coated with buffer films as well. In order to calculate the diffusion and sticking coefficients of precursors using the method described by Siimon and Aarik [17,23,24] the reactant pulse delay times [24] were measured. The chemisorption kinetics was investigated at 250°C which was verified to be inside the temperature range of self-limited growth [19].

3. Results and discussion

3.1. Effects of cycle time parameters on growth rate

Fig. 1 demonstrates a typical QCM response during an ALE cycle for $Ta(OC_2H_5)_5/H_2O$ precursor system at 250°C. After switching on the $Ta(OC_2H_5)_5$ pulse, the QCM signal increased due to the mass of adsorbed molecules and stabilized at a certain new level, Δm_1, above the initial signal level during the exposure time t_1, thereby showing the self-controlled adsorption of $Ta(OC_2H_5)_5$ molecules. During the H_2O exposure time, t_3, the oscillation period of QCM decreased by Δm_2, referring to the surface mass reduction after the reaction between H_2O and the surface species formed during the preceding $Ta(OC_2H_5)_5$ pulse releasing volatile products e.g. CH_3CH_2OH. After a complete ALE cycle the mass-sensor signal stabilized at a new level, $\Delta m_1 - \Delta m_2$, above the initial one indicating the amount of additional mass deposited during this cycle. Similar cycles were repeatedly plotted during the deposition process.

The effect of different cycle times on the film growth rate was investigated at the reactor temperature of 250°C. Fig. 2 demonstrates that the precursor pulse length equal to 2.5 s or longer is needed in order to achieve the saturation of substrate surface. It was observed that the deposition rate, $\Delta m_1 - \Delta m_2$, does not depend on the purge time between $Ta(OC_2H_5)_5$ and following H_2O pulse, t_2. At the same time the deposition rate decreased significantly

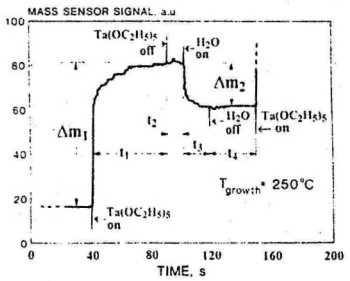

Fig. 1. Plot of QCM response to precursor adsorption in real time. t_1, t_2, t_3 and t_4 are the lengths of $Ta(OC_2H_5)_5$ exposure, the first purge, H_2O exposure and the second purge periods, respectively.

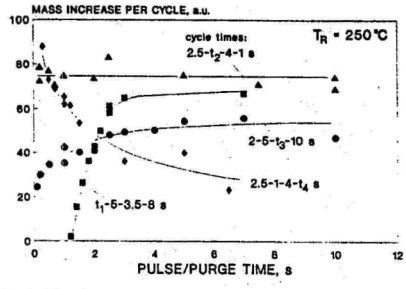

Fig. 2. Mass increase per complete ALE cycle, $(\Delta m_1 - \Delta m_2)$, as function of $Ta(OC_2H_5)_5$ exposure. t_1, the first purge, t_2, H_2O pulse, t_3 and the second purge time, t_4.

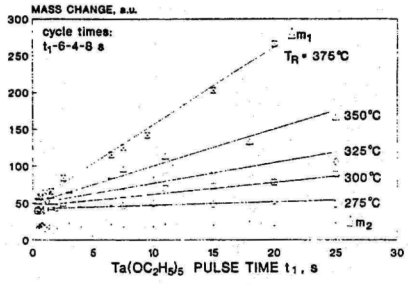

Fig. 3. Mass changes Δm_1 and Δm_2 measured during $Ta(OC_2H_5)_5$ and H_2O exposure periods, respectively, as function of $Ta(OC_2H_5)_5$ pulse time at different growth temperatures, T_R. Averaged Δm_2 was nearly a constant in the given temperature range.

when longer purge times, t_4, after the H_2O pulse were applied (Fig. 2). The latter effect was observed at all temperatures investigated and can be attributed to the partial dehydroxylation of OH-terminated oxide surface after the H_2O pulse [25]. The dehydroxylation causes deficiency of favoured surface sites for the subsequent adsorption of $Ta(OC_2H_5)_5$ molecules in the first step of the next cycle. However, one should not exclude the possible effect of mixing the front of the ethoxide pulse with the tail of the preceding water pulse. This might cause a CVD-like growth with higher growth rate especially in case of short purge times.

3.2. Temperature effect on the film growth

When the QCM was exposed to $Ta(OC_2H_5)_5$ at reactor temperatures below 150°C, Δm_1 did not stabilize but increased with t_1. In addition, the QCM signal decreased somewhat during subsequent purge time, t_2. This decrement became more significant when the growth temperature was raised from 90 to 130°C. One can suggest that at these lowest temperatures some amount of adsorbed precursor remained in the physisorbed state and partially desorbed during t_2, causing the decrease of QCM signal. At higher temperatures physisorption was suppressed and in the range between 150 and 275°C, approximately, the self-controlled growth mode was achieved.

At temperatures higher than 275°C, the non-saturative increase in QCM signal was again observed (Fig. 3). The rate of the uncontrolled deposition increased exponentially with reactor temperature. This effect can be attributed to the decomposition of $Ta(OC_2H_5)_5$. From the slope of the QCM signal plots the rate of decomposition can be estimated. An Arrhenius plot of the $Ta(OC_2H_5)_5$ decomposition rate (Fig. 4) gives the activation energy $E_a = 100 \pm 6$ kJ/mol. For comparison, for the CVD growth of Ta_2O_5 from $Ta(OC_2H_5)_5$ and O_2, Rauch and Burte [12] and Lane [26] have calculated the activation energies equal to 96.5 and 106 kJ/mol.

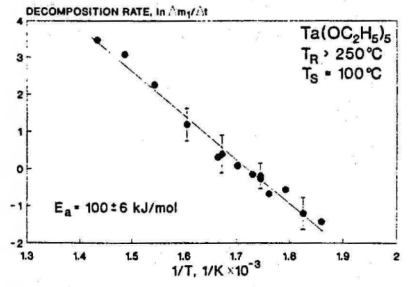

Fig. 4. $Ta(OC_2H_5)_5$ decomposition rate versus inverted value of reactor temperature. E_a is the activation energy of decomposition, T_R is reactor temperature and T_S is ethoxide evaporation temperature. Decomposition rate is expressed as a rate of steady-state QCM signal increase achieved at sufficiently long $Ta(OC_2H_5)_5$ exposures.

respectively. The CVD of Ta_2O_5 films is described as a surface reaction rate limited process [26]. The latter values compare well to our results. However, while using only $Ta(OC_2H_5)_5$, Tominaga et al. [14] obtained CVD-processed Ta_2O_5 with an activation energy of 39 kJ/mol.

In the QCM measurements, the growth rate per cycle could be expressed as $\Delta m_1 - \Delta m_2$ (Fig. 1). In the present study, the growth rate increased monotonously when plotted against the growth temperature (Fig. 5). Such a behaviour of growth rate differs from that reported in our previous study about Ta_2O_5 growth onto glass substrate [19]. In those experiments the growth rate per cycle, determined by optical thickness measurements, slightly diminished above 300°C, reached its local minimum at 375°C and increased thereafter due to the thermal decomposition of $Ta(OC_2H_5)_5$. The reduction of growth rate due to the thermal desorption of surface species is not likely because, in the present study, no mass decrease referring to desorption was detected during t_2 regardless of its length. One can suggest that before the decomposition-enhanced growth starts to dominate, the increasing temperature reduces the density of favoured adsorption sites, most likely OH-groups, thus suppressing the growth rate. For instance, Sakharov et al. [27] have reported that hydrated tantalum oxide significantly dehydroxylates in the temperature range of 230–330°C. It is suggested that at temperatures higher than 275°C the precursor decomposition and dehydroxylation occur as two competing mechanisms. It was also observed in the present study at these temperatures that the film growth took place even when the water supply was cancelled (Fig. 5). In the case of long ethoxide exposure times the uncontrolled decomposition overcomes the effect of possible dehydroxylation and has a superior effect to the response of QCM. For this reason, no local minimum of growth rate could be detected in the present measurements.

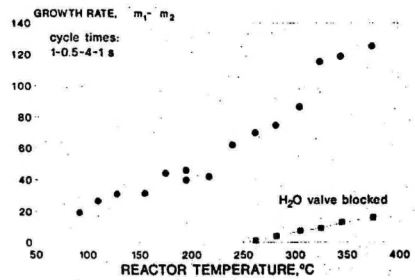

Fig. 5. Growth rate as mass increase per complete ALE cycle, $(\Delta m_1 - \Delta m_2)$, versus growth temperature.

3.3. Growth mechanism

In the two-step surface reactions taking place during the ALE growth, two growth mechanisms can formally be considered. The first is the film formation without decomposition or exchange reactions in the first step of ALE cycle:

$$2Ta(OC_2H_5)_5\,(g) \rightarrow 2Ta(OC_2H_5)_5\,(ad) \quad (1)$$

$$2Ta(OC_2H_5)_5\,(ad) + 5H_2O\,(g) \rightarrow Ta_2O_5\,(ad) + 10CH_3CH_2OH\,(g) \quad (2)$$

Another possibility is to consider the reactions proceeding via intermediate formation of surface hydroxyls and their exchange reactions with the adsorbing $Ta(OC_2H_5)_5$:

$$n(-OH)\,(ad) + Ta(OC_2H_5)_5\,(g) \rightarrow (-O-)_nTa(OC_2H_5)_{5-n}\,(ad) + nCH_3CH_2OH\,(g) \quad (3)$$

$$(-O-)_nTa(OC_2H_5)_{5-n}\,(ad) + (5-n)H_2O\,(g) \rightarrow (-O-)_nTa(OH)_{5-n}\,(ad) + (5-n)CH_3CH_2OH\,(g) \quad (4)$$

Here one can calculate the surface mass exchange ratio during the two-step reaction per one ethoxide molecule reached and bound at the surface in the first reaction step. Furthermore, the analogous surface mass exchange ratio, $S = (\Delta m_1 - \Delta m_2)/\Delta m_1$, can be measured experimentally from the plots of QCM signal (Fig. 1) assuming that the species adsorbed cover the surface uniformly. S is the ratio of mass remained at the surface after the 2nd step of ALE cycle to the mass adsorbed during the first step. Thus we get for the reactions expressed by Eqs. (3) and (4) that $S = 1$, 0.874, 0.791, 0.732 and 0.689 if $n = 5$, 4, 3, 2 and 1, respectively, and for the reactions expressed by Eqs. (1) and (2) $S = 0.544$.

It appears that the experimental values of S presented in Fig. 6 mainly correspond to the growth mechanism which includes contribution of surface OH-groups. However, detailed analysis shows that Eqs. (1) and (2) also contribute to the film growth, in particular, at higher temperatures and longer purge times after H_2O pulse. In addition, it is worth noting that at 250°C, S decreases with increasing $Ta(OC_2H_5)_5$ pulse time. At $t_1 = 1$ s its value is close to 0.8. Thus at least three OH-groups react with an adsorbing $Ta(OC_2H_5)_5$ molecule under these conditions. At $t_1 = 5$ s, $S = 0.68$ showing that the averaged number of OH-groups per $Ta(OC_2H_5)_5$ molecule adsorbed is diminished down to 1, approximately. This indicates that OH-groups become exhausted before the adsorption of $Ta(OC_2H_5)_5$ saturates and, thus, the last portion of $Ta(OC_2H_5)_5$ adsorbs according to Eq. (1). Furthermore, even at $t_1 = 1$ s, S decreases with increasing growth temperature and, at 375°C, its value coincides with that corresponding to the reaction mechanism where no OH-groups are involved.

Similarly it was observed that the role of OH-groups was significantly limited in the case of long purge times after H_2O pulse. Indeed, when t_4 was changed at 250°C from 0.5 to 12 s, S was reduced from 0.9 down to 0.6. This is most likely due to dehydroxylation of the film surface which becomes more completed along with the increase of purge time and results also in a remarkable decrease in the growth rate (Fig. 2) which is consistent with results discussed in Section 3.1.

At 325 and 375°C, the value of S increases

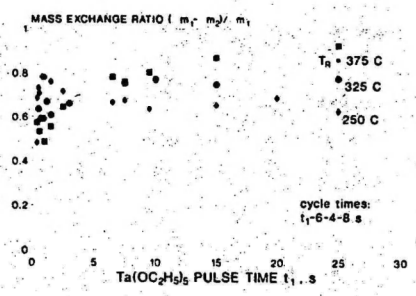

Fig. 6. Mass exchange ratio $(\Delta m_1 - \Delta m_2)/\Delta m_1$ versus tantalum ethoxide exposure time at different growth temperatures, T_R.

together with t_1. This is most likely due to the decomposition of $Ta(OC_2H_5)_5$ described in Section 3.2. Desu [13] has proposed the following decomposition mechanism of tantalum ethoxide during the CVD growth of Ta_2O_5:

$$2Ta(OC_2H_5)_5\,(g) \rightarrow Ta_2O_5\,(s) + 5C_2H_4\,(g) + C_2H_5OH\,(g) + 2(C_2H_5)_2O\,(g) + 2H_2O\,(g) \quad (5)$$

This supports raising the experimental ratio S, because the growth of tantalum oxide during t_1 is naturally followed by a significant increment of Δm_1. No decrease of the adsorbate mass, Δm_2, would be observed during the H_2O pulse if all $Ta(OC_2H_5)_5$ molecules adsorbed were decomposed according to Eq. (5). However, Δm_2 remains nearly constant at all temperatures examined (Fig. 3). Indirectly, the latter fact verifies that $Ta(OC_2H_5)_5$ adsorbs only on those sites where no ethoxy groups exist. Such vacant sites are created either as a result of the preceding H_2O pulse or, later during the $Ta(OC_2H_5)_5$ exposure, due to the decomposition of the $Ta(OC_2H_5)_5$ molecules adsorbed previously. Thus, the monolayer coverage of $Ta(OC_2H_5)_5$, once formed, is sustained due to the immediate adsorption of new $Ta(OC_2H_5)_5$ molecules on those sites where ethoxy groups have decomposed. Regardless of the composition of layer deposited during $Ta(OC_2H_5)_5$ exposure, only the topmost layer of Ta_2O_5 is still covered by ethoxy groups which interact with subsequential H_2O pulse in ordinary exchange reaction (Eqs. (3) and (4)).

3.4. Precursor reactivities

Reactivities of ALE precursors can be characterized by sticking coefficient, k. Determination of k is based on the dependence of the surface coverage variation rate on k. On the other hand, the change in surface coverage is linearly related to the change of mass deposited during a precursor pulse, hence, to the QCM signal. The time dependence of the surface coverage is also affected by the parameters characterizing the growth conditions and the precursors [23]. Diffusion coefficient, D, of $Ta(OC_2H_5)_5$ in N_2 and the initial concentrations of the precursors at the inlet, c_0, must be previously determined [17].

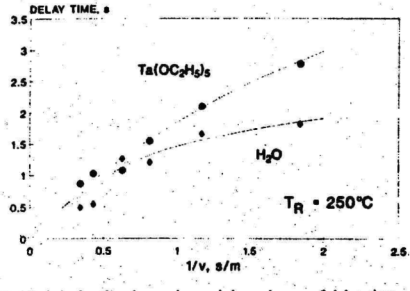

Fig. 7. Calculated and experimental dependences of delay time on reciprocal velocity of carrier gas $1/v$. Solid curves are calculated for $D = 0.00075$ m^2/s ($Ta(OC_2H_5)_5$) and $D = 0.026$ m^2/s (H_2O).

It is known that, when the adsorption wave travels through adsorbing channels, the precursor molecules leave the carrier gas stream and adsorb onto the channel surface thus reducing the propagation rate of the adsorption wavefront along the reactor axis. This results in the delay time between the moment of precursor inlet and its detection by QCM. It has been shown [17] that the gas phase diffusivity of a precursor can be found from the dependence of the delay time on the velocity of the carrier gas, v (Fig. 7). The delay time is inversely proportional to c_0 and the shape of the curve depends on D [24].

The diffusivity of $Ta(OC_2H_5)_5$ and the sticking coefficients were determined at 250°C. As a result of the best approximation the value $D = 0.0075$ m^2/s for $Ta(OC_2H_5)_5$ was obtained. This value coincides with D determined earlier for $TaCl_5$ [17]. Comparing the experimental values of the maximum mass variation rate with the calculated one and averaging the results for different carrier gas velocities, we obtained $k = 0.0035$ for $Ta(OC_2H_5)_5$ and $k = 0.0004$ for H_2O. For comparison, earlier it has been obtained that $k = 0.02$ and $k = 0.0004$ for $TaCl_5$ and H_2O, respectively [17].

4. Conclusions

In the present work, ALE deposition process of Ta_2O_5 from $Ta(OC_2H_5)_5$ and H_2O was studied by means of QCM. The temperature effect on the adsorption processes and the influence of precursor dosing on the deposition rate and mechanism was investigated. It is suggested that $Ta(OC_2H_5)_5$ favourably reacts with surface hydroxyls producing intermediate surface species $(\text{-O-})_n Ta(OC_2H_5)_{5-n}$ where n varies with the reactor temperature. During the subsequent water pulse these species react further converting the surface back to hydroxyl-terminated. At higher growth temperatures and/or longer purge periods after the H_2O pulse, the dehydroxylation of the surface reduces the growth rate. The decomposition of tantalum ethoxide with the activation energy of 100 ± 6 kJ/mol was observed at temperatures higher than 275°C. The value of diffusion coefficient $D = 0.0075$ m^2/s for gas-phase $Ta(OC_2H_5)_5$ at 250°C has been calculated. The sticking coefficient of H_2O is $k = 0.0004$ on ethoxide-terminated surface while that of $Ta(OC_2H_5)_5$ was estimated as high as 0.0035 on H_2O-treated surface. The latter value is about one order of magnitude lower than that of $TaCl_5$.

Acknowledgements

The authors are thankful to A.-A. Kiisler for the assistance in the study.

References

[1] P. Balk, Adv. Mater. 7 (1995) 703.
[2] W.S. Lau, K.K. Khaw, P.W. Qian, S.P. Sandler and P.K. Chu, J. Appl. Phys. 79 (1996) 8841.
[3] H. Kimura, J. Mizuki, S. Kamiyama and H. Suzuki, Appl. Phys. Lett. 66 (1995) 2209.
[4] A. Nagahori and R. Raj, J. Am. Ceram. Soc. 78 (1995) 1585.
[5] T. Aoyama, S. Saida, Y. Okayama, M. Fujisaki, K. Imai and T. Arikado, J. Electrochem. Soc. 143 (1996) 977.
[6] H. Yang, F. Tamoue, S. Hibino, S. Sakakibara, K. Yokoi and T. Hotta, Jpn. J. Appl. Phys. 34 (1995) L757.
[7] J.W. Li, Y.K. Su and M. Yokoyama, Jpn. J. Appl. Phys. 32 (1993) 5591.
[8] R.Z. Bakhtizin, S.S. Ghots and E.K. Ratnikova, IEEE Trans. Electron Devices 38 (1991) 2398.
[9] M. Cevro and G. Carter, Opt. Eng. 34 (1995) 596.
[10] D.W. Graham and D.P. Stinton, J. Am. Ceram. Soc. 77 (1994) 2298.
[11] H. Koyama, S. Tanimoto, K. Kuroiwa and Y. Tarui, Jpn. J. Appl. Phys. 33 (1994) 6291.
[12] N. Rauch and E.P. Burte, Microelectron. J. 24 (1993) 421.
[13] S.B. Desu, Mater. Chem. Phys. 31 (1992) 341.

[14] K. Tominaga, R. Muhammet, I. Kobayashi and M. Okada, Jpn. J. Appl. Phys. 31 (1992) L585.
[15] T. Suntola, Atomic Layer Epitaxy, in: Handbook of Crystal Growth 3, Thin Films and Epitaxy, Part B: Growth Mechanics and Dynamics, ed. D.T.J. Hurle (Elsevier Science B.V., 1994) p. 654.
[16] J. Aarik, K. Kukli, A. Aidla and L. Pung, Appl. Surf. Sci., in press.
[17] H. Siimon and J. Aarik, J. Phys. IV 5 (1995) C5–277.
[18] M. Ylilammi, J. Electrochem. Soc. 142 (1995) 2474.
[19] K. Kukli, M. Ritala and M. Leskelä, J. Electrochem. Soc. 142 (1995) 1670.
[20] K. Kukli, J. Ihanus, M. Ritala and M. Leskelä, Appl. Phys. Lett. 68 (1996) 3737.
[21] K. Kukli, J. Ihanus, M. Ritala and M. Leskelä, J. Electrochem. Soc., in press.
[22] J. Aarik, A. Aidla, A. Jaek, M. Leskelä and L. Niinistö, J. Mater. Chem. 4 (1994) 1239.
[23] H. Siimon and J. Aarik, J. Phys. IV 5 (1995) C5–245.
[24] J. Aarik and H. Siimon, Appl. Surf. Sci. 81 (1994) 281.
[25] M. Ritala and M. Leskelä, Appl. Surf. Sci. 75 (1994) 333.
[26] A.P. Lane, Mater. Res. Soc. Symp. Proc. 250 (1992) 331.
[27] V.V. Sakharov, N.B. Korovkina, B.G. Korshunov and Yu.B. Muravlev, Rus. J. Inorg. Chem. 28 (1983) 1093.

V

Reprinted from *Chemical Vapor Deposition*, Vol. 4 (1998),
K. Kukli, M. Ritala, M. Leskelä and R. Lappalainen,
Niobium oxide thin films grown by atomic layer epitaxy, pp. 29–34,

Chemical Vapor Deposition

Full Paper

Niobium Oxide Thin Films Grown by Atomic Layer Epitaxy**

By *Kaupo Kukli, Mikko Ritala,* Markku Leskelä,* and *Reijo Lappalainen*

Nb_2O_5 thin films were grown by atomic layer epitaxy (ALE) in the temperature range of 150–350 °C using $Nb(OC_2H_5)_5$ and H_2O as precursors. All the films grown on glass substrates were amorphous, as indicated by X-ray diffraction analysis. The films exhibited smooth surfaces as observed by scanning electron microscopy and uniform thickness profiles with less than 7 % variation in the gas flow direction. The refractive index of the films increased with deposition temperature, stabilizing at 2.4 at temperatures higher than 230 °C. Backscattering spectrometry analysis indicated that the films were stoichiometric Nb_2O_5.

Keywords: Atomic layer epitaxy, Thin films, Niobium, Niobium oxide, Dielectrics

1. Introduction

Nb_2O_5 is a dielectric material applicable in capacitor technology,[1–3] waveguides,[4–6] oxygen sensors,[7] and corrosion-resistant[8] and electrochromic coatings.[9,10] Furthermore, niobium is a component of various important compound oxides such as barium or lithium titanium niobates, which are used in waveguides and modulators, for instance.[11,12] Nb_2O_5 has also been used as dopant material to modify the electronic properties of various ferroelectric materials[13–15] and tin dioxide–based varistor ceramics.[16] Niobium also eliminates oxygen vacancies in microwave dielectrics, increasing their dielectric constant,[17] and affects the structural and electrical characteristics of zirconia.[18–20] Niobium oxide is recognized also as a catalyst or catalyst-supporting oxide material.[21]

Nb_2O_5 thin films have been grown mainly using physical deposition techniques such as sputtering[3,5–7,22] or ion plating.[4] Pyrolysis,[1] the sol-gel process,[9,23] and anodization[2] are less frequently used methods of obtaining Nb_2O_5 films. There are also relatively few reports on CVD of niobium oxide.[8,11] In CVD, $Nb(thd)_2Cl_3$ (thd = 2,2,6,6-tetramethyl-3,5-heptanedione) as well as niobium ethoxide, $Nb(OC_2H_5)_5$, have been used as metal precursors for Nb_2O_5.[1,8,11] Besides for CVD, $Nb(OC_2H_5)_5$ has been exploited as a Nb precursor also in the sol-gel process.[9]

The relatively few reports on the controlled growth of Nb_2O_5 thin films provided us with a motivation to deposit and investigate the properties of niobium oxide films using advanced CVD methods such as atomic layer epitaxy (ALE).[24,25] ALE is a digital CVD method where the substrate surface is alternately exposed to the vaporized precursor fluxes. The reactant pulses are separated by purging periods to eliminate gas-phase reactions and remove reaction products. For instance, in the case of metal oxide film growth the complete growth cycle consists of metal precursor exposure, the first purging period, oxygen precursor exposure, and the second purging period. A characteristic feature of ALE growth is the self-limited adsorption of a given precursor onto the substrate surface, providing inherent control of the film thickness. The film thickness depends only on the number of deposition cycles used. The stepwise growth via self-controlled adsorption processes allows one to expect the formation of thin films with high density and thickness uniformity over large substrate areas.

To date, successful deposition of Nb_2O_5 films by ALE has not been reported. An attempt has been made to deposit Nb_2O_5 films by ALE using $NbCl_5$ and H_2O as precursors.[26] However, these experiments failed due to the desorption of stable niobium oxychlorides formed as intermediate species in surface reactions. In the present work we have studied the possibility of obtaining controlled growth of Nb_2O_5 films by ALE using $Nb(OC_2H_5)_5$ and H_2O as precursors. In addition to the interest in the pure Nb_2O_5 films, if proper conditions for controlled ALE growth of Nb_2O_5 could be established, this would also open up new possibilities for depositing novel structured materials, e.g., oxide nanolaminates with improved dielectric characteristics.[27–29]

[*] Dr. M. Ritala, Dr. K. Kukli,[+] Prof. M. Leskelä
Department of Chemistry, University of Helsinki
PO Box 55, FIN-00014 Helsinki (Finland)
Dr. R. Lappalainen
Accelerator Laboratory, University of Helsinki
PO Box 43, FIN-00014 Helsinki (Finland)

[+] On leave from the Institute of Experimental Physics and Technology, University of Tartu, EE2400 Tartu, Estonia.

[**] This work was supported in part by the Academy of Finland and the Technology Development Centre (TEKES), Helsinki, Finland. The authors are thankful to the EM Unit at the University of Helsinki for access to the SEM technique. K.K. expresses gratitude to the Finnish Centre for International Mobility (CIMO) for the research grant.

2. Results and Discussion

2.1. Film Growth

Figure 1 shows the dependence of the film growth rate on H_2O exposure time. Stabilization of the growth rate at about 0.03 nm/cycle with pulse times longer than 2.0 s is

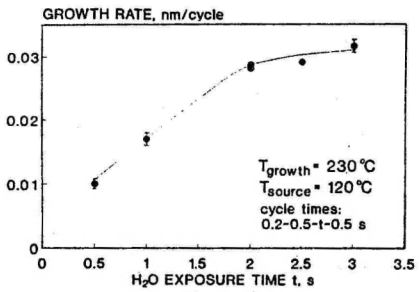

Fig. 1. Growth rate of Nb_2O_5 thin films versus H_2O exposure time.

observable, thereby verifying the self-limiting film growth. The effect of the $Nb(OC_2H_5)_5$ pulse length was also studied. There were no changes in the average film thickness when the $Nb(OC_2H_5)_5$ exposure times were longer than 0.2 s, but then the films became more profiled. Therefore, $Nb(OC_2H_5)_5$ and H_2O pulse lengths of 0.2 and 2.0 s, respectively, resulting in the self-limiting film growth, were chosen to be employed in subsequent experiments. The growth rate was not affected considerably by purge times varied between 0.5 and 2.0 s and purge time length of 0.5 s was used in further experiments. Thus we can use the notation 0.2–0.5–2.0–0.5 s, for instance, to express the time sequence of a growth cycle consisting of ethoxide exposure, the first purge time, water exposure, and the second purge time.

The effect of $Nb(OC_2H_5)_5$ evaporation temperature on the growth rate was also examined. The films were grown at 230 °C using different source temperatures in the range of 70–120 °C. The growth rate was rather insensitive to the evaporation temperature (Fig. 2). However, the films grown using 80 °C source temperature became slightly profiled perpendicular to the gas flow direction. With source temperature of 70 °C, the amount of precursor evaporated was obviously insufficient to cover all the substrate surface area since the film grew only on that part of the substrate which was closest to the precursor inlet (Fig. 2). The boundary between the growth and non-growth regions was very sharp, having a width of only few millimeters, thereby indicating how the precursors become effectively adsorbed while they are flowing through the narrow channel between the two substrates.[24,30] In further experiments $Nb(OC_2H_5)_5$ was evaporated at 90 °C, which is high enough

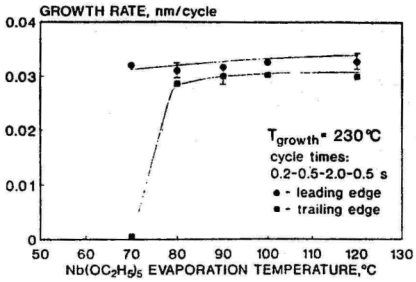

Fig. 2. Growth rate of Nb_2O_5 films versus source temperature at the leading and trailing edges of the substrate. Solid lines are guides for the eye.

to supply a sufficient precursor dose for saturation of the whole substrate surface and, at the same time, optimizes the precursor consumption.

Figure 3 demonstrates the dependence of the growth rate on the deposition temperature. The consistent decrease of the growth rate below 230 °C is apparently due to

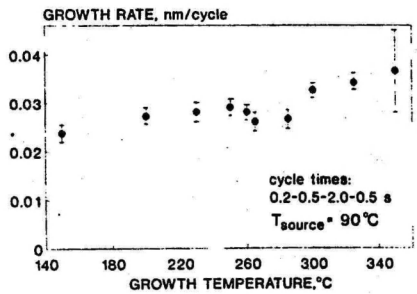

Fig. 3. Dependence of the growth rate of Nb_2O_5 films on growth temperature.

kinetic factors.[25] The film growth rate of 0.028 nm/cycle can be considered as quite a stable value in the narrow temperature range between 230 and 260 °C. The linear relationship between the film thickness and the number of growth cycles, which is characteristic for the ALE deposition process with inherent thickness control, was also verified in the present work. The films grown between 215 and 275 °C using optimum cycle times exhibited 7 % maximum variation in thickness in the gas flow direction (Fig. 4) and less than 5 % perpendicular to the gas flow.

In the case of amorphous material it is complicated to estimate the thickness of one monolayer. Nevertheless, it is obvious that the average growth rate of about 0.03 nm/cycle is lower than the one monolayer per cycle that would be obtained in ideal layer-by-layer growth. An evident rea-

0948-1907/98/0101-0030 $ 17.50+.50/0 *Chem. Vap. Deposition* 1998, 4, No. 1

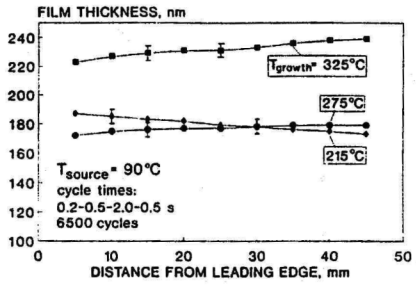

Fig. 4. Thickness profiles of Nb_2O_5 films measured along the gas flow direction.

son for the low growth rate is the steric hindrances caused by the ethoxide ligands.[30–32] Because of these hindrances, the number of niobium atoms in the saturatively chemisorbed $Nb(OC_2H_5)_{5-x}$ monolayer is too low for the formation of a complete monolayer of Nb_2O_5. Nevertheless, even if only a submonolayer is deposited during each cycle, the growth still involves a saturative formation of $Nb(OC_2H_5)_{5-x}$ monolayers, i.e., it is self-limiting, allowing films with good uniformity to be obtained.

Within a temperature region of 260–280 °C the growth rate decreases slightly with an increase in temperature (Fig. 3). This decrease can be attributed to re-evaporation/desorption of the chemisorbed species, dehydroxylation of the film surface or reduction of the $Nb(OC_2H_5)_5$ flux due to its decomposition in the source line.[25] However, above 300 °C the growth rate exhibits a noticeable increase, and therefore the reduction of the precursor flux reaching the substrate can be neglected. At temperatures higher than 325 °C, some film was obtained also in the experiments where only $Nb(OC_2H_5)_5$ was dosed onto the substrate surface without any H_2O pulsing. Thus, the growth above 280 °C is partially enhanced by thermal decomposition of $Nb(OC_2H_5)_5$ on the substrate surface.

It is noteworthy that the thickness profiles of the films became inverted with increasing growth temperature. The films deposited at 215 °C were thicker at the leading edge of the substrate while the films deposited at 275 °C and higher were clearly thicker near the trailing edge of the substrate (Fig. 4). Between 215 and 275 °C, films with minor thickness variations close to 1–2 % could be obtained. At growth temperatures higher than 350 °C, the Nb_2O_5 films became strongly profiled. Films with considerable thickness could be obtained only near the trailing edge of the substrate; the leading edge of the substrate glass remained bare.

The thickness profile with decreasing film thickness along the flow direction is characteristic of the F-120 reactor. It has been attributed to a desorption of one precursor from reactor walls upstream from the substrate during a pulse sequence of the other reactant, thereby resulting in CVD-like growth in the vicinity of the crossing point of the two flow routes.[30,33–35] Since in the F-120 reactor this point is located only about 1 cm ahead of the substrates, the CVD region extends over the substrates, causing a thickness profile at their leading edges. In general, this profile is the narrower the more facile the reactions are. For example, in many processes where metal chlorides are used as precursors the desorbed species become rapidly exhausted and the thickness profile is sharp and narrow, covering only an approximately 1–2 cm wide region at the leading edge.[30,33–35] By contrast, in the present and the other processes[36–38] employing metal alkoxides as precursors the reactions are less facile and, consequently, the thickness profile is smoother and wider. Additional factors possibly affecting the thickness profile are a change of the adsorption density along the flow direction due to an increasing adsorption site blocking by reaction by-products,[39] a consistent decrease of surface density of adsorbing species along the gas flow direction due to the decrease in partial pressure of precursor molecules leaving the adsorption wave[40] and, in the case of processes where alkoxides are used as precursors, weak precursor decomposition.[37,38] These additional factors dominate in the other kind of ALE reactor, where the substrates are located at a distance of up to 10 cm from the source gas flow crossing point, but still nearly identical thickness profiles can be observed.[41]

At temperatures above 275 °C, where inverted thickness profiles were observed, one can account for this by the competitive effect of enhanced thermal desorption of adsorbed ethoxide molecules or hydroxyl groups. In addition, possible impurities in the $Nb(OC_2H_5)_5$ source material, e.g., chlorine, may cause the formation and desorption of volatile compounds such as NbO_xCl_y, resulting in the etching of the film.[26] These processes can explain not only the inverted thickness profile but also the moderate decrease of the film growth rate in the temperature range of 250–280 °C, above which the thermal decomposition of $Nb(OC_2H_5)_5$ begins to dominate and the growth rate increases again (Fig. 3).

2.2. Film Properties

All the films grown on a glass substrate in the present experiments were found to be amorphous when examined by XRD. This is consistent with the reports that CVD-grown Nb_2O_5 films do not crystallize below 400 °C regardless of the substrate material.[1,8,11] However, it is to be noted that the Nb_2O_5 films grown in the present study on a polycrystalline indium tin oxide (ITO) layer tended to crystallize. In the XRD patterns one peak corresponding to the (040) reflection of the monoclinic Nb_2O_5[42] could be clearly distinguished besides peaks characteristic of ITO (Fig. 5). For comparison, no traces of crystallization were detected in the Nb_2O_5 films sputtered onto water-cooled glass sub-

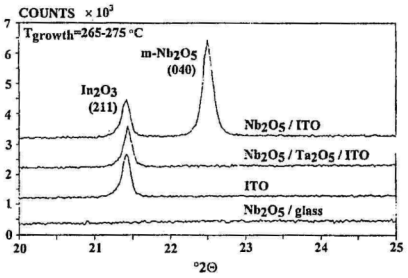

Fig. 5. X-ray diffraction patterns of Nb_2O_5 films grown on bare glass, on an amorphous Ta_2O_5 layer on polycrystalline ITO film, and on polycrystalline ITO film.

strates coated with polycrystalline tin oxide films.[10] Also no crystallization was observed in the present study when a thin (10 nm) amorphous Ta_2O_5 film was grown by ALE between ITO and the Nb_2O_5 films.

Figure 6 shows a cross-sectional SEM image of a Nb_2O_5 film grown at 325 °C. No evident cracks and/or pinholes are observable. The smoothness of the surface is evidently due

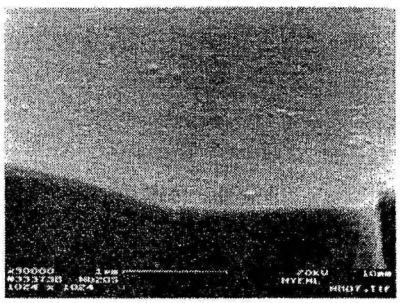

Fig. 6. Cross-sectional SEM image of a Nb_2O_5 film grown at 325 °C on soda lime glass.

to its amorphous nature. Comparison of various films grown by ALE reveals that smooth surfaces are characteristic of the amorphous films[36,43] while the formation of polycrystalline structure is accompanied by significant surface roughening.[30,33–35,38,44,45]

Optical transmission spectra for the films grown at 215, 275, and 325 °C are depicted in Figure 7. This plot implies that the films were transparent and possessed a high refractive index. The refractive index was, in practice, independent of source temperature, cycle times, and film thickness but was influenced by the growth temperature. The refractive index measured at the wavelength λ = 580 nm increased with the deposition temperature, stabilizing at 2.40

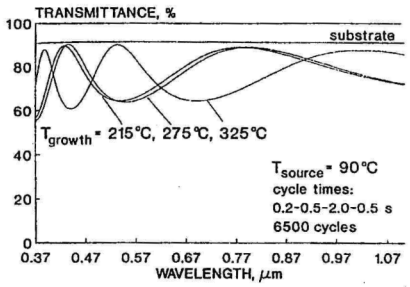

Fig. 7. Transmission spectra of Nb_2O_5 films deposited at different temperatures.

at temperatures of 230 °C and higher (Fig. 8). This value of refractive index is rather high and is equal to that of films grown by ion plating (n = 2.4),[4] which is generally known as a technique that enables highly dense oxide films to be

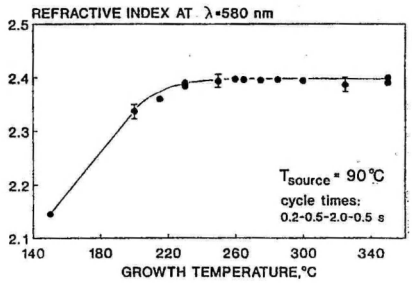

Fig. 8. Dependence of refractive index of Nb_2O_5 films on growth temperature. Solid line is a guide for the eye.

obtained. The high refractive index of thin films can be attributed directly to their high density, as has been shown in the case of TiO_2 films by Ottermann and Bange.[46] For comparison, n = 2.22, 2.31–2.32, and 2.30–2.35 have been achieved in pyrolyzed,[1] sputtered,[5,6] and CVD-grown[8] Nb_2O_5 films, respectively. Thus, a dense amorphous phase of Nb_2O_5 was evidently deposited by ALE in the present study in the temperature range of 230–340 °C.

A backscattering spectrometry (BS) spectrum of the Nb_2O_5 film grown at 325 °C is depicted in Figure 9. Within the accuracy of the BS measurements, the niobium to oxygen atomic ratio in the films grown at 230, 270, and 325 °C corresponded to the stoichiometric Nb_2O_5. The films did not contain any heavy contaminants with concentrations above the detection limit of BS, 0.01–0.1 at.-%. The film thicknesses were evaluated from the BS spectra using the bulk density (4.47 g/cm³ [48]) of crystalline Nb_2O_5. These

  0948-1907/98/0101-0032 $ 17.50+.50/0 *Chem. Vap. Deposition* **1998**, *4*, No. 1

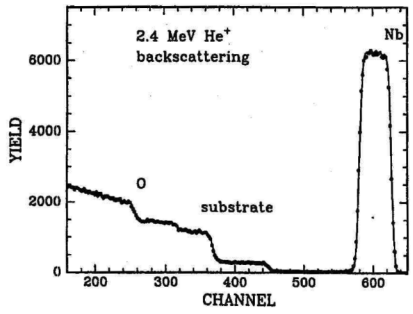

Fig. 9. BS spectrum of a Nb_2O_5 film grown at 325 °C on soda lime glass substrates. The filled circles are measurement data while the solid line is a fitted spectrum obtained using an interactive backscattering simulation program GISA [47]. Labels Nb and O correspond to the step edges of the components. The label "substrate" means all the signals from the substrate, e.g., Ca, Si, and Na (from right to left).

thickness values were found to coincide well with those calculated from optical transmission spectra. Thus it can be concluded that the Nb_2O_5 film density is close to the density of the corresponding bulk material.

3. Conclusions

High-quality niobium oxide thin films were deposited by atomic layer epitaxy in the temperature range of 150–350 °C using $Nb(OC_2H_5)_5$ and H_2O as precursors. All the films grown on amorphous substrates were found to be amorphous when examined by XRD. Reflections of monoclinic Nb_2O_5 were observed in the films deposited onto polycrystalline ITO layers. SEM analysis revealed that the films possessed smooth surfaces. The films deposited at temperatures up to 325 °C exhibited weak thickness profile with maximum variations of around 7 % along the gas flow direction. Inside the narrow temperature range of 230–275 °C films with thickness variations of around a few per cent could be obtained. The refractive index measured at the wavelength λ = 580 nm increased with the deposition temperature, stabilizing at 2.4 above 230 °C. Within the accuracy of BS, the films consisted of stoichiometric Nb_2O_5.

4. Experimental

Niobium oxide films were grown by sequential exposure of 5 cm × 5 cm soda lime glass substrates to niobium and oxygen precursor flows in a hot-wall F120 ALE reactor (Microchemistry Ltd., Espoo, Finland) [24]. Some films were deposited also onto a polycrystalline indium tin oxide layer in order to examine the possible effect of substrate material on structural changes. Nitrogen was used as a carrier and purging gas. The total pressure in the reactor was about 10 mbar. $Nb(OC_2H_5)_5$ (ABCR) as a Nb precursor was evaporated from an open boat held at 70–120 °C inside the reactor. The pulsing of the $Nb(OC_2H_5)_5$ vapor was accomplished by means of inert gas valving [24]. Water vapor as oxygen precursor was generated in an external reservoir at 20 °C and led into the reactor through needle and solenoid valves.

Transmittance spectra of the films were measured within a wavelength range of 380–1100 nm using a Hitachi U-2000 spectrophotometer. A fitting method developed and described by Ylilammi and Ranta-aho [49] was applied to evaluate film thicknesses and refractive indices from these spectra. Comparative thickness measurements and verification of the film stoichiometry were carried out using backscattering spectrometry (BS). The measurements were performed using a 2.4 MeV $^4He^+$ beam with a detection angle of 170 °C. The measuring time was 15 min. Since the samples are dielectrics, special care needs to be taken to prevent charging of the sample. Masks made of high-purity graphite plates were used for this purpose [50]. Structural analysis was carried out with a Philips MPD 1880 powder X-ray diffractometer using Cu Kα radiation. Surface morphology and cross-section of the films were examined by means of a Zeiss DSM 962 scanning electron microscope at the Department of Electron Microscopy at the University of Helsinki.

Received: May 27, 1997
Final version: August 18, 1997

[1] M. T. Duffy, C. C. Wang, A. Waxman, K. H. Zaininger, *J. Electrochem. Soc.* **1969**, *116*, 234.
[2] N. Fuschillo, B. Lalevic, N. K. Annamalai, *Thin Solid Films* **1975**, *30*, 145.
[3] A. Pignolet, G. M. Rao, S. B. Kruphanidhi, *Thin Solid Films* **1995**, *261*, 18.
[4] J. Edlinger, J. Ramm, H. K. Pulker, *Thin Solid Films* **1989**, *175*, 207.
[5] Y. Saito, T. Shiosaki, *Jpn. J. Appl. Phys.* **1992**, *31*, 3164.
[6] H. Onodera, I. Awai, M. Nakajima, J. Ikenoue, *Appl. Opt.* **1984**, *23*, 118.
[7] D. Rosenfeld, R. Sanjinés, F. Lévy, B. A. Buffat, V. Demarne, A. Grisel, *J. Vac. Sci. Technol. A* **1994**, *12*, 135.
[8] N. Hara, E. Takahashi, J. H. Yoon, K. Sugimoto, *J. Electrochem. Soc.* **1994**, *141*, 1669.
[9] N. Özer, D.-G. Chen, C. M. Lampert, *Thin Solid Films* **1996**, *277*, 162.
[10] T. Maruyama, S. Arai, *Appl. Phys. Lett.* **1993**, *63*, 869.
[11] S.-C. Jung, N. Imaishi, H.-C. Park, *Jpn. J. Appl. Phys.* **1995**, *34*, L775.
[12] G. L. Roberts, R. J. Cava, W. F. Peck, J. J. Krajewski, *J. Mater. Res.* **1997**, *12*, 526.
[13] C. K. Barlingay, S. K. Dey, *Thin Solid Films* **1996**, *272*, 112.
[14] K. H. Yoon, Y. S. Kim, E. S. Kim, *J. Mater. Res.* **1995**, *10*, 2085.
[15] R. D. Klissurska, A. K. Tagantsev, K. G. Brooks, N. Setter, *J. Am. Ceram. Soc.* **1997**, *80*, 336.
[16] P. N. Santhosh, H. S. Potdar, S. K. Date, *J. Mater. Res.* **1997**, *12*, 326.
[17] K. H. Yoon, E. S. Kim, *Mater. Res. Bull.* **1995**, *30*, 813.
[18] F. Wang, D. O. Northwood, *J. Mater. Sci.* **1995**, *30*, 4003.
[19] D.-Y. Kim, H.-J. Park, D.-H. Cho, *Solid State Ionics* **1995**, *80*, 67.
[20] X. J. Huang, W. Wepper, *J. Chem. Soc. Faraday Trans.* **1996**, *92*, 2173.
[21] See articles in *Catal. Today* **1996**, *28*, Nos. 1–2.
[22] R. Y. Chau, W.-S. Ho, J. C. Wolfe, D. L. Licon, *Thin Solid Films* **1996**, *287*, 57.
[23] T. Hashimoto, T. Yoko, *Mater. Trans., JIM* **1996**, *37*, 435.
[24] T. Suntola, *Mater. Sci. Rep.* **1989**, *7*, 266. T. Suntola, *Thin Solid Films* **1992**, *216*, 84.
[25] L. Niinistö, M. Ritala, M. Leskelä, *Mater. Sci. Eng. B* **1996**, *41*, 23.
[26] K.-E. Elers, M. Ritala, M. Leskelä, E. Rauhala, *Appl. Surf. Sci.* **1994**, *82/83*, 468.
[27] K. Kukli, M. Ritala, M. Leskelä, *Nanostruct. Mater.*, in press.
[28] K. Kukli, J. Ihanus, M. Ritala, M. Leskelä, *Appl. Phys. Lett.* **1996**, *68*, 3737.
[29] K. Kukli, J. Ihanus, M. Ritala, M. Leskelä, *J. Electrochem. Soc.* **1997**, *144*, 300.
[30] M. Ritala, *Ann. Acad. Sci. Fenn., Ser. A2* **1994**, *257*, 1.
[31] M. Leskelä, M. Ritala, *J. Phys. IV (Paris)* **1995**, *5*, C5-937.
[32] M. Ylilammi, *Thin Solid Films* **1996**, *279*, 124.
[33] M. Ritala, M. Leskelä, L. Niinistö, T. Prohaska, G. Friedbacher, M. Grasserbauer, *Thin Solid Films* **1994**, *250*, 72.
[34] M. Ritala, M. Leskelä, L.-S. Johansson, L. Niinistö, *Thin Solid Films* **1993**, *228*, 32.
[35] M.Ritala, M. Leskelä, E. Rauhala, P. Haussalo, *J. Electrochem. Soc.* **1995**, *142*, 2731.
[36] K. Kukli, M. Ritala, M. Leskelä, *J. Electrochem. Soc.* **1995**, *142*, 1670.
[37] M. Ritala, M. Leskelä, L. Niinistö, P. Haussalo, *Chem. Mater.* **1993**, *5*, 1174.
[38] M. Ritala, M. Leskelä, E. Rauhala, *Chem. Mater.* **1994**, *6*, 556.

  0948-1907/98/0101-0033 $ 17.50+.50/0

[39] H. Siimon, J. Aarik, *J. Phys. D: Appl. Phys.* **1997**, *30*, 1725.
[40] M. Ylilammi, *J. Electrochem. Soc.* **1995**, *142*, 2474.
[41] K. Kukli, J. Aarik, A. Aidla, H. Siimon, M. Ritala, M. Leskelä, *Appl. Surf. Sci.* **1997**, *112*, 236.
[42] Joint Committee of Powder Diffraction Data, Card 27-1312.
[43] M. Ritala, H. Saloniemi, M. Leskelä, T. Prohaska, G. Friedbacher, M. Grasserbauer, *Thin Solid Films* **1996**, *286*, 54.
[44] T. Asikainen, M. Ritala, M. Leskelä, T. Prohaska, G. Friedbacher, M. Grasserbauer, *Appl. Surf. Sci.* **1996**, *99*, 91.
[45] J. Ihanus, M. Ritala, M. Leskelä, T. Prohaska, R. Resch, G. Friedbacher, M. Grasserbauer, *Appl. Surf. Sci.*, **1997**, *120*, 45.
[46] C. R. Ottermann, K. Bange, *Thin Solid Films* **1996**, *286*, 32.
[47] E. Rauhala, J. Saarilahti, *Nucl. Instrum. Methods B* **1992**, *64*, 734.
[48] *CRC Handbook of Chemistry and Physics*, 68th ed., CRC Press, Boca Raton, FL **1966**, p. B-111.
[49] M. Ylilammi, T. Ranta-aho, *Thin Solid Films* **1993**, *232*, 56.
[50] R. Lappalainen, J.-P. Hirvonen, P. Pokela, J. Alanen, *Thin Solid Films* **1989**, *181*, 259.

VI

Reprinted with permission from *Journal of the Vacuum Science and Technology*, Vol. A 15 (1997), K. Kukli, M. Ritala, M. Leskelä and J. Jokinen, Atomic layer epitaxy growth of aluminium oxide thin films from a novel $Al(CH_3)_2Cl$ precursor and H_2O, pp. 2214–2218,

Atomic layer epitaxy growth of aluminum oxide thin films from a novel $Al(CH_3)_2Cl$ precursor and H_2O

Kaupo Kukli,[a] Mikko Ritala,[b] and Markku Leskelä
Department of Chemistry, Laboratory of Inorganic Chemistry, University of Helsinki, P. O. Box 55, FIN-00014, University of Helsinki, Finland

Janne Jokinen
Accelerator Laboratory, P. O. Box 43, FIN-00014, University of Helsinki, Finland

(Received 25 July 1996; accepted 7 February 1997)

The deposition of Al_2O_3 thin films by atomic layer epitaxy was investigated using $Al(CH_3)_2Cl$ as a new aluminum precursor. All the films grown in the temperature range of 125–500 °C were amorphous as examined by x-ray diffraction analysis. The residual contents of carbon, chlorine, and hydrogen in the film deposited at 200 °C were 0.2, 2.1, and 12 at. %, respectively, and diminished rapidly with increasing growth temperature. The refractive index of the films increased with deposition temperature, stabilizing at the highest value of 1.68 above 300 °C. The permittivity of the films increased from 7.3 to 8.7 with increasing growth temperature from 200 to 500 °C. The leakage current density was lowest in the film deposited at 200 °C and increased markedly at higher deposition temperatures. © *1997 American Vacuum Society*. [S0734-2101(97)03104-7]

I. INTRODUCTION

Al_2O_3 thin films have been characterized by high chemical and thermal stability; high resistivity and dielectric strength; good adhesion, and small number of pinholes.[1,2] Al_2O_3 has been used as dielectric, ion barrier, and passivation material for thin film electroluminescent displays.[3–5] Al_2O_3 is applicable as corrosion and wear resistant[2,6] and optical coatings.[7,8]

Different growth methods, such as reactive dc magnetron sputtering[8] and chemical vapor deposition (CVD)[2] have been used to produce high-quality aluminum oxide films. In CVD, a large number of aluminum precursors including aluminum halides, alkoxides, β-diketonates, and metalorganic compounds have been employed for the CVD growth of Al_2O_3 films. Amorphous Al_2O_3 films grown by CVD at low temperatures have demonstrated excellent dielectric properties.[2,9]

Besides conventional CVD, atomic layer epitaxy (ALE)[5] has been used to deposit Al_2O_3 films.[7,10–21] The ALE growth is based on alternate exposure of the substrate surface to different precursors. Between the precursor pulses the reactor is purged with an inert gas. A characteristic feature of the ALE growth is the self-limiting adsorption of a given precursor onto the substrate surface. Therefore, the film thickness is proportional to the number of deposition cycles used. ALE can be used to produce large-area thin films with excellent uniformity and reproducibility. ALE also enables one to obtain high-quality material at relatively low growth temperatures. $AlCl_3$ (Refs. 7, 11–13, and 17–21) and $Al(CH_3)_3$ (Refs. 9, 14–16, and 18) have been the most widely used metal precursors for ALE-processed Al_2O_3 while H_2O (Refs. 7, 10, 11, 13, and 18) or H_2O_2 and N_2O (Refs. 14 and 16) have been the most common oxygen precursors. In the present work we report the preparation of Al_2O_3 films by ALE from a less-known dimethylaluminum chloride $Al(CH_3)_2Cl$ (DMACl) as a metal precursor while H_2O is applied as an oxygen precursor. The vapor pressure of DMACl is comparable to that of $Al(CH_3)_3$, thereby allowing a more convenient transportation than the solid $AlCl_3$. In addition, a smaller amount of corrosive byproduct HCl is formed than in the case of $AlCl_3$, and also a reduced chlorine contamination of the films can be expected. On the other hand, due to the one chlorine ligand, DMACl is assumed to exhibit somewhat better stability against decomposition than $Al(CH_3)_3$.

II. EXPERIMENT

Aluminum oxide films were grown onto 5×5 cm^2 soda lime glass substrates using a hot-wall flow-type F120 ALE reactor (Microchemistry Ltd., Espoo, Finland).[5] Nitrogen was used as a carrier and purging gas. The total pressure in the reactor was about 10 mbar. DMACl and water were evaporated from external reservoirs held at room temperature. Precursors were led into the reactor through needle and solenoid valves.

Transmittance spectra of the films grown were measured within a wavelength range of 370–1100 nm using a Hitachi U-2000 spectrophotometer. All optical measurements were carried out at the same point on different substrates. A fitting method developed and described by Ylilammi and Ranta-aho[22] was exploited for evaluating film thicknesses and refractive indices from these spectra. Structural analysis was carried out with a Philips MPD 1880 powder x-ray diffractometer using Cu $K\alpha$ radiation. The depth profiling of residual contaminants was carried out using time-of-flight elastic recoil detection analysis (TOF-ERDA)[23] for chlorine and carbon and nuclear resonance broadening (NRB) technique with the 6.39 MeV resonance of the reaction

[a]On leave from Institute of Experimental Physics and Technology, University of Tartu, EE2400 Tartu, Estonia.
[b]Electronic mail: mikko.ritala@helsinki.fi

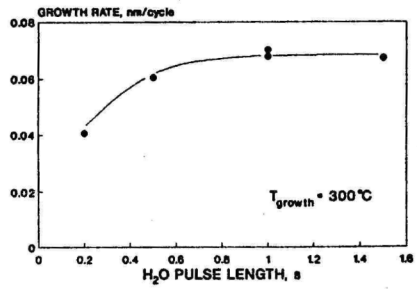

FIG. 1. Dependence of Al_2O_3 growth rate on water pulse length. The growth cycle consisted of $Al(CH_3)_2Cl$ exposure time 0.2 s, the first purge period 0.5 s, H_2O exposure time, and the second purge period 0.5 s. Solid line is drawn for convenience. Experimental measurement error is covered by the size of data points.

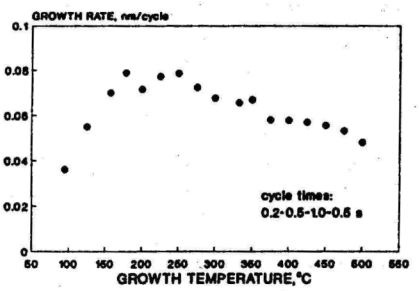

FIG. 2. Dependence of Al_2O_3 growth rate on growth temperature. Experimental measurement error is covered by the size of data points.

$^1H(^{15}N,\alpha\gamma)^{12}C$ for hydrogen.[23,24] 37 MeV $^{197}Au^{7+}$ beam for TOF-ERDA and $^{15}N^{2+}$ beam for NRB were obtained from a 5 MV tandem accelerator EGP-10-II at the Accelerator Laboratory.

In order to measure basic electrical characteristics, aluminum oxide films with thicknesses of 140–180 nm were deposited onto sputtered indium-tin oxide (ITO) electrodes. An array of aluminum electrodes was evaporated onto the aluminum oxide layer enabling the measurement of the dielectric properties over an approximate surface area of 20 cm^2. The effective area of a single electrode was 29.4 mm^2. Capacitances were measured at a frequency of 10 kHz using a HP 4275A multifrequency *LCR* meter, and the current–voltage characteristics with a HP 4140B pA meter/dc source. All measurements were carried out at room temperature.

III. RESULTS

Figure 1 shows the dependence of the film growth rate on H_2O exposure time. The stabilization of the growth rate at about 0.07 nm/cycle with pulse times longer than 1.0 s is evident. This saturative behavior of the growth rate is analogous to that reported for films grown from $Al(CH_3)_3$ and H_2O.[10] The effect of the DMACl pulse length was also studied but no essential differences were found between films grown using 0.2 and 1 s pulses. Therefore, DMACl and water pulse lengths of 0.2 and 1.0 s, respectively, were chosen to be employed in subsequent experiments. The purge time, when varied from 0.5 to 1.0 s, had no effect to the deposition rate either. The films grown using optimum cycle times exhibited about 7% deviation in thickness, as a maximum, in the gas flow direction and about 3% perpendicular to the gas flow.

Figure 2 demonstrates the dependence of the growth rate on the deposition temperature. The maximum growth rate of approximately 0.08 nm/cycle is achieved in the narrow temperature range of 180–250 °C. The lower growth rate below 180 °C is apparently due to the incomplete surface reactions at temperatures close to the reaction threshold. Within a temperature region of 250–500 °C the growth rate decreases with an increase in temperature. This decrease can be attributed, most probably, to the dehydroxylation of the Al_2O_3 surface during purging period after H_2O exposure, thereby

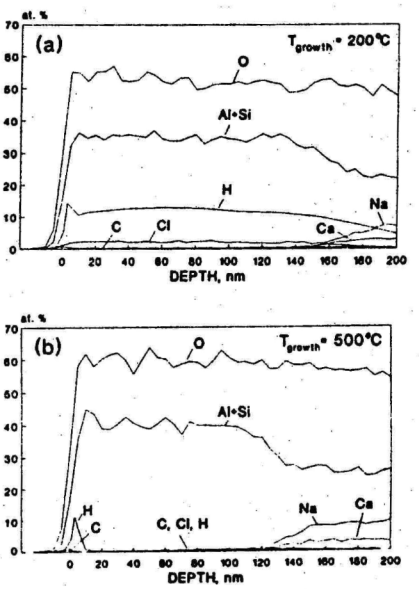

FIG. 3. Composition depth profiles in the films deposited at (a) 200 and (b) 500 °C. The substrate atom concentrations are only relative since, in the data analysis, the density of the film was used also for the substrate. Due to the overlap of signals from Al and Si, the mass separation of these elements is not reliable away from the surface and spectra of Al and Si were analyzed together.

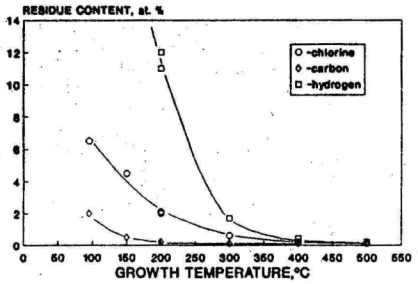

FIG. 4. Temperature dependences of Cl, C, and H residual contents in Al_2O_3 thin films measured by TOF-ERDA and NRB. Solid lines are guides to eye.

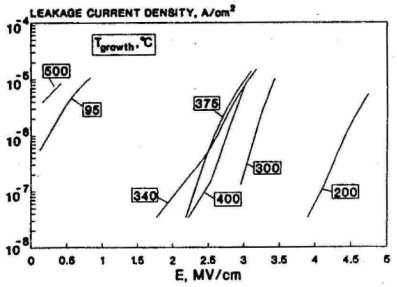

FIG. 6. Plots of leakage current density vs electric field applied to Al_2O_3 thin films deposited at different growth temperatures from $Al(CH_3)_2Cl$ and H_2O.

reducing the amount of reactive surface sites for the adsorption of DMACl supplied subsequently. All the films grown in the present experiments were amorphous as examined by x-ray diffraction (XRD). This is consistent, in general, with several data published about the structure of aluminum oxide films deposited by ALE onto amorphous glass substrates using different source materials.[1,7,13,17,18]

The results of composition analysis are depicted in Figs. 3 and 4. The contents of hydrogen, chlorine, and carbon residues are relatively high in the films deposited below 200 °C (Fig. 4) but they diminished rapidly with the increase in deposition temperature, decreasing below 1 at. % level in the films grown at 400 °C. It is likely that at low temperatures oxide hydroxide and oxide chloride are formed together with pure aluminum oxide. The hydrogen content was as high as 60 at. % in the film grown at 95 °C. In the film grown at 500 °C only a relatively weak surface peak of hydrogen was detected [Fig. 3(b)].

The refractive index measured at a wavelength $\lambda = 580$ nm increased with the deposition temperature from 1.59 to 1.68, obviously stabilizing at the highest value when temperatures higher than 300 °C were used (Fig. 5). It is noteworthy that this value of refractive index is rather high referring to the relatively dense amorphous phase of Al_2O_3.[10,14,15] Also, the dielectric constant increased from 7.3 to 8.5 when the growth temperature increased from 200 to 500 °C (Fig. 5). For comparison, Kattelus *et al.*[13] reported $n = 1.67$ and $\varepsilon = 8.4$ for Al_2O_3 films grown by ALE at 300 °C using $AlCl_3$ as an aluminum precursor. Below 200 °C the films grown in the present study were too conductive for the reliable determination of the dielectric constant. The dramatic increase in ac conductivity is most likely due to the remarkable increment of impurity content in the low temperature films (Fig. 4).

Samples examined in the present study exhibited rather uniform current–voltage dependences over the 20 cm^2 measurement area. Typical leakage current density versus electric field curves are depicted in Fig. 6 for the films grown at different temperatures. The film deposited at 200 °C exhibited clearly superior resistance to leakage current in comparison with the other samples.

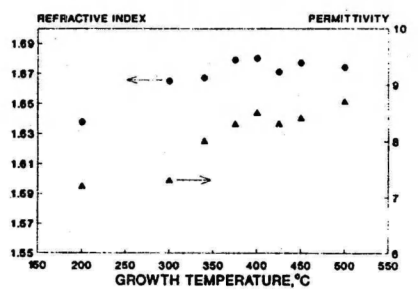

FIG. 5. Behavior of refractive index and dielectric constant vs growth temperature.

IV. DISCUSSION

The growth temperature was found to have a strong effect on the film composition, refractive index, and dielectric constant. Changes in the film composition, i.e., trace element contents, affected also the physical properties of the films. The decrease of contamination level is likely the reason for the film densification and, consequently, for the increase in refractive index and dielectric constant (Figs. 4 and 5). However, it seems that the impurity contents detected in these films are still moderate and actually too low to directly affect the conduction properties (Fig. 6) even at 200 °C. Moreover, though the residue contents decreased, the leakage current increased with the increase in growth temperature from 200 to 500 °C (Figs. 4 and 6). Of course, the growth temperatures close to 100 °C are obviously too low to attain oxide films with well defined dielectric properties, as indicated especially by the extremely high hydrogen content in the film grown at 95 °C.

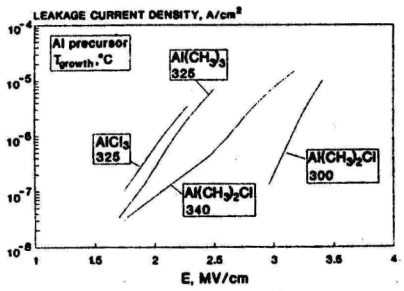

FIG. 7. Plots of leakage current density vs electric field applied to Al_2O_3 thin films deposited by ALE using different Al precursors and water.

It should be noted that high dielectric constant and low leakage current often contradict one another.[25,26] In the case of sufficiently thick oxide films (>50 nm, approximately) and at high electric fields the electronic conduction often tends to be bulk limited in accord with the Poole–Frenkel potential barrier model.[25,26] Analysis of the data given in Fig. 6 shows that our aluminum oxide films display nearly a linearly correlated $\log(I/E)$ vs $E^{1/2}$ curve. Thus, the Poole–Frenkel conduction mechanism at high fields can be considered in the present case as well.

The Poole–Frenkel emission is due to field-enhanced thermal excitation of electrons from trap levels into the conduction band and can be expressed as

$$I/E = \sigma_0 \exp[-(\Phi - \Delta\Phi)/2kT], \quad (1)$$

where I is the leakage current density, E is the external electric field, σ_0 is the low field conductivity, Φ is the Poole–Frenkel potential barrier, $\Delta\Phi$ is the field-induced potential barrier lowering, k is the Boltzmann's constant, and T is the absolute temperature. $\Delta\Phi$ is square-root dependent on the external field and inverse-square-root dependent on the permittivity.[27,28] The height of potential barrier Φ is independent of electric field applied and inversely proportional to the dielectric constant of the material.[28,29] Thus the magnitude of leakage current is predominantly dependent on permittivity; the higher the permittivity the higher the leakage current. This trend was verified also in the present work as can be seen by comparing the behavior of dielectric constant (Fig. 5) and leakage current (Fig. 6) versus growth temperature.

In Fig. 7 Al_2O_3 thin films deposited in the present study are compared with those deposited by ALE from $AlCl_3$ and $Al(CH_3)_3$.[18] revealing that the films grown from $Al(CH_3)_2Cl$ exhibited remarkably lower leakage current densities. Better breakdown resistance as well as well-defined optical properties refer directly to the preferences of the new precursor and higher quality of the films deposited. As the ALE deposited Al_2O_3 films have been amorphous regardless of the Al precursor used,[7,10–21] the improvement of the dielectric properties is most likely assigned to lower contamination level, not to structural differences.

There exist rather few reports on the contamination analysis of ALE-grown aluminum oxide films. It can be noted, however, that the impurity contents in Al_2O_3 films grown by ALE from $AlCl_3$ exhibit similar decreasing behavior with increasing growth temperature from 100 to 500 °C[11,19–21] as observed in the present study. However, the chlorine content in the films grown in the present study from DMACl was 5%–60% of that in films prepared from $AlCl_3$.[19–21] The difference in the chlorine content seemed to increase toward higher growth temperatures. In this respect the usage of DMACl seems to be advantageous.

V. CONCLUSION

Amorphous aluminum oxide thin films were deposited by atomic layer epitaxy via sequential surface reactions in the temperature range of 95–500 °C using $Al(CH_3)_2Cl$ and H_2O as precursors. The maximum growth rate of about 0.08 nm/cycle was determined in the temperature range of 180–250 °C using the optimum precursor pulse lengths. The refractive index measured at the wavelength λ=580 nm increased with the deposition temperature, stabilizing at 1.68 when temperatures higher than 300 °C were used. The value of permittivity ε increased from 7.3 to 8.7 with the increase in growth temperature from 200 to 500 °C. The residual contents of carbon, chlorine, and hydrogen in the film deposited at 200 °C were 0.2, 2.1, and 12 at. %, respectively, and diminished rapidly with increasing growth temperature. Leakage current density increased with the deposition temperature. The leakage current density in the films deposited at 200 °C was as low as 5×10^{-8} A/cm^2 at the electric field strength of 4 MV/cm. The leakage current density in the films deposited from $Al(CH_3)_2Cl$ was remarkably lower than in those deposited from $Al(CH_3)_3$ and $AlCl_3$.

ACKNOWLEDGMENTS

The authors are indebted to Erkki Soininen and Juha Viljanen from Planar International Ltd. for the access to the electrical measurement techniques. This work was supported in part by the Academy of Finland and Technology Development Centre (TEKES, Helsinki, Finland). K. K. expresses gratitude to the Finnish Centre for International Mobility (CIMO) for a research grant.

[1] M. Leskelä and M. Ritala, J. Phys. (France) IV **5**, C5-937 (1995).
[2] E. Fredriksson and J.-O. Carlsson, J. Chem. Vapor Dep. **1**, 333 (1993).
[3] S. Shih, P. D. Keir, J. E. Wagner, and J. Viljanen, J. Appl. Phys. **78**, 5775 (1995).
[4] W. Barrow, R. Coovert, E. Dickey, T. Flegal, M. Fullman, C. King, and C. Laakso, SID 94 Digest, 448 (1994).
[5] T. Suntola, Thin Solid Films **216**, 84 (1992).
[6] H. D. van Gorbach, V. A. C. Haanappel, T. Fransen, and P. J. Gellings, Thin Solid Films **239**, 31 (1994).
[7] D. Riihelä, M. Ritala, R. Matero, and M. Leskelä, Thin Solid Films **289**, 250 (1996).
[8] S. M. Edlou, A. Smajkiewicz, and G. A. Al-Jumaily, Appl. Opt. **32**, 5601 (1993).
[9] V. P. Ovsyannikov, G. V. Lashkarov, and E. A. Mazurenko, J. Phys. (France) IV **5**, C5-705 (1995).

[10]S. Higashi and C. G. Fleming, Appl. Phys. Lett. **55**, 1963 (1989).
[11]L. Hiltunen, H. Kattelus, M. Leskelä, M. Mäkelä, L. Niinistö, E. Nykänen, P. Soininen, and M. Tiitta, Mater. Chem. Phys. **28**, 379 (1991).
[12]J. Aarik, A. Aidla, A. Jaek, A.-A. Kiisler, and A.-A. Tammik, Acta Polytech. Scand. Chem. Technol. Ser. **195**, 201 (1990).
[13]H. Kattelus, M. Ylilammi, J. Saarilahti, J. Antson, and S. Lindfors, Thin Solid Films **225**, 296 (1993).
[14]H. Kumagai, K. Toyoda, M. Matsumoto, and M. Obara, Jpn. J. Appl. Phys. **32**, 6137 (1993).
[15]H. Kumagai and K. Toyoda, Appl. Surf. Sci. **82/83**, 481 (1994).
[16]V. E. Drozd, A. P. Baraban, and I. O. Nikiforova, Appl. Surf. Sci. **82/83**, 583 (1994).
[17]M. Ritala, H. Saloniemi, M. Leskelä, T. Prohaska, G. Friedbacher, and M. Grasserbauer, Thin Solid Films **286**, 54 (1996).
[18]K. Kukli, J. Ihanus, M. Ritala, and M. Leskelä, J. Electrochem. Soc. **144**, 300 (1997).
[19]M. Hamilo, M. S. thesis, Helsinki University of Technology, Espoo, Finland, 1983.
[20]J. Aarik, A. Jaek, A.-A. Kiisler, and V. Sammelselg, Acta Comment. Univ. Tartuensis **964**, 12 (1993).
[21]M. Nieminen, L. Niinistö, and R. Lappalainen, Mikrochim. Acta **119**, 13 (1995).
[22]M. Ylilammi and T. Ranta-aho, Thin Solid Films **232**, 56 (1993).
[23]J. Jokinen, J. Keinonen, P. Tikkanen, A. Kuronen, T. Ahlgren, and K. Nordlund, Nucl. Instrum. Methods Phys. Res. B **119**, 533 (1996).
[24]J. Jokinen, P. Haussalo, J. Keinonen, M. Ritala, D. Riihelä, and M. Leskelä, Thin Solid Films **289**, 159 (1996).
[25]P. Balk, Adv. Mater. **7**, 703 (1995).
[26]P. Balk, J. Non-Cryst. Solids **187**, 1 (1995).
[27]J. G. Simmons, J. Phys. D **4**, 613 (1971).
[28]J. Frenkel, Phys. Rev. **54**, 647 (1938).
[29]X. M. Wu, S. R. Soss, E. J. Rumaszewski, and T. M. Lu, Mater. Chem. Phys. **38**, 297 (1994).

VII

Reprinted from *Journal of the Electrochemical Society*, Vol. 144 (1997),
K. Kukli, J. Ihanus, M. Ritala and M. Leskelä,
Properties of Ta_2O_5 based dielectric oxide multilayers
deposited by atomic layer epitaxy, pp. 300–306,

Properties of Ta_2O_5-Based Dielectric Nanolaminates Deposited by Atomic Layer Epitaxy

Kaupo Kukli,* Jarkko Ihanus, Mikko Ritala,* and Markku Leskelä

Department of Chemistry, University of Helsinki, FIN-00014, Helsinki, Finland

ABSTRACT

Dielectric thin films and multilayers suitable for application as insulating layers in electroluminescent display devices have been studied. In this work, ZrO_2-Ta_2O_5 and Al_2O_3-Ta_2O_5 nanolaminates with improved dielectric characteristics were grown by atomic layer epitaxy. The films were evaluated by capacitance and current-voltage measurements. The pure Ta_2O_5, Al_2O_3, and ZrO_2 films possessed charge-storage factors up to 8, 16, and 19 nC/mm^2, respectively, at a leakage current density of 1 μA/cm^2. The Al_2O_3-Ta_2O_5 nanolaminates were completely amorphous and their storage factors did not exceed 30 nC/mm^2. The ZrO_2-Ta_2O_5 nanolaminates showed remarkably improved dielectric properties when compared with those of the pure oxide films, especially when the interlayer thicknesses were optimized. Nanosize crystallites of monoclinic and metastable tetragonal ZrO_2 were observed in the nanolaminates by x-ray diffraction. The ZrO_2-Ta_2O_5 nanolaminates possessed high charge-storage factors up to 64 nC/mm^2 and showed superior stability of the dielectric properties.

Introduction

The performance and reliability of ac thin-film electroluminescent (ACTFEL) displays depend a great deal on the quality of dielectric layers which prevent the active phosphor layer from breakdown.[1] There are several requirements for good dielectrics. The dielectric strength must be as high as possible and the dielectric constant has to be high enough so that a low driving voltage is possible. The dielectric material has to be mechanically stable and chemically inert to prevent reactions with other films in contact with it. In addition, film defects should be avoided.[1] To be able to use inexpensive soda lime glass as a substrate in ACTFEL devices, the deposition process has to be carried out at relatively low temperatures, below 500°C. For the same reason, the dielectric films should possess sufficient quality in the as-deposited state, because high-temperature annealing processes cannot be used.

ACTFEL structures have been prepared using physical[2,3] as well as chemical deposition methods, particularly atomic layer epitaxy (ALE).[1,4,5] The ALE method is based on sequential exposures of the substrate surface to different precursors separated with purging periods, thus providing digital growth rate control.[6] ALE is recognized as a suitable technique for the growth of complex layered structures.[4,6] Other merits of ALE are the possibility to obtain abrupt interfaces and uniformity over large areas[6] and deposition convenience when low growth temperatures are needed.

Owing to its relatively high dielectric permittivity and breakdown field strength, Ta_2O_5 is a potential material for dielectric layers in ACTFEL devices.[7] Ta_2O_5 has also been reported to have beneficial effects on crystallinity and luminance levels of the subsequently deposited blue emitting SrS:Ce films.[8] Unfortunately, high permittivity is often accompanied with high leakage current.[9-12] Generally, the presence of defect states, such as oxygen vacancies and Cl, C, or OH residues, has been reported to be responsible for the inferior dielectric properties of Ta_2O_5.[7,9,10,13] The increase of leakage current has also been related directly to the high permittivity of Ta_2O_5 causing lowering of the Poole-Frenkel conduction barrier.[11]

Ta_2O_5 thin films have been grown by ALE using both $TaCl_5$[14,15] and $Ta(OC_2H_5)_5$ [16] in combination with water as precursors. The ALE-grown films had high leakage currents[14-16] as is common with Ta_2O_5 films prepared by other methods. There was, however, an order of magnitude difference between the two processes: the leakage currents at 1 MV/cm electric field were 40 mA/cm^2 for the films grown from $TaCl_5$ [14,15] but only 2.3 mA/cm^2 for those prepared from $Ta(OC_2H_5)_5$.[16] Although semi-insulating Ta_2O_5 layers can be employed as carrier injectors in the ACTFEL devices,[17] the search for ways to reduce leakage currents is of importance. In general, two approaches have been employed to improve the dielectric properties of Ta_2O_5 thin films: postdeposition annealing[9,10] and preparation of oxide mixtures from Ta_2O_5 and some other metal oxide, *e.g.*, Al_2O_3,[7,18] TiO_2,[7,19] WO_3, Nb_2O_5, BiO_3, SiO_2,[7] or ZrO_2.[7,20]

Kattelus *et al.*[14,15] demonstrated that leakage currents through the Ta_2O_5 films grown by ALE from $TaCl_5$ can be significantly reduced with the aid of composite films consisting of thin alternate layers of Ta_2O_5 and either HfO_2 or Al_2O_3. In the HfO_2-Ta_2O_5 composites, the dielectric constants remained above 20, which made them more interesting than the Al_2O_3-Ta_2O_5 composites which suffered from a decrease of the dielectric constant along with increasing Al_2O_3 content. The HfO_2-Ta_2O_5 multilayers combined the positive features of both constituents, *i.e.*, the reversible breakdown of Ta_2O_5 and the low leakage current of HfO_2 at moderate electric fields below 2 MV/cm. The HfO_2-Ta_2O_5 composites possessed leakage currents of 40 nA/cm^2 under 1 MV/cm field strength, which is a remarkably low value considering the fact that the films had not experienced temperatures higher than 325°C.[21] Li *et al.*[2] and Yoshida *et al.*[3] reported the use of HfO_2-Ta_2O_5-HfO_2 triple-layer insulators in ACTFEL devices, resulting in increased charge density, brightness, and efficiency as compared with analogous devices with single-layer dielectrics.

The aim of this study was to examine if the dielectric properties of Ta_2O_5 films grown by ALE from a chlorine-free tantalum precursor, $Ta(OC_2H_5)_5$, could be improved using a multilayer configuration with ZrO_2 and Al_2O_3. Since the leakage currents through pure Ta_2O_5 film grown from $Ta(OC_2H_5)_5$ were an order of magnitude lower than those of the films grown from $TaCl_5$, $Ta(OC_2H_5)_5$ appears to be a promising Ta precursor also for multilayer deposition. In our previous work, we examined the deposition and properties of HfO_2-Ta_2O_5 nanolaminates.[21] By optimizing the interlayer thicknesses in these multilayer structures, the dielectric properties, especially leakage current densities, were improved markedly. In the present work, the composite films were prepared from sequential layers of Ta_2O_5 and alternative oxides ZrO_2 or Al_2O_3, which are known as materials of low conductivity and high chemical stability[22-24] and have earlier been deposited by ALE.[24]

Experimental

Metal oxide films were grown on 5 × 5 cm^2 soda lime glass substrates using a hotwall flow-type F120 ALE reactor (Microchemistry, Limited, Espoo, Finland).[6] Nitrogen was used as a carrier and purging gas. The total pressure in the reactor was about 10 mbar. $Ta(OC_2H_5)_5$, $ZrCl_4$, and

* Electrochemical Society Active Member.
* Permanent address: Institute of Experimental Physics and Technology, University of Tartu, EE2400 Tartu, Estonia.

$AlCl_3$ were evaporated from open boats held at 105, 150, and 95°C, respectively, inside the reactor. The pulsing of the metal precursors was accomplished by means of inert gas valving.[8] Trimethylaluminum, $Al(CH_3)_3$, was led into the reactor from an external reservoir held at room temperature. Water vapor was generated in an external reservoir thermostated at 20°C and led into the reactor through needle and solenoid valves. All the films were grown at 325°C reactor temperature, because in our earlier work[16] this was established as the upper edge of the ALE window, *i.e.*, the highest temperature where the growth of Ta_2O_5 takes place in the self-controlled mode. Films grown at this temperature exhibited better dielectric properties than those deposited at lower temperatures. The optimum metal precursor and water exposure times used for the multilayer deposition were 0.2 and 2.0 s for $Ta(OC_2H_5)_5$ and H_2O, respectively, as established earlier.[16] Exposure times of 0.2/0.5 s were applied for the $ZrCl_4/H_2O$ system and 0.2/0.2 s for both $AlCl_3/H_2O$ and $Al(CH_3)_3/H_2O$ processes. Purge times between the precursor pulses were 0.5 s in all cases.

Growth rates of single-oxide interlayers (expressed as Å/cycle) were evaluated from pure binary oxide films grown to the thickness of about 160 nm. These growth rates were used in calculating the appropriate amount of deposition cycles needed to achieve the target thicknesses of the thin single layers in the multilayer structure. Because the growth rates may be somewhat different during the early stages of film growth, the real layer thicknesses may differ slightly from the target values.

In order to measure the basic electrical characteristics, metal oxide nanolaminates and single binary oxide films were deposited onto indium-tin oxide (ITO) electrodes (Fig. 1). The ITO electrodes were sputtered onto an Al_2O_3 layer acting as a barrier against sodium diffusion from the glass substrate. In most cases, a Ta_2O_5 film with an approximate thickness of 10 nm was first deposited onto the ITO electrodes. The nanolaminates were grown onto this underlayer (Fig. 1). The thicknesses of the Ta_2O_5 single layers in different samples were in the range 1.2 to 18 nm. Correspondingly, the thicknesses of the other oxide layers were varied in a way that the total thickness of one MO_x-Ta_2O_5 bilayer remained constant in a particular sample series. Three main sample series with different bilayer thicknesses of 20, 10, and 5 nm were prepared. The total thickness of all samples was held in the range of 150 to 200 nm. In all the samples described, the topmost layers were Ta_2O_5. In addition, some ZrO_2-Ta_2O_5 multilayers where both the underlayers and the topmost layers consisted of ZrO_2 were prepared as well. For comparative measurements, single Ta_2O_5, ZrO_2, and Al_2O_3 films were also deposited. The capacitors were completed by evaporating the aluminium electrodes onto the multilayers (Fig. 1).

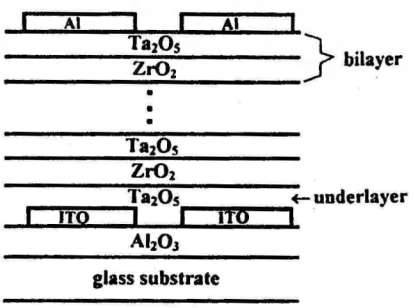

Fig. 1. A schematic representation of the nanolaminate structure. Al_2O_3 replaces ZrO_2 in the alternative structure type studied.

enabling the measurement of the dielectric properties at different points on the 5 × 5 cm^2 sample area. The effective area of a single electrode was 29.4 mm^2. Capacitances were measured at a frequency of 10 kHz using an HP 4275A multifrequency LCR meter, and the current-voltage characteristics were analyzed with an HP 4140B pA meter/dc voltage source or HP 4142B modular dc source. All measurements were made at room temperature.

Transmittance spectra of the single oxides as well as nanolaminates deposited onto bare glass substrates were measured within a wavelength range of 370 to 1100 nm using a Hitachi U-2000 spectrophotometer. A fitting method developed and described by Ylilammi and Rantaaho[25] was exploited for evaluating film thicknesses and refractive indexes from these spectra. Since the thicknesses of the single layers in the sandwich structures were below 20 nm, their determination with the aid of transmission measurements was not possible. Instead, the transmission spectra were fitted using a single-layer model which gave only the total thickness and the effective refractive index of the multilayer structure. In general, the total thicknesses determined this way were within 5% of their target values.

The crystallinity of the nanolaminates was examined with a Philips MPD 1880 powder x-ray diffractometer using Cu K_α radiation. The mean crystallite size, D, was estimated from the peak broadening at the full width at half maximum (FWHM) by using the Scherrer-Warren formula[26]

$$D(\text{nm}) = 0.9\lambda/(\text{FWHM})\cos\Theta$$

where λ is the x-ray wavelength and Θ is the Bragg angle. The FWHM was determined assuming that the observed broadening arises exclusively from the small crystallite size. This is a reasonable assumption as far as the crystallite size remains low, below about 20 nm, which is the case in our nanolaminates.

Results

Ta_2O_5 films.—The growth and properties of Ta_2O_5 thin films grown from tantalum ethoxide and water have been investigated in detail in our earlier paper.[16] The permittivity, ϵ_r, of the Ta_2O_5 films deposited onto ITO electrodes at 325°C was 25 and the refractive index, n, at the wavelength λ = 580 nm was 2.24. The tantalum oxide films as-deposited were relatively leaky (Fig. 2). The leakage current density at the 1 MV/cm electric field strength was 2.3 mA/cm^2.[16]

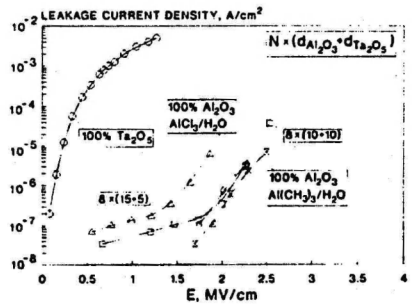

Fig. 2. Dependence of leakage current density on applied electric field strength in Al_2O_3-Ta_2O_5 nanolaminates. The labels describe sample configuration $N(d_{Al_2O_3} + d_{Ta_2O_5})$ where N is the number of bilayers and $d_{Al_2O_3}$ and $d_{Ta_2O_5}$ are thicknesses of single Al_2O_3 and Ta_2O_5 layers, respectively, expressed in nanometers.

In order to compare the properties of dielectric structures, the charge-storage factors[27] were measured

$$Q = U_{cr} \cdot C/S$$

where C is the capacitance measured, S is the effective electrode area, and U_{cr} is the critical voltage inducing a specified value of leakage current. We have measured U_{cr} when the leakage current reached 1 $\mu A/cm^2$. The charge storage factor considers simultaneously the two essential dielectric characteristics, *i.e.*, dielectric constant and leakage current, and provides information about the charge stored per unit surface area at a given leakage current density level. Thus it can be used as a figure of merit for the comparative evaluation of different dielectric materials. In our pure tantalum oxide samples, the charge-storage factor Q is as low as 8 nC/mm^2.

Al_2O_3 films and Al_2O_3-Ta_2O_5 nanolaminates.—Al_2O_3 films were deposited using both $AlCl_3$ and $Al(CH_3)_3$. Water was used as an oxygen precursor in both cases. The permittivity values of the oxides prepared by the two methods were the same, 8.1. This value is comparable with that usually measured for ALE-grown Al_2O_3 films.[15] The refractive index was 1.65, corresponding to relatively dense Al_2O_3. The Al_2O_3 films deposited using $Al(CH_3)_3$ exhibited somewhat lower leakage current densities than those deposited from $AlCl_3$ (Fig. 2). The charge storage factor Q was about 16 nC/mm^2 for both aluminum precursors.

The Al_2O_3-Ta_2O_5 nanolaminates were grown using $Al(CH_3)_3$ as an aluminum precursor. In these films the values of n and ϵ decreased nearly linearly with the increase in Al_2O_3 layer thickness (Fig. 3 and 4), very similarly to the results obtained by Kattelus *et al.*[15] for their Al_2O_3-Ta_2O_5 composites grown from the corresponding chlorides. In the present study the Al_2O_3-Ta_2O_5 composite oxides showed markedly improved leakage currents compared with that of the single Ta_2O_5 films but were in this respect somewhat worse than the single aluminium oxide films (Fig. 2). Charge storage factors of the Al_2O_3-Ta_2O_5 nanolaminates did not exceed 30 nC/mm^2 (Fig. 4). Nevertheless, this Q value was already almost twice that of the single Al_2O_3 films and four times of that of the pure Ta_2O_5.

ZrO_2 films and ZrO_2-Ta_2O_5 nanolaminates.—ZrO_2 films were deposited from $ZrCl_4$ and H_2O at 325°C. The permittivity, ϵ, of these films was 19.6 and the refractive index, n, at λ = 580 nm was 2.15. The latter value is somewhat higher than that reported for metallorganic chemical vapor deposited (MOCVD) films (n = 2.04).[28] In this study pure ZrO_2 films showed markedly lower leakage current densities when compared with the pure Ta_2O_5 but were relatively leaky when compared with the multilayers (Fig. 5). For comparison, at high electric fields above 1.5 MV/cm, our

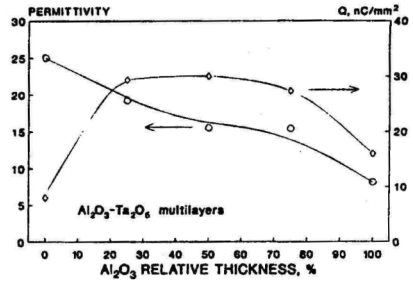

Fig. 4. Permittivity and charge storage factor Q vs. Al_2O_3 relative thickness. The bilayer thickness was held at ~20 nm.

ZrO_2 films were similar to those MOCVD-deposited by Shapphir *et al.*[29] The Q value of the pure ZrO_2 was not higher than 19 nC/mm^2. When a 10 nm thick Ta_2O_5 underlayer was deposited between ITO and ZrO_2 film with a thickness of 160 nm, the permittivity was lowered to 18, but the storage factor was not changed.

In the ZrO_2-Ta_2O_5 nanolaminates, the refractive index was scarcely dependent on the ZrO_2 content, which differs from the case of the HfO_2-Ta_2O_5 and Al_2O_3-Ta_2O_5 films where the monotonous decrease of n with the increase in HfO_2 or Al_2O_3 interlayer thickness was obvious (Fig. 3). The average permittivity of these ZrO_2-Ta_2O_5 nanolaminates was even higher than that of the pure Ta_2O_5 films, rising slightly with ZrO_2 content, although the permittivity of the pure ZrO_2 was remarkably lower than that of Ta_2O_5 (Fig. 6). The leakage current density was hardly correlated with the ZrO_2 thickness in the particular sample series with a constant 20 nm bilayer thickness (Fig. 5). The reduction of the bilayer thickness to 10 nm caused an obvious decrease of leakage current (Fig. 5), but further reduction down to 5 nm resulted again in dramatic increase of leakage current density. In the latter samples also the permittivity decreased down to 23.5 (Fig. 6). It has to be noted that the samples with equal bilayer thicknesses and ZrO_2 interlayer thicknesses exhibited similar dielectric properties regardless of the under- and topmost oxide layer material.

Figure 7 depicts the behavior of charge storage factors *vs.* relative thickness of the ZrO_2 layer in the ZrO_2-Ta_2O_5 nanolaminates. Three regions corresponding to different multilayer configurations can be distinguished. The sam-

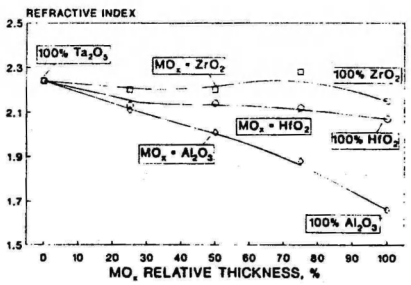

Fig. 3. Refractive index *vs.* relative thickness of the oxide laminated with Ta_2O_5. The bilayer thickness was held at ~20 nm. For comparison, the data concerning the properties of previously reported HfO_2-Ta_2O_5 multilayers[21] are also shown.

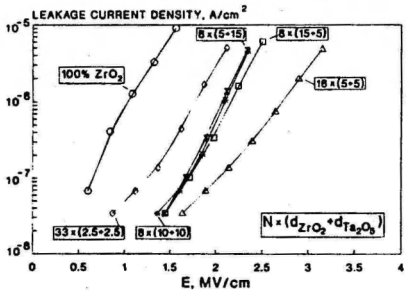

Fig. 5. Dependence of leakage current density on applied electric field strength for ZrO_2-Ta_2O_5 nanolaminates. For labeling, see Fig. 2.

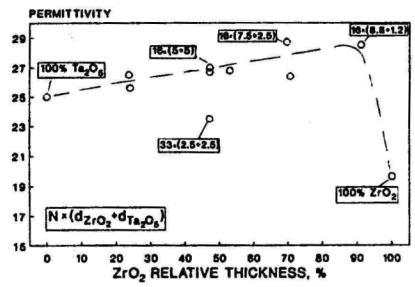

Fig. 6. Permittivity of ZrO_2-Ta_2O_5 nanolaminates *vs.* thickness of ZrO_2 layers. For labeling, see Fig. 2.

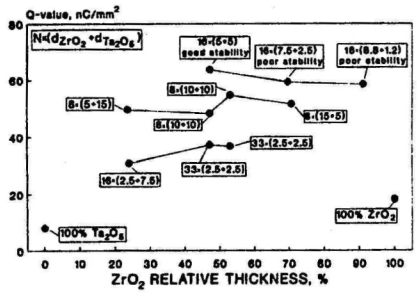

Fig. 7. Charge storage factor *Q* of ZrO_2-Ta_2O_5 nanolaminates *vs.* relative thickness of ZrO_2 layers. For labeling, see Fig. 2.

ples containing 33 or 16 ZrO_2-Ta_2O_5 bilayers with an approximate ZrO_2 thickness of only 2.5 nm exhibit the lowest *Q* values around 37 nC/mm², which is due to their high leakage current densities and poor permittivity values. It should be emphasized, however, that these *Q* values are already higher than those measured for the single oxide films. The samples with 16 double layers and ZrO_2 thicknesses in the range of 5 to 8.8 nm possessed high charge storage factor values of $Q \leq 64$ nC/mm². The nanolaminates containing 16 ZrO_2-Ta_2O_5 bilayers with equal single-oxide layer thicknesses of 5 nm exhibited the best stability of the electrical properties and the highest *Q* value (64 nC/mm²) among all the oxide films investigated. The drawback of the increase in the ZrO_2 single-layer thickness above 5 nm was the instability of the dielectric properties and markedly increased breakdown probability.

Film structure.—The pure Ta_2O_5 and Al_2O_3 films as well as Al_2O_3-Ta_2O_5 nanolaminates were amorphous; no peaks were detected in the x-ray diffractograms. At the same time, the ZrO_2 single-oxide films and their nanolaminates exhibited some crystallinity (Fig. 8). Low peak intensity and peak broadening imply that these single-oxide films and nanolaminates are not entirely crystallized.

X-ray diffraction (XRD) measurements showed that the crystalline ITO electrode layer enhances crystallization of the thick ZrO_2 films. If ZrO_2 films of 160 nm thick were deposited directly onto the electrodes, the most intense peaks appeared about ten times more intense than in the corresponding films deposited on glass. However, the effect of ITO could not be observed after deposition of 10 nm Ta_2O_5 film between ITO and ZrO_2; the XRD patterns of these films were identical to those deposited on glass covered by an identical Ta_2O_5 underlayer. Likewise, no major difference in the XRD peak intensities or dielectric properties could be observed between samples having either Ta_2O_5 or ZrO_2 underlayer. Therefore, in the following we focus only on those samples which were deposited on glass.

The most intense reflection from a 160 nm thick ZrO_2 film at $2\Theta = 30.3°$ could be assigned as the tetragonal (111) polymorph (t-ZrO_2) while the peaks appearing at $2\Theta = 28.2°$ and 31.7° are characteristic monoclinic ZrO_2 (m-ZrO_2) (−111) and (111) reflections.[30] Further, two significant peaks appearing at $2\Theta = 34.3°$ and 34.8° in the pure ZrO_2 films (Fig. 8) could be attributed to the monoclinic (020) and (002) reflections, respectively.[30] However, the width and position of these peaks do not allow one to exclude the presence of the tetragonal ZrO_2, because m-ZrO_2 (002) and t-ZrO_2 (002) have very close interplanar distances of 2.62 and 2.60 Å, respectively.[30,31] Nevertheless, various authors attributed these peaks to the m-ZrO_2.[32,33] In addition, five weaker peaks, which were detected in the 160 nm thick film (Fig. 8), can be attributed to the monoclinic ZrO_2.

In the ZrO_2-Ta_2O_5 nanolaminates with layer thicknesses of 15 nm for ZrO_2 and 5 nm for Ta_2O_5, the broad peak of tetragonal (111) ZrO_2 appeared even more intensively than in the pure ZrO_2 films (Fig. 8). The peak at $2\Theta = 50.4°$ can

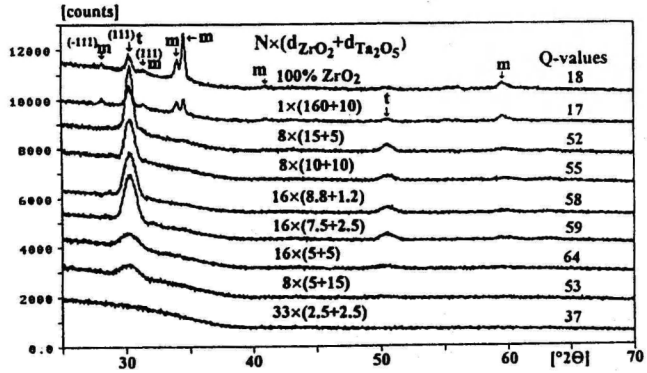

Fig. 8. XRD patterns of ZrO_2 films and ZrO_2-Ta_2O_5 nanolaminates.

be assigned as t-ZrO_2 (220).[30] This peak vanishes in the pure ZrO_2 film (Fig. 8). On the other hand, no reflections of the monoclinic phase were observed in the nanolaminates. It is also easy to notice from the diffractograms (Fig. 8) that the first traces of crystallization can be detected when the thickness of the ZrO_2 layer is still as low as 5 nm.

The minimum possible value of average crystallite dimension, D, perpendicular to the surface plane, was calculated for the most intense peaks appearing in the XRD patterns in the range $2\Theta = 28$ to 32°. The crystallite size calculated from (111) t-ZrO_2 at $2\Theta = 30.3°$ increased from 5 to 13.6 nm along with the increase of the ZrO_2 layer thickness from 5 to 15 nm.

Discussion

To improve dielectric properties and especially to reduce the high leakage currents characteristic of as-deposited Ta_2O_5, nanolaminates were prepared by ALE from Ta_2O_5 and ZrO_2 or Al_2O_3 films. In the nanolaminates having the highest charge storage factors, the high permittivity of Ta_2O_5 and the low leakage current of ZrO_2 have been successfully combined. Although an exact treatment of the leakage current and conduction mechanism remains beyond the scope of this work, possible reasons for the improvement of electrical properties are discussed qualitatively.

It has been suggested[13] that the high leakage current densities through as-deposited Ta_2O_5 films are caused by defect states arising from oxygen vacancies and impurities in the films. A possible explanation for the leakage current reduction in the nanolaminates is the creation of a large number of electron traps at the interfaces between the adjacent layers. Electron trapping[12] at the interface states may reduce the injecting field and hence counteract leakage current through weak spots, causing dramatic decrease of leakage current in nanolaminates when compared with that of single-oxide films.

Leakage properties of polycrystalline films, like ZrO_2 in this case, are strongly affected by their structure,[34,35] the grain boundaries often acting as leakage channels.[12,13,36] In the polycrystalline ZrO_2 films the grain boundary region is also the most convenient route for leakage current through the film. On this basis it seems that leakage current reduction in the nanolaminates is due to the elimination of grain boundaries extending through the whole insulator film by intermediate amorphous Ta_2O_5 layers.

On the other hand, if the influence of electron trapping at interfaces and elimination of grain boundaries were the only mechanisms for the successful reduction of leakage currents, no difference should be observable in leakage currents between different samples as far as the Ta_2O_5 film is thick enough to form a continuous well-defined interlayer with its characteristic dielectric properties. In practice, however, it was observed that the dielectric properties, including also the leakage current density, can be optimized further by varying the thicknesses of the single layers constituting the nanolaminates. At the same time, the crystal structures of the nanolaminates were found to be dependent on the layer thickness. This leads to a suggestion that there is a connection between the dielectric and structural properties of the nanolaminates.

Resistivity may be much higher across the grain boundaries than within the grains.[37] The resistivity of a dielectric sample is strongly dependent on the carrier depletion layer at the grain boundary.[34] In the samples where the grain boundary potential is the same regardless of grain size, the total resistivity is the product of the single grain boundary resistance and the number of boundaries in the film. This seems to be the case in the ZrO_2-Ta_2O_5 nanolaminates where the leakage current decreased with the decrease in crystallite size and with the decrease of bilayer thickness (Fig. 5).

In the films consisting of very fine crystallites the size of which does not exceed the layer thickness, the leakage current evidently flows across the grain boundaries. The smaller the crystallite size, the larger the number of boundaries and the lower the voltage drop across the electrical junction at the boundary. Thus the breakdown probability at possible weak points should decrease, and therefore, the breakdown voltage increases. This is supported by the fact that superior dielectric characteristics are achieved in the ZrO_2-Ta_2O_5 nanolaminates with the $16 \times (5 + 5)$ configuration (Fig. 5 and 7) containing the smallest ZrO_2 crystallites (Fig. 8).

Technically, as it has been clearly demonstrated, the dielectric properties of the multilayer structures can be optimized by optimizing the thicknesses of the single layers. For example, in the ZrO_2-Ta_2O_5 nanolaminates the leakage current was at minimum when ZrO_2 thickness was about 5 nm (Fig. 5). When the ZrO_2 layer thickness was increased above 5 nm, both the leakage current density and breakdown probability were increased, and consequently, the charge storage factor was decreased (Fig. 7). Because the film thickness increase was accompanied by an increase of crystallite size, it appears likely that to achieve the optimum dielectric properties the thickness of the ZrO_2 layers should be kept small enough (about 5 to 9 nm) to prevent the formation of larger crystallites and hence, formation of grain boundaries linking the layers of higher conductivity and thus acting as weak points. On the other hand, the ZrO_2 layers should be thick enough (at least 5 nm) to enable some crystallization during growth, because ordering is accompanied by the closest packed growth. Consequently, densification[28,38] evidently improves the dielectric properties. Deposits of completely amorphous ZrO_2 layers with thicknesses below 5 nm (Fig. 8), probably result in increased void and defect densities, causing poor dielectric characteristics.

An interesting feature observed in this study is that the permittivity values of about all the ZrO_2-Ta_2O_5 nanolaminates exceed somewhat those of both pure ZrO_2 and pure Ta_2O_5 films (Fig. 6). The permittivity of ZrO_2 is known to be principally determined by crystallographic form rather than by the amount and nature of additives.[39] Thompson *et al.*[19] have shown that monoclinic to tetragonal transformation of ZrO_2 was followed by a large increase of permittivity from 23 up to 40 due to the decrease of the unit cell volume. The average bulk density calculated for t-ZrO_2 is in excess of about 6% in comparison with that of m-ZrO_2.[22] Because only t-ZrO_2 was detected in the nanolaminates (Fig. 8), this could explain the surprisingly high permittivities of the ZrO_2-Ta_2O_5 nanolaminates. For comparison, the HfO_2-Ta_2O_5 nanolaminates contained both tetragonal and monoclinic HfO_2[21]; therefore, possible differences in dielectric properties between these HfO_2 phases cannot be discussed. In addition, in the Al_2O_3-Ta_2O_5 nanolaminates deposited here, no crystallization was detected; therefore, no crystallinity related effects could be observed.

It is worth noting that the monoclinic phase is generally recognized to be stable below 1150°C while the t-ZrO_2 can be present as a metastable phase at low temperatures.[22,40] Tetragonal ZrO_2 can be stabilized due to the influence of dopants or defects[37,41-44] or surface energy, *i.e.*, grain size effect.[28,40-42,45,46] The exact mechanism for the initial nucleation and growth of the tetragonal ZrO_2 remains an open question. The initial formation of metastable t-ZrO_2 is in many cases followed by further transformation to the monoclinic phase.[28,31,45,47] The displacive (martensitic) transformation can be initiated not only by an increase of temperature but also by the surface energy difference between t- and m-ZrO_2 crystallites already at relatively low temperatures.[38,40]

The formation of the metastable oxide seems to be favored also in the early stage of ALE growth. By comparing XRD patterns of 160 nm thick ZrO_2 layers deposited onto bare glass and on a Ta_2O_5 underlayer (Fig. 8), it is seen that Ta_2O_5 as the starting surface favors the formation of the metastable tetragonal phase. Stabilization of the t-ZrO_2 may be due to the higher content of defects at the interface with the Ta_2O_5 sublayer. At the same time, the monoclinic ZrO_2 crystallite size in single-oxide films evi-

dently exceeds that of t-ZrO_2. This suggests that further film growth includes either the tetragonal to monoclinic transformation or direct growth of the m-ZrO_2 crystallites.

The estimated crystallite size of t-ZrO_2 in the ZrO_2-Ta_2O_5 nanolaminates is well below the value of the critical particle size for the t → m transformation, which has been found to be 15 to 80 nm for undoped ZrO_2 powders and thin films.[31,38,40,48] Scanlan *et al.*[38] have reported that sputtered Al_2O_3-ZrO_2 multilayers with single-oxide thicknesses less than 25 to 30 nm consisted of t-ZrO_2, while the pure zirconia films were entirely monoclinic ZrO_2. The ZrO_2 crystallite size was dependent only on the ZrO_2 layer thickness between the amorphous Al_2O_3 layers. According to Garvie,[40] 325°C used as the growth temperature is the t → m transformation temperature of zirconia with crystallite size of about 20 nm. Moreover, if internal strain was considered, the corresponding critical crystallite size as well as the temperature range where the phases can coexist due to incomplete transformation may be enlarged.[40] This is in accordance with the observation that only t-ZrO_2 is detected in the ZrO_2 interlayers with thickness below 20 nm (Fig. 8). For comparison, in the case of HfO_2, the established volume expansion during the t → m transformation is smaller than that in ZrO_2. Consequently, the critical grain size for the t → m transformation in HfO_2 is 4 to 10 nm, *i.e.*, remarkably smaller than for ZrO_2.[48] Thus, the XRD reflections originating from the monoclinic phase in thin HfO_2 layers appear at earlier stages of growth[21] as compared with ZrO_2.

There is a possibility that when the ZrO_2 layer thickness is high enough, the size of t-ZrO_2 crystallites exceeds some critical value and initiates displacive transformation to the monoclinic phase. The transformation process as well as the crystallization itself are evidently incomplete so that the mixture of different ZrO_2 phases remains in the thick films. Another suggestion for the formation of the phase mixture is that due to strain effects the surface energy of growing crystallites increases along with their size and once exceeding a certain value, inhibits further growth of the tetragonal phase, resulting in subsequent growth in the monoclinic phase.

Conclusions

In this work, the dielectric properties of various Ta_2O_5-based, two-component oxide nanolaminates deposited by ALE were evaluated. The ZrO_2-Ta_2O_5 nanolaminates exhibited markedly better dielectric properties than those of the corresponding single-oxide layers. The leakage currents of the Al_2O_3-Ta_2O_5 nanolaminates were not lower than those of the pure aluminum oxide film. Due to the low permittivity of Al_2O_3, the charge storage factors of the Al_2O_3-Ta_2O_5 nanolaminates did not exceed 30 nC/mm^2. However, this is remarkably higher than the values evaluated for the pure oxides, 16 nC/mm^2 for Al_2O_3 and 8 nC/mm^2 for Ta_2O_5.

The permittivity of the ZrO_2-Ta_2O_5 multilayers increased up to 28 in comparison with the pure Ta_2O_5 ($\epsilon \approx 25$) or ZrO_2 ($\epsilon \approx 19$) films. The electrical properties were optimized by adjusting the layer thickness. The most stable dielectric characteristics were obtained with sequential Ta_2O_5 and ZrO_2 layers with equal thicknesses of 5 nm. This sandwich structure possessed a charge storage factor as high as 64 nC/mm^2. The storage factor for the pure ZrO_2 films was 19 nC/mm^2.

The ZrO_2 layers growing onto an amorphous Ta_2O_5 layer began to crystallize at 5 nm thick. In the nanolaminates only the metastable tetragonal ZrO_2 crystallites were present. In the single-oxide films larger crystallites of monoclinic ZrO_2 appeared.

As compared with the general approach of preparing oxide mixtures, the application of nanolaminated structures with separate single-oxide phases should be preferred when high-quality dielectric films are needed in the as-deposited state. The use of oxide mixtures does not always suffice for desired improvement of electrical properties, because as a rule, the use of various stabilizing materials often complicates the deposition process and creates defects, consequently increasing conductivity. Thus, where high-quality insulators are needed, a material of high permittivity and breakdown resistance such as Ta_2O_5 is to be used. In order to suppress the leakage currents, nanolaminates of different oxides can be prepared where the interlayers of low leakage current density material like ZrO_2 have to be added. The additional oxide may exhibit thickness- and phase-dependent dielectric properties. In the multilayer structures these properties can be controlled successfully and stabilized by adjusting layer thicknesses. While preparing nanolaminates, ALE is an advantageous technique, since it allows an accurate film thickness control and uniformity over large areas enabling the growth of single-oxide phases with well-defined properties.

Acknowledgments

The authors are indebted to Erkki Soininen from Planar International, Limited, and Hannu Kattelus from Technical Research Centre of Finland for access to electrical measurement. This work was partly supported by the Academy of Finland and Technology Developing Centre (TEKES). K.K. expresses gratitude to the Nordic Council of Ministers - Nordic Baltic Scholarship Scheme and the Magnus Ehrnrooth Foundation for research grants.

Manuscript submitted April 1, 1996; revised manuscript received Sept. 25, 1996.

The University of Helsinki assisted in meeting the publication costs of this article.

REFERENCES

1. D. H. Lee, Y. S. Cho, J. K. Lee, and H. J. Jung, *Mater. Res. Soc. Symp. Proc.*, **310**, 397 (1993).
2. J. W. Li, Y. K. Su, and M. Yokoyama, *Jpn. J. Appl. Phys.*, **32**, 5591 (1993).
3. M. Yoshida, T. Yamashita, K. Taniguchi, K. Tanaka, T. Ogura, A. Mikami, H. Nakaya, S. Yamaue, and S. Nakayima, in *Electroluminescence*, S. Shionoya and H. Kobayashi, Editors, Vol. 38, p. 232, Springer-Verlag Berlin, Heidelberg (1989).
4. L. Niinistö and M. Leskelä, *Appl. Surf. Sci.*, **82/83**, 454 (1994).
5. S. Shih, P. D. Keir, J. F. Wager, and J. Viljanen, *J. Appl. Phys.*, **78**, 5775 (1995).
6. T. Suntola, in *Handbook of Crystal Growth-3, Thin Films and Epitaxy, Part B: Growth Mechanics and Dynamics*, D. T. J. Hurle, Editor, Chap. 14, Elsevier Science, B.V., Amsterdam (1994).
7. H. Fujikawa and Y. Taga, *J. Appl. Phys.*, **75**, 2538 (1994).
8. H. Yang, F. Tanoue, S. Hibino, S. Sakakibara, K. Yokoi, and T. Hotta, *Jpn. J. Appl. Phys.*, **34**, L757 (1995).
9. H. Kimura, J. Mizuki, S. Kamiyama, and H. Suzuki, *J. Appl. Phys. Lett.*, **66**, 2209 (1995).
10. S. R. Jeon, S. W. Han, and J. W. Park, *J. Appl. Phys.*, **77**, 5978 (1995).
11. X. M. Wu, S. R. Soss, E. J. Rumaszewski, and T-M. Lu, *Mater. Chem. Phys.*, **38**, 297 (1994).
12. P. Balk, *J. Non-Cryst. Solids*, **187**, 1 (1995).
13. W. S. Lau, T. S. Tan, N. P. Sandler, and B. S. Page, *Jpn J. Appl. Phys.*, **34**, 757 (1995).
14. H. Kattelus, M. Ylilammi, J. Salmi, T. Ranta-aho, E. Nykänen, and I. Suni, *Mater. Res. Soc. Symp. Proc.*, **284**, 511 (1993).
15. H. Kattelus, M. Ylilammi, J. Saarilahti, J. Antson, and S. Lindfors, *Thin Solid Films*, **225**, 296 (1993).
16. K. Kukli, M. Ritala, and M. Leskelä, *This Journal*, **142**, 1670 (1995).
17. J. Mita, M. Koizumi, H. Kanno, T. Hayashi, Y. Sekido, I. Abiko, and K. Nihei, *Jpn. J. Appl. Phys.*, **26**, L541 (1987).
18. K. Nomura and H. Ogawa, *This Journal*, **138**, 3701 (1991).
19. S. R. Kurtz and R. G. Gordon, *Thin Solid Films*, **147**, 167 (1987).
20. R. A. Russell and P. P. Phule, *Mater. Sci. Eng.*, **B21**, 88 (1993).

21. K. Kukli, J. Ihanus, M. Ritala, and M. Leskelä, *Appl. Phys. Lett.*, **68**, 3737 (1996).
22. J. Nawrocki, M. P. Rigney, A. McCormick, and P. W. Carr, *J. Chromatogr.*, **A657**, 229 (1993).
23. E. Fredriksson and J-O. Carlsson, *J. Chem. Vapor Deposition*, **1**, 333 (1993).
24. M. Leskelä and M. Ritala, *J. Phys. IV*, **5**, C5-937 (1995).
25. M. Ylilammi and T. Ranta-aho, *Thin Solid Films*, **232**, 56 (1993).
26. H. P. Klug and L. E. Alexander, *X-Ray Diffraction Procedures for Polycrystalline and Amorphous Materials*, p. 491, John Wiley & Sons, Inc., New York (1954).
27. D. Gerstenberg, in *Handbook of Thin Film Technology, Thin Film Capacitors*, L. I. Maissel and R. Glang, Editors, p. 19-8, McGraw-Hill, Inc., New York (1970).
28. J. Si, S. B. Desu, and C-Y. Tsai, *J. Mater. Res.*, **9**, 1721 (1992).
29. J. Shapphir, A. Anis, and I. Pinsky, *IEEE Trans. Electron Devices*, **ED-33**, 442 (1986).
30. Joint Committee on Powder Diffraction Standards, Cards 17-923 and 13-307.
31. I. A. El-Shanshoury, V. A. Rudenko, and I. A. Ibrahim, *J. Am. Ceram. Soc.*, **53**, 264 (1970).
32. A. Bastiniani, G. A. Battiston, R. Gerbasi, M. Porchia, and S. Daolio, *J. Phys. IV*, **C5-525**, 5 (1995).
33. C. S. Hwang and H. J. Kim, *J. Mater. Res.*, **8**, 1361 (1993).
34. X. Guo and R. Z. Yuan, *Solid State Ionics*, **80**, 159 (1995).
35. D-H. Kim, I-K. Park, W-S. Um, and H-G. Kim, *Jpn. J. Appl. Phys.*, **34**, 4862 (1995).
36. Q. X. Jia, L. H. Chang, and W. A. Anderson, *Thin Solid Films*, **259**, 264 (1995).
37. S-Y. Chen and H-Y. Lu, *J. Mater. Sci.*, **30**, 1321 (1995).
38. C. M. Scanlan, M. Gajdarziska-Josifovska, and C. R. Aita, *Appl. Phys. Lett.*, **64**, 3548 (1994).
39. D. P. Thompson, A. M. Dickins, and J. S. Thorp, *J. Mater. Sci.*, **27**, 2267 (1992).
40. R. C. Garvie, *J. Phys. Chem.*, **82**, 218 (1978).
41. B. J. Gould, I. M. Povey, M. E. Pemble, and W. R. Flavell, *J. Mater. Chem.*, **4**, 1815 (1994).
42. Y. Takahashi, T. Kawae, and M. Nasu, *J. Cryst. Growth*, **74**, 409 (1986).
43. F. Tsheliebou and A. Boyer, *Mater. Sci. Eng.*, **B26**, 175 (1994).
44. R. Srinivasan, T. R. Watkins, C. R. Hubbard, and B. H. Davis, *Chem. Mater.*, **7**, 725 (1995).
45. E. D. Whitney, *Trans. Faraday Soc.*, **61**, 1991 (1965).
46. G. J. Exarhos, L. Q. Yang, and T. Dennis, *Thin Solid Films*, **253**, 41 (1994).
47. N. Michiura, T. Tatekawa, Y. Higuchi, and H. Tamura, *J. Am. Ceram. Soc.*, **78**, 793 (1995).
48. J. Wang, H. P. Li, and R. Stevens, *J. Mater. Sci.*, **27**, 5397 (1992).

Reprinted from JOURNAL OF THE ELECTROCHEMICAL SOCIETY
Vol. 144, No. 1, January 1997
Printed in U.S.A.

VIII

Reprinted with permission from *Applied Physics Letters*, Vol. 68 (1996),
K. Kukli, J. Ihanus, M. Ritala and M. Leskelä,
Tailoring the dielectric properties of HfO_2-Ta_2O_5 nanolaminates, pp. 3737–3739,

Tailoring the dielectric properties of HfO_2–Ta_2O_5 nanolaminates

Kaupo Kukli,[a] Jarkko Ihanus, Mikko Ritala, and Markku Leskela
Department of Chemistry, University of Helsinki, FIN-00014 Helsinki, Finland

(Received 14 March 1996; accepted for publication 23 April 1996)

Dielectric thin films applicable, for instance, as insulating layers in electroluminescent display devices have been studied. In order to improve dielectric characteristics HfO_2–Ta_2O_5 nanolaminates were prepared by atomic layer epitaxy at 325 °C. The nanolaminates were evaluated in capacitance and current–voltage measurements. By optimizing the layer thicknesses in the nanolaminate structures the dielectric properties, especially leakage current densities, could be tailored remarkably. The best nanolaminates showed charge storage factors improved up to 8 times when compared with those of the single oxide films. The presence of nanosize crystallites of monoclinic and metastable tetragonal HfO_2 was observed by x-ray diffraction analysis, © *1996 American Institute of Physics.* [S0003-6951(96)03526-7]

The search for high permittivity and low leakage dielectric thin films is actual for the development of many micro- and optoelectronic devices.[1,2] In this study dielectric films have been examined from the point of view of thin-film electroluminescent (TFEL) displays.[3,4] High dielectric constant, breakdown resistance, mechanical stability, and chemical inertness are the intrinsic properties required from the insulators in contact with phosphor layers.[4] Furthermore, the already as-deposited insulators in an unannealed state must be of a high quality due to glass substrates. Here, we describe a remarkable improvement of Ta_2O_5 based high permittivity dielectrics by preparing Ta_2O_5–HfO_2 nanolaminates. In memory capacitors, only very thin layers could be used in such layer structures,[5] but in TFEL devices the insulators are thicker, typically a few hundred nanometers, thereby allowing a broader variation of the individual layer thicknesses in the nanolaminates.[4,6,7]

Owing to its unique self-limiting growth process the atomic layer epitaxy (ALE) technique[8,9] is capable of meeting the challenge to deposit films with accurately controlled layer thicknesses uniformly over large area substrates. Pure Ta_2O_5 and HfO_2 films and their nanolaminates were grown onto patterned indium-tin-oxide (ITO) electrodes on 5 $\times$5 cm^2 glass substrates using a hot-wall flow-type F120 ALE reactor, operated under a 10 mbar nitrogen pressure.[8] $Ta(OC_2H_5)_5$ and $HfCl_4$ were evaporated from open boats held at 105 and 140 °C, respectively, inside the reactor. Water vapor was exploited as an oxygen precursor. The films were grown at 325 °C, which is the highest temperature for self-controlled growth regime for Ta_2O_5.[10]

Figure 1 depicts schematically the structure of the HfO_2–Ta_2O_5 nanolaminates. The thicknesses of the Ta_2O_5 interlayers were varied in a range of 1.2–18.8 nm. The thicknesses of the HfO_2 layers were varied in a way that the total thickness of one HfO_2–Ta_2O_5 bilayer remained constant. Three main sample series with different bilayer thicknesses of 20, 10, and 5 nm were prepared. The total thickness of all multilayers was kept at about 170 nm. This was independently checked by fitting transmittance spectra measured within a wavelength range of 370–1100 nm.[11] In most samples both under and top layers were Ta_2O_5. For comparative measurements some HfO_2–Ta_2O_5 nanolaminates where both under and top layers consisted of HfO_2 were prepared as well. Aluminum electrodes were evaporated onto the as-deposited nanolaminates. The area of a single electrode was 29.4 mm^2. Capacitances were measured at 10 kHz frequency using an HP 4275A multifrequency LCR meter. The current–voltage characteristics were analyzed with an HP 4140 B pA meter/dc voltage source, or HP 4142B modular dc source. All measurements were made at room temperature. Film crystallinity was examined with x-ray diffraction (XRD) using a Philips MPD 1880 diffractometer with Cu K_α radiation.

To compare the properties of the different insulators for given capacitor structure, charge-storage factors (Q) as figures of merit were evaluated:[12]

$$Q = U_{cr} \cdot C/S,$$

where C is the capacitance measured, S is the electrode area, and U_{cr} is the critical voltage inducing a certain, arbitrarily chosen value of leakage current density (1 $\mu A/cm^2$). The charge-storage factor provides information about the charge stored per surface area at a given leakage current density level.

The permittivities of the pure Ta_2O_5 and HfO_2 films were 25 and 16, respectively. Due to the relatively high leak-

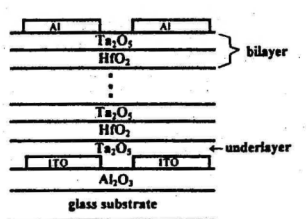

FIG. 1. Schematic representation of the nanolaminates prepared onto 5 $\times$5 cm^2 glass substrates. The Al_2O_3 layer serves as an ion barrier against sodium diffusion from soda lime glass.

[a]Permanent address: Institute of Material Science, University of Tartu, EE2400 Tartu, Estonia.

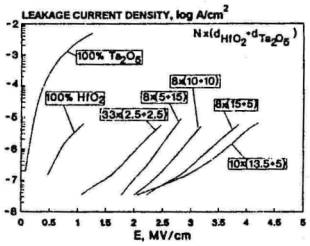

FIG. 2. Dependence of leakage current density on applied electric field strength in single Ta_2O_5 and HfO_2 films and HfO_2–Ta_2O_5 nanolaminates. Labels describe the sample configuration N $(d_{HfO_2}+d_{Ta_2O_5})$ where N is the number of bilayers, d_{HfO_2} and $d_{Ta_2O_5}$ are thicknesses of single HfO_2 and Ta_2O_5 layers, respectively, expressed in nanometers.

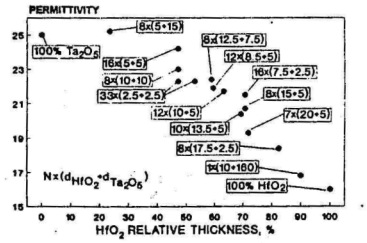

FIG. 4. Permittivities of HfO_2–Ta_2O_5 nanolaminates vs the relative thicknesses of HfO_2 layers. For labeling, see Fig. 2. For 33(2.5+2.5) configuration the results from the samples with HfO_2 lower and top layer are both indicated.

age currents (Fig. 2) the charge-storage factor Q was as low as 8 nC/mm^2 in both cases. XRD measurements indicated remarkable crystallization in the HfO_2 films (Fig. 3) while the Ta_2O_5 films were amorphous.

By preparing HfO_2–Ta_2O_5 nanolaminates the leakage currents were dramatically reduced (Fig. 2). By varying the layer thicknesses within the multilayer structure the leakage current properties could be tailored markedly (Fig. 2). The leakage current for the configuration 33(2.5+2.5) is rather similar to that measured by Kattelus *et al.*[5] in their multilayers of 32(3+3) configuration grown by ALE from $TaCl_5$, $HfCl_4$, and H_2O at 300 °C. However, a further reduction in the leakage current density was achieved when the layer thicknesses were increased up to 15 nm (Fig. 2). An additional increment of the HfO_2 interlayer thickness above 15 nm was followed by an apparent increase in breakdown probability.

The permittivity of the multilayers decreased with increasing HfO_2 content (Fig. 4). The charge storage factor exhibited a rather broad maximum between 50% and 75% relative HfO_2 content (Fig. 5). Q values up to 66 nC/mm^2 were achieved in these films. Reduction of the bilayer thickness and/or the increase of the HfO_2 interlayer thickness generally led to a decrease of the permittivity (Fig. 4) and increased dielectric instability as compared with other samples having the same relative HfO_2 contents.

Polycrystalline ceramic films may exhibit increased conductivity along the grain boundaries.[2,13,14] In the nanolaminates the intermediate amorphous Ta_2O_5 layers inhibit the continuous crystal growth of HfO_2 and, thereby, eliminate the grain boundary channels extending from one electrode to the other. The leakage current reduction in the nanolaminates can also be due to electron trapping at the interface states at the end of leakage channels extending through single sublayers, thereby causing a decrease of the injecting electric field in the vicinity of these channels.[2]

If the above two effects were the only mechanisms for the successful reduction of leakage currents, no differences should be observable between different configurations, provided that the films are thick enough to form continuous well-defined interlayers with their characteristic dielectric properties. In practice it was observed that the dielectric properties, also including the leakage current density, can be optimized further by varying the thicknesses of the single layers constituting the nanolaminate film. To rationalize these observations the structural properties of the nanolaminates were examined with XRD (Fig. 3).

The crystalline ITO electrode layer was found to have a strong effect on the crystallization of the HfO_2 films depos-

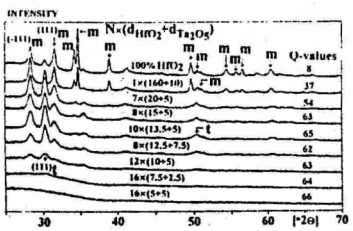

FIG. 3. XRD patterns of HfO_2 thin films and HfO_2–Ta_2O_5 nanolaminates. The labels m and t refer to the monoclinic and tetragonal HfO_2 (Ref. 15). The intensity scale is linear.

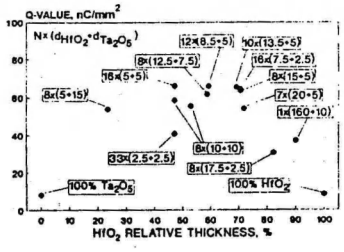

FIG. 5. Charge storage factors of HfO_2–Ta_2O_5 nanolaminates vs the relative thicknesses of HfO_2 layers. For labeling, see Fig. 2. For 8(10+10) configuration the results from the samples with HfO_2 lower and top layer are both indicated.

ited upon it. However, the effect of ITO was already eliminated after a deposition of 10 nm amorphous Ta_2O_5 between the ITO and HfO_2 films; the XRD patterns of these films were identical to those deposited on glass covered by an identical Ta_2O_5 underlayer. The XRD patterns shown in Fig. 3 were measured from samples deposited on glass.

The XRD pattern of the pure HfO_2 film (Fig. 3) is dominated by reflections of the monoclinic HfO_2 (m-HfO_2) phase.[15] In addition, the tetragonal (111) reflection is observed as well.[15] The tetragonal HfO_2 (t-HfO_2) is known to be a metastable phase at room temperature[16] but it may be stabilized by film stress and/or grain size effects.[16,17]

In the HfO_2–Ta_2O_5 nanolaminates crystallization of the HfO_2 is observed when the HfO_2 layer thicknesses exceed 10 nm (Fig. 3). With increasing HfO_2 layer thickness the XRD reflections become more intense and the peak widths decrease. The crystallite sizes calculated from the XRD peak widths for the t-HfO_2 increase from 7.5 to 14.5 nm when the thicknesses of the HfO_2 layers increase from 7.5 to 20 nm. The crystallite sizes of the m-HfO_2 are in a range of 9.0–11.8 nm in samples having 10–20 nm HfO_2 layer thicknesses.

The third effect of increasing layer thickness is a decrease of the relative fraction of the t-HfO_2 (Fig. 3). Nevertheless, in the thicker films the relative content of the t-HfO_2 is increased when a 10 nm thick Ta_2O_5 layer is deposited between glass and HfO_2. Thus it is suggested that the Ta_2O_5 underlayer enhances nucleation and growth of the t-HfO_2.

Correlation of the XRD data with the dielectric properties indicates that the nanolaminates with optimized characteristics contain a remarkable amount of t-HfO_2. Apparently, to attain the optimum dielectric properties the thicknesses of the HfO_2 layers should be high enough for crystallization and, on the other hand, low enough to prevent the formation of larger crystallites and leaky grain boundaries acting as weak points, and/or to keep the relative fraction of the t-HfO_2 high.

No differences in electrical properties were observed in the samples with otherwise similar configurations but with different under and topmost layers (Figs. 4 and 5). This enables to choose the oxide layer in TFEL structures in accord with interface properties and structural compatibility with phosphor material. For instance, Ta_2O_5 is known to have a positive effect on the structural and luminescent properties of the subsequently deposited phosphor layer,[7] while HfO_2 generates a larger density of deep interface states.[6]

In conclusion, it has been shown that by preparing HfO_2–Ta_2O_5 nanolaminates, the lowest leakage currents measured were about 3×10^{-8} A/cm^2 at 2 MV/cm which is a remarkably low value for unannealed samples. It seems that the tailoring of dielectric properties is related to the crystallization of HfO_2, though the exact mechanism cannot yet be unambiguously identified. The highest storage factors for the HfO_2–Ta_2O_5 nanolaminates exceeded that of single oxide films by about 8 times.

Thus, in the nanolaminates where high storage factors are needed, a high permittivity material with high breakdown resistivity such as Ta_2O_5 is to be used. In order to suppress the leakage currents, interlayers of low leakage current density material, e.g., HfO_2, have to be added. In such multilayer structures the amorphous Ta_2O_5 layers interrupt the grain boundaries acting as leaky channels through the polycrystalline films. While preparing nanolaminates ALE is an advantageous technique since it allows an accurate film thickness control and uniformity over large areas.

The authors are indebted to Erkki Soininen and Hannu Kattelus for access to electrical measurements. This work was supported in part by the Academy of Finland, Technology Development Centre (TEKES), Helsinki, Finland, K. Kukli expresses gratitude to the Nordic Council of Ministers and Magnus Ehrnrooth Foundation for research grants.

[1] R. F. Cava, W. F. Peck, Jr. and J. J. Krajewski, Nature **377**, 215 (1995).
[2] P. Balk, J. Non-Cryst. Solids **187**, 1 (1995).
[3] K. Derbyshire, Solid State Technol. **37**, 55 (1994).
[4] J. W. Li, Y. K. Su, and M. Yokoyama, Jpn. J. Appl. Phys. **32**, 5591 (1993).
[5] H. Kattelus, M. Ylilammi, J. Salmi, T. Ranta-aho, E. Nykänen, and I. Suni, Mater. Res. Soc. Symp. Proc. **284**, 511 (1993).
[6] C. T. Hsu, J. W. Li, C. H. Liu, Y. K. Su, T. S. Wu, and M. Yokoyama, J. Appl. Phys. **71**, 1509 (1992).
[7] H. Yang, F. Tanoue, S. Hibino, S. Sakakibara, K. Yokoi, and T. Hotta, Jpn. J. Appl. Phys. **34**, L757 (1995).
[8] T. Suntola, Thin Solid Films **216**, 84 (1992).
[9] T. Suntola, in *Handbook of Crystal Growth 3, Thin Films and Epitaxy, Part B: Growth Mechanics and Dynamics*, edited by D. T. J. Hurle (Elsevier, Amsterdam, 1994), p. 601.
[10] K. Kukli, M. Ritala, and M. Leskelä, J. Electrochem. Soc. **142**, 1670 (1995).
[11] M. Ylilammi and T. Ranta-aho, Thin Solid Films **232**, 56 (1993).
[12] D. Gerstenberg, in *Handbook of Thin Film Technology, Thin Film Capacitors*, edited by L. I. Maissel and R. Glang (McGraw-Hill, New York, 1970), p. 19-8.
[13] G. J. Exarhos, L. Q. Yang, and T. Dennis, Thin Solid Films **253**, 41 (1994).
[14] Q. X. Jia, L. H. Chang, and W. A. Anderson, Thin Solid Films **259**, 264 (1995).
[15] Joint Committee on Powder Diffraction Standards, Cards 6-318 and 8-342.
[16] J. Wang, H. P. Li, and R. Stevens, J. Mater. Sci. **27**, 5397 (1992).
[17] R. C. Garvie, J. Phys. Chem. **82**, 218 (1978).

IX

Reprinted from *Nanostructured Materials*, Vol. 8 (1997),
K. Kukli, M. Ritala and M. Leskelä,
Properties of $(Nb_{1-x}Ta_x)_2O_5$ solid solutions and $(Nb_{1-x}Ta_x)_2O_5$-ZrO_2
nanolaminates grown by atomic layer epitaxy, pp. 785–793,

Pergamon

NanoStructured Materials, Vol. 8, No. 7, pp. 785–793, 1997
Elsevier Science Ltd

0965-9773/97 $17.00 + .00

PII S0965-9773(98)00003-8

PROPERTIES OF $(Nb_{1-x}Ta_x)_2O_5$ SOLID SOLUTIONS AND $(Nb_{1-x}Ta_x)_2O_5$-ZrO_2 NANOLAMINATES GROWN BY ATOMIC LAYER EPITAXY

K. Kukli*†, M. Ritala* and M. Leskelä*

Department of Chemistry, University of Helsinki, P.O. Box 55, FIN-00014, Helsinki, Finland
†On leave from Institute of Experimental Physics and Technology, University of Tartu, EE2400 Tartu, Estonia

(Accepted September 28, 1997)

Abstract *— $(Nb_{1-x}Ta_x)_2O_5$ solid solution films and $(Nb_{1-x}Ta_x)_2O_5$-ZrO_2 nanolaminates have been deposited by Atomic Layer Epitaxy. Amorphous $(Nb_{1-x}Ta_x)_2O_5$ films were obtained by sequential pulsing of tantalum and niobium ethoxide and water. The composition of the films was checked by Energy Dispersive X-ray Spectroscopy. $(Nb_{1-x}Ta_x)_2O_5$ films exhibited 1.6-4 times higher permittivity than that of Ta_2O_5 films. Leakage currents through the $(Nb_{1-x}Ta_x)_2O_5$ films were reduced drastically by adding intermediate ZrO_2 layers with thickness of 5-10 nm, i.e. by constructing nanolaminate structures. The ZrO_2 interlayers contained nanosize tetragonal ZrO_2 crystallites.* ©*1998 Acta Metallurgica Inc.*

INTRODUCTION

The investigation of new dielectric materials with high permittivity and low leakage current is an important subject of thin film research (1). Referring, for instance, to the significance of the insulating layers in thin film electroluminescent (TFEL) devices, it is recognized that the luminance of TFEL device increases with the phosphor layer thickness to a level which is only limited by the insulating layer capacitance (2). Due to the high electric fields used in these large area devices, the insulator capacitance cannot be increased simply by reducing the layer thickness without meeting reliability problems. Therefore, insulators with increased permittivity have to be sought. The usage of ferroelectrics in TFEL devices results in higher luminous intensity value versus drive voltage when compared to binary oxide dielectrics (3). However, the efficiency of TFEL device with ferroelectric layer suffers from much higher density of transferred charge as compared with devices where binary oxides such as Ta_2O_5 are used (3). In general, the problems concerning leakage current, time-dependent polarization and long-term reliability are still substantial barriers for the wider application of ferroelectric materials (4,5). Thus it is challenging to search for binary dielectric oxides or their combinations possessing simultaneously high permittivity and high electric field strength.

Atomic Layer Epitaxy (ALE) is an attractive technique for the deposition of capacitor dielectric materials (6-9). The ALE growth is based on alternate self-limited adsorption of precursors on the substrate surface (10). One metal oxide growth cycle in the ALE process consists of the metal precursor exposure, the first purge period, oxygen precursor exposure, and the second purge period. The saturation of the substrate surface with the adsorbing species ensures a surface-controlled growth instead of the source-controlled growth used in conventional thin film deposition techniques. At proper growth temperatures, the film thickness depends only on the number of deposition cycles used. Thus ALE provides a controlled growth of solid films with high thickness uniformity and low defect density over large substrate area (10), making possible, for instance, an industrial production of TFEL displays (2,11). A further merit of ALE stems from the possibility of depositing stacked atomic layers of different materials in one continuous process. Such a film growth technique, with inherent precision at a nanometer level, is appropriate for the production of one-dimensionally modulated multilayer materials, where the repeat distance is of the order of nanometers.

Ta_2O_5-HfO_2 (8) and Ta_2O_5-ZrO_2 (9) nanolaminates prepared by ALE have shown excellent dielectric performance with a dramatic reduction of leakage current in comparison to their single constituents and, in the case of Ta_2O_5-ZrO_2, also some increment in permittivity. Furthermore, other researchers have shown that the performance of TFEL device can be improved by using SiO_xN_y-Ta_2O_5 and Al_2O_3-Ta_2O_5 stacked dielectrics with high breakdown resistance (12). It has also been reported that sputtered composite films of Ta_2O_5 and Nb_2O_5 show much higher dielectric constant in comparison with the single constituent oxides (13-15). In this study, we report the possibility to deposit by ALE $(Nb_{1-x}Ta_x)_2O_5$ solid solutions and $(Nb_{1-x}Ta_x)_2O_5$-ZrO_2 nanolaminates showing concurrently high permittivity and low leakage current density.

EXPERIMENTAL

$(Nb_{1-x}Ta_x)_2O_5$ solid solutions and $(Nb_{1-x}Ta_x)_2O_5$-ZrO_2 nanolaminates were grown onto 5 cm x 5 cm soda lime glass substrates using a hot-wall flow-type F120 ALE reactor (Microchemistry Ltd., Espoo, Finland) (10). Nitrogen was used as a carrier and purging gas. The total pressure in the reactor was about 10 mbar. $Nb(OC_2H_5)_5$ (ABCR), $Ta(OC_2H_5)_5$ (Aldrich, 99.98%) and $ZrCl_4$ (Aldrich, 99.99%) were evaporated from open boats held at 90, 105 and 150°C, respectively, inside the reactor. The pulsing of the precursors was accomplished by means of inert gas valving (10). Water vapor as oxygen precursor was generated in an external reservoir at 20°C and led into the reactor through needle and solenoid valves. Precursor pulsing times in one ALE cycle were chosen in accord with our earlier results (7,16).

Film thicknesses and refractive indices were calculated, using the method by Ylilammi and Ranta-aho (17), from transmittance spectra measured by a Hitachi U-2000 spectrophotometer within a wavelength range of 370-1100 nm. Structural analysis was carried out with a Philips MPD 1880 powder X-ray diffractometer (XRD) using CuK_α radiation. The relative Ta content in the $(Nb_{1-x}Ta_x)_2O_5$ films was measured by a Link ISIS Energy Dispersive X-Ray Spectrometer (EDX) installed to a Zeiss DSM 962 scanning electron microscope.

A sample series with thicknesses of 90-210 nm were deposited onto sputtered indium-tin oxide (ITO) electrodes at 230, 270 and 325°C. An array of aluminum electrodes was evaporated onto the film surface, enabling electrical measurements over substrate area of 9.5 cm^2. The area

of a single electrode was 29.4 mm^2. Capacitances were measured at a frequency of 10 kHz using an HP4275A multifrequency LCR meter and the current-voltage characteristics with an HP4140B pA meter/d.c source. All measurements were carried out at room temperature.

$(Nb_{1-x}Ta_x)_2O_5$ solid solutions were prepared by supplying a few subsequent deposition cycles of each constituent (Table 1). Such a cycling sequence is not expected to result in true multilayer deposition because only a fraction of a monolayer is deposited during each cycle. In most samples, a 10 nm thick Ta_2O_5 single layer was grown below and above the $(Nb_{1-x}Ta_x)_2O_5$ film.

RESULTS AND DISCUSSION

The ALE growth rates of Ta_2O_5 films were 0.039, 0.040 and 0.039 nm/cycle at 230, 270 and 325°C, respectively (7), while the respective growth rate values for Nb_2O_5 were 0.028, 0.026 and 0.035 nm/cycle (16). Due to their identical ionic radii, it may be assumed that Nb and Ta become incorporated into the film in quantities determined by their deposition cycle numbers multiplied with the deposition rates. Thus, the Ta/(Ta+Nb) ratio may be estimated (Table 1) from an equation

$$Ta/(Ta+Nb) = N_{Ta} \cdot R_{Ta}/(N_{Ta} \cdot R_{Ta} + N_{Nb} \cdot R_{Nb}), \quad [1]$$

TABLE 1
Composition, Optically Determined Thickness, d, Permittivity, ε, and Refractive Index, n (λ=580 nm), of $(Nb_{1-x}Ta_x)_2O_5$ Films

cycling, Nx(X cycles Nb_2O_5 + Y cycles Ta_2O_5)	Ta/(Ta+Nb) from Eq. 1	Ta/(Ta+Nb) by EDX	d, nm	n	ε
T_{growth} =230°C					
600x(3 + 3)	0.58	0.56	210	2.24	28
200x(10 + 10)	0.58	0.54	117	2.24	28
200x(16 + 3)	0.21	0.21	104	2.32	98
T_{growth} = 270°C					
750x(6 +1)	0.21	0.24	152	2.33	44
300x(16 + 3)	0.23	0.25	162	2.35	62
T_{growth} = 325°C					
500x(3 + 3)	0.53	0.60	93	2.30	31
250x(10 +10)	0.53	0.52	135	2.31	37
250x(16 + 3)	0.17	0.22	140	2.34	45

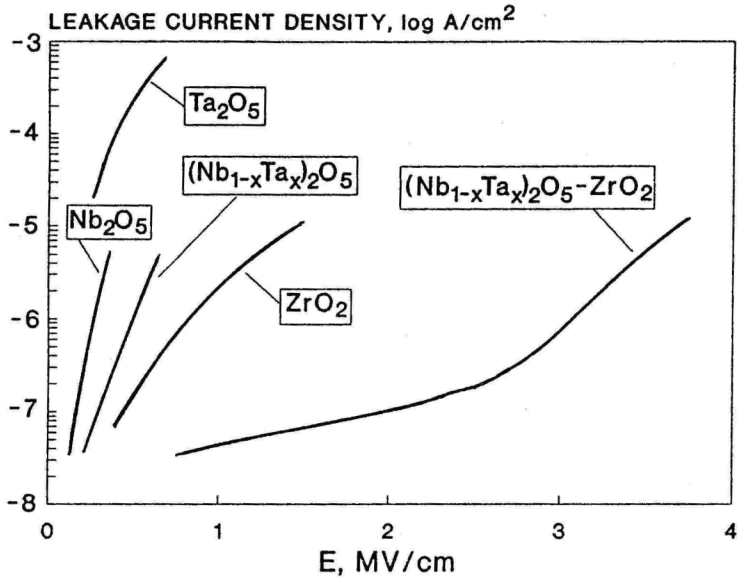

Figure 1. Leakage current density *vs.* electric field applied. The films are grown at 325°C.

where N and R are the number of deposition cycles used for each constituent and growth rates of the corresponding binary oxide films, respectively. This calculated ratio is in a good consistency with the ratio evaluated by EDX (Table 1). At 325°C, thermal decomposition of the Ta and Nb ethoxides already occurs with a considerable rate (7,16), and thus the growth is not strictly self-limiting. Therefore, some discrepancy between calculated and measured content ratios appears (Table 1).

XRD measurements showed that all the $(Nb_{1-x}Ta_x)_2O_5$ films grown in the present experiments were amorphous. Also, the Ta_2O_5 and Nb_2O_5 films grown in the earlier experiments (7,16) were amorphous.

Electrical measurements showed that the leakage current, I_{leak} in the $(Nb_{1-x}Ta_x)_2O_5$ films was reduced in comparison to the Ta_2O_5 and Nb_2O_5 films (Figure 1). However, $(Nb_{1-x}Ta_x)_2O_5$ films were still too leaky to resist fields higher than 0.7 MV/cm.

Earlier results have shown that the permittivity, ε, of ALE-grown Ta_2O_5 films was 25 (7). Due to the high a.c. conductivity of the Nb_2O_5 films, we could not determine their permittivity reliably. Literature data give $\varepsilon = 10$ for Nb_2O_5 films obtained by a pyrolysis of $Nb(OC_2H_5)_5$ (18), $\varepsilon = 30$ for sputtered crystalline Nb_2O_5 films (14), and $\varepsilon = 45$-48 for amorphous anodized or sputtered Nb_2O_5 films (19,20). The leakage current in the sputtered amorphous films (20) in their as-deposited state was somewhat higher than that reported in the present study. Crystallization induced by annealing caused considerable increment in both ε and I_{leak} (20).

It is obvious that the ALE-grown $(Nb_{1-x}Ta_x)_2O_5$ films possess stabilized permittivity value (Table I) and, at the same time, decreased leakage current (Figure 1). The permittivity increases somewhat with growth temperature in the films where the same number of deposition cycles was applied for both oxides (Table 1). By contrast, in the series of samples where 16 cycles of Nb_2O_5 and 3 cycles of Ta_2O_5 were applied, ε increases considerably with decreasing growth temperature. Even more pronounced increment of ε was achieved by increasing the number of Nb_2O_5 deposition cycles in relation to those of Ta_2O_5 (Table 1). It is to be noted that the refractive index as an independently measured optical parameter is in accordance with the permittivity (Table 1). Regardless of the rather complex dependence of permittivity and refractive index on the growth temperature and the Ta to Nb cycling ratio, it is obvious that the compositional tuning of optical and electrical parameters is possible by choosing an appropriate cycling ratio.

The reason for the increment of the dielectric constant in the solid solutions remains an open question due to the lack of knowledge about microstructure and bonding in these solutions. Cava *et al.* (15) have proposed a possibility that Nb_2O_5 could itself be a borderline ambient temperature ferroelectric, and the accommodation of the even more polarizable TaO_x coordination polyhedra in the Nb_2O_5 crystal structure initiates distortions giving rise to the weak ferroelectricity of $Nb_xTa_yO_z$ solid solutions. Although no XRD reflections from the solid solution films were observed, one might still expect some short-range ordering, *i.e.* the formation of very small crystalline nuclei in the amorphous oxide matrix, undetectable by XRD. In addition, changes in growth temperature and deposition cycles can affect the adsorption of different precursors, resulting in creation of growth parameter dependent defects in solid solution films. These defects are supplementary to those possibly existing in the binary oxide films and are formed in spite of the similar properties and ionic radii of Nb and Ta. The defects create additional bulk traps for charge carriers. Charge trapping during leakage current conduction could cause the observed moderate decrease in the leakage current of the $(Nb_{1-x}Ta_x)_2O_5$ films as compared to that of Nb_2O_5 and Ta_2O_5 films (Figure 1). The effect of charge trapping can appear also as a formation of space charge which polarizes under an external electric field applied. Here it is to be noted that permittivity decreased 10-20% in the solid solutions when the measurement frequency was increased from 10 to 30 kHz. The corresponding decrease in the Ta_2O_5 films was only 2%. This refers to the possible influence of additional charge polarization mechanism contributing to the measured permittivity value.

To suppress leakage current, ZrO_2 interlayers were deposited between $(Nb_{1-x}Ta_x)_2O_5$ layers. ZrO_2 interlayers with thicknesses between 5 and 10 nm were deposited using 85 or 150 deposition cycles (Table 2). Though the 160 nm thick ZrO_2 films crystallized in the monoclinic phase (m-ZrO_2) (21) already when deposited at 230°C (Figure 2b,c), in the nanolaminate structures only the broad peak characteristic to the tetragonal ZrO_2 (t-ZrO_2) (21) was detected with XRD (Figure 2a). The crystallite size calculated from the width of this peak was 8.0 nm. No crystallization was observed when the ZrO_2 interlayer thickness was held at 5 nm.

The amorphous $(Nb_{1-x}Ta_x)_2O_5$ layers deposited between ZrO_2 layers inhibit the growth of large m-ZrO_2 crystallites, the grain boundaries of which may otherwise act as leaky channels for electronic conduction. Thus, in the leakage current conduction process, the charge carriers are trapped at the nanosize crystallite boundaries crossing the field direction. The amount of the electron trapping centers increases with the decrease of crystallite dimensions (22). Charge carriers are most probably trapped also at the interfaces of different oxide layers. Thus, the electric field should be divided between several potential barriers. This results in the dramatic decrease

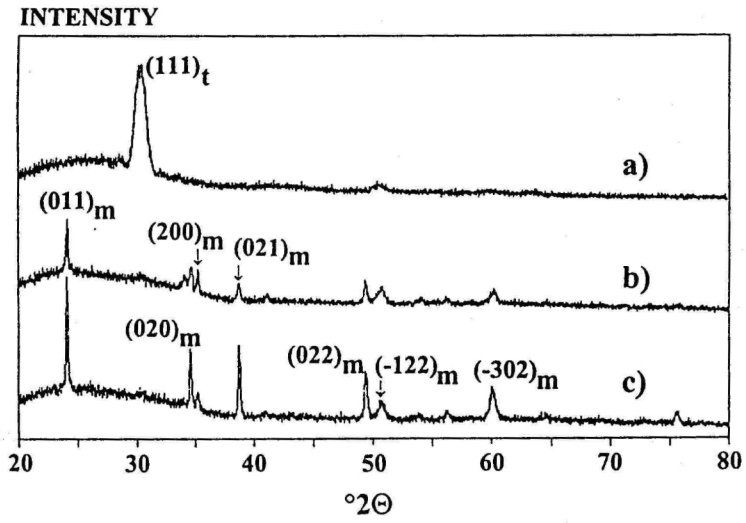

Figure 2. Typical X-ray diffractograms for (a) $(Nb_{1-x}Ta_x)_2O_5$-ZrO_2 nanolaminate grown at 325°C, (b) ZrO_2 film grown onto 10 nm Ta_2O_5 underlayer at 230°C, and (c) ZrO_2 film grown onto glass substrate at 230 °C. The intensity scale is linear. The thickness of ZrO_2 films is close to 160 nm. The nominal thickness of the separate layers in the nanolaminate is 10 nm.

of the breakdown probability and leakage current in the $(Nb_{1-x}Ta_x)_2O_5$-ZrO_2 nanolaminates in comparison with binary oxides (Figure 1).

It is known that m-ZrO_2 is the equilibrium phase at normal temperature and pressure (23). Nonetheless, it is also recognized as a general rule that, if the initial system in the solid formation process deviates from the equilibrium state, metastable phases tend to form first during crystallization (24,25). At the early stage of the deposition process, the nucleation is initiated by the formation of nanoscale clusters which are characterized by a large surface area to volume ratio. A large fraction of atoms/molecules resides at the surface of these mesoscopic material clusters and therefore is coordinatively unsaturated and have broken bonds. At this stage, the generation of metastable phases is often favored (26). Thus the formation of the metastable tetragonal ZrO_2 nanocrystals can take place during the deposition of first oxide layers by ALE. Nb_2O_5 additives (27,28) or mechanical stress arising from the difference between the thermal expansion coefficients or elastic moduli of ZrO_2 and underlying material (29) may serve as additional factors stabilizing the t-ZrO_2 phase with crystallite sizes over several tens of nanometers. The nanocrystallites may have specific characteristics different from those of bulk film material. In the case of $(Nb_{1-x}Ta_x)_2O_5$-ZrO_2 nanolaminates, the beneficial effect of the stabilization of the fine-

TABLE 2
Thickness, d, Permittivity, ε, and Charge Storage Factor, Q, of $(Nb_{1-x}Ta_x)_2O_5$-ZrO_2 Nanolaminates. Q is the Capacitance per Surface Area multiplied by Critical Voltage inducing the arbitrarily chosen Leakage Current Density of 1 $\mu A/cm^2$.

cycling, 16[Z cycles ZrO_2 + 12(Ycycles Ta_2O_5 + X cycles Nb_2O_5) + 10 cycles Ta_2O_5]	d, nm	ε	Q, nC/mm^2
T_{growth} =230°C			
16x [85+12x(10 + 10)+10]	227	28	27
T_{growth} = 270°C			
16x[150+12x(10+ 10)+10]	248	31	83
T_{growth} = 325°C			
16x[150+12x(10 + 10)+10]	238	33	84

grained t-ZrO_2 probably arises from its remarkably higher density and dielectric constant in comparison to that of m-ZrO_2 (30). It was already earlier suggested that, for this reason, the permittivity of Ta_2O_5-ZrO_2 nanolaminates containing only t-ZrO_2 crystallites always exceeded that of both constituent binary oxides (9). For comparison, the Ta_2O_5-HfO_2 nanolaminates having HfO_2 interlayer thicknesses between 5 and 15 nm contained a mixture of the t- and m-phases and their permittivity decreased rapidly with the increase in HfO_2 interlayer thickness (8).

The creation of the t-ZrO_2 can be followed by a size-dependent metastable-to-stable phase transformation if the size of t-ZrO_2 crystallites exceeds some critical value. The critical crystallite size for t→m transformation may vary in the range of 5-30 nm, depending on the ZrO_2 preparation technique and conditions (31,32), being weakly sensitive to the temperature changes in the temperature range investigated in the present study. Nevertheless, the structural properties of the interlayers remain, in practice, to be determined by the multilayer dimensions rather than deposition and/or measurement temperatures. Obviously, the thickness of ZrO_2 layers in the ALE-grown nanolaminates can be optimized between 5-10 nm to obtain a high content of t-ZrO_2 with as small crystallite size as possible.

The permittivity values calculated for the $(Nb_{1-x}Ta_x)_2O_5$-ZrO_2 nanolaminates (Table 2) containing nanosize t-ZrO_2 crystallites were higher than those of Ta_2O_5 (ε=25) and ZrO_2 films (ε=19.6) as well as Ta_2O_5-ZrO_2 nanolaminates (ε=28) (9). The charge storage factor, Q, which gives information about the substrate area needed for the given capacitance value (33) at arbitrarily chosen leakage current value (here 1 $\mu A/cm^2$) can be calculated as a figure of merit for the dielectric

films. In the $(Nb_{1-x}Ta_x)_2O_5$-ZrO_2 nanolaminates Q = 84 nC/mm^2 (Table 2) while 8, 16 and 64 nC/mm^2 has been achieved in case of the Ta_2O_5, ZrO_2, and Ta_2O_5-ZrO_2 films (9), respectively. When the ZrO_2 interlayer thickness was held at 5 nm, it was amorphous and the $(Nb_{1-x}Ta_x)_2O_5$-ZrO_2 nanolaminates were more leaky, possessing Q-value as low as 27 nC/mm^2.

CONCLUSIONS

Amorphous $(Nb_{1-x}Ta_x)_2O_5$ solid solution films and $(Nb_{1-x}Ta_x)_2O_5$-ZrO_2 nanolaminates containing nanosize tetragonal ZrO_2 crystallites grown by Atomic Layer Epitaxy demonstrated remarkably improved dielectric performance. $(Nb_{1-x}Ta_x)_2O_5$ films exhibited 1.6-4 times higher permittivity than that of Ta_2O_5 single oxide film. The addition of niobium in the nanolaminates resulted in an increase of permittivity value which stabilized above that of Ta_2O_5-ZrO_2 nanolaminates. Leakage current through $(Nb_{1-x}Ta_x)_2O_5$-ZrO_2 nanolaminates was reduced by several orders of magnitude in comparison with Ta_2O_5 and Nb_2O_5 films and $(Nb_{1-x}Ta_x)_2O_5$ solid solutions. The charge storage factor of nanolaminates was remarkably higher in comparison to that of binary oxide films.

ACKNOWLEDGMENTS

The authors are indebted to the Department of Electron Microscopy for the access to EDX apparatus and to Dr. E. Soininen and Dr. J. Viljanen from Planar International Ltd. for the possibility to use electrical measurement techniques. This work was supported in part by the Academy of Finland and Technology Development Centre (TEKES), Helsinki, Finland. K. Kukli expresses gratitude to the Finnish Centre for International Mobility (CIMO) for the research grant.

REFERENCES

1. Moazzami, R., Hu, C. and Shepherd, W.H., *IEEE Transact. Electron Devices*, 1992, 39, 2044.
2. Ono, Y.A., *Electroluminescent Displays*, World Scientific Series on Information Display - Vol. 1, World Scientific, Singapore, 1995.
3. Fukao, R., Fujikawa, H., Nakamura, M., Hamakawa, Y. and Ibuki, S., in *Electroluminescence, Springer Proceedings in Physics* Vol. 38, eds. S. Shionoya and H. Kobayashi, Springer-Verlag, Berlin Heidelberg, 1989.
4. Streiffer, S.K. and Kingon, A.I., *Nature*, 1995, 377, 194.
5. Rack, P.D., Naman, A., Holloway, P.H., Sun, S.-S. and Tuenge, R.T., *MRS Bulletin*, 1996, 21, 49.
6. Kattelus, H., Ylilammi, M., Salmi, J., Ranta-aho, T., Nykänen, E. and Suni, I., *Materials Research Society Symposium Proceedings*, 1993, 284, 511.
7. Kukli, K., Ritala, M. and Leskelä, M., *Journal of the Electrochemical Society*, 1995, 142, 1670.
8. Kukli, K., Ihanus, J., Ritala, M. and Leskelä, M., *Applied Physics Letters*, 1996, 68, 3737.
9. Kukli, K., Ihanus, J., Ritala, M. and Leskelä, M., *Journal of the Electrochemical Society*, 1997, 144, 300.
10. Suntola, T., *Thin Solid Films*, 1992, 216, 84.
11. Suntola, T., *Materials Science Report*, 1989, 7, 266.
12. Tiku, S.K. and Rustomji, S.H., *IEEE Transactions of Electronic Devices*, 1989, 36, 1947.
13. Fujikawa, H. and Taga, Y., *Journal of Applied Physics*, 1994, 75, 2538.

14. Cava, R.J., Peck, Jr, W.F., Krajewski , J.J. and Roberts, G.L., *Materials Research Bulletin*, 1996, 31, 295.
15. Cava, R.J., Krajewski, J.J., Peck, Jr., W.F., and Roberts, G.L., *Journal of Materials Research*, 1996, 11, 1428.
16. Kukli, K., Ritala, M. and Leskelä, M., Advanced Materials CVD, 1998, 4, in press.
17. Ylilammi, M. and Ranta-aho, T., *Thin Solid Films*, 1993, 232, 56 .
18. Duffy, M.T., Wang, C.C., Waxman, A. and Zaininger, K.H., *Journal of the Electrochemical Society*, 1969, 116, 234 .
19. Fuschillo, N., Lalevic, B. and Annamalai, N.K., *Thin Solid Films*, 1975, 30, 145.
20. Pignolet, A., Rao, G.M. and Kruphanidhi, K.B., *Thin Solid Films*, 1995, 261, 18.
21. Joint Committee of Powder Diffraction Standards, Cards 17-923 and 13-307.
22. Gazaux, J., *X-Ray Spectrometry*, 1996, 25, 265.
23. Amberg, M. and Gunter, J.R., *Solid State Ionics*, 1996, 84, 313.
24. Gutzow, I. and Avramov, I., *Thin Solid Films*, 1981, 85, 203.
25. Gopalakhrisnan, J., *Chemistry of Materials*, 1995, 7, 1265.
26. Chakravorty, D. and Giri, A.K., in *Chemistry of Advanced Materials, Nanomaterials*, ed. C.N.R. Rao, p. 217, Blackwell Scientific Publications, Oxford, 1993.
27. Wang, F. and Northwood, D.O., *Journal of Materials Science*, 1995, 30, 4003.
28. Kim, D.-Y., Park, H.-J. and Cho, D.-H., *Solid State Ionics*, 1995, 80, 67.
29. Scanlan, C.M., Gajdardziska-Josifovska, M. and Aita, C.R., *Applied Physics Letters*, 1994, 64, 3548.
30. Thompson, D.P., Dickins, A.M. and Thorp, J.S. *Journal of Materials Science*, 1992, 27, 2267.
31. Garvie, R.C. and Goss, M.F., *Journal of Materials Science*, 1986, 21, 1253.
32. Aita, C.R., Wiggins, M.D., Whig, R., Scanlan, C.M. and Gajdarziska-Josifovska, M., *Journal of Applied Physics*, 1996, 79, 1176.
33. Gerstenberg, D., in *Handbook of Thin Film Technology, Thin Film Capacitors*, ed. L. I. Maissel and R. Glang, p.19-8, McGraw-Hill, New York, 1970.

CURRICULUM VITAE

Kaupo Kukli

Citizenship:	Estonian
Birth:	22.12.1967, Valga, Estonia
Address:	University of Tartu, Institute of Experimental Physics and Technology, Tähe 4, Tartu 51010, Estonia
Phone:	+37 27 376 294
Fax:	+37 27 375 858
E-mail:	kaupok@ut.ee

Education

1975–1986	Põlva Secondary School
1986–1987,	
1989–1992	University of Tartu, diploma in physics
1992–1993	University of Tartu, M. Sc. (Phys.)

Scientific experience

1993–1996	Visiting researcher at the Laboratory of Inorganic Chemistry, University of Helsinki
1996–1997	Researcher at the Laboratory of Inorganic and Analytical Chemistry, Helsinki University of Technology
1998	Visiting researcher at the Laboratory of Inorganic Chemistry, University of Helsinki

Publications

Total number of publications: 15
1 poster and 5 oral presentations in international scientific meetings and conferences

ELULUGU

Kaupo Kukli

Kodakondsus:	Eesti
Sündinud:	22.12.1967 Valgas
Aadress:	Tartu Ülikool, eksperimentaalfüüsika ja tehnoloogia instituut, Tähe 4, Tartu 51010
Telefon:	(27) 376 294
Faks:	(27) 375 858
E-post:	kaupok@ut.ee

Hariduskäik

1975–1986	Põlva Keskkool (Põlva Ühisgümnaasium)
1986–1987, 1989–1992	Tartu Ülikool, diplom füüsikas
1992–1993	Tartu Ülikool, magistrikraad füüsikas

Teadusalane enesetäiendus

1993–1996	Helsingi Ülikooli anorgaanilise keemia laboratooriumi külalisteadur
1996–1997	Helsingi Tehnoloogiaülikooli anorgaanilise ja analüütilise keemia laboratooriumi teadur
1998	Helsingi Ülikooli anorgaanilise keemia laboratooriumi külalisteadur

Publikatsioonid

Publikatsioonide üldarv: 15
1 poster ja 5 suulist ettekannet rahvusvahelistel sümpoosiumidel või konverentsidel

DISSERTATIONES PHYSICAE UNIVERSITATIS TARTUENSIS

1. Andrus Ausmees. XUV-induced electron emission and electron-phonon interaction in alkali halides. Tartu 1991.
2. Heiki Sõnajalg. Shaping and recalling of light pulses by optical elements based on spectral hole burning. Tartu 1991.
3. Sergei Savihhin. Ultrafast dynamics of F-centers and bound excitons from picosecond spectroscopy data. Tartu 1991.
4. Ergo Nõmmiste. Leelishalogeniidide röntgenelektronemissioon kiiritamisel footonitega energiaga 70–140 eV. Tartu 1991.
5. Margus Rätsep. Spectral gratings and their relaxation in some low-temperature impurity-doped glasses and chrystals. Tartu 1991.
6. Tõnu Pullerits. Primary energy transfer in photosynthesis. Model calculations. Tartu 1991.
7. Olev Saks. Attoampri diapasoonis voolude mõõtmise füüsikalised alused. Tartu 1991.
8. Andres Virro. AlGaAsSb/GaSb heterostructure injection lasers. Tartu 1991.
9. Hans Korge. Investigation of negative point discharge in pure nitrogen at atmospheric pressure. Tartu 1992.
10. Jüri Maksimov. Nonlinear generation of laser VUV radiation for high-resolution spectroscopy. Tartu 1992.
11. Mark Aizengendler. Photostimulated transformation of aggregate defects and spectral hole burning in a neutron-irradiated sapphire. Tartu 1992.
12. Hele Siimon. Atomic layer molecular beam epitaxy of A^2B^6 compounds described on the basis of kinetic equations model. Tartu 1992.
13. Tõnu Reinot. The kinetics of polariton luminescence, energy transfer and relaxation in anthracene. Tartu 1992.
14. Toomas Rõõm. Paramagnetic H^{2-} and F^+ centers in CaO crystals: spectra, relaxation and recombination luminescence. Tallinn 1993.
15. Erko Jalviste. Laser spectroscopy of some jet-cooled organic molecules. Tartu 1993.
16. Alvo Aabloo. Studies of crystalline celluloses using potential energy calculations. Tartu 1994.
17. Peeter Paris. Initiation of corona pulses. Tartu 1994.
18. Павел Рубин. Локальные дефектные состояния в CuO_2 плоскостях высокотемпературных сверхпроводников. Тарту 1994.
19. Olavi Ollikainen. Applications of persistent spectral hole burning in ultrafast optical neural networks, time-resolved spectroscopy and holographic interferometry. Tartu 1996.
20. Ülo Mets. Methodological aspects of fluorescence correlation spectroscopy. Tartu 1996.

21. Mikhail Danilkin. Interaction of intrinsic and impurity defects in CaS:Eu luminophors. Tartu 1997.
22. Ирина Кудрявцева. Создание и стабилизация дефектов в кристаллах KBr, KCl, RbCl при облучении ВУФ-радиацией. Тарту 1997.
23. Andres Osvet. Photochromic properties of radiation-induced defects in diamond. Tartu, 1998.
24. Jüri Örd. Classical and quantum aspects of geodesic multiplication. Tartu, 1998.
25. Priit Sarv. High resolution solid-state NMR studies of zeolites. Tartu, 1998.
26. Сергей Долгов. Электронные возбуждения и дефектообразование в некоторых оксидах металлов. Тарту, 1998.

ISSN 1406–0647
ISBN 9985–56–388–3